Department of Chemical Engineering

Modelling and Simulation of Chromatographic Processes for Whey Proteins

Sanket H. Jadhav

This thesis is presented for the Degree of

Doctor of Philosophy

of

Curtin University

March 2019

Declaration

To the best of my knowledge and belief, this thesis contains no material previously published by any other person except where due acknowledgement has been made.

This thesis contains no material which has been accepted for the award of any other degree or diploma in any university.

Signature:

Date: 27/03/2019

Dedicated To,

My Mother,

Father, & Sister

Acknowledgement

Sometimes saying a simple 'thank you' may not be enough to show the actual feeling behind it. Nevertheless, here is an attempt to pen down the acknowledgement.

I want to express my deepest gratitude to my Ph.D. supervisor, Dr. Ranjeet Utikar for giving me all the freedom in my research work. He has been such an inspiration to work with. There are numerous things to enlist that I have learned from his approach towards scientific problems. I appreciate his way of encouraging self learning over giving direct answers, which helped me gain knowledge and hone my skills for the research work. Most importantly, he taught me simplistic thinking towards complex problems which will help me in addressing problems in my professional and personal life. He emphasised the fact that Ph.D. is all about learning new skills to get ready for future challenges.

I would also like to extend my thanks to Head of School, Prof Vishnu Pareek for providing me with the infrastructure for the research work. I gratefully acknowledge Department of Chemical Engineering, Curtin University for providing funding during my PhD. Laboratory work wouldn't have been possible without the technical staff of Chemical Engineering department. I would like to thank specially to Andrew and Melina for their efforts to answer and arrange solutions for the problems with the chemicals and set-ups in the lab.

It is true that there were testing times in the tenure but they were made simpler by presence of so many great individuals. I would like to take this opportunity to make some special mentions. Mrunmai has been such a wonderful friend. She was always there to listen when I had to talk about technical or personal problems. Subhra has been such a fantastic friend. His constant care and ever smiling attitude helped me relax throughout this tenure. His encouragement helped a lot

in developing my cooking and baking hobbies. Adhirath has been an inspiring friend and a person to look up to in the testing times. It was amazing to find a friend in him who had almost similar goals for life, to mine. His passion towards research and problems in society is something I will always appreciate. I would like to extend my thanks to Sharmilee for making my transition from India to Australia seamless. I would like to acknowledge Vaibhav and Himanshu for their timely advise in difficult times.

My special thanks to Majushree Utikar for her super delicious food treats and encouragement in baking. I express my heartfelt gratitude to Cathy, David, Joshua, and Jesslyn (The Wongies). It never felt away from home as they welcomed me into their family with open hearts. Special thanks to Cathy for the encouraging conversations which uplifted me when I was not sure of the situations. Furthermore, I found an amazing friend in Navdeep. The conversations, coffee times, and random drives with her made me feel mindful in stressful situations.

In this long journey, I was blessed with presence of so many colleagues at Curtin university. I will always cherish the road trips we have been to and I would like to acknowledge all of them for making this tenure a fun ride. I would also like to express special thanks to friends from home, Kalpana, Manasee, and Sayali, who were a continuous source of positive energy and encouragement.

Last, but not least, I am indebted to my family, **'Aai', 'Pappa', and 'Tai'**, for understanding my goals and ambitions. Specially my **'Tai' and 'Jeeju'** (sister and brother- in-law) who have been taking care of my parents in my absence in spite of their busy lives. This lightened my responsibilities so that I could stay focused. I dedicate this thesis to them. They have been an endless source of encouragement, love, happiness, and support through the thick and thins of my Ph.D. They made me stronger which helped me pursue my passion wholeheartedly.

Lastly, it is needless to state that this thesis has been a milestone in an ever evolving journey for becoming a better student, engineer, scientist, explorer, and a human being. Again, I thank all those who have contributed in it.

I quote my inspiration for life here to end this acknowledgement!

"Arise, Awake, Stop not till the goal is reached"

Abstract

Introduction of mechanistic models for chromatography first started for improving understanding of the mechanism of the process and since then, the focus of research in chromatography is shifted to mathematics based concepts. Nowadays, modelling and simulations of chromatography are being conveniently used with process development tools such as; DoE, QbD, and PAT to enhance research. With advent of novel molecules at rapid rates and continuously rising market potential, effective utilisation of time and resources has become very crucial. With upcoming advanced techniques and their integration, tremendous amount of data is being generated which needs to be understood in order to use it for process improvement and monitoring. This makes simulation driven process optimization highly significant in the current research era.

Current research presents a systematic methodology of experiments and simulation of ion exchange chromatography process. Ion exchange chromatography is chosen for the study considering its wide implementation for capture and intermediate polishing steps for variety of protein molecules.

A brief literature review was presented for various aspects of modelling and simulations of ion exchange process are touched upon along with potential mass transfer and thermodynamic models which can be implemented. Different facets of model based process design were introduced to give a brief idea about role of simulation tools in the overall methodology. Overview of current tools for simulation of chromatography was given further to highlight the advantages and disadvantages. Criteria for selecting an experimental system for validation were presented further to emphasise why whey protein stream was chosen as an experimental system for model validation.

A simulation tool, Extenstible Process Simulator for Ion exchange Chromatog-

raphy (*ExProSim:IC*) was introduced further along with its computational framework, data analysis methodology, and different models involved. The tool gives flexibility of solving equilibrium dispersive model (EDM) in combination with thermodynamics models such as; Langmuir, steric mass action (SMA), and mobile phase modulator (MPM). Tool verification was presented further by checking functionality with respect to change in variation of model constants. The variation was found to be inline with physical significance of the model constants. Code to code verification with CADET as a reference tool and mesh independency studies to get convergent solutions further emphasised the workability of the tool. The predictions from the tool showed a decent match to experimental and simulation case studies from the literature as average Coefficient of determination (CoD) was above 0.95. The cases from the literature were chosen to give a wide array of process parameters for a thorough validation of all three thermodynamic models solved with EDM.

To build data for *ExProSim:IC* validation based on experiments, binding characteristics of major whey protein standards; bovine serum albumin (BSA), β-Lactoglobulin (BLG), and α-Lactalbumin (ALA) were studied for both cation and anion exchange chromatography. Model constants were determined for three thermodynamic models; Langmuir, SMA, and MPM . Inverse fit method was employed in parameter estimation module of *ExProSim:IC* for determination of the model constants from batch, gradient, and breakthrough experimental data. It was proved that anion exchange was a better technique for separation of major whey proteins considering their electrokinetic potential at operating pH of 6.9. Ability of *ExProSim:IC* to predict the breakthrough curves was further examined and effect of model constants and process parameters on breakthrough curve prediction for all the thermodynamic models was investigated. Lessons from tool verification exercise were utilised to make changes in the model constants to fit the simulation data to breakthrough curve. Changes in model constants was discussed in detail to understand the importance of physical and chemical properties involved. Higher error was observed for BSA breakthrough as the experimental unsaturation was not predicted by *ExProSim:IC*. The unsaturation was an outcome of possible weaker hydrophobic interactions of BSA leading to continuous adsorption-desorption of

protein which was not efficiently predicted by EDM. Experimental multicomponent breakthrough for cation exchange showed displacement of BLG by BSA due to higher hydrophobicity of BSA. Predictions of multi component breakthrough showed inability to accurately predict the overshoot of the protein molecule due to displacement (CoD values down to 0.85 and DBC errors>10% and errors >20% at saturation).

The average 'point to point' error for predictions of single component anion exchange breakthrough was found to be <5% for all the models and average CoD was more than 0.96. ALA and BSA were displaced by BLG owing to existence of high proportions of BLG dimers at the operating pH. Dimerisation increases binding due to increased ionic strength leading to higher binding capacity. Prediction for multicomponent breakthrough for anion exchange were better than cation, however the overshoot was not predicted well (CoD values>0.90 and DBC errors>5% and errors >20% at saturation).

Similar studies were carried out for minor whey protein standards; Lactoferrin (LF) and Lactoperoxidase (LP). Standards obtained were first purified to >98% in order to use them for adsorption kinetic studies. Experimental data was used to generate model constants which were utilised further for investigation of effect of process parameters and variation in model constants on single component and multicomponent breakthrough curves. It was observed that the predictions were excellent match to the experimental data for single component breakthrough. Multicomponent breakthrough predictions were observed (CoD>0.95 and DBC errors<5% and errors >10% at saturation). That may be due to absence of overshoot in the data. Potential learning from earlier chapters was implemented in examining the predictability of the tool for simulation of multicomponent breakthrough for crude whey protein concentrate (WPC) on anion exchanger. It was observed that BLG, being in high concentration, dominated the binding pattern, and the accuracy of predictions was compromised (CoD<0.95 and error>10%) while predicting the overshoot of displaced protein concentration.

The results presented in this thesis lay a systematic methodology towards developing basic understanding of implementation of modelling and simulation for ion exchange chromatography. The experimental system developed here for ma-

jor and minor whey proteins not only served as a comprehensive dataset for experimental validation but also laid a basic framework for designing a prospective separation process for individual whey proteins. Experiments and major learning about model constant calibration formed a preliminary platform for creating a prospective database of thermodynamic constants for protein molecules for building a framework for model based process development.

Nomenclature

Symbols

μ_f	Mean residence time/first moment (min)
W_h	Width at half height
d_p	Resin particle diameter
h	Reduced plate height
Re	Reynolds number
Pe	Peclet number
c	Protein concentration in the mobile phase (mg/ml)
q	Protein concentration in the solid phase (mg/ml)
δ	Variance of the peak
ϵ_e	Column porosity
ϵ_t	Total porosity
ϵ_p	Particle porosity
D_{ax}	Dispersion coefficient (cm^2/min)
L	Length of the column (cm)
F	Flow rate (ml/min)
u	Flow linear velocity cm/min

D_m	Molecular diffusivity (cm^2/min)
M	Molecular weight (KDa)
η	Viscosity (cP)
T	Temperature in Kelvin (K)
r_p	Radius of particle (cm)
$c_{i,0}$	Concentration at the inlet (mg/ml)
Q_{max}	Maximum binding capacity for Langmuir (mg/ml resin)
k^l_{ads}	Adsorption coefficient in Langnmuir (ml/mg.min)
k^l_{des}	Desorption coefficient in Langmuir (min^{-1})
k_d	Dissociation constant for Langmuir (mg/ml)
c_{eq}	Concentration in mobile phase at equilibrium
q_e	Equilibrium adsorbed concentration in Freundlich isotherm (mg/ml)
Q_f	Equilibrium adsorption capacity for Freundlich isotherm (mg/ml)
c_e	Equilibrium concentration in mobile phase (mg/ml)
n	Adsorption intensity for Freundlich isotherm
k_1	Pseudo first order kinetic constant (min^{-1})
k_2	Pseudo second order kinetic constant (ml/mg.min)
q_t	Adsorbed concentration at instantaneous time 't' (mg/ml)
Λ	Ionic capacity of the resin (mM)
σ_i	Steric hindrance factor for SMA
v_i	Characteristic charge of the protein
k_{eq}	Equilibrium constant in SMA
$k^s_{ads,i}$	Adsorption coefficient in SMA

$k^s_{des,i}$	Desorption coefficient in SMA
cv	Volume of column (ml)
v_r	Retention volume (ml)
v_g	Gradient volume (ml)
$c_{a,s}$	Salt concentration at gradient begin (mM)
$c_{e,s}$	Salt concentration at gradient end (mM)
c_0	Salt concentration in the buffer during breakthrough (mM)
q_0	Total salt concentraion in the stationary phase (mM)
$\bar{q}_0$	Salt ion in stationary phase available for exchange (mM)
v_b	Breakthrough volume at 10% of the complete breakthrough (ml)
t_r	Retention time (min)
t_0	Dead void time (min)
v_d	Column dead volume (ml)
v_0	Breakthrough volume at 10% of a nonretarded tracer (ml)
k_{ads0}	Adsorption coefficient in MPM (ml/mg.min)
k_{des0}	Desorption coefficient in MPM (ml/mg.min)
$k^m_{ads,i}$	Adsorption coefficient in MPM
$k^m_{des,i}$	Desorption coefficient in MPM
k_{dmpm}	Resultant desorption constant for MPM
γ_i	Hydrophobicity index for MPM model (ml/mg)
β_i	Salt interaction index for MPM model
t	Time (min)
x	Axial coordinate (cm)

T	Temperature (°C)
R_L	Equilibrium constant in Langmuir
R_{min}	Minimum radius of protein molecule
ρ	Density of the mobile phase (gm/cm^3)
c_{NaOH}	Concentration of NaOH for titration (mM)
v_{NaOH}	Volume required of NaOH for titration (ml)
ψ	Phase ratio from chromatography column
$v_{10\%bt}$	Breakthrough volume at 10$\%$
N_{comp}	Number of protein components in a mixture
t_p	Time of pulse injection (min)
t_f	Tailing factor
$\%B$	$\%$ of mobile phase B in chromatography
S_{BSA}	slope of BSA curve in the mixture for SEC:HPLC calibration
S_{BLG}	slope of BLG curve in the mixture for SEC:HPLC calibration
c_{BSA}	concentration of BSA in the mixture for SEC:HPLC calibration
c_{BLG}	concentration of BLG in the mixture for SEC:HPLC calibration
A_{tot}	Total peak area for the mixture of BSA and BLG
N_x	Number of axial mesh points
n_t	Number of time mesh points
Δx	axial grid interval
Δt	time grid interval
r_{min}	radius of protein (m)

Abbreviations

AC	Affinity chromatography
ALA	α-lactalbumin
ANN	Artificial neural network
BLG	β-lactoglobulin
BSA	Bovine serum albumin
CFD	Computational fluid dynamics
CQA	Critical quality attributes
CADET	Chromtography analysis and design tool
CV	Column volume
DBC	Dynamic binding capacity
DoE	Design of Experiments
EDM	Equilibrium dispersive model
FDM	Finite difference method
FEM	Finite element method
FVM	Finite volume method
GALib	Genetic algorithm library
GRM	General rate model
HIC	Hydrophobic interaction chromatography
IC	Ion exchange chromatography
IDM	Ideal model
IgG	Immunoglobulin G

LC	Liquid chromatography
LF	Lactoferrin
LMA	Levenberg-Marquardt algorithm
LP	Lactoperoxidase
MBE	Model based engineering
MOO	Multi objective optimisation
MPM	Mobile phase modulator
NGC	Next generation chromatography
NMR	Nuclear magnetic resonance
NTU	Net transfer units
ODEs	Ordinary differential equations
PAT	Process analytical technology
PDEs	Partial differential equations
pI	Isoelectric point
POR	Pore diffusion model
PVDF	Poly vinylidine fluoride
QbD	Quality by Design
RPC	Reverse phase chromatography
RSM	response surface methodology
RV	retention volume
SAS	Self association model
SBC	Static binding capacity
SDM	Stoichiometric dispersion model

SEC	Size exclusion chromatography
SMA	Steric mass action
SPFF	Sulphopropyl sepharose fast flow
SUNDIALS	SUite of Nonlinear and DIfferential/ALgebraic Equation
TDM	Transport dispersive model
WENO	Weighted essentially non oscillatory
WPC	Whey protein concentrate
SE	Standard error
SD MSE	Standard deviation in mean standard error
RMSE	Root mean square error
CoD	Coefficient of Determination

Subscripts

i	: 'i'th component
e	: exit
s	: salt
eq	: equilibrium

Contents

List of Figures

List of Tables

Chapter 1

Introduction

1.1 Introduction

In the past few decades, breakthrough scientific explorations have led to faster production at upstream processes moving the bottleneck to downstream operations in food and bio-pharmaceutical industries [7]. Significantly higher process development rate in upstream processes compared to the downstream processes is due to multiple steps involved in the purification, where every step needs to be improved to make a mark on the efficiency [8]. Liquid chromatography (LC) is one of the most prominent platforms for purification however, its cost effective design and operation is very challenging. At the same time, increasing raw material costs and quality constraints on the final products makes it difficult to design a cost effective and self sufficient process. It is believed that answers must be sought in the fundamentals of LC in order to solve current problems such as excessive experimentation, time consuming scale ups, tedious troubleshooting, and slower implementation of process improvements.

LC is a complex unit operation that has number of different processes occurring in parallel. Along with the complexity of the operation it is also considered to be one of the most costliest operations in purification assembly. Therefore, attempts must be made in order to reduce the costs. Mathematical modelling has proved to be an effective tool for prediction of outputs of numerous operations. It has been used to efficiently design of multiple unit operations such as; fluidised beds, distillation columns, dryers, crystallisers etc. This research at-

tempts to study chromatography models and their simulation methodology in the hope to reach an effective approach to unravel, understand, and improve the way chromatography is approached in research and industries.

1.2 Motivation

LC is a unit operation in which a mixture of molecules to be separated, flow through a packed adsorbent bed along with a mobile phase. Differential migration of molecules takes place depending on their relative interaction with the bed and mobile phase. It is crucial to understand these interactions for improving current approaches of process design. Various key approaches such as; heuristic approach, experimental approach, platform approach, and combined approach have been practised for designing of chromatography. In heuristics, decisions are taken based on prior knowledge and experience about the molecule in consideration [9, 10]. Though it takes less efforts, heuristic approaches lack new methodologies which can prove to be a limitation for the capability of the process. Experimental approaches rely on trial and error based intensive experimentation which consume a lot of time, efforts, and resources in order to get desired outcomes. Though it is the safest of all other approaches, limited sample availability and strict time lines for getting the product do not make it a wise choice. Platform approach relies on designing a process based on already established data for a similar molecule. This method is widely used in industries where stringent deadlines are to be followed and the molecules to be produced are costly species like antibodies [11]. Despite of above mentioned strategies and their practise in LC over last three decades, further improvement in the speed of development is required to keep desired quality and quantity in check. It is true that, recent introduction of concepts such as; design of experiments (DoE) and quality by design (QbD) ensure robustness and flexibility of the process[12], however these approaches involve plentiful experiments which may be time consuming for a market driven development. Furthermore, these techniques along with process analytical technology (PAT), generate a lot of data which needs to be assessed meaningfully to design further steps.

A more strategic approach which has been explored widely, involves model

based development of chromatographic processes. Various tools for chromatography simulation have been proposed and implemented [13, 14, 15] which offer varying degree of accuracy and efficiency for design. However, it is important to note that there is a further scope in discussing the implementation of models based on fundamental understanding of determination of model parameters by using experimental basis to determine them. This research focuses on building an understanding about the parametric calibration which is to be done to get the right predictions and further understand their significance for three thermodynamic models. It is also important to understand before the actual process development, the causes of possible variations in the governing parameters when different feed streams are involved. Considering this, simplification of the pathway of understanding what experiments should be performed to pave the way to implement modelling for simulations of chromatography is what is sought here.

1.3 Research objectives

Major aim of this work is to provide a better outlook of how modelling and simulations can be used for understanding of ion exchange chromatographic operations. Following are the objectives of this research;

1. To formulate a simple tool, *ExProSim:IC* offering flexibility of using various thermodynamic models for simulation of chromatographic operation.
2. To verify the tool for its functionality by assessing effect of variation in model constants, code to code verification, and mesh independency
3. To check the predictability and accuracy of the tool based on literature data.
4. To understand separation characteristics of major and minor whey protein standards for ion exchange chromatography.
5. To establish an experimental system by determining model constants and validate *ExProSim:IC* for five whey proteins.
6. To discuss in detail how the isotherm parameters affect the simulation curves for better understanding of the process and further assess applicability for

crude protein systems such as whey protein concentrate.

1.4 Thesis outline

The thesis is divided into 7 chapters based on the research objectives.

1. Chapter 1 gives a brief introduction to the research problem along with the motivation for the research.

2. Chapter 2 discusses basic concepts of modelling in chromatography. Further a comprehensive review of literature is given for modelling and simulation of chromatographic operations with emphasis on thermodynamic and mass transfer models along with their applications. Various tools available for implementation of these models are discussed further with a brief summary and their implementation followed by a summary of model based process development for chromatography. In addition to this selection of whey proteins as an experimental system is justified. Furthermore, challenges associated with implementation of modelling and simulation in chromatography is discussed to state significance of the thesis.

3. Chapter 3 discusses summary of formulation of the tool *ExProSim:IC* including data analysis, mathematical models, and mechanistic framework. Materials and methodology for experiments for chromatography and sample analysis is discussed in detail. Furthermore, tool verification and literature based validation is demonstrated for the chosen thermodynamic models for *ExProSim:IC*.

4. Chapter 4 shows experimental validation of *ExProSim:IC* in continuation to the literature based validation from chapter 3. Assessment of experimental characteristics of major whey proteins for anion and cation exchange chromatography is performed. This is accompanied by prediction of breakthrough curves for single and multicomponent systems using *ExProSim:IC* with further explanation pertaining to change of experimental and simulation parameters.

5. Chapter 5 continues the experimental validation for *ExProSim:IC* for basic whey proteins. Assessment of minor whey proteins for cation exchange chromatography is performed for finding model parameters. *ExProSim:IC* is used further for breakthrough prediction of single and multicomponent mixture of standard proteins.

6. Chapter 6 shows applicability of *ExProSim:IC* for prediction of experimental breakthrough of crude whey protein concentrate (WPC). Furthermore, comparison of model parameters for standards and crude is discussed in detail.

7. Chapter 7 summarises the research work by stating important observations and findings. This is followed by insights on prospective areas of improvements for taking the work forward.

Chapter 2

Literature review

2.1 Introduction

2.1.1 Liquid chromatography (LC)

Liquid chromatography is one of the most critical operations in the food, pharmaceuticals, and biopharmaceutical industries. For optimisation of LC, several steps should be followed with careful considerations towards the desired outcomes such as; type of product, yields, purity, and costs. There are various types of chromatography techniques depending on the chemistry used for separation. These include ion exchange chromatography (IC), reversed phase chromatography (RPC), hydrophobic interaction chromatography (HIC), affinity chromatography (AC) etc. IC uses charge interactions between resin and protein molecules for fractionation based on change in the degree of ionic interactions with a changing salt gradient. In HIC, hydrophobic interactions between protein and resin are exploited for fractionation by changing the salt concentration of the mobile phase. For RPC, hydrophobicity of the protein is explored further for binding to non polar resin under an organic modifier. AC is designed based on specific interactions of a protein to a ligand which is attached to the resin for enhanced adsorption. Among these, IC is one of the most widely used chromatographic methods in the industries because of its simple application at capture, intermediate, and polishing stages of a separation process.

2.1.2 Ion Exchange chromatography

IC explores the fact that protein exerts no surface charge at its isoelectric point (*pI*) and pH of the solution can be changed in order to change the charges on the protein molecule. If the pH is higher than the *pI* of the protein, the net charge on the protein is negative and it will bind to a positively charged adsorbent. On the other hand, when the pH is lower than the *pI* of the protein, it shows positive charge to further bind to a negatively charged adsorbent. IC can be described further as follows.

1. IC offers high resolution between the protein peaks as the separation criteria is easy to modify and control, based on pH and salt concentration of the solution.

2. IC adsorbents offer high protein-binding capacity due to high density of charged ligands on the adsorbent.

3. IC is operated with aqueous mobile phases which does not raise an extra concern for removal of organic solvent from the product peaks. The product peaks are generally concentrated in salt which can be easily addressed by desalination process if required.

4. IC provides flexibility in terms of processing. It can operate at very high flow rates. It can be used to separate wide range of protein molecules and do not have specific criteria as required for size exclusion or affinity chromatography. IC is also a non-denaturing technique and it can be used at all stages and scales of purification. It also serves as a concentration step for crude stream with high impurities.

5. Modern IC adsorbents offer macroporous structures allowing the processes to be operated at high flow rates which is an indicative of high productivity.

Considering all these advantages IC has high popularity in enzyme and food industries [16] and it is chosen for the work in this thesis. Further sections will discuss modelling aspects of IC.

2.2 Modelling and simulations in chromatography

Any ion exchange chromatography interaction in the column is an effect of charge driven thermodynamics between the protein and resin, and mass transfer of the protein through the porous bed towards or away from the charged ligands. Hydrodynamics of the proteins due to flow conditions is another aspect which affects the binding kinetics. It is very difficult to assess and control these mechanisms by experimental means hence numerous models are proposed for understanding IC better. These are presented in the further sections.

2.2.1 Thermodynamic models

Linear model is a simplest adsorption model where the rate of adsorption is linearly proportional to the concentration of molecules of the components present in the mobile phase. As this is the simplest of all kinetics, most of the basic theories were based on linear model [17, 18, 19]. Langmuir model based on homogeneity of the sites is a monolayer isotherm which follows pseudo second order kinetics [20]. For Langmuir, the physical phenomena was represented by two constants; Q_{max} and k_d, where first one gives maximum binding towards the resin and second one represents the dissociation equilibrium coefficient or binding strength (k^l_{des}/k^l_{ads}). Though Langmuir model captures competitive binding of proteins to the ligand sites, it has certain drawbacks. The isotherm is thermodynamically inconsistent if the saturation capacities of proteins are not identical [21, 22]. Binding is considered proportional to the vacant sites on the adsorbent and salt interactions are lumped into a binding constant when they are major driving forces for the adsorption and desorption [23]. It doesn't account for the steric effects between the salt-protein and protein-protein molecules, or hydrophobic surface interactions because of their conformation. Nevertheless, it has been used widely for determining chromatographic profiles to certain accuracy [24, 25, 26].

To account for the salt interactions, Langmuir model was further modified to mobile phase modulator model (MPM). MPM considers both ionic and hydrophobic interactions during binding and desorption by modification of the rate constants to; k_{des0} and k_{ads0} from Langmuir constants [27]. Karlsson et al. [28] con-

sidered the factor γ to be zero, to simulate breakthrough curves for insulin and transferrin successfully. Furthermore, antibody purification was studied by Karlsson to give a perfect prediction for experimental profile due to accurate parameter estimation [29].

Another isotherm referred as steric mass action model (SMA), accounts for the steric effects based on the electronegativity of the salt ions present with protein molecules and their effect on the adsorption-desorption kinetics [30]. Isotherm formalism was based on completely new set of constants such as; λ (Ionic capacity), υ (characteristic charge), σ (steric factor), and $k_{eq} = k^s_{des}/k^s_{ads}$ (equilibrium dissociation constant). SMA has been implemented widely for binding predictions for ion exchange displacement chromatography as it describes the mass transfer of proteins in exchange of salt ions [31, 32, 33]. The parameter determination for SMA is explored widely for its easy implementation for any experimental setup [34, 35, 36]. However, aggregation between the protein molecules is not considered in SMA. Effects such as aggregation or changes in the secondary and tertiary structure of the protein can occur because of physical forces like van der Waals and electrostatic interactions between adsorbed proteins and the salt ions, or protein-protein interactions[37]. These are mostly applicable to macro-molecules and can lead to anti-Langmuir multi layered adsorption at lower concentrations and Langmurian kinetics at higher concentrations [38]. For such a situation, self association model (SAS) was proposed [39]. For current chromatography applications, applicability of linear model is obsolete, whereas Freundlich describes mostly multilayered adsorption with poor accuracy. SAS is an isotherm which is applicable in special cases where large molecules are involved. Langmuir, SMA, and MPM are widely applied isotherms for predicting ion exchange chromatography processes hence, these were primarily chosen for further simulation studies in this work. Further modifications in these basic models for capturing specific interactions have been proposed based on more complex phenomena such as self association, unfolding, refolding etc. [40, 41, 42]; however, they are not considered here.

2.2.2 Mass transfer models

Along with thermodynamics of the interaction, it is also critical to understand the mass transfer kinetics of a chromatography process. Mass transfer models are based on certain assumptions in order to make them simple to apply [43]. Various models are proposed based on the complexity of the process. The general rate model (GRM) captures all possible mass transfer resistances such as; molecular diffusion, surface diffusion, film diffusion, pore diffusion etc. [44]. All the equations for implementation of GRM are given in Section A.1.1. GRM is used in model based process development as it considers most mass transfer processes involved. GRM is mostly applied for small molecules and slow processes where pore diffusion is prevalent but it was also successfully applied for big molecules [45]. GRM was successfully implemented for many experimental systems at small and large scales [46, 47, 48, 49]. However, application of GRM is also complex because of the relatively large number of parameters needed to characterize the axial dispersion, the external mass transfer, and the effective diffusion through the pores and external bed. These parameters are often difficult to measure experimentally for accurate predictive modelling [50].

Pore diffusion model (POR) is a simplification of GRM where pore and surface diffusion are neglected by simplifying gradient pore concentration to the average concentration [51]. Binding kinetics, overall diffusion coefficient at surface and medium are considered further to assess mass transfer. All the required equations from formulation of POR to determination of diffusion coefficients are given in Appendix B Section A.1.2. Different formulations of POR are applied for simulation of LC based on pore structure, particle shape, pore diameter and pore distribution [52, 53, 54, 55, 56].

Further simplification of POR led to formulation of equilibrium dispersive model (EDM). EDM considers that the variability from the equilibrium can be represented by an apparent axial dispersion coefficient (D_{ax}) [57]. D_{ax} is also considered to be independent of the low protein concentration in less viscous medium. At higher concentrations and higher velocities, the effect of axial dispersion coefficient was considered to be zero [58]. However, it was realised that it can be estimated and even though the value is minimal it is not negligible [59]. As most of the processes

in analytical and industrial scales are relatively fast, EDM is the most widely used model for simulating chromatography [60, 61]. It is proved that applicability of EDM is not limited to specific resin structure [62, 63] or chromatography technique [64, 65], hence it can be applied to a variety of modelling applications. As EDM is a focus of this work, expressions for EDM are discussed further in section 3.2.1

Transport dispersive model (TDM), Ideal model (IDM) are few other mass transfer models which have been used for prediction purpose. In the TDM, contributions of slow mass transport kinetics are lumped into the mass transport rate coefficient, k_m [66, 67]. TDM uses same equation as EDM except that the $\frac{\partial q}{\partial t}$ term is replaced by equation A.21 [68].

IDM is the simplest of all models, it has been explored since last 3 decades [69, 70, 71, 72]. It does not consider any diffusion and it was often found that such is not the case for LC processes [73]. The accuracy of predictions for IDM is questionable; however, it can be applied for very fast processes. Considering simplicity of implementation, minor requirements of model constants as compared to other mass transfer models, and accuracy of predicting industrial processes, EDM was chosen further for simulation purpose in this work. Equations for all other models are given in Appendix A for further reference.

2.2.3 Hydrodynamic approaches

As chromatography is a continuous adsorption and desorption process under a flowing regime, it is very hard to know what exactly happens inside the column.

Packing and nature of the resin, and velocity and nature of the mobile phase decide the flow patterns inside the column. Current analysis techniques rely on inlet and outlet sample analysis and they are insufficient to give complete idea of how the adsorption happens throughout the column. Studying the flow patterns inside the column can facilitate in understanding nature of band broadening in the column and help design better matrices. With simultaneous mass transfer between mobile and stationary phase along with the flow, it is evident that multiple resistances are present throughout the column which need to be accounted. Most analysis techniques rely on inlet and outlet sample analysis and it may not give a

complete picture of the adsorption phenomena. Non-invasive column visualisation tools such as; X-rays, Nuclear magnetic resonance (NMR), Computed Tomography(CT), and gamma rays were employed for measuring the velocity patterns inside the packed column under operation [74, 75, 76]. This can help in finding the governing mechanisms inside the column. Even the scales at which the velocity changes take place can be understood. Such techniques can help in assessing radial heterogeneity. Though all the mass transfer models discussed earlier assume that the column is radially homogeneous, it is worth investigating radial heterogeneity of the column for better understanding. This can help assessing irregular flows, uneven packings, and improve distributor design. Modelling techniques such as computational fluid dynamics (CFD) were applied for simulation of chromatographic column to get further insights of the mechanism of mass transfer [77].

CFD is defined as study of systems involving fluid flow, heat transfer and associated phenomena such as chemical reactions by means of computer simulation. CFD softwares serve as an easy to use interfaces where process parameters can be given (pre-processor), processed (solver), and the results can be analysed (post-processor). For example, for studying fluid flow in a chromatography column, a packed bed geometry can be created by giving column dimensions, resin particle specifications such as particle size, pore size, overall porosity, and particle geometry [78]. CFD of columns at different scales can be performed and the flow patterns can be related for consistency of flow to assess if the scale up is achieved as desired [79]. Even distributor designs can be compared for optimising flow patterns inside the column [80].

Advanced visualisation and modelling techniques if combined with mechanistic modelling tool, can give a complete picture of column hydrodynamics in terms of velocity and mass distribution. Recently, simulating a separation of lutein molecule in a preparative chromatography column using CFD was attempted by employing mass transfer equations such as EDM and IDM [81]. Though it is a good idea to combine the hydrodynamics and mass transfer models under a collaborative solver approach, the computational requirements are very high.

2.2.4 Statistical approaches

Numerous mass transfer models described earlier can simplify the way chromatography process is understood but it is often a case that the solution of these models becomes computationally intensive. Statistics can provide an easier approach towards modelling and simulation of chromatography with less intensive computational requirements. It can either serve as a stand alone model system which can predict simpler processes or can pave a way for better analysis of traditional mass transfer models. Major statistical approaches which have been widely used for modelling and simulation of chemical engineering operations are design of experiments (DoE) and artificial neural networks (ANN).

2.2.4.1 Design of Experiments (DoE)

DoE provides a combination of statistical techniques based on empirical models for a process under scrutiny. It describes a relation between input and output variables, and helps to assess and model the process in a more systematic way. This helps in faster scanning of the design space and reach to the optimum solution in terms of quality and yield, in least number of experiments and time. Input variables are generally called as 'decision variables' whereas the output variables are termed as 'response variables' or 'response functions'. Aim is to achieve the best possible output for a system by optimizing decision variables to create a model which can help predict the results. A detailed method of experimental design for chromatography is reviewed by Hibbert [82]. There are multiple decisions to be taken when DoE is to be used for LC process optimization. These include, screening of decision variables, choice of experimental statistical design, choice of experimental design space, response variables, and regression analysis techniques to be used. Screening of all possible variables is necessary to know what process parameters affect the process output significantly. For example; Designs such as factorial designs, Plackett-Burman, Box-behnken can be used a screening designs where preliminary DoE for screening of important variable is to be performed. More complex designs such as central composite design, D-optimal, and Dohlert designs can be used for generating the final surface in response surface methodology (RSM) to get an optimized design space. Details of statistical param-

eters involved, methodology, and different designs available for DoE-RSM have been described in detail in a review by Bezerra et al.[83]. An account of various screening designs for multivariate and multilevel analytical designs, and mixture designs along with respective data interpretation techniques is described in detail by Dejaegher and Heyden [84]. Designed set of experiments are then carried out in laboratories. Alternative to this is to make predictions in a validated simulation tool to construct the surface plots for responses. Furthermore, the surface model equation should be validated by carrying out experiments in the laboratories. It is also important to test the desirability of the design used by comparison with other competitive designs and optimality of the chosen design [85]. DoE may also be used for comparison with results produced from mechanistic models for further strengthening of the model validation process.

Numerous applications of DoE are seen in LC design and development. Response surface methodology is used effectively for designing LC process [86, 87, 88]. Multiobjective optimisation (MOO) is carried out for creating a statistical models for LC systems; however, most of the work is experimentally driven [89, 90, 91].

DoE definitely helps in narrowing down the experiments towards process optimisation; however, it is important to realise that those experiments are still to be performed for every step of the process. Mechanistic modelling can aid in reducing the efforts taken for DoE. If a validated tool is available, all the experiments in experimental designs can be performed in the tool and simulated response surface can be obtained. Validation experiments can be performed further to ensure the desirability model equation of the surface. Secondly, if the experimental designs can be compared through a tool, many designs can be compared within short span of time with ease for their optimality. The data being generated from simulations can be linked to statistical analysis or probabilistic methods and further analysed to give an optimal solution in no time[92]. Application of high throughput screening and simulations together can give a faster way of both experimental as well as mechanistic model based validation [93, 94].

2.2.4.2 Artificial neural networks (ANN)

ANN is a network of nodes and inter-nodes which are interconnected to each other defining their interrelations. The system is then trained by adjusting the interlinks to get close to the desired outputs or minimize the error. During training, transfer of signal happens to each neuron from the input neurons, its summed up at intermediate nodes, and passed further after applying a suitable mathematical function to it which is defined in the hidden layers. Once the training is performed, ANN serves as a good predictability tool even without physical and chemical characteristics of the system. ANN also provides a model system which can describe complex relationships between the variables which can be quite useful for LC process development. Role of ANN in pharmaceutical process and product development has been well described [95]. ANN is used for estimation of adsorption isotherm and mass transfer parameters for TDM and stoichiometric dispersion model (SDM) for protein chromatography application [96]. The predictability was further compared with mechanistic model predictions. The accuracy of estimated parameters was proved by decent agreement with simulation and experimental data from two salt gradient experiments. Havel et al. demonstrated that combination of ANN modelling with experimental design, experiments required for the optimal solution were reduced considerably proving ANNs ability of quick optimization [97]. As the major advantage of ANN is to handle large amount of data effectively, it has been used successfully for modelling of hyphenated techniques including chromatography and mass spectrometry [98]. It should be noted that the quality and accuracy of results from ANN depends on the quality of training data used. This data can be from retrospective experiments or fresh experiments. For DoE, definitive experimental design is formulated and experiments are carried out to build the model. Though comparison of ANN and DoE is not intended here, it is important to mention that the computation times for both ANN and RSM-DoE models are insignificant; however, accuracy of the model solutions may vary based on training data and experimental design respectively.

Major drawback of ANN is requirement of large amount of data for training purpose. Getting so much data can be possible for product running in the industry for years but generating the data for new molecules is cumbersome. Typical

approach for a chromatography process optimization can be carrying out simulation experiments on a validated tool in a multivariate experimental design space to generate data which can be used for training ANN systems with appropriate structure specific to the process in consideration. Once the ANN is calibrated for a system, it can simulate the experimental results in minimal time facilitating the on-line monitoring and troubleshooting. Even though, solving complex equations by using appropriate tool for predictions is making difference in processing, it is important to make such a complex information accessible in a simpler form.

2.3 Model based process development

Though mechanistic modelling using the mathematical models has been widely explored in last two decades, it is necessary to understand its implementation in process development. Major advantage of model simulations is reduction in the extensive experimentation required to get to the developed process. For process development at both small and preparative scales, main objectives are maximum possible loading and highest possible flow rates with desired resolution, quality, and yield for the target molecules. Traditionally, numerous experiments are performed to find the optimal conditions for achieving required quality product. Recently FDA approved QbD for manufacturing design which gives further flexibility to manufacturers without compromise on the quality requirements. Approaches like DoE and process analytical technology (PAT) allow the user to optimize the points in the design space at which the experiments can give desired results [99]. With the help of prediction tools available, it is now possible to assess the whole design space with more scrutiny. For having confidence in the tools, it should be made sure that the tools are well validated for the process systems under consideration.

2.3.1 Model validation

Tools discussed ensure accurate implementation of the model mathematically but it is also important to ensure that the simulated data matches well with the experimental data. This process is called as model validation. Model validation can be

carried out in two ways. Primarily, data from the literature can be chosen. Results obtained from simulations are then compared with the data from the literature to identify the error. If the error is high, it is attempted to tune the parameters in order to fit to the target data. This process is also called as model calibration. Care must be taken while choosing the literature data as it should be able to provide all the required parameters for the execution of simulations. It should also provide range of variations in the process parameters to ensure that the validation is robust enough to apply for future predictions. Another type of validation is experimental validation. In house experiments are performed for finding out model parameters [100]. Experiments which define different aspects of resin-protein interactions are planned in the design space to cover all possible process variations. Model parameters are determined by fitting the equations to the experimental data produced. For example, experiments such as batch studies can give model parameters such as Q_{max}, k_d for Langmuir isotherm or charge value (v), equilibrium dissociation constant (k_eq) for SMA. Column moment analysis with tracers such as blue dextran or acetone, can be used to determine diffusion and porosity values. Details of such experiment is given in literature which can be referred further [101, 102, 35]. Once the model parameters are determined, they can be used in the tools for simulation for a successful prediction. Further tuning of parameters might be required and should be performed based on process knowledge about how the parameters affect the curves to be predicted. Overview of model validation is shown in Figure 2.1

2.3.2 Optimisation

Process development is a challenging task due to complex interactions in between adsorption variables. These interactions play an important role in the output of the system and finding how input affects the output responses becomes important. For this, choice of responses and decision variables, and priority given to them is very important while defining the process development objective. Though it is hard to find generic rules for process optimisation, current approaches in the industries and academia are mostly influenced by QbD. QbD is a multi-objective optimisation based approach which is targeted to achieve predefined process ob-

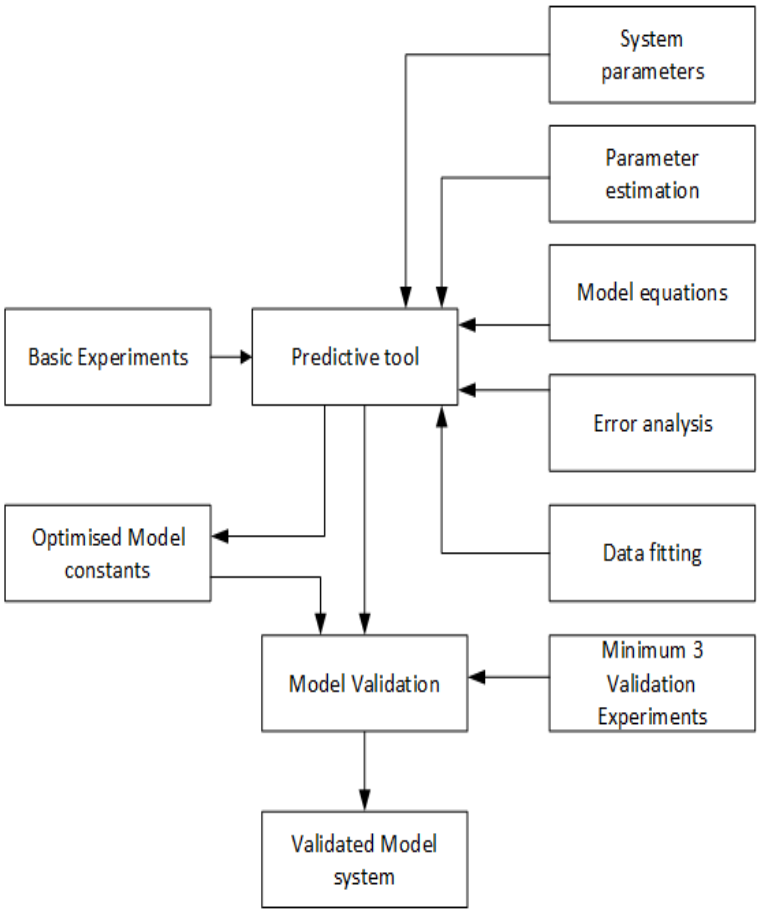

Figure 2.1: Generalised model calibration and validation philosophy

jectives by using basic knowledge of the process [103]. Tricky part in QbD is setting a measurable objective function which can describe the desired outcomes. A significant work by Rathore gives an outline of a road map of QbD for process development of a biotherapeutic products along with a detailed case study for purification of a biosimilar [104]. Principles described by Kanwar et al.[105] about enablers of QbD implementation for model based development of ion exchange membrane chromatography apply well for LC. There have been numerous other case studies on implementation of QbD for process development emphasising its importance in industries [106, 107]. Recently, QbD principles were implemented to the development of an analytical chromatography method aimed to the quality control of a vaccine product [108]. Furthermore, McBrien has discussed practical implications of QbD for chromatography processes [109].

Though QbD based thinking provides a full proof approach towards highly successful process, it requires a detailed understanding of the process mechanism. Even though QbD approaches along with DoE reduces overall experimentation re-

quired for optimisation, it is based on statistical guess work based on fundamental process knowledge [110]. It order to implement QbD based development, numerous experiments are to be performed which take time and efforts. On top of that if the CQAs are not defined with critical consideration, all the process has to be repeated which can be laborious. Degerman et al.[111] have demonstrated how optimisation can be carried out by amalgamating simulation and QbD approaches and choice of the model is a critical step in such a methodology. Comparison of DoE and mechanistic modelling is also done to prove mechanistic models can give better meaning to the system under process development [112]. This shows that a simulation tool can not only ease the way for faster QbD implementation but also can help in controlling it [113].

Before simulation studies can be applied to QbD, the model to be used has to undergo calibration. This includes testing the tool in a wider design space [114]. Simulations are beneficial in this regard, as lot of time and efforts can be saved. It is also advised to check the representative simulations by performing experiments for additional validation. In a study by Persson et al. [115], the dependency of flow rate and bead size on the film mass transfer and axial dispersion coefficient was checked for further calibration of the model for its implementation for simulations. Teoh et al. tested dynamic model of a high performance LC unit experimentally [116]. It was further used for optimisation of a preparative chromatographic separation by use of closed-loop recycling resulting in improved purity and yield of the process. This is an indicative of model calibration and simulations aiding in process improvement. For detailed understanding of the model optimization strategies, it is highly advised to refer to work by Guiochon [43].

2.3.3 Design space characterisation

Design space characterization is a logical selection of input process parameters and respective ranges which can make the process flexible for operation. It is very important to understand and thoroughly assess the relationships between the selected CPPs and responses so that significant CPPs can be picked up to register a manufacturing design space. According to U.S. FDA Q8 [117] regulatory guidelines, 'the process changes inside an authorized or registered design space

is not considered as a process change as it does not affect the quality of the product'. This gives more operational flexibility to the manufacturers. Scanning of design space can be performed by experimentation [118]; however, modelling and simulation can accelerate the process and make it more cost effective. This suggests that the overall aim of characterisation is to get to a design space which provides flexibility for CPPs to operate within wider range without compromising on the quality. While characterisation, it may happen that experiments may not be able to access few coordinates in the design space due to practical or financial constraints. These inaccessible design points can be examined by simulations. The only requirement here is a well validated simulation tool for the protein-adsorbent system which can give accurate predictions.

Simulations also help in repeating the experiments for number of times without further investments throughout the design space. However, the validity of the simulation tool needs to be further supported by the experimental proof. Experiments for validation must be chosen in order to cover the entire range of the CPPs. In fact such intensive simulation exercise can help in ranking process parameters in the order of their impact and sensitivity. Experiments from the design space for robust model validation can be planned considering the most sensitive variables. If the simulation tool is thoroughly validated for the accessible design space, it can be assumed that it makes accurate predictions for inaccessible part of the space. For seeking additional proof, experimentation on the maximum accessible boundaries or experiments immediately outside the design space to show failure cases may be carried out [119]. Degerman et al. used mathematical models to determine the impact of design space for purification of IgG from BSA by a hydrophobic interaction purification process [120]. Optimisation was performed for both cost and quality. Another optimization study was performed by Getaz et al. in order to optimize linear and bi-linear gradient for purification process of polypeptide crude mix [121]. Westerberg et al. carried out a design space based sensitivity analysis for hydrophobic interaction chromatography and reversed phase chromatography using mathematical models to optimise purity and optimal pooling criteria [122]. Shan and Shiedel implemented ANN for design space characterisation to investigate the effect of parameters for gradient chromatography on

the productivity of the target compound from a multicomponent mixture. Experimental design and ANN were used together to compare different modes for operation such as isocratic and different gradient slopes to identify the effect of parameters on the shape of the peaks obtained and respective purity [123]. Many more such implementations have been demonstrated in the literature [124, 124]

2.3.4 Scale up and design

Every process developed in the lab is destined to undergo scale up if it has to reach to manufacturing stage. A systematic experimental scale up for chromatography is well defined [125]; however, lot of experimentation is involved in doing so. Application of simulation tools for scale up can save a lot of efforts. In fact, intermediate scales can also be assessed for which infrastructure may not be available. Gerontas et al. [46] demonstrated successful implementation of modelling and simulation for scale up of two protein processes. They emphasised on the fact that understanding model parameters and their implementation is the key for a model based scale up. This can also help in design of columns of appropriate size based on the product requirements. Furthermore, advanced set-ups of chromatography such as; simulated moving bed [126, 127], liquid solid circulating fluidised bed [128], and expanded bed [129] can be designed based on understanding of a single column data.

Model based approach for LC design can provide additional benefits after the process is optimised. Optimization gives parameter values for which desired result can be obtained; however, it is important to find a wider design space which can sustain the desired output. Model based process design can help account for those variabilities and their effect which cannot be realised in experimentation [130]. This can further increase the knowledge about the process under development which may not happen with experimental approach [131]. For a successful implementation of the simulation approach, it is important to validate the tool for such innate changes and account the sensitivity for the same [132]. For a robust implementation of a modelling tool for uncertainty and sensitivity determination, it has to be validated exhaustively for range of variables, different scales of column, adsorbents, different chemistries of a technique such as; cation and an-

ion exchange for ion exchange chromatography etc. There are many such tools available currently which can combine one or more requirements of the model based process development. These are discussed further.

2.4 Chromatography simulation tools

It is seen that the bottlenecks in the process industries are currently being addressed to accelerate the time to market; however, industry continues to demand new technologies in downstream processing [133, 134]. This is an indicative of the fact that process development still remains a main problem to address to improve on time and investments. With advances in computer technology and improved understanding of chromatography process, many researchers have formulated potential simulation tools for chromatographic predictions. Brief summary of the tools is given below and details are shown in Table 2.1. It has been claimed by respective literatures referred here for each tool that they are accurate in predicting the experimental outcomes to the desired accuracy. In any way, it is not intended to compare them here for their capabilities as that requires code to code comparison. This thesis just intends to put forward a short summary of features of the codes and methodologies implemented in the current tools.

2.4.1 Chromatography Analysis and Design Tool (CADET)

CADET is an acronym for chromatography analysis and design tool which was formulated by 'ModSim' group at Forschungszentrum Jülich GmbH, Julich, Germany. The inventor list includes Eric Von Lieres, Joel Anderson, Sebastian Schnittert, Andreas Puttman, Samuel Leweke, and William Heymann (written as Lieres et al., in Table 2.1). CADET allows implementation of mass transfer models such as; GRM, POR, EDM, and TDM with isotherms such as; Linear, multi component Langmuir, MPM, SMA, SAS etc [135]. Finite volume method (FVM) is used for basic discretisation. To reduce the time required to solve the complex models, several scientific computing techniques such as; weighted essentially non-oscillatory (WENO), suite of nonlinear and differential/algebraic equation solvers (SUNDIALS), and parallel computing have been incorporated [15]. The solver can take up

variable step-width and order, for space and time integration, based on user defined mesh intervals. While the simulation engine is designed in C^{++} for the best possible performance, modelling framework is laid in MATLAB for easy customisation. An easy implementation of CADET can be accessed at (CADET web user interface) [136]. The interface is capable of solving both single component and multi component systems along with sensitivity and robustness optimisation. All the code of CADET is freely available to the research community as an open source on CADET github website. Here the codes can be downloaded and implemented in MATLAB or Python without recompiling the code and further modified to the desired use if required. This allows any researcher across the world to contribute with their own extension codes in order to enhance the framework of the tool. Latest release of CADET can solve systems of multiple unit operations such as simulated moving bed chromatography, stirred tanks, or plug flow systems. CADET is being used successfully for predicting chromatography process outcomes for almost 8 years internationally in 15 countries [137, 138]. Diedrich et al. [40] have presented application of CADET for ion exchange adsorption of monoclonal antibody on a tentacle resin with high accuracy using a multistate SMA model which is an extension of original SMA model [139] given by Brooks and Cramer. Complex peaks and shoulder were predicted under overloaded conditions and the consistency of the model was checked by comparing the simulated salt concentrations with experimental conductivity data. Freier at al. demonstrated use of CADET for elution chromatography predictions and its robust multi-objective optimisation [140]. Recently, Leweke and Lieres described latest updates in CADET with multiple case studies showcasing extensive capabilities of the tool [135].

2.4.2 ChromX

ChromX provides a customisable simulation tool, in which POR, TDM, EDM, GRM models can be solved with either Langmuir or SMA adsorption isotherms [141]. Built on finite element method (FEM), tool provides multiple time discretisation models.ChromX offers interfaces to various libraries for linking the simulations to heuristics. These include; Levenberg–Marquardt algorithm (LMA), Cminpack, and the genetic algorithm optimizer GAlib. ChromX also gives a sampling module

for recommended pooling criteria for *insilico* peak collection. ChromX has been widely used for laboratory and industrial research. It has been used for *insilico* process development of ion exchange chromatography [142, 143] and Hydrophobic interaction chromatography [144]. Hahn et al. used ChromX has for modelling of industrial level antibody purification [145]. They used TDM and SMA for prediction of profiles at industrial scales. Baumann et al. performed Pareto optimization for yield and purity by predicting ion exchange chromatography profiles in ChromX using TDM and SMA [146]. The simulations were also validated further by performing chosen experiments. Chromatographic separation using core shell metal organic frameworks were explored for prediction using multi component Langmuir and GRM where single component data was found out to give basic parameters which were further used to predict multi component isotherms [147]. ChromX was used to devise a new method to determine the ionic capacity in column and batch chromatography, based on the adsorption/desorption of the natural, uv-detectable amino acid Histidine [148].

2.4.3 Chromulator

Chromulator is built around GRM and provides various modules for solving different chromatography problems. It uses FEM and orthogonal collocation for discretisation of model equations. The bulk fluid phase PDEs are discretised by FEM, whereas particle phase equations are discretised by orthogonal collocation. This gives rise to a coupled ODE system which can be further solved easily using an ODE solver. As the complete code is implemented in Fortran 77, a Fortran based public domain VODE (variable coefficient ODE) solver was used for giving numerical solution. Chromulator provides several modules such as; Rate.exe, Kinetic.exe, Gradient.exe, Affinity.exe, and Raterfc.exe. For example; Raterfc.exe and Ratecored.exe are same as Rate.exe, except they are used for Radial Flow Chromatography (RFC) and superficially porous particles which are different class of resins [149]. Chromulator was the first tool to capture these kind of simulations. These modules provide various chromatographic simulations; however, additional operational simulations need editing the code which may not be possible for a researcher from non-coding background. This reduces the flexibility of Chromula-

tor as compared to CADET or ChromX. It is highly recommended to refer to a book on Chromulator which provides detailed guidelines for its implementation [150].

2.4.4 Aspen Chromatography

Aspen Chromatography is a highly customizable flow sheet simulator which is used to design and simulate batch and continuous chromatographic processes [151]. It is also used to optimize yield, product quality, capacity, and operating costs. Aspen is highly customisable over other simulation tools for its capability of linking to various unit operations so that series of operations can be optimized together. Aspen chromatography accommodates hydrodynamic models such as; TDM, EDM,GRM, and POR. Aspen provides a huge database to extract parameters specific to molecules being separated, which can help to configure model constants based on heuristic approach and can incorporate in-line model fitting and regression analysis with access to database of model constants [152]. Aspen chromatography is used widely for continuous chromatography operations like SMB [153]. Two zone and three zone SMB has been well explored by using Aspen chromatography tool [154, 155].

2.4.5 gProms

gProms is another highly customisable tool which can perform modelling and simulation of series of operations. One of the most attractive modules of gProms is a model-based engineering (MBE) module which can be used for process development of scale up and scale down operations with the help of process models. MBE relies on three main approaches:

- First principles modelling: Process models applied mainly describe in detail the heat transfer, mass transfer, and kinetics of the the process
- Multiscale modelling: Modelling can be done at various scales of the process. For example, in case of chromatography, single particle models can be used and extrapolated further to simulate flows in the column. Separate column flow models can also be applied to check the validity

- Integration with experiments: Data driven from experiments can be used to modify the model to increase the effectiveness of the experiments being carried out

MBE has obvious advantages over conventional engineering approaches as it can accelerate exploration of the design space. It also provides an effective interface for use of current R&D results into the model in order to improve further processing by reducing errors [156, 157]. MBE relies on a set of model-based experimentation methodologies for parameter estimation which can help refine the models being used [158]. gProms has optimization features ranging from single operation to a whole plant which can be used flexibly for modelling and simulation of series of chromatography operations [159]

It is discussed here that so many efficient tools are present for modelling various aspects of LC. Few of them describe the way they are designed and source codes are shared in an open source platform, while others are marketed software for industrial and academic use. In academia, effort is made to understand how these tools operate on the mathematical level; however, in industries, they might be used as a black box for process design. Understanding these tools provides a better way to design a process. In addition to this, it also helps in troubleshooting the process with much ease and confidence.

These tools also demonstrate the fact that a successful simulation tool which can mimic the experimental systems, needs to undergo number of steps such as; (i) Mathematical verification of the tool for desired precision and accuracy, (ii) Exhaustive experimental validation to showcase tha accuracy of simulations is maintained for wide range of input parameters (iii) Demonstrating that the tool is robust and shows sensitivity of the process towards process parameters. For IEX LC, most important parameters from experimental perspective are;

- Properties of protein such as; molecular weight, isoelectric point, amino acid content which decides the structure, hydrophobicity, and ionicity.
- Process flow properties such as flow rate, protein concentration, total protein in the feed.
- Thermodynamic properties such as ionic content of the mobile phase, resin

Table 2.1: Comparison of current available tools for simulation of chromatographic operations

Criteria Aspen Chromatography	CADET	ChromX	Chromulator	Aspen Chromatography
Inventor	Lieres et al., IBG-1, Germany	Dr. Tabias Hahn, Karlsruhe Institute of Technology, Germany	Prof. Tinguye Gu,Ohio University,Ohio, USA	Aspentech
Hydrodynamic models	GRM	GRM, TDM, POR, Edm	GRM	GRM,TDM,POR,EDM
Thermodynamic models	Langmuir, SMA, MPM, SAS	Langmur, SMA,single and multicomponent	Langmuir, first order	Langmuir & Freundlich variants
Discretisation scheme	Finite volume method	finite element method and method of lines	Finite element method	-
Additional Mathematical solvers	WENO, SUNDIALS, offers additional solvers like Schur solver	Explicit Euler, Implicit Euler, Crank Nicolson	DVODE, Orthogonal collocation	-
Coding platform	Simulation codes: C^{++}, MATLAB Interface:Django based interface with connection to PostgreSQL database	Simulation codes: C^{++}	Simulation codes: Fortran 77 Interface: C^{++}	-
Interface	1. Web interface available for everyone for free 2. MATLAB interface and standard routines for parameter estimation, process optimization and experimental design	Available in executable software format	Available in executable software format	Available in executable software format
Processing modules	1. Interface allows simulation a single chromatography column with multiple steps and components 2. DoE simulation allows to run a simulation by changing a parameter based on earlier completed simulation 3. loading and elution analysis with flexible flow an time settings	1. sampling module for collection of the peak 2. Highly customisable flow parameters 3. Provides control on dimensions, flow rates, buffer concentrations, sample injection 4. ChromX supports direct simulation in [mAU] instead of molar or mass concentrations. 5.Latin hypercube sampling can be used to evaluate the robustness of the process and relate them to CQAs for process optimisation	1. Rate.exe: for Langmuir along with GRM. Useful for setting elution with step changes. 2. Kinetic.exe: Uses second order kinetics instead of langmuir 3. Gradient.exe: gradient elution in various modes of step, linear and non linear regime 4. Affinity.exe: specially for affinity chromatography 5. Raterfc.exe: For radial flow chromatography	1. Provides tools for fast construction and configuration of SMB and TMB 2.Flexibility in defining flow rates of process streams, time cycles, step or ramped inputs 3. Regression analysis by fitting of model data to experimental data
Compatibility and Add-ons	Export to Microsoft Excel in both xlsx and csv file format	Export to Microsoft Excel, VTK format further to ParaView for 3D visualisation		Highly integrated tool compatible with various other softwares like excel, MATLAB where analysis and visualization can be done
Special mentions	1. Allows sensitivity analysis for all the parameters involved 2. Allows to share simulation online with other user	DoE, interface to libraries such as LMA, Cminpack and Galib	provides several methods of visualizing the solution such as position-time plots, effluent histories and several animations.	1. Can be linked to number of different unit operations for overall process design and simulation 2. Database can provide thermodynamic parameters to select from for various molecules
Availability	Web interface available for free to all	ChromX academic is available free of cost whereas ChromX industrial version is a licensed software	Chromulator is available free of cost for academics whereas Chromulator-IEX is given on license to industries.	Marketed software
Tie-ups	AMGEN, GlaxoSmithKline, Fraunhofer IME, KBI Biopharma, BOKU	Academic version of ChromX is meanwhile used in more than 15 countries.	Licensed by 3M, Pfizer, Genentech, Novo Nordisk, Milipore	It is being used by many research institutes and companies for whole process development
References	[15, 136, 138, 140, 40, 137]	[142, 143, 144, 145, 148]	[160, 161, 149]	[153, 154, 155, 152]

ligand density, mode of ion exchange (cation or anion)

This makes the choice of validation system very critical. Next section describes the experimental system selected in this work.

2.5 Experimental system

2.5.1 Whey proteins

Use of chromatography in biopharmaceuticals is prevalent. In recent times, even food industries, have adopted chromatography for analysis and purification of high value enzymes and proteins of therapeutic importance [162, 163]. A review from Tranchida et al. emphasises on the importance of chromatography in food analysis [164]. Another review from Mane et al. showcases importance of chromatography in purification of anti-diabetic protein γ conglutin from agricultural sources such as Lupin [165]. Latest techniques such as simulated moving bed chromatography have also been implemented in food processing industries [166]. Dairy industry is one of the largest food sectors, widely spread out in every corner of the world. Cheese is one of the major products of dairy industries, which is manufactured on large scale. Huge amount of waste generated during cheese and casein manufacturing is called as whey which is a potential source of significant milk proteins [167]. Whey proteins are marketed in the form of whey protein concentrates (WPC) such as; WPC 35 (35$\%$ protein), WPC 80 (80$\%$ protein), and WPI (isolates: 90-95$\%$ protein). Detailed literature on recovery of protein concentrates from whey has been discussed in detail in a recent review with emphasis on ultrafiltration [168]. WPC has multiple proteins with different characteristics. These include; α-Lactalbumin (ALA) , β-Lactoglobulin , Bovine serum albumin (BSA) , Lactoferrin [169], and Lactoperoxidase [170]. Out of these, first three are major proteins and latter are present in minor quantities. It is important to understand the protein properties before they can be used for experimental studies. For separation of individual whey proteins, most common technique is ion exchange chro-

matography [171, 172, 173, 174]. Individual proteins are discussed in brief here and are summarised in Table along with the literature references 2.2.

β-Lactoglobulin (BLG)

BLG is a major protein from whey which is almost 60% by weight of total whey proteins. It has 162 amino acids all present in one peptide chain. BLG is known to exist in different molecular forms depending on the pH and ionic strength of the medium [175]. As the isoelectric point(*pI*) of BLG is 5.2, the protein is highly hydrophobic at its *pI*. A stable dimer is found for pH between 7 and 5 and below that the protein exists as an octamer upto pH 3.5. Two disulfide bonds and a thiol group exhibits increased reactivity above pH 7 leading to monomer formation [176]. Such structural changes in the molecule may influence the binding of the protein to charged matrices during chromatography. Purification of BLG from whey is attempted.

α-Lactalbumin (ALA)

ALA is a major protein roughly 20% of the total whey proteins. It is a globular protein with 123 amino acids with molecular weight of 14.1 kDA and a *pI* of 4.2. It has high affinity for calcium is mostly stabilised by four disulphide bonds [177]. It is tricky to detect ALA by spectral techniques as the conformation of the protein changes drastically with slight changes in pH and ionic strength of the buffering medium making it difficult to monitor the absorbance [178].

Bovine serum albumin (BSA)

BSA is approximately 10-15% of the total whey proteins. It has 582 amino acids with a molecular weight of 66 kDA and *pI* of 4.7. The structure of BSA is stabilised by a highly hydrophobic core with 70% α helices and 17 disulphide bonds [179]. It is proved that, buffer pH and ionic strength can have a major impact on BSA due to its highly hydrophobic centre [180].

Lactoferrin (LF)

Lactoferrin belong to minor proteins from whey which is present about 1-2% of total whey proteins. It has ≈700 amino acids with a molecular weight of 76-80 kDA and a *pI* of 8.2. It has a Fe^{+2} binding domain a the centre which gives the protein positive charge naturally which can be used to isolate it on cation exchange resins [169], whereas the intensity of the charge can be optimised by changing pH and ionic strength of the solution.

Lactoperoxidase (LP)

LP is a minor protein which is present in 0.5-1% of the total whey proteins. It is 612 amino acid long protein with molecular weight of 78 kDA. There are five helices in LP which gives a strero chemistry in the shape of a heme binding centre which has one iron molecule per LP [170]. LP has highly active hydrophobic centre which can interfere in the ionic binding of the protein to an adsorbent [181].

2.5.2 Model calibration system

Following are the reasons why whey proteins are used as an experimental system to aid in understanding the model calibration approaches for experimental validation of a simulation tool.

1. The system should be well explored in the literature as the objective here is to validate the tool. Basic properties and the standard samples of the proteins under consideration should be available so that they can be used easily to find the model parameters when required.

2. The experimental system should provide a complex protein mixture offering wide variety of proteins, whey protein mixture offers 5 different proteins of wide range of properties which can be used separately and in a mixture for validation.

3. It should be possible to explore both cation and anion exchange chromatography for separation of individual proteins from the mixture. Major proteins from whey are acidic in nature and minor proteins are basic in nature

making it possible to explore both ion exchange mechanisms at the same operating pH at which sweet whey is industrial obtained from the industry.

4. Industrial significance: High value products such as pure individual proteins can improve process economy for dairy industry.

Table 2.2: Comparison of properties of whey proteins used here as an experimental validation system

Protein	% in Whey	MW (kDa)	pI	Nature	Function	Structure	Purification and simulation references
β lactoglobulin	60	18.3	5.25-5.39	Acidic	Transfer of passive immunity,	Globular, 162 amino acids, tendency of aggregation with change in pH	[182, 183, 184, 100, 185, 186]
α Lactalbumin	20	14.1	4.2-4.5	Acidic	Cancer prevention, lactose synthesis	Globular, 123 amino acids, natural calcium binding domain	[187, 188, 1, 189, 190, 191, 192]
BSA	5 to 6	66.26	4.7	Acidic	Anti mutagenic, source of essenital amino acids, gelation at acidic pH	Globular, 582 amino acids, 17 intermolecular disulphidebridges	[3, 193, 194, 195, 196]
Lactoferrin	1-1.5	76.5-80	8-8.5	Basic	Antimicrobial, antiviral, and antifungal responses, shows immunomodilatory activities, influences cell growth and differentiation	Globular, 692 amino acids, Fe+2 binding site	[197, 198, 199, 200, 201]
Lactoperoxidase	0.5-0.7	78.4	9.5	Basic	Protective factor against infectious microbes	Globular, 612 amino acids, contains one iron molecule per LP	[202, 203, 204, 205, 206]

2.6 Significance of this research

It is clear from the preceding discussion that modelling and simulation can aid in process development for research and industries. However, there are number of challenges in the implementation of mechanistic models for simulation and it is important to understand the gaps between the present status and the futuristic process development approach.

Two important pillars of simulation driven process development are a simulation tool and experiments assisting in successful simulations. The current state of chromatography tools provide fast and accurate mathematical solvers. The codes are well developed for the available models. In order to implement such tools with more confidence, it is important to understand the model calibration and experimental validation philosophy in more details. Every model parameter has a physical/chemical significance which needs to be understood. Few parameters highly affect the predictions while rest don't have significant impact. Once it is understood which parameters are critical for the process and what kind of physical or chemical changes they cause, it can help in relating establishing a link between process and simulations. Also, it is imperative that model results are dependent on the accuracy of model constants. Model constants can be determined from number of experiments; however, further tuning of model constants is often required to adequately simulate the experimental data.

Secondly, there are several theoretical models available to simulate a chromatographic process. These models are based on process assumptions and a priori choice of an appropriate model is often challenging for a given chromatographic process. System specific physical and chemical interactions are described by mass transfer and thermodynamic models respectively and it should be made sure that the model system selected is appropriate for the application under development. Also, lack of robust database for thermodynamics constants results in increased uncertainty for application of the model, making the validation challenging.

To correlate the experiments and simulations, Chapter 4 and 5 attempt to show model calibration and validation methodologies based on exhaustive experiments on major and minor whey protein standards for the model validation.

These learnings can help in refining the simulation approach on real systems. Chapter 6 describes how learnings from experimental validation were applied for crude whey protein concentrate. Figure 2.2 describes the overview of the thesis in a nutshell. In the current process development paradigm, focus is on using simulations for efficient reduction of the experiments incurred during development, scale up, and operations. Fundamental understanding of chromatography system parameters for exhaustive experimental validation of the simulation tool is a prime step in a simulation tool calibration and validation.

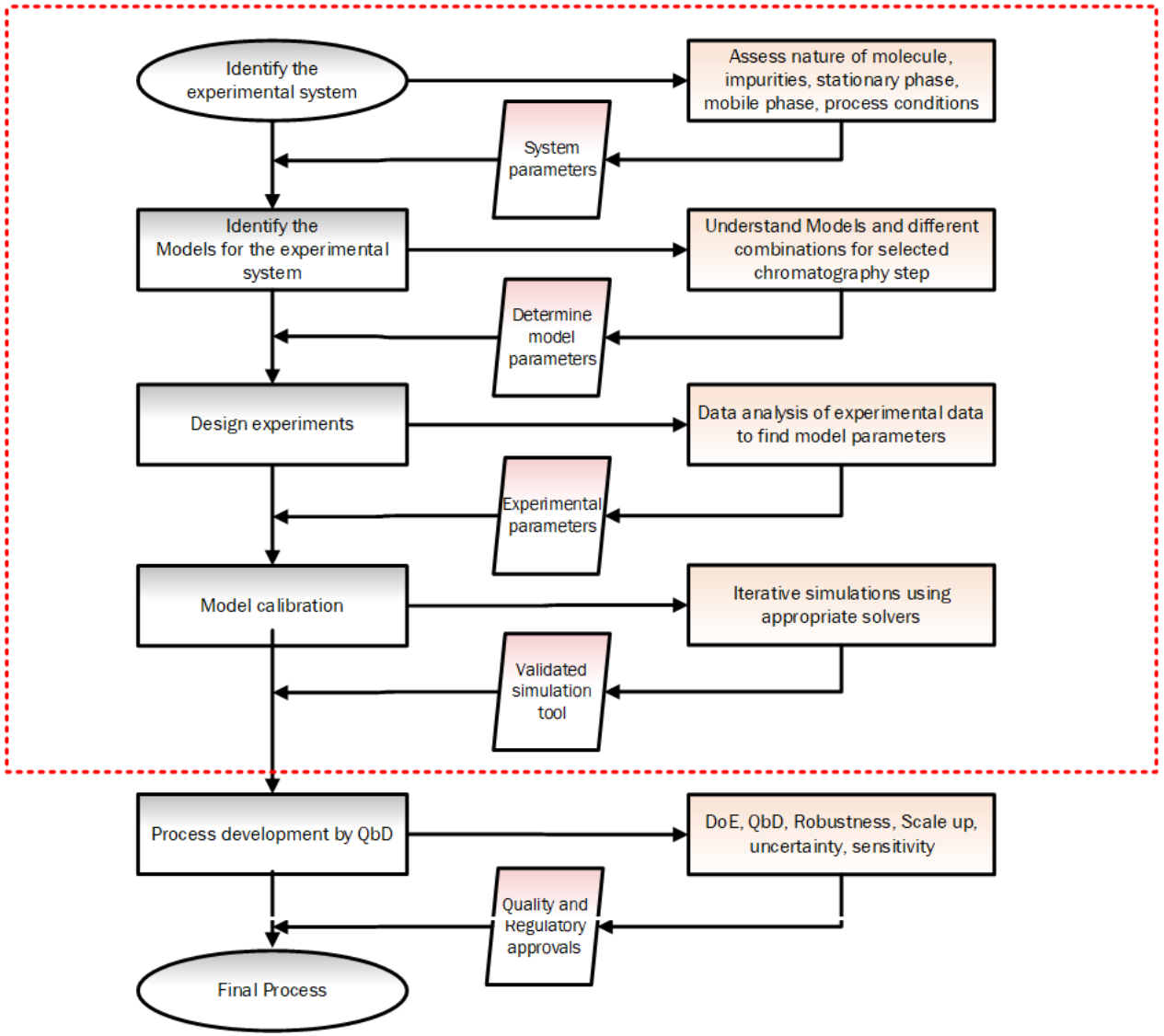

Figure 2.2: Overview of the thesis. Red dotted box signifies the role of the thesis in a broader picture

Chapter 3

Materials and Methodology

3.1 Introduction

It has been emphasised earlier that modelling and simulation can aid to accelerate process development of liquid chromatography processes. Numerous models have been proposed which can help predict the outcomes of the experiments, hence it is beneficial to compile these models in a tool which be helpful for better understanding and application. This chapter discusses a new tool; Extensible Process Simulator for Ion exchange Chromatography (*ExProSim:IC*), which can be efficiently used for predicting outcomes of chromatographic experiments. In the following sections firstly computational philosophy is described along with mathematical models involved in the tool. Outline of the tool is given. Experimental methods required for parameter estimation and validation experiments for whey proteins are discussed in the subsequent sections. The chapter closes with tool verification and literature based validation for *ExProSim:IC*.

3.2 Computational basis

Simulation of chromatography has matured significantly in last three decades and several models are available to predict possible outcomes [207]. Depending on the underlying assumptions, these models range from the simplest ideal model to most comprehensive GRM, and offer varying degree of accuracy [68, 208]. Assumptions which we have made are as follows;

1. **Column is radially homogeneous**

   Radial heterogeneity is highly dependent on the size of the column and it has been proved experimentally that columns up to 80 cm diameter can be as homogeneous as the analytical scale columns present in the market [68]. This requires input profile of the load and mobile phase to be evenely distributed across the column area [209]. With developments in design of distributor plates, homogeneity can be easily achieved [210].

2. **Mobile phase velocity remains constant throughout the column**

   It is rarely seen at preparative scale that the column is being operated at more than 200 bar. From 0-200 bar, the compressibility of the mobile phase can be neglected [211]. Thus according to the Darcy's law, the mobile phase velocity can be considered as constant as it is a function of pressure gradient which remains constant throughout the column during the operation [212, 213]

3. **Dispersion coefficient remains constant throughout the column**

   It is proven that the change in dispersion coefficient in mobile phase for the solutes with respect to pressure is insignificant at lower concentrations, however at higher concentrations this effect can be significant [214]. This effect might be further enhanced in case of micro-porous resins, where high pressure drops are observed with increase in the flow rates [215]. Macroporous resins offer lower pressure drops at higher flow rates, lowering the variation in dispersion coefficient even at higher concentrations. It is important to note that the value of dispersion coefficient is not negligible but the variation can be considered negligible [216].

4. **Mobile phase is not adsorbed**

   Though it is hard to check the mass balance for the mobile phase, it can be assumed that losses of the mobile phase in th column are negligible [217]. This can be said as systems are in place which deliver the flow consistently and there is no change in the viscosity and density of the mobile phase at isothermal and adiabetic conditions at which the columns are operated.

5. **The column is operated under constant conditions of pressure and temperature**

   This ensures least variability in the thermodynamics of the adsorption-desorption process

Though with advances in computers and mathematical algorithms, it has got easier to solve complex models such as GRM, it is challenging to find the input parameters for the same by doing experiments. Models like EDM where, diffusion consideration are relaxed can be handy for predictions as experimental procedures can be used to find lumped parameters to be used in the model equations [216]. Hence, it was decided to start with EDM. On the other hand thermodynamic models such as Langmuir, Freundlich, SMA, and MPM are well established to predict the nature of interactions between proteins and adsorbent. *ExProSim:IC*, a tool formulated here incorporates a mathematical solver for EDM along with the thermodynamic models. Details of these models are given in sections 3.2.1 and 3.2.2. Mathematical models incorporated in the tool are discussed in the next section.

3.2.1 Mass transfer models

Numerous models have been proposed for chromatography simulations depending on the diffusion considerations. GRM considers all the possible diffusion phenomena like pore diffusion, film diffusion, and surface diffusion within the packed bed[218]. For fast processes, the GRM can be significantly simplified by preferential selection of extent of slow diffusion processes. EDM used here, is a simple modification of GRM[219]. In this model, diffusion is represented by a lumped coefficient termed as axial dispersion coefficient (D_{ax})[68]. Pore and surface diffusion are neglected to assume faster mass transfer resulting in lumped coefficient[220]. The mathematical form of EDM is represented by Equation 3.1,

$$\epsilon_e \frac{\partial c_i}{\partial t} + (1 - \epsilon_e) \frac{\partial q_i}{\partial t} + u \frac{\partial c_i}{\partial x} = \epsilon_e D_{ax,i} \frac{\partial^2 c_i}{\partial^2 x} \tag{3.1}$$

Initial conditions along with Danckwerts and Neumann boundary conditions were used further for solving model equations [221].

Initial conditions:

$$c_i(t=0) = c_{i,0} \quad \text{for} \quad x = 0 \tag{3.2}$$

$$q_i(t=0) = 0 \quad \text{for} \quad 0 \leq x \leq L \tag{3.3}$$

Boundary conditions:

$$c_i(x=0,t) = c_{i,inj} \quad \text{for} \quad 0 \leq t \leq t_p \tag{3.4}$$

$$q_i(x=0,t) = 0 \quad \text{for} \quad 0 \leq t \leq t_p \tag{3.5}$$

$$\frac{\partial c_i}{\partial t}(x=L,t) = 0 \quad \text{for} \quad 0 \leq t \leq t_p \tag{3.6}$$

$$\frac{\partial q_i}{\partial t}(x=L,t) = 0 \quad \text{for} \quad 0 \leq t \leq t_p \tag{3.7}$$

3.2.2 Thermodynamic models

3.2.2.1 Langmuir model

The Langmuir isotherm takes into consideration consistency of sites where there are fixed number of adsorption sites having equal energy. This suggests minimal interactions between adjacent binding sites on a resin and only one molecule is adsorbed per adsorption site. Equation 3.8 shows a single component generalised Langmuir model equation. Dissociation constant, k_d is defined as the ratio of desorption coefficient (k^l_{des}) to the adsorption coefficient (k^l_{ads}). Equation 3.9 shows a kinetic form of Langmuir isotherm for multicomponent mixtures.

$$q = \frac{Q_{max} c_{eq}}{k_d + c_{eq}} \tag{3.8}$$

$$\frac{\partial q_i}{\partial t} = k^l_{ads,i} c_i Q_{max,i} \left(1 - \sum_{j=1}^{N_{comp}} \frac{q_j}{Q_{max,j}}\right) - k^l_{des,i} q_i \tag{3.9}$$

As the equation describes the competitive behaviour of the protein molecules, it has been widely applied for prediction purposes. However, Langmuir isotherm is a single layer isotherm which may not be able to describe behaviour for all the proteins. Adsorption is an effect of exchange of salt ions to protein molecules, which is not separately defined in the isotherm equation. This means that, salt interactions are considered in the lumped form of experimental constants. Considering this, it may be tricky to implement Langmuir isotherm for different salt concentrations based on experiments performed at single salt conditions. In case of gradient elution, where salt concentration changes with time, model constants determined from constant salt concentration experiments, may not aid in right predictions. It further neglects steric effects due to size of the protein and interaction of the protein with the adjacent binding sites which might hinder overall binding.

3.2.2.2 Freundlich isotherm

Freundlich isotherm was proposed to describe non-ideal systems with reversible adsorption. It is applicable to adsorption on heterogeneous surfaces and accounts for multilayer nature of the kinetics. Equation for Freundlich isotherm is as given by 3.10.

$$q_e = Q_f c_{eq}^{1/n} \tag{3.10}$$

It suggests that the stronger binding sites are occupied first followed by weak linkages and multilayer linkages. As the mass of the adsorbed concentration increases, the energy is exponentially decreased for each adsorbed interactions leading to saturation. Q_f is a coefficient of partition and '1/n' is an exponent of non-linearity. '1/n' also decides the curvature of the adsorption isotherm across the protein concentrations range. Value of '1/n' =1 signifies that the relative adsorption was same across the concentration range. Typical value of '1/n'ranges between 0.7-1 which indicates saturation of binding sites with increase in concentration of the protein under investigation. It has been observed that, at higher concentrations the value of n is large reducing the value of $1/n$ to zero. In these conditions adsorption becomes random and independent of the protein concentration. Therefore, Freundlich isotherm is not advisable at high protein concen-

trations for both experiments or simulations.

3.2.2.3 Steric mass action model (SMA)

SMA overcomes drawbacks of the Langmuir isotherm. It considers salt interactions during ion exchange of proteins onto resin. For electrostatic interactions during adsorption, the exchange between salt and protein molecules can be shown as Equation 3.11.

$$c_i + vq_0 \longleftrightarrow q_i + vc_0 \tag{3.11}$$

Where, charge factor v is a stoichiometric exchange coefficient for salt and proteins. Further, the equilibrium constant can be defined as Equation 3.12;

$$k_{eq,i} = \left(\frac{q_i}{c_i}\right)\left(\frac{c_0}{q_0}\right)^{v_i} \tag{3.12}$$

The total concentrations of the sites in the resin is given by 3.13.

$$\Lambda = \bar{q}_0 + \sum_{i=1}^{N_{comp}} (v_i + \sigma_i)q_i \tag{3.13}$$

Furthermore, from the electroneutrality on the stationary phase, q_0 and dq_0/dt can be calculated as Equation 3.14 and 3.15 respectively.

$$q_0 = \bar{q}_0 + \sum_{i=1}^{N_{comp}} \sigma_i q_i \tag{3.14}$$

$$\frac{dq_0}{dt} = -\sum_{i=1}^{N_{comp}} \sigma_i \frac{dq_i}{dt} \tag{3.15}$$

Where, $\bar{q}_0$ is salt ions available for exchange, q_0 is total salt ions on stationary phase, c_0 is total salt ions in the mobile phase, Λ is the ionic capacity (total binding sites on the resin), and σ is steric hindrance factor [139, 222]. From these, equation for $\frac{dq}{dt}$ by SMA model is given by Equation 3.16.

$$a\frac{\partial q_i}{\partial t} = k^s_{ads,i} c_i \bar{q}_0^{v_i} - k^s_{des,i} c_0^{v_i} q_i \tag{3.16}$$

Where, a is a quasi-stationarity indicator. a =0 signifies the rapid equilibrium model and a=1 signifies the kinetic model. Equilibrium constant $k_{eq} = k^s_{des,i}/k^s_{ads,i}$ is a measure of the affinity of the macro-molecule towards the resin surface [223]. For a rapid equilibrium model (represented by 'a=0'), only the value of k_{eq} is relevant and not the individual rate constants, whereas kinetic model (represented by 'a=1') is sensitive to both the rate constants. Value of 'a' also decides if the problem is to be solved as algebraic equations ('a=0') or as differential equations (a=1'). In this case, value of a was set to 1 to follow kinetic regime. Equilibrium formulation of SMA is given by Equation 3.17 and was used further for fitting the isotherm with experimental data,

$$c_i = \left(\frac{q_i}{k_{eq,i}}\right)\left(\frac{c_s}{\Lambda - (v_i + \sigma_i)c_i}\right)^{v_i} \tag{3.17}$$

Multicomponent form of SMA model is represented by Equation 3.18.

$$\frac{\partial q_i}{\partial t} = k^s_{ads,i}c_i(\Lambda - \sum_{j=1}^{N_{comp}}(\sigma_i + v_i)q_j)^{v_i} - k^s_{des,i}q_i c_0^{v_i} \tag{3.18}$$

3.2.2.4 Mobile phase modulator Langmuir model (MPM)

Adsorption and desorption of a protein are regarded as competitive processes where inclusion of salt shows its effect on the retention of the protein. Salt (S) is considered inert in MPM isotherm. This means that $\frac{dq_{salt}}{dt}$ can be considered as zero. Adsorption and desorption kinetics were represented by two separate kinetic coefficients $k^m_{ads,i}$ and $k^m_{des,i}$ respectively as in case of Langmuir isotherm as shown in Equation 3.19.

$$\frac{dq}{dt} = k^m_{ads,i}c_i(Q_{max.i} - q_i) - k^m_{des,i}q_i \tag{3.19}$$

The constants were further modified to include effect of hydrophobicity and salt interactions as shown in Equations 3.20 and 3.21. During the binding step, $k_{ads0,i}$, the adsorption coefficient of component i $(m^3/mol/s)$, is much larger than $k_{des0,i}$, the desorption coefficient of component i $(1/s)$, while at elution $k_{des0,i}$ dominates.

$$k^m_{ads,i} = k_{ads0,i} e^{\gamma_i S} \tag{3.20}$$

$$k^m_{des,i} = k_{des0,i} S^{\beta_i} \tag{3.21}$$

Main advantage of the MPM model is that it can be applied for both loading and elution steps as given in Equations 3.20 and 3.21. 'S' denotes salt concentration of elution component and $k_{ads0,i}$ (ml/mg.min) and $k_{des0,i}$(ml/mg.min) are constants. β_i is a constant describing the ion exchange characteristic and γ_i (ml/mg) describes the hydrophobic interactions. Under loading conditions adsorption dominates and during elution, desorption dominates. For loading conditions, S is given by the buffer salt concentration only, i.e. $k^m_{ads,i}$= $k_{ads0,i}$ and $k_{des0,i}$= 0 unlike the elution conditions ($S > 0$), where $k^m_{ads,i}$ is reduced by the factor $e^{\gamma S}$ and $k^m_{des,i}$ is increased by a factor S^{β}_i. In case of ion exchange chromatography, the value of γ can be assumed to be negligible, however in this work γ was determined by inverse fitting and is considered to see if it affects the predictions. Overall computational methodology is shown in Fig. 3.2.

3.3 Experimental methodology

Once the tool is developed and data analysis methods are decided, it is important to validate the computational methodology for ensuring its applicability. For the practical validation of *ExProSim:IC*, experiments were planned which can serve as a robust system for assuring its usability. Whey protein mixture was chosen for this purpose as it gives a wide array of protein molecules varying in their electrokinetic properties, molecular weights, and structural conformations (Section 2.5). It is also important to note that along with the validation purpose, separation of individual whey proteins from industrial whey protein concentrate was targeted further. Before validating for crude sample, it was easier to handle the standard protein solutions in order to find out the model constants to be used for prediction. Following Sections will discuss the details of materials, experimental setups, general methodologies, and sample analysis which were involved in the work. As the primary aim was to find the model constants for simulation purpose, the

methods have been categorised based on their applicability for models in consideration.

3.3.1 Materials

Protein standards for Bovine Serum Albumin (BSA), α-lactalbumin (ALA), and β-lactoglobulin (BLG) were purchased from Sigma-Aldrich Pty. Ltd. Sydney, Australia. Standards for LF, LP, and WPC were received from Tatua Co-operative Dairy Company Ltd., Morrinsville, New Zealand. Blue dextran for porosity studies was procured from Bio-rad laboratories, New South Wales, Australia. Acetic acid (CH_3COOH), sodium acetate (CH_3COONa), mono-sodium phosphate (NaH_2PO_4), di-sodium phosphate (Na_2HPO_4), sodium nitrate ($NaNO_3$), sodium hydroxide (NaOH), sodium chloride (NaCl), acetone (CH_3CHO), acetonitrile HPLC grade (CH_3CN), trifluoro acetic acid/TFA ($C_2HF_3O_2$), and ethanol (C_2H_5OH) were purchased from Sigma Aldrich, Pty. Ltd. Sydney, Australia.

Resin SP sepharose FastFlow (SPFF^{TM}), Capto Q^{TM}, and Capto S^{TM} resin in both free form and in the form of prepacked columns of HiTrap (2.5×0.7 cm) were bought from GE Healthcare, Sweden. XK-16/20 from GE Healthcare was used as a column for higher scale processing. Column for size exclusion chromatography, BIO-SEC 3 (30×0.45 cm) was purchased from Agilent technologies, Victoria. These columns, packed with 3 μ silica particles are coated with hydrophilic layer with pore size of 100 A^0 are ideal for high pressure size based separation of proteins ranging within 0.1-100 kDa. High performance liquid chromatography (HPLC) column zorbax 300SB (4.5 $\times$300 mm), with 5μm particle size was purchased from Agilent technologies, Victoria. Larger pore size of the column is advantageous for separating proteins and peptides above 4000 Daltons with a good resolution. Column chromatography experiments were performed on NGC Bio-Rad system. HPLC experiments for SEC was performed on Varian ProStar system, whereas, HPLC for analytical resolution of proteins was performed on Agilent 1260LC system. Details of the methodologies have been explained in Section 3.3.2.

3.3.2 Sample analysis

3.3.2.1 Spectrophotometric analysis

Spectrophotometry can be used for chemicals and bio-molecules which show absorbance or transmittance of the intense light beam passing through the solution. The wavelengths at which the maximum absorbance is obtained is a property of the molecule and its constituents. Protein molecules are shown to show maximum absorbance at UV 280 nm due to presence of aromatic amino acids. It is imperative to understand that the absorbance shown by a specific protein is a property of its amino acid sequence and structural conformation. It has been stated by Beer-Lambert law that there is a linear relationship between the absorbance and the concentration of a sample, however this is valid only at lower concentration corresponding to absorbance less than 1 absorbance unit. Beer-Lambert law can be stated as Equation 3.22.

$$A = A_0 \times l \times c \tag{3.22}$$

UV-vis spectrophotometer Jasco V-670 was used for analysis of protein samples generated during batch studies. Path length chosen was 1 cm and the absorbance was measured using quartz cuvettes.

3.3.2.2 Elemental analysis

Elemental analysis was performed to find out total protein based on carbon, hydrogen, and nitrogen content of the sample. It is often the most crude methods of protein analysis as it gives the total protein and not concentrations of specific proteins as HPLC does. Sample kept for analysis undergoes combustion and elements in the sample get oxidised into their gaseous forms. Carbon is converted to carbon dioxide, hydrogen to water, nitrogen to nitrogen gas/ oxides of nitrogen, and sulphur to sulphur dioxide. For a protein sample, as the peptide bond is made of $CONH$ linkage, $\%$ nitrogen is considered for further calculations. For a class of protein, multipliers have been defined to convert total nitrogen content into protein content. For whey proteins, multiplier used is 6.25. This is based on the assumption that total protein content in food is 16% and all the nitrogen in wpc is protein bound [224].

3.3.2.3 SDS-PAGE analysis

Sodium dodecyl sulphate-polyacrylamide gel electrophoresis was performed to separate proteins based on their molecular weights. The techniques was used as a qualitative tool to check if the protein standards are in their usual state or not. The bands misplaced from the expected place, suggest that the sample is either degraded or has formed aggregates [225]. Mini-Protean TGX 12% acrylamide gels (Bio-Rad Laboratories, New South Wales, Australia) were used for loading protein samples on fixed amount basis and further run in Mini-PROTEAN Tetra Cell System (Bio-Rad Laboratories, New South Wales, Australia) for conducting the electrophoresis at a voltage of 150 mV. Staining was carried out by silver staining [226] method to visualise presence and removal of impurities in the successive process step samples.

3.3.2.4 SEC-HPLC

Size exclusion chromatography (SEC) of molecules is mainly based on their molecular weights (size) and particle size of the resin used for the permeation. SE-HPLC provides a better solution for analytical purpose as it provides size exclusion and better resolutions. Here, SEC-HPLC was used for finding concentrations of BLG (16kDa) and BSA (66kDa) from multicomponent breakthrough samples for major proteins. Varian ProStar HPLC system was used for carrying out chromatography experiments and data anlysis was performed in 'Galaxie' tool from Varian.Inc. Agilent Bio SEC-3 HPLC ($4.6 \times 300mm$) columns with a particle size of 3 μm and pore size of 100 was used for the analysis. These columns have proven to give higher loading capacity, higher stability for salt based injections, and reproducibility for the size based separation. They also provide faster separations than large particle columns for a size range of 0.1 kDa to 100 kDa.

3.3.2.5 HPLC analysis

HPLC analysis method was developed for finding unknown concentrations of whey proteins form the experimental samples. Samples generated in multicomponent breakthrough experiments for both acidic and basic proteins, and optimisation experiments for crude whey separation. Two different HPLC methods (*HPLC method*

1 and method 2) were used for the analysis of basic proteins and acidic proteins. *Method 1* was developed to resolve basic proteins and *method 2* was used for acidic protein as well as crude whey analysis. As method development was based on the molecules involved, details of method development and analysis is given in respective sections. 1260 Infinity Micro-Scale purification system purchased from Agilent Technologies, Victoria was used for HPLC analysis. Zorbax 300SB-C18 5 μm ($4.6 \times 250mm$) column for HPLC analysis was procured from Agilent Technologies, Victoria, Australia. These columns have 5 μ silica particles coated with highly hydrophobic c18 stationary phase. With a wide pore size of 300 , these columns are ideal for high pressure analysis and separation of proteins and peptides based on their hydrophobicity irrespective of their molecular size [227].

3.3.3 Determination of Langmuir isotherm parameters

Langmuir isotherm parameters were obtained by performing batch experiments on a smaller scale. Resin was washed thoroughly with water to remove storage solution (20% ethanol) and then contacted with equilibration buffer twice to ensure ionic consistency throughout the resin. Resin quantities were carefully portioned by making a slurry of 50% resin to buffer and then pipetting out twice the amount of volume that of required. The resin was then allowed to settle naturally, supernatant was carefully removed, and then the tubes were weighed to ensure equivalent weight of resin for all the tubes used (with <2% error).

3.3.3.1 Batch experiment

For adsorption isotherm experiment, 0.2 ml of pre-equilibrated resin was taken in a centrifuge tube and was contacted with 5 ml of individual protein solutions of different concentrations. The tubes were kept for mixing on a rocker shaker for minimum of 3 hours at 25°C and allowed to achieve equilibrium. Once the equilibrium was achieved, tubes were centrifuged at 4000 rpm for 10 min to take the samples out for further analysis of protein concentration. All the samples were kept in triplicates to ensure the accuracy of the experiment. Further the plot of adsorbed concentration to equilibrium concentration in the mobile phase for all samples was estimated. All the constants (Q_{max} and k_d for Langmuir, Q_f and n for

Freundlich) in the isotherm models were found out by non-linear optimization using MATLAB R2014b (MathWorks, Inc., Massachusetts, USA). The curve also served in determination of SMA and MPM isotherm parameters by inverse fitting.

3.3.3.2 Uptake kinetics

Uptake experiments were conducted in equilibration buffer in a centrifuge tube. Pre-equilibrated 0.5 ml of resin was taken in a 50 ml centrifuge tube and contacted with 25 ml of individual protein solutions of fixed concentration. The mixture was kept on a rocker shaker for mixing and sample of 200 μl were withdrawn, centrifuged at 10000 rpm, and analysed by spectrophotometry for finding the concentration at every time point. Analysis and withdrawal was done in parallel so that sampling could be stopped after saturation was reached. Total reduction in the volume was found to be less than 5$\%$ therefore a constant volume was assumed throughout the experiment. Experimental data was further used to fit pseudo first order and pseudo second order models to check which one describes the kinetics better. The obtained constants were used further in simulations. Same kinetic constant were used in SMA isotherm parameters for representing adsorption rate constant.

3.3.4 Determination of steric mass action parameters

For column experiments, NGC^{TM} medium pressure chromatography system (NGC) was used. The system provides automated buffer blending systems with a flow rate as high as 20 ml/min. Conductivity and pH can be measured on-line along with UV-visible absorbance giving a better control on the experimental progression. Automatic sampler provides an error free continuous sampling of longer chromatography runs such as breakthrough experiments. ChromLab^{TM} software was used for data collection and continuous monitoring of pH and conductivity during the runs. The system was utilised for pulse experiment, gradient experiments on HiTrap columns, and breakthrough experiments.

3.3.4.1 Gradient elution experiments

Gradient experiments were performed to estimate the charge constant v_i and equilibrium constant $k_{eq,i}$. Column was equilibrated with the buffer. Protein solutions at specific concentrations and fixed injection volume were injected on a HiTrap column (0.96 ml) packed with the chosen resin. the column was washed with 4 CV wash buffer to remove losely bound proteins. Bound protein was further eluted by gradient elution at varying gradient slopes such as 5, 10, 15, 20, and 30 column volumes (CV) between 0-100$\%$ of the mobile phase B. The values of v and k_{eq} were determined by fitting experimental data to Equation 3.23 for various gradient lengths[228]. Standard deviation was found out for the same and mean of the fitted constants were carried forward for prediction. Repeating the experiments at different gradients lengths was needed to ensure that the constants are valid for faster as well as slower changes in the elution mobile phase.

$$v_r = \left(\left(c_{a,s}^{v+1} + \frac{v_d k_{eq} \epsilon_e \Lambda^v (v+1)(c_{e,s} - c_{a,s})}{v_g} \right)^{\frac{1}{v+1}} - c_{a,s} \right) \tag{3.23}$$

Where; $c_{a,s}$ is concentration of protein in mobile phase at the inlet, $c_{e,s}$ is concentration of protein in mobile phase at column exit, v_d is column dead volume.

3.3.4.2 Breakthrough experiments

Breakthrough experiments are needed to determine the steric hindrance factor for proteins (σ_i). Therefore, breakthrough profiles for respective proteins were obtained at operating pH at different flow rates to ensure accurate estimation of σ_i. Breakthrough curves were also used further for validation of *ExProSim:IC*. Inlet concentrations were chosen for major proteins based on their actual concentrations in crude whey as they were high enough for breakthrough analysis. On the other hand, as the concentration of minor proteins is very low in the crude whey, higher concentration solutions of standard minor proteins were preferred in order to achieve the individual breakthroughs. Breakthrough curves were performed at different flow rates (linear velocities) in order gauge if the simulation tool can make predictions, consistent with experimental data at different flow rate conditions. Time and volumes for breakthrough point, 10$\%$ breakthrough,

halfway concentration and exhaustion were recorded for comparison with simulations to assess accuracy of prediction. Steric hindrance factor, σ_i was estimated by using Equation 3.24[229].

$$\sigma_i = \frac{\psi}{c_{in,i}(\frac{v_b}{v_0} - 1)} \left[\Lambda - c_s \left(\frac{(\frac{v_b}{v_0} - 1)}{\psi k_{eq}} \right)^{\frac{1}{v_i}} \right] - v_i \tag{3.24}$$

Where, ψ is the phase ratio; $\frac{(1-\epsilon_e)}{\epsilon_e}$. Breakthrough curves were further used to find out dynamic binding capacity (DBC) of the proteins towards the resin. DBC was found out as given in Equation 3.25

$$DBC = \frac{(v_{10\%bt} - v_d) \times c_0}{cv} \tag{3.25}$$

It was important to assess the competitiveness of the proteins during adsorption and hence multicomponent protein breakthrough were performed for both major and minor proteins. It was expected to find the changes in relative affinity and hence dynamic binding capacity of the individual proteins due to presence of the other contenders for the binding sites. For multicomponent breakthrough, solutions of major and minor proteins were prepared based on their percentage contribution in whey, and loaded continuously on to HiTrap column at 0.5 ml/min flow rate. Samples were collected throughout the experiment till the saturation. Few samples were selected based on the shape of the curve towards saturation and used for further analysis by using HPLC method developed for resolution of whey proteins. Injection volume for all the samples was 100 μl.

3.3.5 Column physical parameters

3.3.5.1 Column evaluation:

Though most of the columns used were freshly bought pre-packed columns and were already tested for the integrity at the factories, it was decided to check the asymmetry and Number of transfer units(NTU) before and after usage of the column. 2% acetone was injected (2% CV) on a water equilibrated column at 20 cm/hr linear velocity and the peak was analysed for its symmetry. NTU was found

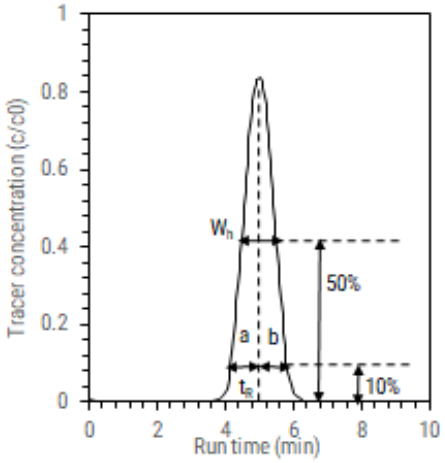

Figure 3.1: An example of a typical chromatography peak analysis

out by Equation 3.26.

$$NTU = \frac{\mu_f^2}{\delta^2} = 5.54\left[\frac{v_r}{W_h}\right]^2 \tag{3.26}$$

Where, W_h is the peak width at half height, v_r is retention volume, μ and σ are first and second moments, and L is length of the column. Height equivalent to theoretical plates (HETP) was simply given by L/NTU. Furthermore, reduced plate height was given by $HETP/d_p$. found out by using Equation 3.27.

$$h = \frac{L}{5.54 d_p}\left[\frac{W_h}{V_R}\right]^2 \tag{3.27}$$

Where, d_p is the resin particle diameter. A typical chromatography can be seen in Figure 3.1

3.3.5.2 Pulse experiments:

Porosity of the column was determined by injecting pulses of tracers blue dextran (0.5 mg/ml) and sodium nitrate (100 mM). 200 μl of these tracers were injected and detected at 640 ηm for blue dextran and 310 ηm for sodium nitrate to determine external(ϵ_e) and particle porosity (ϵ_p) respectively. Moment analysis (Equations 3.28,3.29,3.30) for the peaks obtained at different flow rates ranging from 0.2 ml/min to 1 ml/min was done in order to ensure accurate estimation of diffusion coefficient (equation 3.32[5]. The column was washed and equilibrated thoroughly after every run to target least possible tailing for blue dextran. Most

of the experiments showed tailing factor of 1.6-2.05. The recommendation by FDA for tailing factor for analytical purpose is t_f<2 [230]. For sodium nitrate, the peak tailing factors were close to 1 showing gaussian behaviour. Total porosity ϵ_t was then obtained using the values of ϵ_e and ϵ_p (Equation 3.31[231]). This process was repeated for all the columns used in the work for breakthrough analysis (SPFF, Capto S™, and Capto Q™).

$$\mu_f = \frac{\int_0^t c.t.dt}{\int_0^t c.dt} \tag{3.28}$$

$$\delta = \frac{\int_0^t c.(t-\mu_f)^2 dt}{\int_0^t c dt} \tag{3.29}$$

$$\mu_f = \frac{L}{u}\left(\epsilon_e + (1-\epsilon_e)\epsilon_p b_0\right) \tag{3.30}$$

$$\epsilon_t = \epsilon_e + (1-\epsilon_e) \times \epsilon_p \tag{3.31}$$

$$D_{ax} = \frac{\delta^2}{\mu^2}\frac{Lu}{2} \tag{3.32}$$

This gives a dispersion coefficient for the tracer elements. Furthermore, to find the fluid properties specific to the protein, Peclet and Reynolds number were estimated. Peclet number (Equation 3.34) gives the ratio of convective mass transfer to the diffusive mass transfer, whereas Reynolds number (Equation 3.33) gives the ratio of convective forces in the medium to the viscous forces. To find out dispersion coefficient of the protein molecules, Reynolds number and Peclet number were determined using Equation 3.35.

$$Re = \frac{u\rho\epsilon_e d_p}{\eta} \tag{3.33}$$

$$Pe = \frac{1}{2}(0.2 + 0.011Re^{0.48}) \tag{3.34}$$

$$Pe = \frac{ud_p}{D_{ax}} \tag{3.35}$$

Molecular diffusivity was found out by Equation 3.36 to compare the diffusivity of different protein molecules through the medium. Though there are numerous equations to find the diffusivity, this was chosen as it was proposed specifically for proteins and has been validated for more than 150 proteins [232].

$$D_m = \frac{8.34 \times 10^{-8} T}{\eta M^{0.33}} \tag{3.36}$$

3.3.5.3 Ionic capacity

Ionic capacity is a representation of ligand density for the resin. To estimate ionic capacity of Capto S™, a displacement experiment was carried out. Initially column was saturated with 0.5 M HCl ions to ensure all the cationic sites are blocked by H^+ ions. Further column was washed by 0.1 M NaOH to displace H^+ ions by Na^+ ions[229]. Conductivity and pH were monitored to detect the presence of pure NaOH at the outlet. The value of ionic capacity, Λ was calculated using Equation 3.37. Ionic capacity was measured for all the HiTrap columns in the work (SPFF, Capto S™, and Capto Q™)

$$\Lambda = \frac{c_{NaOH} v_{NaOH}}{cv \times (1 - \epsilon_t)} \tag{3.37}$$

3.3.6 Buffer preparation

Buffers being an integral part of the experimental systems used here, were precisely prepared in ultra pure water (resistivity $18.4 M\Omega - cm$). pH of the buffer was chosen based on isoelectric points of both the proteins to ensure enough binding on the resin. Equilibration and wash buffer were prepared at the chosen pH. De-ionized water was used for ionic capacity determination. All the buffers were filtered by using 0.45 μm Whatman filter paper using vacuum filtration. Protein solutions for all experiments were filtered through Pall Biosciences PVDF filters of 0.45 μm syringe filter.

3.3.7 Crude whey processing

Breakthrough experiment of crude whey protein concentrate was performed on HiTrap Capto Q column at 0.5 ml/min. 4 mg/ml concentration of WPC was prepared. As the solution was turbid, it was centrifuged at 10000 rpm and further filtered through 0.45 μm filter before loading on the column.

3.4 *ExProSim:IC*

Overview of *ExProSim:IC* is shown in Figure 3.2. *ExProSim:IC* is designed to gain basic understanding of the process, in order to practice goal oriented separation. *ExProSim:IC* is a customisable numerical tool for solving various kinds of binding models such as; Langmuir isotherm, Freundlich isotherm, steric mass action isotherm (SMA), and mobile phase modulator isotherm (MPM), which can be solved in combination with mass transfer models such as Equilibrium dispersive model (EDM). Details of the models included are discussed in Section 3.2.1 and 3.2.2.

ExProSim:IC has two different modules. First module is a 'parameter estimation' module in which curve fitting is performed for models and experimental results for determination of coefficients. Second stage is 'prediction' module which can be used for predicting the experimental profiles using model constants from the first module.

3.4.1 Parameter estimation module

The models have coefficients, which govern the behaviour of the phenomena they describe, and signify physical or chemical characteristic of the proteins. These coefficients or model constants are found out by performing basic experiments. These include experiments such as; pulse flow to determine porosity's and column consistency, adsorption and uptake experiments to find basic binding characteristics of the protein-resin interaction, breakthrough experiments for flow kinetics of the protein through the resin column. Detailed methodology of experiments carried out for finding model constants is given in Section 3.3. It can be

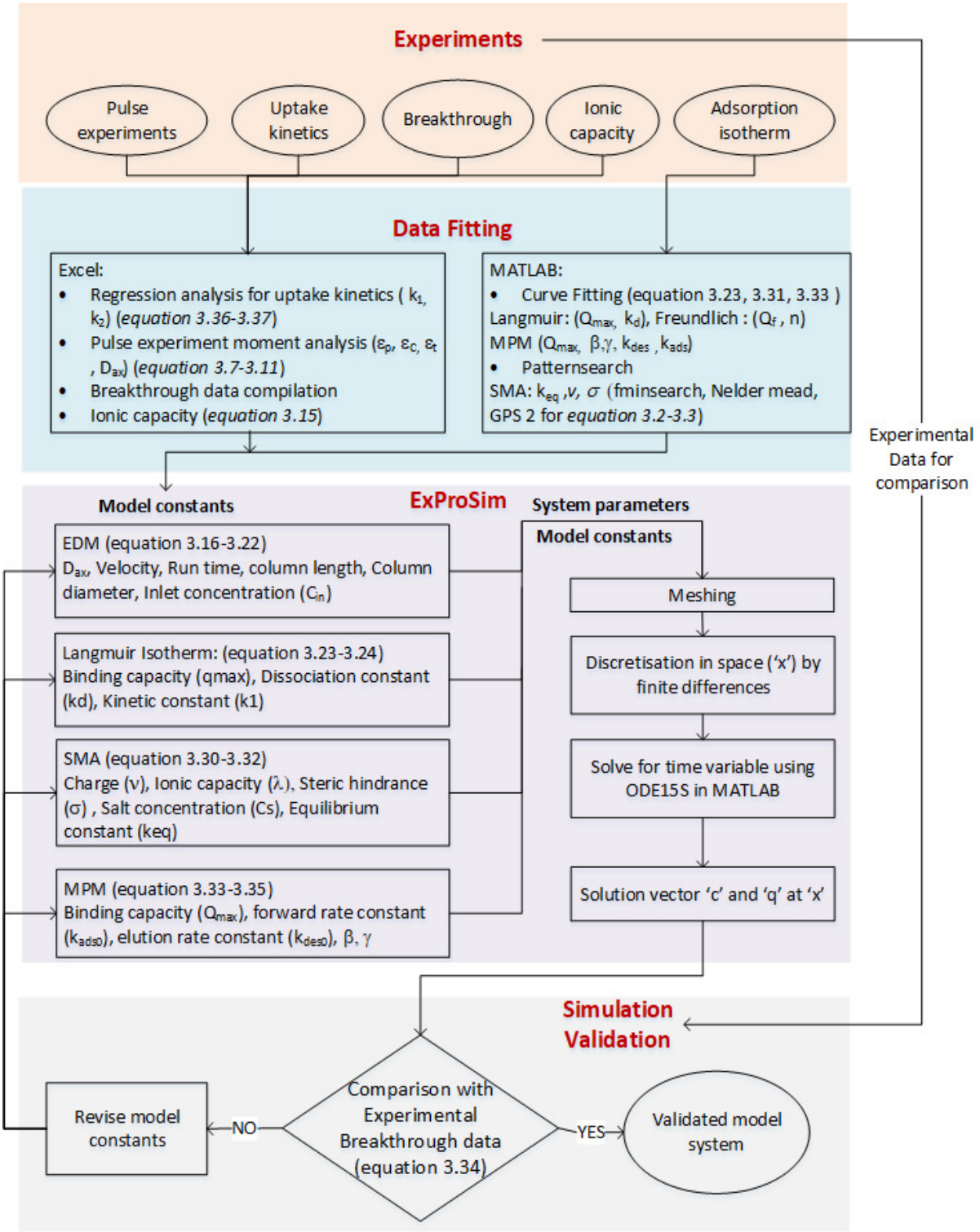

Figure 3.2: Schematic representation of data analysis and computational methodology

said that substantial amount of experiments may be required for parameter estimation and question can be is it worth to follow such methodology rather than investing resources directly onto developmental experiments. As parameter esti-

mation experiments lead towards a platform for accurate prediction, it can help in reducing number of experiments during process development phase of the system. Experiments performed for parameter estimation are described in Section 3.3.3 to 3.3.5

In the first stage, data from number of experiments were further used in *ExProSim:IC* for data fitting to equilibrium models in order to find model constants. Estimation of parameters for Langmuir, Freundlich, and MPM model was done by 'inverse fitting' the model equation parameters by using *curve fitting* application in MATLAB 2014b to fit the equation to the experimental data (Q_{max}, k_d for Langmuir, Q_f and n for Freundlich, and Q_{max}, k^m_{des}, k^m_{ads}, γ for MPM). The error between the fitted curve and experimental curve was minimised based on equation 3.38. Parameters for SMA were found by two different methods and compared for their predictability. First method was an experimental approach as discussed in Section 3.3.4. Second method was 'inverse fitting' where, *patternsearch* optimisation tool was used to fit the Equation 3.17 to the adsorption data. Curve fitting was performed to minimise the error where y_{exp} is an experimental value and y_{calc} is value obtained from the model fit. model constants were changed strategically to get the best fit.

$$Err_{fun} = \sum_{i=1}^{N} [y_{exp} - y_{calc}]^2 \tag{3.38}$$

The minimisation function *fminsearch* was chosen for optimisation. Logical initial guesses were made in order to start the iterative estimation for minimum. Considering the learning's from one of the research works about error induced because of initial guesses [229], global optimisation tool was used to avoid the effect of local minimal during the iterations and hence to reduce the dependency on the initial guesses. 3000 iterations were done for the minimisation algorithm along with use of *GPS Positive basis 2N* and *Nelder-Mead* methods to ensure minimum error. Uptake kinetics experimental data was used to fit the unadsorbed concentration c vs $time$ for pseudo first order (Equation 3.39) and pseudo second order equations (Equation 3.40). The model constant for a better fit was chosen further (k_1 or k_2).

$$ln(q_e - q_t) = lnq_e - k_1 t \tag{3.39}$$

$$\frac{t}{q_t} = \left(\frac{1}{k_2 q_e^2} + \frac{t}{q_e}\right) \tag{3.40}$$

Where, q_e is stationary phase concentration at equilibrium and q_t is stationary phase concentration at any time t from start of contact to saturation of the stationary phase.

The values of the model constants obtained here were used further for breakthrough predictions in *ExProSim:IC*.

3.4.2 Prediction module

Parameters from the chosen models, for all the proteins in the mixture to be fractionated are put into input matrix in the tool. This is followed by defining the experimental system including column configuration, flow conditions, properties of mobile and stationary phases. Column is further divided into number of intersections called meshes at which the model equations are solved (N_x for axial coordinate and N_t for time coordinate). ExProSim:IC uses 'method of lines' [233] which is implemented in *'pdepe'* function in MATLAB. *'pdepe'* solves initial-boundary value problems in the one space variable 'x' and time 't' for system of parabolic or and elliptic equations. Functions for system parameters, inlet conditions, boundary conditions were solved together using this function. According to 'method of lines', axial coordinate is discretised first to convert the partial differential equations into ordinary differential algebraic equations in time. Further discretisation in the time domain is performed using *'ode15s'* which ensures efficient treatment of Jacobian matrices. This reduces the differential algebraic equations into simple algebraic equations which can be easily solved for the solution on axial mesh as defined in the program. Solution at any point in the column can be extracted from the program and a profile for breakthrough at given time points can be plotted.

3.4.3 Tool verification

There are two methods to validate a code. Firstly, code to code validation can be done where predictions from the current code are compared with another al-

ready established code for same experimental and model constants. This can be performed exhaustively on numerous datasets to gain more confidence. Another way of validation is experimental validation, where at least 3 experiments for a system of proteins are used as a framework for calibrating model constants in iterative way by minimising the errors to least possible value. This section is called as code verification and not code validation as preliminary work on verification of the workability of the tool is presented.

Initially, an assessment of model constants is carried out for gaining more understanding about the effectiveness of the tool to handle and represent these model constants. This was followed by a basic comparison of simulations from the tool to CADET simulations in order to check if it is workable for simulating chromatography processes. For the tool, meshing is a critical step in the discretisation process as it affects the accuracy and computational time. High number of mesh points give higher accuracy but they also increase the computational time. On the other hand, accuracy is compromised when mesh points are too low. Here, aim was to find out criteria for optimum mesh size which will give required accuracy without compromising on computational time. To gauge the criteria for mesh independency, number of meshes along axial and time coordinate are varied, and predictions obtained at consecutive mesh points were compared for root mean square error and coefficient of determination between the curves. Value of Δx and Δt were found out from this exercise for which the RMSE and CoD remained constant for further change. These values of Δx and Δt were considered for simulating rest of the scenarios in the thesis. In case of change in column length or run time, Δx and Δt were adjusted back to obtained values by changing number of discretisation intervals.

3.4.4 Experimental validation

As the thesis is also to gain insights about the separation of whey proteins, exhaustive code to code validation is not carried out and more emphasis is given on experimental validation. Initial experimental validation of the tool was carried out with experimental and simulation data from the literature. Each model combination was validated for minimum of three literature cases which are discussed

further in Section 3.5.3. Exhaustive experimental validation was carried out on experiments performed for major and minor whey proteins in Chapters 4 and 5 respectively. Errors between predicted and experimental breakthrough curves were determined by calculating mean square error (MSE), standard deviation of mean square error (SDMSE), root mean square error (RMSE), and coefficient of determination (CoD) between the curves. Standard error is defined as standard deviation divided by the square root of the sample size. This is shown in equation 3.41. The standard error is also a measure of variability as the standard deviation (SD). As the data sets chosen are processed by interpolation of data for experimental time data, standard error gives a better estimate of the variability of the chosen data set from the curve predicted curve with respect to experiments.

$$SE = \sum \frac{(y - y')^2}{n} \tag{3.41}$$

Where, y and y' are values of respective points of two data sets being compared and n is number of points. Important error parameters used here for comparing the curves were RMSE which gives the variability of the predictions with respect to experimental data. This was calculated by equation 3.42. It can be said that lower the RMSE value, closer are the two curves to each other.

$$RMSE = \sqrt{\sum \frac{(y - y')^2}{n}} \tag{3.42}$$

It is also true that RMSE is a function of the sample size and may not give a statistically significant picture. If the number of points under consideration are too many, standard error automatically goes down which may not reflect the complete variability of the sample. For making the comparison independent of the sample size, correlation coefficient between experimental and predicted data sets was determined. The squared value of correlation coefficient is called as CoD. Higher the value of CoD towards 1, shows higher overlap between the data sets. CoD was determined as in Equation 3.43.

$$CoD = \left(\frac{1}{n} \sum \frac{(y - \bar{y})(y' - \bar{y}')}{SD_{exp}.SD_{pred}} \right)^2 \tag{3.43}$$

Where, SD is standard deviation. $\bar{y}$ and $\bar{y}'$ are mean values of the datasets.

3.5 Results and discussions

For ion exchange chromatographic processes, factors such as; protein concentration, flow velocity, column dimensions, resin characteristics, and properties of proteins play an important role. Their effect on separation characteristics is predominant [234, 235]. It is important to know if the tool developed can predict the changes induced by variation of these parameters. Easiest way to check that was to pick cases from the literature and assess if they are predicted well by *ExProSim:IC*. Minimum of three cases were chosen for each model combination in order to confirm if the predictability of the tool is acceptable however, few preliminary checks for the verification of the tool were required before its implementation.

3.5.1 Tool verification

3.5.1.1 Assessment of model constants

It was important to assess if the code developed is solving the model equations correctly. As thermodynamic model constants are important in solving the equations accurately, it is important to know if the code is sensitive to changes in the model constants. Hence, effect of model constants on breakthrough curves was determined by choosing extreme values (three values; low, middle and high) of the model constants in the context of the protein data sets chosen from literature. Values of other model constants were kept at reported values when one parameter was varied during these verification runs. For Langmuir isotherm, an example of BLG from the literature was chosen to see if changes in Q_{max}, k_d, and k_1 brings any change in the breakthrough profile or not [1]. For SMA, Insulin breakthrough profile from Karlsson et al was chosen and changes in charge value υ, σ, k_{eq}, and ionic capacity λ were checked for changes in the breakthrough profiles. For MPM, changes in Transferrin breakthrough profiles were analysed for respective changes in k_{ads0}, k_{des0}, β, and γ. The representative values at which the data is presented here, are given in Table 3.1.

Table 3.1: Representative values at which the tool verification was performed for all three isotherms

	Langmuir BLG			**SMA Insulin**				**MPM Transferin**			
	Q_{max}	k_d	k_1	v	σ	k_{eq}	λ	k_{ads0}	k_{des0}	β	γ
Low	0	0.008	0	0	35.1	0.54	0	0	0	0.58	0
Mid	339	0.8	0.035	1.25	175.5	5.4	1050	0.055	5	2.9	2
High	678	8	3.5	2.5	351	540	2100	0.55	50	11.6	4

Langmuir Isotherm verification

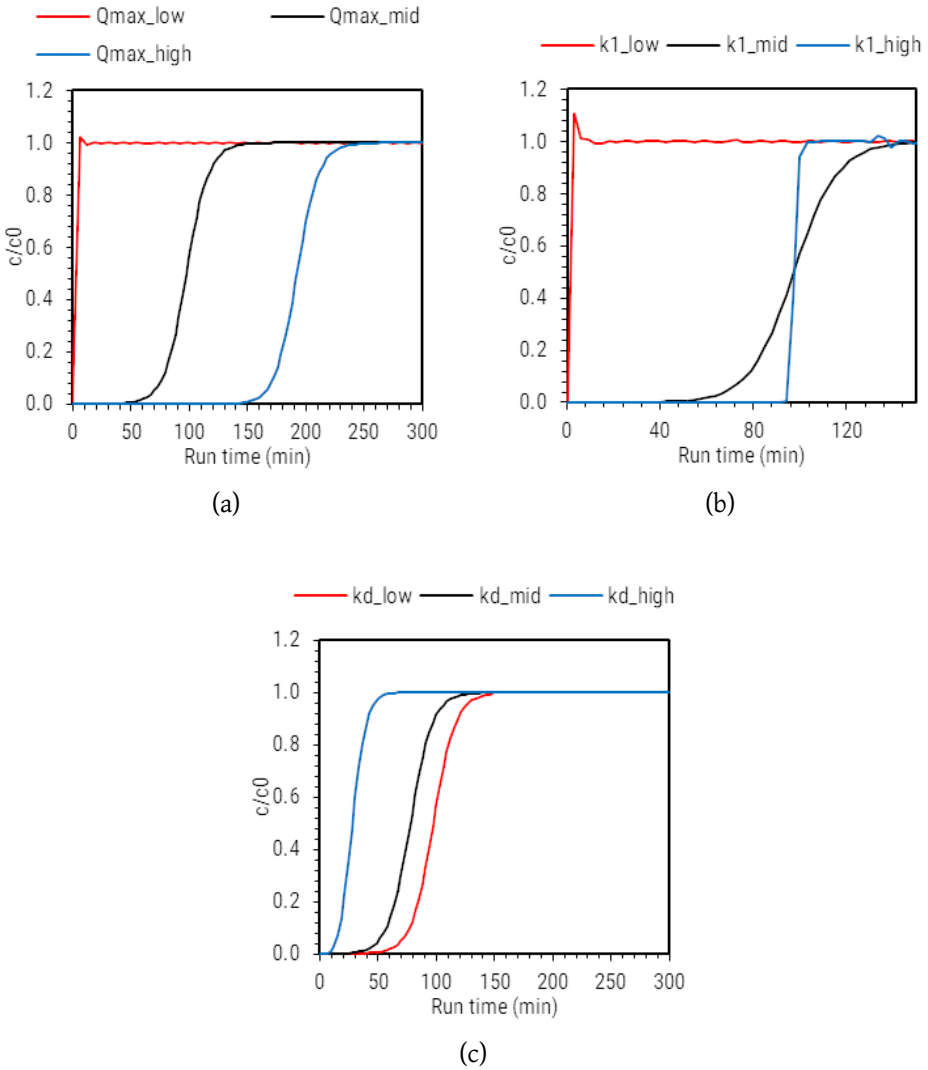

Figure 3.3: Tool verification for variation in Langmuir isotherm model constants based on data from Elsayed et al. [1]. a) Q_{max} b) k_d c) k_1

For Langmuir isotherm values optimised in the literature were taken as reference. For Q_{max}, value seemed very high, hence it was doubled to achieve a high

value and set to zero to see what happens at lowest possible binding capacity. Figure 3.3(a) shows a steep breakthrough for the lowest values of Q_{max} suggesting no binding in the column. For a higher value of binding capacity, prolonged retention of the protein was observed and breakthrough was achieved much later. For k_d, it was expected that with increase in the value, the desorption should increase leading to earlier breakthrough. As k_d value from the paper is very low, it was decided to consider it as a low and multiply it 100 and 1000 times for a middle and high values. Figure 3.3(b) shows an expected trend. For values of k_1, optimised value was considered as a mid value. For higher value it was multiplied by 100 and lowest value was set to zero. k_1 value shows the adsorption rate coefficient so it is expected that with increase in k_1 value, the breakthrough point should move farther. It was also observed in Figure 3.3(c), that the breakthrough slope became steeper with increase in adsorption rate coefficient. At zero k_1 value the adsorption was found to be zero.

SMA Isotherm verification

For SMA, charge values are used in exponential function. The charge value reported in the literature was very high hence it was considered as the highest value. The lowest value was set to zero and middle value was considered at 50$\%$ of the reported value. It can be seen in Figure 3.4(a) that variation in charge value is directly proportional to the binding capacity of the protein. It is obvious that the relation is not linear as the function is exponential. As the charge value decides the binding strength of the protein, this is an expected outcome. It can also be observed that the slope of breakthrough did not change with change in the charge value. The equilibrium constant for SMA is a ratio of desorption constant to adsorption constant, hence it is expected that with increase in the value of k_{eq}, the breakthrough capacity should decline. It was necessary to gauge an effect of equilibrium constant in a wider range as the adsorption and desorption rate constants can vary in multiples of 10 with respect to each other even with a smaller change in the process conditions. Hence, the value from the literature was considered as a middle point and lowest and highest values were defined at a factor of 10.

Figure 3.4(b) shows a similar profile. High value of equilibrium constant can

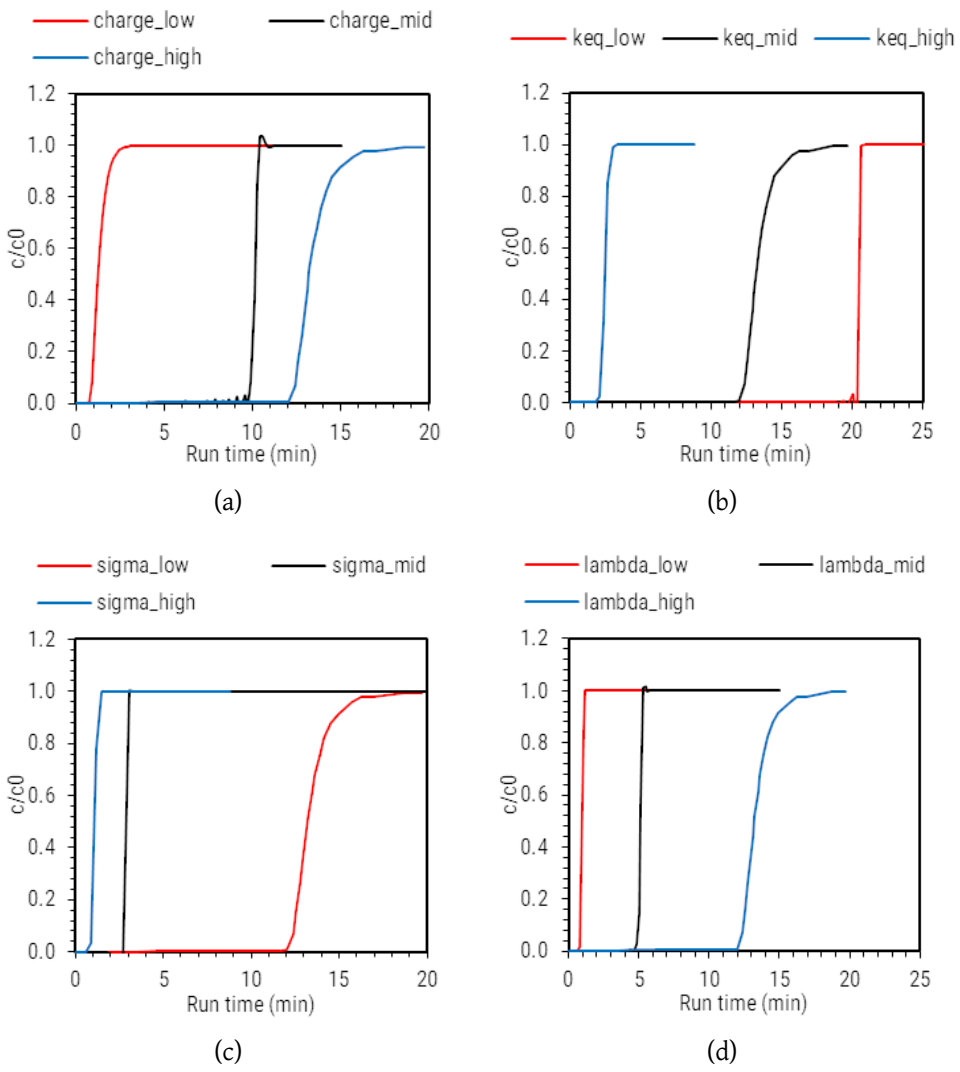

Figure 3.4: Tool verification for variation in SMA isotherm model constants based on data from Karlsson et al. [4]. a) Charge v b) k_{eq} c) σ d)λ

mean either higher desorption constant or lower adsorption constant. It is expected that if the desorption rate changes, the slope of the breakthrough should change, however, change in adsorption constant might only reflect in change in binding capacity. Steric hindrance factor works against the binding of the protein as higher the resistance of protein against each other, lower will be their binding on the resin.

The trend shown in Figure 3.4(c) supports this hypothesis. The range of values for σ were derived by considering the data from the referred literature as the minimum. Furthermore, ionic capacity gives an estimate of number of binding sites on the resin. It is obvious that more number of binding sites can allow higher binding for the proteins. The values selected for λ were based on ion capacity

values of resins available in the market. The resin used in the work referred, offered very high capacity hence it was set at high level. Lowest was defined as zero and middle values were derived as 50% of the highest. As shown in Figure 3.4(d), expected decline in binding capacity was observed with decline in ionic capacity constant.

MPM Isotherm verification

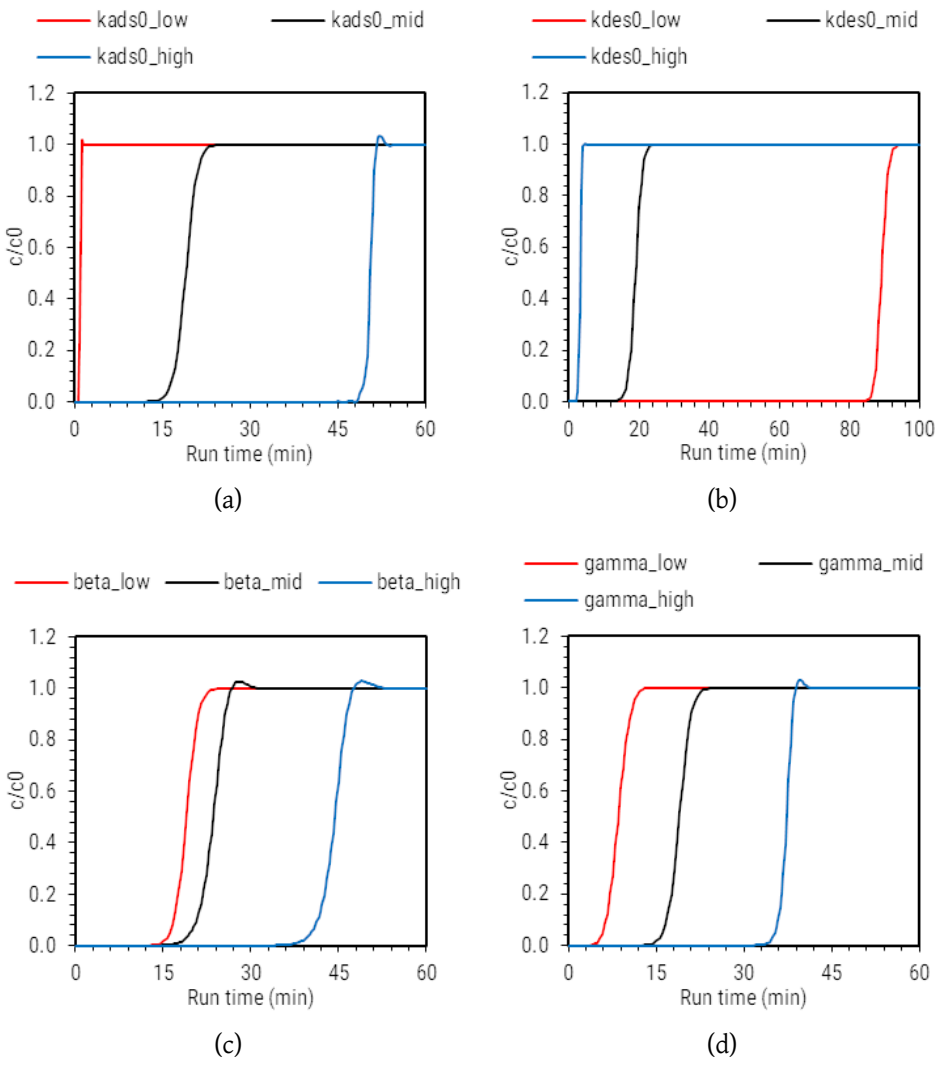

Figure 3.5: Tool verification for variation in MPM isotherm model constants based on data from Karlsson et al. [4]. a) k_{ads0} b) k_{des0} c) β d)γ

For MPM isotherm, the optimised values of k_{ads0} and k_{des0} were considered as middle values. Lowest values were set to zero and highest values were set to 10 times the reported values. It can be observed in Figure 3.5(a) that with increase in k_{ads0}, the binding capacity was improved. At zero k_{ads0}, no protein was adsorbed

as expected. In contrast to this, when the value of k_{des0} was set to zero, the binding capacity was very high. At highest k_{des0}, binding capacity reduced to almost zero. This is expected from the definition of the rate constants. It was expected that the slope would also vary with change in desorption constant, however, it was not observed. Variation of k_{des0} variation can be seen in Figure 3.5(b).

β value is defined for a factor responsible for ionic interactions. It is analogous to v in SMA isotherm hence, similar behaviour was expected for β as well. It can be observed in Figure 3.5(c) that binding capacity increased with increase in the value of β. β is indirectly involved in determination of k_{des}^{m} and is an exponent of salt concentration (S^{β}) as given in Equation 3.21, its effect cannot be directly compared with charge value from SMA. As the salt concentrations are generally very low, β may not be as sensitive as the charge value. γ value captures hydrophobic interactions for the proteins. The variation in γ values is often overlooked in case of ion exchange chromatography, however, as shown in Figure 3.5(d), it has significant impact on the breakthrough curves. When the curves for lowest value of γ (zero) and middle value of γ were compared, it was observed that hydrophobic interactions play significant part in the binding process. For higher γ higher binding was observed. γ is used in determination of adsorption constant k_{ads}^{m} in an exponential function as given in equation 3.20. Effect of γ may also be dependent on salt concentration of the medium.

This exercise gave a picture of how the model constants are related in location and shape of the breakthrough curve. It was repeated for all the experimental systems used in this work (Not shown here). The knowledge gained can be used in adjusting the parameters for the experimental validation studies. Extent of effect of these parameters are system specific and the numerical change in the parameters may be based on trial and error till an expected fit for simulation curves is achieved. Ideally once the parameters are determined for a system by performing this exercise, it should establish a successful set of thermodynamic constant for the system to make future predictions.

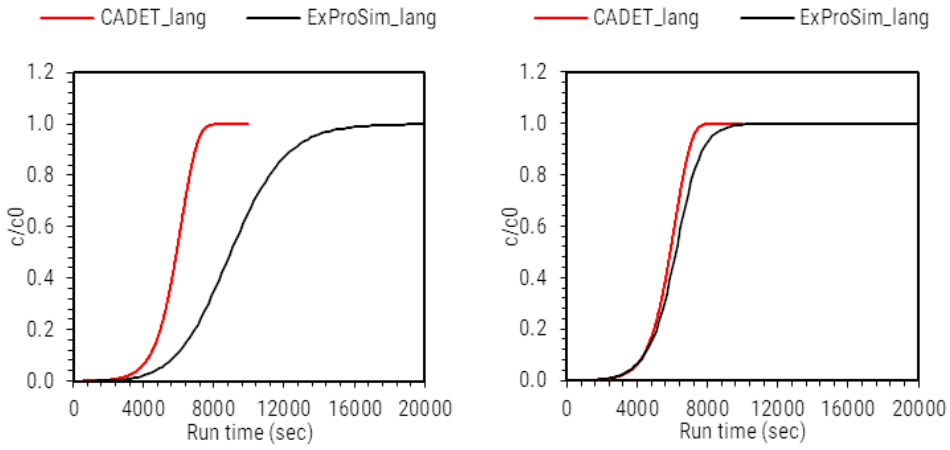

Figure 3.6: Comparison with CADET simulations using Langmuir isotherm model constants. a)initial comparison b) post Q_{max} and k_d modification

3.5.1.2 Verification against a reference tool

To assess *ExProSim:IC* for its predictability, it was decided to compare the simulation results to an established tool such as CADET. Comparison with CADET is not intended here. As both the codes have different framework, direct comparison is not possible. CADET is also a well validated tool hence, intention is to use it as a reference. Overview of features of CADET were discussed in Section 2.4.1. Simulations for CADET can be run on a web interface (CADET web user interface) [136]. It was tricky to find examples from the literature which can provide constants for simulation in CADET, as framework of CADET is detailed and many model constants are required for GRM simulations. For ease of comparison, three examples from the CADET web interface, one for each isotherm were chosen for comparison. Model and system parameters were extracted, used as inputs for *ExProSim:IC*, and the simulations were compared. For Langmuir isotherm, huge error was obtained when compared with CADET simulations as seen in Figure 3.6(a). The difference in number of model constants, mass transfer model, and implementation methodology may be responsible for the error. Also the diffusion coefficient considered here was an overall diffusion coefficient in GRM. Input parameters in *ExProSim:IC* were further modified to fit the simulations to CADET simulations as shown in Figure 3.6(b). The change in model constants was derived from the lessons from earlier sections. For example, as the *ExProSim:IC* simulation curve was farther than

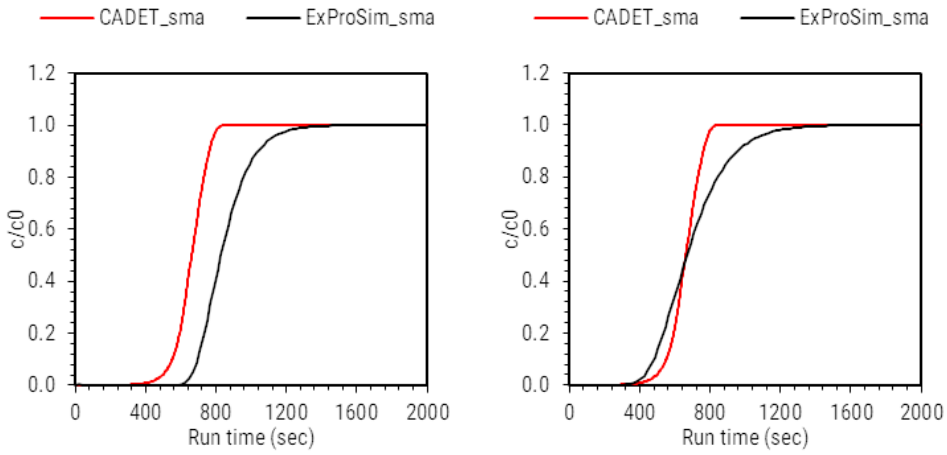

(a) (b)

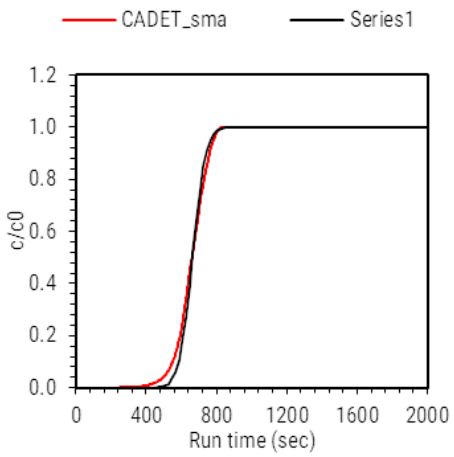

(c)

Figure 3.7: Comparison with CADET simulations using SMA isotherm model constants. a)initial comparison b) post v modification c) post k^s_{ads} modification

CADET, value of Q_{max} was adjusted (RMSE 3.65E-3, CoD 0.8921). k_d was further modified to adjust the slope (RMSE 8.26E-4, CoD 0.9867). These modifications were done on trial and error basis and errors for every simulation fit was measured. Similarly, for SMA isotherm it can be observed in Figure 3.7(a) that CADET simulation was over predicted by *ExProSim:IC* (RMSE 3.08E-3, CoD 0.9034). In order to fit the data, charge value was reduced and improved result were obtained as shown in Figure 3.7(b) (RMSE 3.41E-4, CoD 0.9567). To further adjust the slope, value of k^s_{ads} was adjusted and better results were obtained (RMSE 5.64E-7, CoD 0.9903). In case of MPM isotherm, huge difference in the preliminary predictions was observed (RMSE 5.90E-2, CoD 0.8712). To fit the curves, the value of Q_{max} was reduced to reduce the binding capacity (RMSE 8.03E-7, CoD 0.9867). Figure 3.8(b)

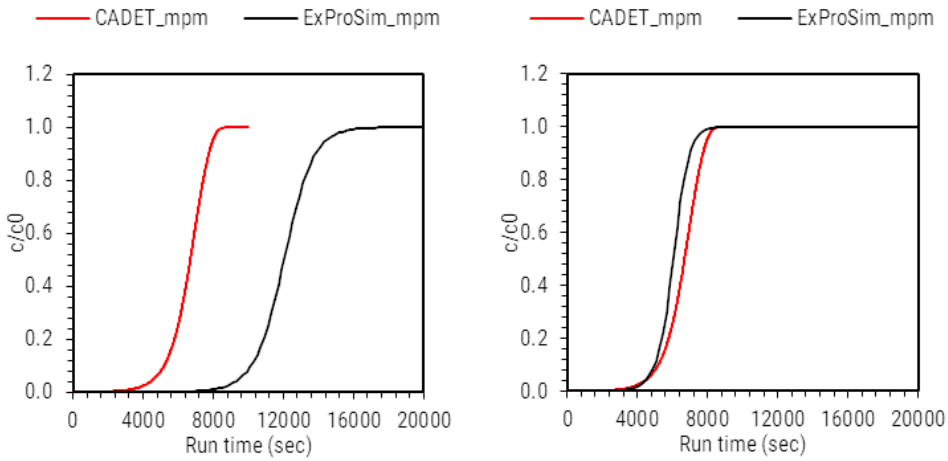

(a) (b)

Figure 3.8: Comparison with CADET simulations using MPM isotherm model constants. a)initial comparison b) post Q_{max} modification

shows the final fit. Initial and final parameters for all three isotherms are given in Table 3.2.

It can be said that enough understanding about the model constants is gained through a tool verification exercise. However, adjustment of these parameters on a trial and error basis may take a long time to reach to the best fit. More confidence should be gained based on exercising data fitting for different protein systems.

3.5.1.3 Mesh independence study

Literature data of El-sayed and Chase [1] was used for mesh dependency studies. For finding out dependency of mesh parameters on the solution. Initially axial mesh points were varied by keeping time mesh points to 50. Once the number of axial mesh points for least variation was optimised, time mesh points were varied from 10-100. Error between the curves were found out and plotted against the mesh points as shown in Figure 3.9 and 3.10. It can be seen that the error for axial coordinate were reduced to minimal at N_x value of 20 and error for time coordinate was reduced to least at N_t value of 50. From these values, Δx and Δt values were found out for the column and were kept constants for all the simulations in this thesis by varying number of mesh points for a different lengths of the column. Error tables for mesh study are given in Appendix B, Tables B.11 and B.12.

Table 3.2: System and model constants from CADET web interface for *ExProSim:IC* code verification

System parameters		
Length (m)	0.014	
Velocity (m/s)	5.75E-4	
porosity	0.37	
Dispersion coefficient (m2/s)	5.75E-08	
Model constants	**CADET**	**Modified**
Langmuir		
c_{in} (mol/m3)	7.14E-03	7.14E-03
Q_{max} (mol/m3)	4.88	2.44
k_1 (1/s)	1.14	1.14
k_d (mol/m3)	0.002	0.001
SMA		
c_{in} (mol/m3)	1	1
v	4.7	1.88
σ	11.83	11.83
λ (molm3)	1200	1200
k^s_{ads} (mol/(m3/s))	35.5	42.6
k^s_{des} (mol/(m3/s))	1000	1000
s (mol/m3)	50	50
MPM		
c_{in} (mol/m3)	7.14E-03	7.14E-03
Q_{max} (mol/m3)	4.88	2.44
β	1	1
γ	1	1
k^m_{ads} (m3/mol.s)	1.14	1.14
k^m_{des} (m3/mol.s)	0.002	0.002
s (mol/m3)	100	100

3.5.2 Preliminary experimental predictions

Initial predictions were made using experimental parameters from the research paper [1]. It can visually be said that there is high error in predictions based on experimental factors, however errors were determined for predicted curve to experimental curve and are shown in Table 3.3. Even if the overall curve to curve error were low (the RMSE values were low and CoD values close to 1 showing an accurate fit), it was observed that the curves differed highly in their shape and nature. For a realistic comparison from experimental perspective, it was decided to compare important experimental events on the breakthrough curve such as

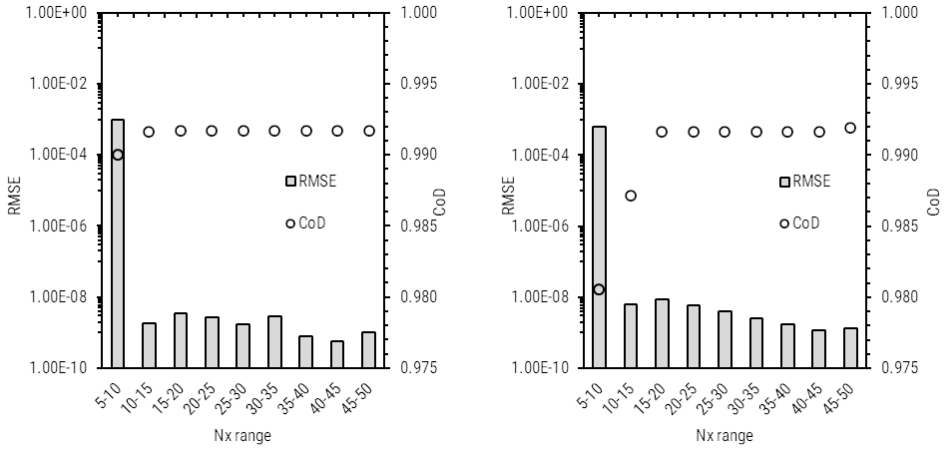

(a) (b)

Figure 3.9: Mesh independency study for *ExProSim: IC* code for axial coordinate. 'RMSE' and 'CoD' show root mean square error and Coefficient of determination between consecutive curves respectively. 'Nx range' shows shows consecutive number of discretisation intervals for axial coordinate between which the error is measured. (a) ALA and (b)BLG

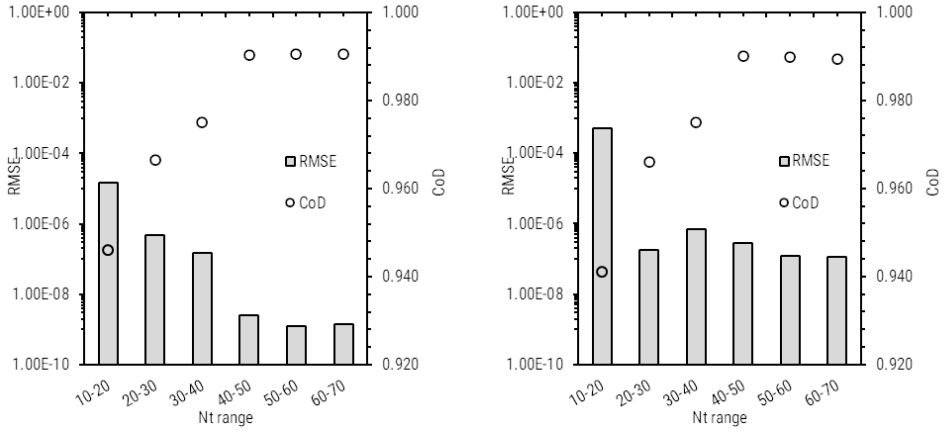

(a) (b)

Figure 3.10: Mesh independency study for *ExProSim: IC* code for time coordinate. 'RMSE' and 'CoD' show root mean square error and Coefficient of determination between consecutive curves respectively. 'Nt range' shows consecutive number of discretisation intervals for time coordinate between which the error is measured. (a) ALA and (b)BLG

0%, 10%, 50%, and 100%. Table 3.4 shows presence of higher error between the predicted and experimental curves suggesting that the change in the model constants is required for a better fit. For CoD values of even 0.8 are considered as good fit for modelling purpose, however in this case, 0.9254 did not show significant match for the predictions. This also shows that the RMSE values of the order

of 10^{-3} do not represent a good fit. It was decided to practise the same comparison method for rest of the breakthrough curves so that predicted results can be compared from experimental perspective.

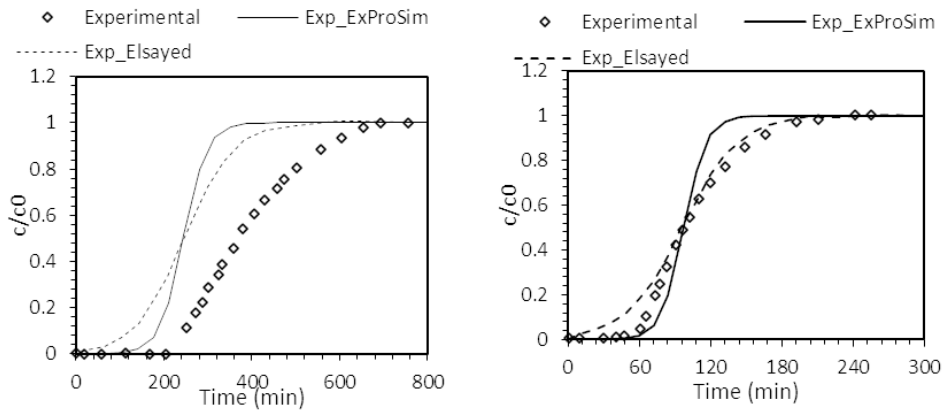

Figure 3.11: Comparison of *ExProSim:IC* predictions with experimental parameters and simulation data from literature [1](a) ALA and (b)BLG

Table 3.3: Errors for Langmuir:EDM single component breakthrough prediction using experimental data from El Sayed and Chase [1]

	ALA		**BLG**	
	Exprosim	sim	Exprosim	sim
MSE	0.0116	0.0051	0.0039	0.0041
CoD	0.0191	0.0070	0.0074	0.0066
RMSE	0.0005	0.0039	0.0000	0.0007
CoD	0.9399	0.9254	0.9538	0.9649

3.5.3 Literature based validation

3.5.3.1 EDM with Langmuir isotherm

1. ALA and BLG breakthrough

   Literature data of El-sayed and Chase [1] was used as a first case study. The work focuses on use of EDM and Langmuir isotherm for prediction of single and multicomponent breakthrough curves for major whey proteins, ALA and BLG. *ExProSim:IC* was used further with modified constants in order to

Table 3.4: Two sets of simulations from *ExProSim:IC* and El-Sayed and Chase [1] by using experimental parameters compared with experimental data

Protein	BT%	Experimental	El sayed simulations	% error	ExProSim:IC	% error
BLG	0	47.06	9.63	79.54	47.89	-1.76
	10	60.25	46.34	23.09	65.83	-9.26
	50	98.61	95.41	3.25	99.34	-0.74
	100	241.63	228.45	5.45	144	40.40
ALA	0	205.01	53.45	73.93	173.41	15.41
	10	246.34	131.36	46.68	195.42	20.67
	50	361.23	245.77	31.96	236.74	34.46
	100	877.98	497.84	43.30	351.35	59.98

fit the experimental data available in the paper for both single and multi-component systems and the data is compared with experimental as well as simulation curves from the paper.

Single component breakthrough prediction

Modified parameters were compared with the reported parameters obtained from experiments and simulations as shown in Table 3.5. Fig. 3.12 shows comparison of *ExProSim:IC* predictions to experimental and simulated data for individual proteins. The data for comparison for predicted profiles is shown in Table 3.6. It can be said that *ExProSim:IC* predicted the experimental data for both the proteins with less than 5%error throughout the breakthrough curve.

Table 3.5: Comparison of modified parameters for *ExProSim:IC* simulations with experimental data and simulation data from [1] for single component breakthrough predictions

	BLG			ALA		
Parameter	**Exp**	**El-Sayed**	***ExProSim:IC:IC***	**Exp**	**El-Sayed**	***ExProSim:IC:IC***
Q_{max} (mg/ml resin)	113	113	113	147	220.5	220.5
k_d (mg/ml)	0.008	0.008	0.008	0.029	0.029	0.029
k_1 (ml/mg.min)	0.035	0.055	0.025	0.030	0.030	0.025

Exp:Experimental, El-Sayed: El-Sayed and Chase simulations,
ExProSim:IC: Simulations from *ExProSim:IC*

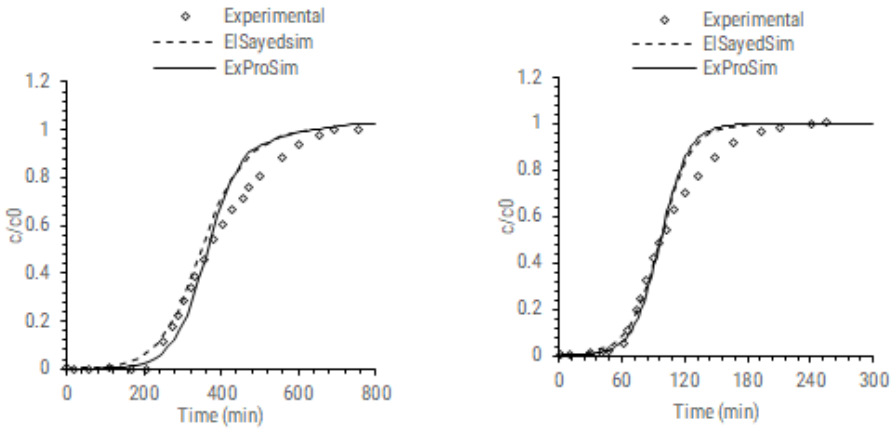

(a) (b)

Figure 3.12: Comparison of *ExProSim:IC* predictions with experimental and simulation data from literature [1](a) ALA and (b)BLG

Table 3.6: Comparison of breakthrough curves for *Exprosim:IC* simulations with experimental data and simulation data from [1] for single component breakthrough predictions

Protein	**BT%**	**Experimental**	**El-Sayed Simulations**	**% error**	***Exprosim:IC***	**% error**
BLG	0	47.06	47.75	-1.47	47.89	-1.76
	10	60.25	62.63	-3.95	63.06	-4.66
	50	98.61	96.23	2.41	97.65	0.97
	100	241.63	182.54	24.45	181.65	24.82
ALA	0	205.01	187.69	8.45	195.92	4.43
	10	246.34	233.35	5.27	264.32	-7.30
	50	361.23	349.67	3.20	364.56	-0.92
	100	877.98	630.52	28.19	653.06	25.62

Multicomponent breakthrough prediction

Figure 3.13 shows comparison of *ExProSim:IC* predictions with experimental data and simulations from El-Sayed and Chase [1] for multicomponent breakthrough curves. Simulations were performed by adjusting the parameters for multicomponent experimental data. Modified parameters are mentioned in Table 3.7.

Simulations performed for breakthrough curves were further compared based on the breakthrough points at 0%, 10%, 50% and 100% to have a closer look

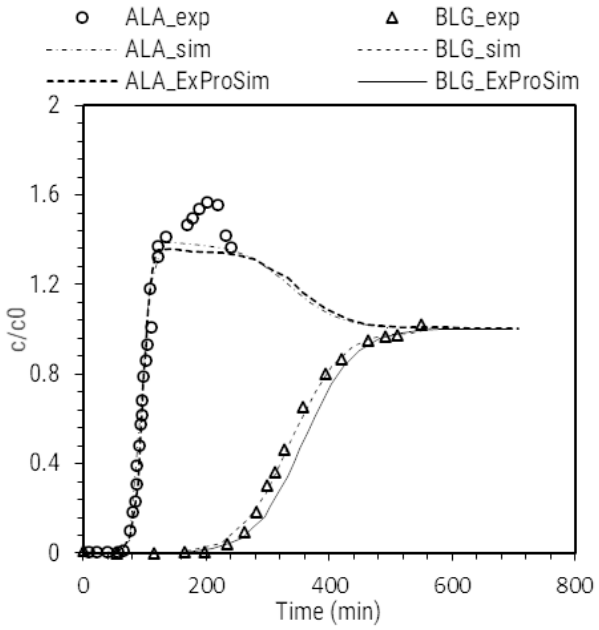

Figure 3.13: comparison of *ExProSim:IC* predictions for multicomponent breakthrough with experimental and simulation data from the literature

Table 3.7: Comparison of modified parameters for *ExProSim:IC* simulations with experimental data and simulation data from [1] for multicomponent breakthrough predictions

	BLG			**ALA**		
Parameter	**Exp**	**El-Sayed**	***ExProSim:IC:IC***	**Exp**	**El-Sayed**	***ExProSim:IC:IC***
Q_{max} (mg/ml resin)	113	339	339	147	220.5	220.5
k_d (mg/ml)	0.008	4.8	4.8	0.029	0.029	0.029
k_1 (ml/mg.min)	0.035	0.035	0.035	0.030	0.030	0.030

Exp:Experimental, El-Sayed: El-Sayed and Chase simulations,
ExProSim:IC: Simulations from *ExProSim:IC*

at the predictive ability of *ExProSim:IC* for multicomponent systems and is shown in Table 3.8. It can be observed that the profiles obtained using *ExProSim:IC* show ≈5% error for most part of the breakthrough however, for 100% breakthrough point the error was high for *ExProSim:IC* simulations as well as for simulations from El-Sayed and Chase [1]. This can be due to slower diffusion of BLG and ALA which may not be captured by EDM due to lumped diffusion coefficient.

2. Immunoglobulin-G breakthrough

   H. Bak et al. studied the effect of varying inlet concentrations on the breakthrough profile [2]. Though binding of IgG with different resins have been

Table 3.8: Comparison of breakthrough curves for *Exprosim:IC* simulations with experimental data and simulation data from [1] for multicomponent breakthrough predictions

Protein	**BT%**	**Experimental**	**El-Sayed Simulations**	**% error**	***Exprosim:IC***	**% error**
BLG	0	66.06	68.2	-3.24	65.97	0.14
	10	69.65	74.36	-6.76	71.2	-2.23
	50	92.1	93.2	-1.19	91.6	0.54
	100	110.21	101.2	8.18	103.92	5.71
ALA	0	196.30	185.89	5.30	179.18	8.72
	10	272.45	246.67	9.46	258.45	5.14
	50	335.47	356.34	-6.22	332.53	0.88
	100	548.85	576.04	-4.95	576.73	-5.08

explored in the paper, this work describes the profiles for MabSelect resin. It can be observed in Figure 3.14 that, *ExProSim:IC* predicts the experimental profile better than lumped parameter model which is used in the paper. This is due to the fact that the lumped parameter model considers axial dispersion to be negligible whereas it is well accounted in *ExProSim:IC*. The input parameters from the paper were adjusted with an appropriate multiplier in order to fit the experimental data better. The adjusted parameters can be seen as in Table 3.9. The predictions were found to be consistent throughout the range of concentration from 20% to 100%. This shows that the simulations performed by *ExProSim:IC* is sensitive to change in concentration of the protein and shows consistent predictions.

Table 3.9: Adjusted model constants for prediction of breakthrough for IgG at varying inlet concentration

Parameter	**Experimental**	**multiplier**	**Modified value**
Q_{max} (mg/ml)	57.5	0.6	34.5
k_d (mg/ml)	3.0	0.5	1.5
k_1 (ml.mg/min)	0.0501	1	0.0501

3. BSA and Lysozyme breakthrough

   The case study was chosen to see how proteins of different sizes (lysozyme-14kDa and BSA-66 kDa) impact on the predictions using simple model such as EDM. Two proteins which are distant in molecular weights [3]. This is

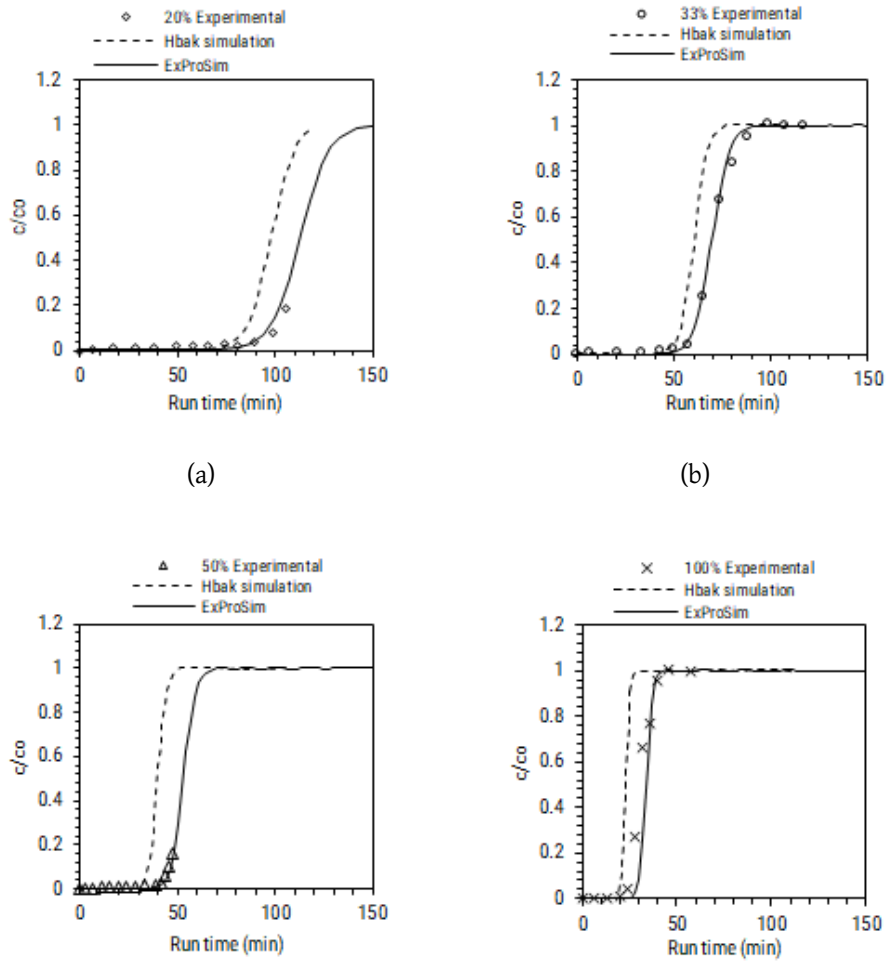

Figure 3.14: Prediction of breakthrough curves for IgG on MabSelect at different inlet concentrations showcasing the prediction accuracy for *ExProSim:IC*. '% Experimental' shows Rabbit IgG antiserum strength diluted in equilibration buffer

important to check, as the diffusion through resin is dependent on the size of the protein. Table 3.10 shows the modified parameters for simulation to fit the data to experiments. For lysozyme, very good fit was observed as shown in Figure 3.15(a), whereas for BSA (shown in Figure 3.15(b)) both the simulations were not able to predict the experimental data till saturation, though the breakthrough point was well predicted.

As both the models, kinetic model from the paper and *ExProSim:IC*: EDM show close predictions with a CoD of 0.9617 and 0.9845 respectively for lysozyme, it can be said that both were able to predict the lysozyme behaviour. Experiment for BSA shows the inability to reach saturation which was attributed to

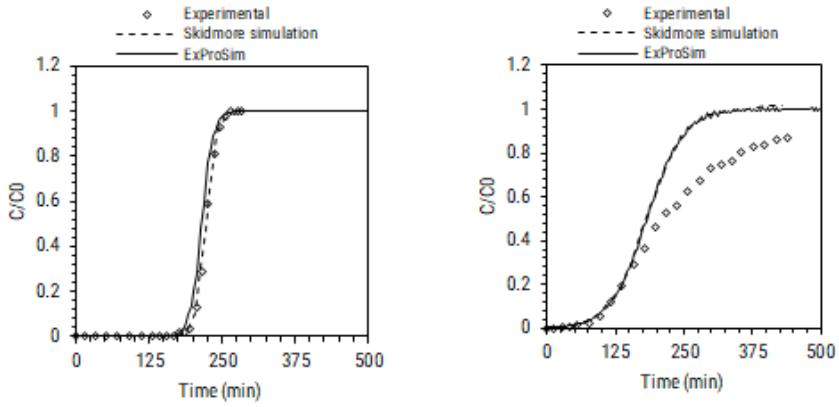

(a) (b)

Figure 3.15: Prediction of breakthrough curves for lysozyme (14 kDa) (a) and Bovine serum albumin (66kDa) (b) covering range of molecular weight proteins for the prediction validity for *ExProSim:IC*

multilayer adsorption of BSA. As EDM:Langmuir model in *ExProSim: IC* does not take into account the multilayer adsorption, it was not able to predict the BSA experimental profile. Even the kinetic model shown in the literature [3] could not predict the data well.

Table 3.10: Adjusted model constants for prediction of breakthrough for BSA and Lysozyme

Parameter	**Experimental**	**multiplier**	**Modified value**
	Lysozyme		
Q_{max} (mg/ml)	120	1	120
k_d (mg/ml)	0.019	1	0.019
k_1 (ml.mg/min)	0.0017	60	0.102
	BSA		
Q_{max} (mg/ml)	113	0.929	105
k_d (mg/ml)	0.133	0.2	0.0266
k_1 (ml.mg/min)	0.0005	60	0.030

3.5.3.2 EDM with SMA isotherm

First two breakthrough case studies for SMA validation are taken from the work of Karlsson et al. [4]. The work uses EDM with SMA to predict the breakthrough profiles for proteins such as Transferrin (80kDa) and Insulin (6kDa) which differ considerably in the molecular weights. Figure 3.16 shows the comparison of exper-

imental and simulated breakthroughs compared to *ExProSim:IC* predictions. The profiles were well predicted by *ExProSim:IC*. Slight variation in the simulation profiles was found due to use of Robin boundary conditions in the paper as compared to Dirichlet in *ExProSim:IC*. For Insulin, similar observation can be made where profiles till 50% of the breakthrough were predicted perfectly whereas slight variation was seen during the saturation of the curve. The modifications done in the input parameters are shown in Table 3.11

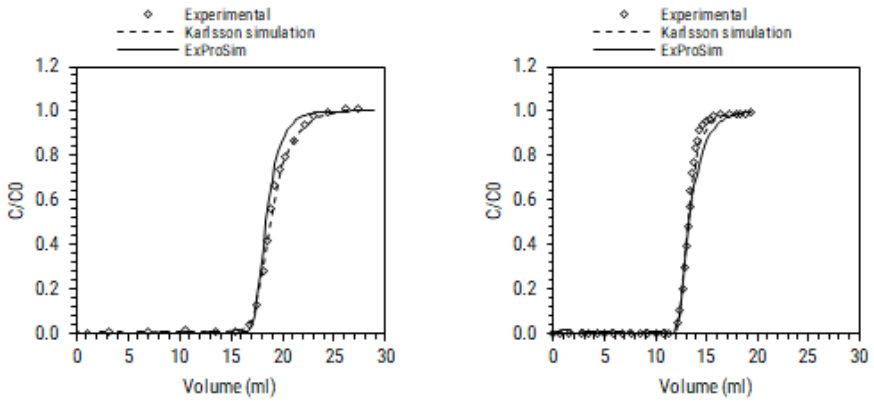

(a) (b)

Figure 3.16: Prediction of breakthrough for Transferrin (80kDa) (a) and Insulin (6kDa) (b) by using EDM and SMA isotherm.

Table 3.11: Modified model constants for prediction of breakthrough for Transferrin and Insulin

Parameter	**Experimental**	**multiplier**	**Modified value**
	Transferrin		
k_{eq}	190	0.5	95
v	5.2	0.385	2
σ	97	0.8	77.6
λ (mmol/ml)	2100	1	2100
	Insulin		
k_{eq}	0.54	10	5.4
v	2.5	1	2.5
σ	7.8	4.5	35.1
λ (mmol/ml)	2100	1	2100

Another literature case study chosen is cytochrome C (12kDa) on UNO S1 monolith column [5] to see if *ExProSim:IC* can predict the data for monolith column at

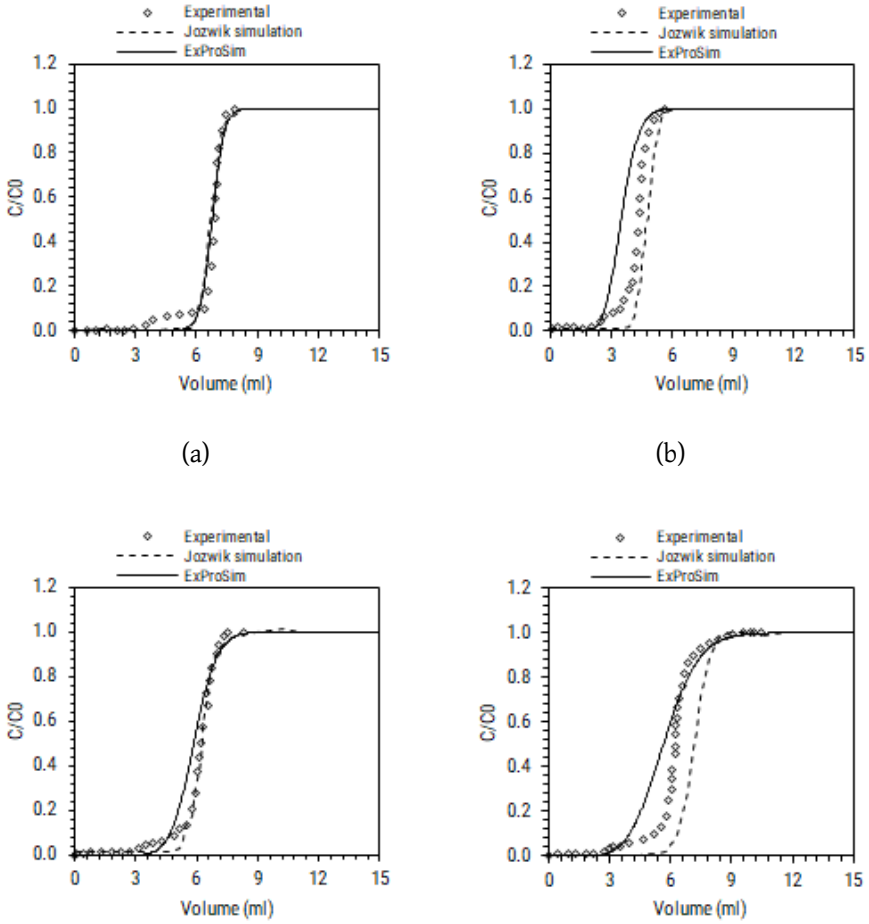

Figure 3.17: Prediction of breakthrough for cytochrome C (12kDa) by using EDM and SMA isotherm at different salt concentrations a) 120mM+0% salt b) 120mM +1% NaCl c) 120mM +3% NaCl d) 120mM + 5% salt

different mobile phase salt concentration.. It can be observed in Figure 3.17 that the breakthrough point was not predicted by both simulation datasets. The profile after the 10% breakthrough was predicted to accuracy of 0.9822 correlation coefficient using *ExProSim:IC*. This can give a precise idea about the binding and elution kinetics in the dynamic conditions at varying salt concentration. Experimental data was predicted more accurately by simulations from Jozwik et al. as the model used was a POR model which considers pore and surface diffusion interactions. The modifications in the parameters is given in Table 3.12

Table 3.12: Modified model constants for prediction of breakthrough for cytochrome C at changing salt concentration

Parameter	Experimental	multiplier	Modified value
k_{eq}	25.5	0.04	1.2
v	0.75	1	0.75
σ	4900	0.8	3920
λ (mmol/ml)	445	0.9	400.5

3.5.3.3 EDM with MPM isotherm

A work from Karlsson et al. was chosen in order to check if the tool can reproduce the experimental and simulation data for various protein molecules varying in chemical properties and molecular weights [4]. Breakthrough curves for all the proteins at 20 mM salt concentration are presented in the literature along with predictions using MPM and EDM models. Transferrin and Insulin breakthrough predictions using *ExProSim:IC* to the experimental and simulation breakthrough profiles to validate its usability have been demonstrated here. *ExProSim:IC* predicted the experimental as well as simulation profiles for both the proteins successfully with < 5% error at 0%, 10%, 50%, and 100% breakthrough points as can be seen in Figure 3.18(a) and Figure 3.18(b). This was achieved by modifying the model constants as shown in Table 3.13 in order to minimize the error between two curves. The simulations in the paper follows different boundary conditions as compared to *ExProSim:IC* (Robin condition instead of Dirichlet condition) which may reflect in different parameters being used to fit the same experimental curve effectively.

Table 3.13: Comparison of model constants from literature and modified model constants for *ExProSim:IC* simulations using EDM and MPM models for transferrin and insulin breakthrough prediction

Parameter	Transferrin			Insulin		
	Karlsson	Multiplier*	*ExProSim:IC***	Karlsson	Multiplier*	*ExProSim:IC**
Q_{max} (mol/m3)	0.770	1	0.770	57.2	1.4	80.08
k_{ads0} (m3/mol.sec)	10	0.2	2	0.0275	2	0.055
k_{des0} (m3/mol.sec)	4000	0.2	800	5	1	5
β	3.0	0.01	0.03	2.9	0.2	0.58
γ (m3/mol)	0	-	3	0	-	2
D_{ax} (m2/sec)	4.4 x 10-6	1	4.4 x 10-6	4.5 x 10-6	1	4.5 x 10-6

*ExProSim:IC***: model constants modified by a multiplier* used for *ExProSim:IC* simulations for the best fit

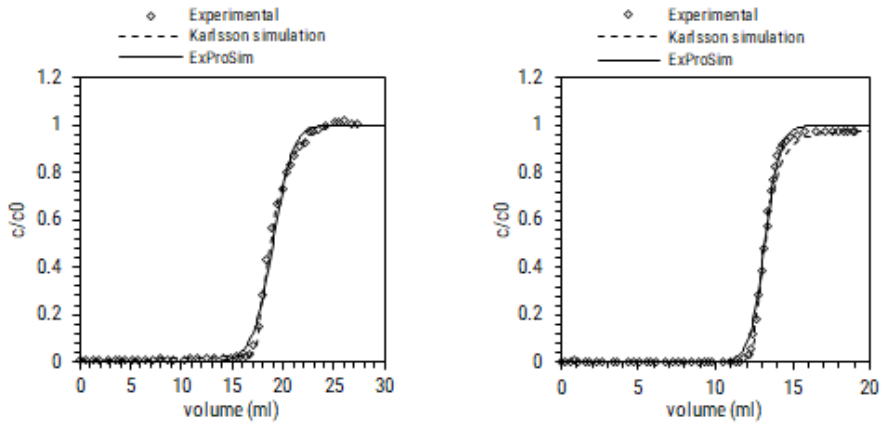

(a) (b)

Figure 3.18: Prediction of breakthrough for Transferrin (80kDa) (a) and Insulin (6kDa) (b) by using EDM and mpm isotherm.

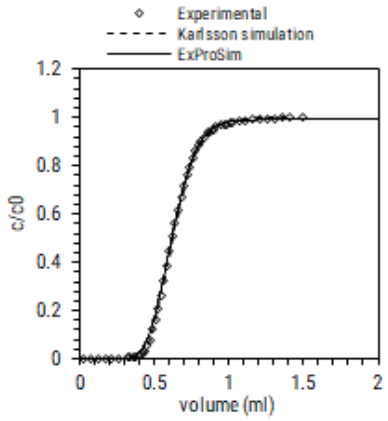

Figure 3.19: Prediction of breakthrough for IgG (150 kDa) (a) and Insulin (6kDa) (b) by using EDM and MPM isotherm.

Breakthrough curve for IgG was not given in this paper so another work by Karlsson et al. was considered further [6]. It describes the model based optimisation for preparative separation of IgG by using a simulation approach which uses EDM, MPM, and particle diffusion model. Breakthrough at high flow rate was performed for IgG which was further predicted by *ExProSim:IC* and compared here. The change in parameters are as shown in Table 3.14. It is often the case that high velocity experiments are more convection driven and are difficult to match by simulations. The comparison of *ExProSim:IC* predicted breakthrough curves to the literature data is shown in Figure 3.19. It can be said that it predicted the experimental and simulation profiles quite effectively. The predictions obtained

Table 3.14: Comparison of literature and modified model constants for *ExProSim:IC* simulations for IgG

Parameter	**IgG**		
	Karlsson	Multiplier	*ExProSim:IC***
Q_{max} (mol/m3)	1.1	1	1.1
k_{ads0} (m3/mol.sec)	0.065	0.2	0.0130
k_{des0} (m3/kmol.sec)	50	0.2	10
β	1.12	0.1	0.112
γ (m3/mol)	0	-	0
D_{ax} (m2/sec)	4.4 x 10-6	1	4.4 x 10-6

ExProSim:IC: model constants modified by a multiplier used for *ExProSim:IC* simulations for the best fit

were equally effective as the simulations from the literature and provided comparatively simpler simulation approach to the problem.

3.6 Conclusion

The chapter provides a detailed summary of computational, data analysis, and experimental philosophies practised throughout this work. Initially models implemented in this work are discussed in detail. Experimental methodology which is used for estimation of model constants is discussed further. Overview of experimental methods for separation of major and minor whey proteins was given, however, specific details were discussed in respective chapters. *ExProSim:IC* was introduced along with description of various aspects such as coding methodology, parameter estimation module, tool verification, mesh independence, and experimental validation.

Tool verification was specifically performed to understand how the simulation profiles vary with respect to model constants. It was realised that Langmuir isotherm parameters follow an expected trend according to their physical significance. Variation in Q_{max} affected the binding capacity and k_1 affected the slope and binding capacity of the protein. k_d impacted on both slope and binding capacity as it defines the equilibrium of the process. In case of SMA, variation in charge factor, v was found very critical. Minor changes in v led to large variation in location and shape of the curve. The equilibrium constant, k_{eq} showed similar

behaviour as that of Langmuir k_d value. Steric hindrance showed inverse relation to the binding capacity as expected. For MPM, β showed a high sensitivity as compared to other parameters and influenced binding capacity. Adsorption and desorption constants showed similar behaviour to that of Langmuir model rate constants, however, variation in slope of the curves is expected when the constants k_{ads}^m and k_{des}^m are varied. It was important to note that all these relations were not linear and were reliant highly on variation in the model constants. Also the variation studies were performed one factor at a time where rest of the model constants were kept at optimised values when one was varied on three levels. Even though this exercise gives a fair estimate of how individual constants affect the breakthrough curve, it can be tricky to gauge the effect when more than one factors are varied together. However, these insights are used further in the literature based validation and in experimental validation later.

Further, a comparison with CADET simulations showed that the accuracy of simulations for preliminary simulations were not good (CoD<0.9). Lessons from model constants assessment section were applied further to change the parameters for a better fit. Modifications performed in the model constants were able to match the CADET simulation data well. As the modifications were performed on trial and error basis, it might take a long time to obtain the best fit. Mesh independence studies carried out for the tool ensured that it gives a convergent solution. Mesh independency can be case specific hence it is important to practise for every system under consideration.

Literature based validation was carried further by choosing the case studies to check the effect of varying process parameters on the prediction ability of *ExProSim:IC*. The tool establishes a reasonable accuracy with changing process conditions and for various protein molecules ranging from 6kDa to 150kDa. 'Curve to curve' error were determined using RMSE and CoD, however they were not efficient enough to give accurate comparison between experiments and simulations. Method of 'point to point' comparison was practised instead where important experimental points were selected and the error was determined for them. Data reproduced for all the thermodynamic models showed good agreement (average error<5$\%$) with the simulations and experimental data from the respective litera-

ture. It is thus can be concluded here that mathematical models were successfully incorporated in a tool, *ExProSim:IC* for predicting the outcomes of the data from the literature.

Furthermore, it is important to look at limitations at this stage of research. It is very difficult to mimic the non-equilibrium interactions in the real process while determining the model constants from equilibrium assumptions and models. Not all the parameters can be directly derived from the experiments and some of them need mathematical approximations based on physical assumptions. This was seen when, parameters were to be adjusted for matching the simulations to the experimental data. Choice of EDM looked appropriate as there are lesser parameters which are empirically derived, however it also comes at a cost of overlooking detailed diffusion phenomena happening in the resin. Such diffusion considerations can be critical while scale up of the process as scale dependent parameters may be left out without adjustment. This makes EDM not an ideal choice for simulations of development data at large scales. In the subsequent chapters experimental validation is presented where more data based conclusions can be derived on the applicability of EDM.

Chapter 4

Major whey proteins separation

4.1 Introduction

Most important aspect to consider before implementation of a simulation tool is its reliability and robustness. For achieving these criteria, it is important to exhaustively validate the tool. Literature based validation of *ExProSim:IC* with variations in process parameters specific to thermodynamic models is discussed in Chapter 3 . However, literature based validation can be limiting in developing an understanding about, how the model constants were determined from experiments performed and their further implementation. Even if the code is working fine mathematically, the results produced can be questionable if the model constants aren't well determined. Hence, it was decided to perform in house experiments to find out model constants. This ensured availability of reliable data for validation. Overall experimental validation is divided into three chapters. Experiments performed on separation of major whey proteins and their simulation is covered in this chapter. The chapter discusses implementation of both anion and cation exchange chromatography techniques by experimental and simulations, and compares them with each other to find out which one is more advantageous. [1]

[1] It is important to note that, extensive resin screening was not included in the scope of the research. Choice of the resin was completely based on the popularity of the resin in the current industries, based on their performance, and usage.

4.2 Methodology

4.2.1 Experimental

4.2.1.1 Materials and Methodology

All the protein standards and buffers required for cation and anion exchange chromatography and sample analysis are mentioned in Section 3.3.1. For cation exchange at pH 4.5, BSA and BLG were used as standards and resin chosen was SPFF^{TM}. For anion exchange at pH 6.9, BSA, BLG, and ALA were used as standards and Capto Q^{TM} was used as resin. Column chromatography experiments were performed on NGC Bio-Rad system. SEC was used for analysis of cation exchange samples, however HPLC was used for analysis of anion exchange samples. Details of the methodologies for sample analysis are explained in Section 3.3.2.

Buffers and protein samples

Buffers used for cation and anion exchange chromatography are shown in Table 4.1. 1 M NaOH was used for regeneration of the resin after the run and it was stored in 20% ethanol when not in use. Standard curves were prepared for all the proteins by taking absorbance at 280 ηm for concentrations between 0-1 mg/ml on a UV-vis spectrophotometer, Jasco V-670. After experiments in triplicates (except for breakthrough), mean values and standard deviation were determined for further analysis.

Table 4.1: Overview of experimental systems

Technique	System	Buffer A	Buffer B
Cation exchange	NGC medium pressure system	10 mM sodium acetate pH 4.5	1 M NaCl in 10 mM sodium acetate pH 4.5
Anion Exchange	NGC medium pressure system	25 mM sodium phosphate pH 6.9	1 M NaCl in 25 mM sodium phosphate pH 6.9
SEC-HPLC	Varian ProStar HPLC sysetm	10 mM sodium acetate pH 4.5	10 mM sodium acetate pH 4.5
HPLC	Agilent 1260 HPLC system	0.1% TFA in 100% purified water	0.1% TFA in 100% acetonitrile

Sample analysis

UV-vis spectrophotometry All the samples from batch studies for adsorption kinetics and uptake kinetics were analysed on a UV spectrophotometer. Standard curve was prepared for the proteins ranging from 0-1 mg/ml concentrations in order to find out the concentration for the unknown samples. Samples from the experiments were diluted so as to keep the absorbance below 1.0 to meet to the linear equation of the standard curve.

SEC-HPLC For cation exchange chromatography with two proteins BSA and BLG, the column was equilibrated with 10 mM sodium acetate buffer at pH 4.5 till a stable baseline was achieved. Initially a mixture of standards was run at different flow rates in order to optimise flow rate to achieve faster and resolved peak separation. Then the standard curve was prepared for injecting known concentration of mixtures at optimised flow rate.

HPLC In case of anion exchange, it was impossible to resolve ALA and BLG using SEC-HPLC as they have very minute difference in their molecular weights (Table 2.2). Hence, alternative HPLC method was developed by injecting a mixture of all the whey proteins (BSA, BLG, ALA, LF, and LP; 1 mg/ml each in equal amounts). Mobile phases used are as given in Table 4.1. Initially baseline was achieved for the column with buffer A. Optimisation of gradient was done for getting maximum resolution possible between proteins from crude whey. This was called as *HPLC method 2*. Furthermore, once the method was optimised, standards of each proteins (ranging in 0-1 mg/ml) were injected at different concentrations to determine the standard curve for the proteins. Multicomponent breakthrough samples were analysed and individual protein concentrations were determined from the standard curves. Injection volume for all the runs was 100μl. It was decided not to perform SDS-PAGE if the standards are pure enough for the adsorption studies.

Chromatography experiments

Adsorption isotherm experiment For cation exchange adsorption equilibrium, experiments were carried out for SPFF resin as given in Section 3.3.3.1. Protein load was (BLG and BSA) 3-8 mg/ml. Similar experiments were repeated for Capto Q for anion exchange chromatography for all three major whey proteins. All the constants (Q_{max} and k_d for Langmuir, Q_f and n for Freundlich) in the isotherm models were determined.

Uptake kinetics 4 mg/ml of each protein solutions were used for the uptake kinetics experiment as given in Section 3.3.3.2. Experiments were carried out for both SPFF and Capto Q. pseudo first order and pseudo second order models were checked for the best kinetic fit. Method for estimation of parameters has been given in Section 3.4.1. Uptake kinetics constant k^l_{ads} was found out from the best fit.

Column physical parameters Column physical parameters for both columns, HiTrap SPFF and HiTrap Capto Q were determined by methods mentioned in Section 3.3.5. These include porosity ($\epsilon_e, \epsilon_p, \epsilon_t$), column asymmetry factor, HETP, NTU, dead volume (v_0), molecular diffusivity, diffusion coefficient, and ionic capacity.

Gradient elution experiments Detailed method for gradient elution is described in Section 3.3.4.1. For cation exchange chromatography, 3 mg/ml solutions of both BSA and BLG were prepared in buffer. For anion exchange chromatography, 3 mg/ml solutions of all the proteins were prepared in equilibration buffer. Injection volume was set to 400 μl. Equation 3.23 was used to estimate v_i and $k_{eq,i}$ for SMA isotherm.

Breakthrough experiments Breakthrough experiments of BSA, ALA, and BLG were carried out as per the procedure given in Section 3.3.4.2. at similar conditions that of gradient experiments. For cation exchange experiments, both protein samples were continuously loaded at 3 mg/ml concentration until the exhaustion point of the curve was achieved. Breakthrough was performed at 0.5 ml/min and 1 ml/min for BSA, and 0.4 ml/min and 1 ml/min for BLG. For anion exchange experiments, breakthrough was performed by loading 3 mg/ml BLG, 2

mg/ml ALA, and 1.5 mg/ml of BSA at 0.5 and 1 ml/min flow rates till the column was saturated with the respective proteins.

For multicomponent breakthrough studies on cation exchange columns, BSA and BLG 3 mg/ml each were mixed in 100 ml buffer. The mixture was loaded continuously at 1 ml/min till the column was saturated. Multicomponent breakthrough for anion exchange was performed by loading a mixture of all acidic proteins (2 mg/ml each) at 0.5 ml/min till the column reaches saturation. All the fractions were collected in 1 ml volumes and then further analysed to find out individual breakthrough curves. Injection volume for analysis runs was 20μl.

Determination of Model parameters

Langmuir parameters Q_{max} and k_d were determined from inverse fitting the data of the adsorption isotherm to Equation 3.8. Uptake kinetics rate constant was determined by fitting both pseudo first order (Equation 3.39) and pseudo second order equations (Equation 3.40) to the uptake kinetics data obtained. MPM constants (k_{ads0}, k_{des0}, γ, and β) were determined by inverse fitting the adsorption isotherm data to Equation 3.19. SMA parameter σ_i was determined from the breakthrough curves (Equation 3.24), whereas values of charge factor and equilibrium dissociation constant were determined from gradient elution experiments (Equation 3.24). Inverse fitting was performed for minimisation of error function from Equation 3.38. The parameters were used as it is or modified into *ExProSim:IC* for simulating the breakthrough curves. If the error with respect to experiments was found to be more than $\pm 5\%$, model constants were revised logically depending on the error obtained and the simulations were repeated until an acceptable fit was obtained. Detailed computational methodology implemented for simulations and data analysis is given in Chapter 3.

4.3 Results and Discussions

Current Section discusses the results from the experiments carried out for cation and anion exchange chromatography along with estimation of model parameters, their importance in binding and elution kinetics, followed by comparison with the

simulation of breakthrough curves using *ExProSim:IC*. For cation exchange chromatography, where adsorbent is negatively charged, protein has to be positively charged. For protein to have a positive charge, the pH of the solution should be lower than the isoelectric point of the protein. For cation exchange chromatography initial batch binding experiments were performed at pH 3.5 to 4.2 to keep positive charge on all the proteins. It was observed that at such lower pH, elution of BLG and BSA was not eluted completely with strong elution buffers such as 1 M sodium chloride. Hence pH was further increased to 4.5. As the isoelectric point of ALA is 4.2, at pH 4.5 the protein has negative charge which is not suitable for cation exchange chromatography. Binding of ALA on cation exchange resin was checked at pH 4.5 and high losses of protein was found in batch studies showing very low binding capacity and strength. Taking this into account, cation exchange was studied for BSA and BLG. On the other hand anion exchange chromatography features all the proteins as they showed complete elution at pH 6.9.

4.3.1 Sample analysis

4.3.1.1 UV-spectrophotometer

Standard curves plotted for the standard protein samples are as shown in Figure 4.1. The regression coefficient was found to be more than 0.99 for all the standard curves supporting an acceptable linear fit. Corresponding equations for the fit are displayed in the Figures which were used for estimation of unknown protein samples from batch adsorption studies.

4.3.1.2 SEC-HPLC

HPLC-SEC was used to exploit the difference in the molecular weights of BSA and BLG to find out the individual fractions in the combined breakthrough curve. Flow rate 0.5 ml/min was chosen for processing the samples as the peaks showed maximum possible separability. As expected, BSA was eluted first followed by BLG. Complete resolution between the proteins was difficult to achieve as dimeric form of BLG is prevalent at pH 4.5 [236]. This can be seen in Figure 4.2. Hence, the peak areas were not directly used to get the concentrations from the standard curves.

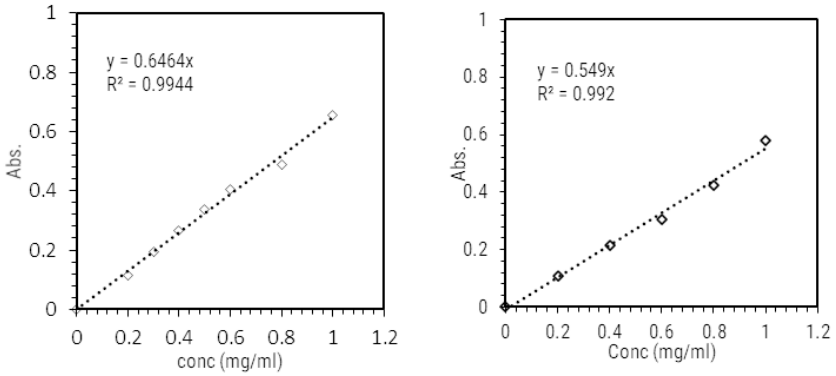

(a) (b)

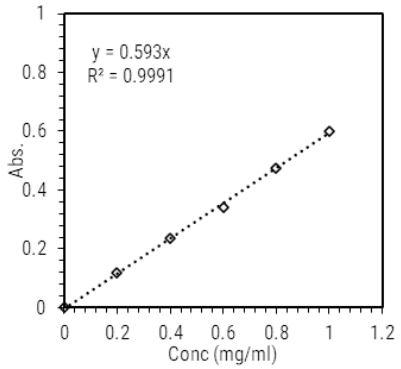

(c)

Figure 4.1: Standard curves on UV spectrophotometer at 280 nm for BSA (a), BLG (b), and ALA (c)

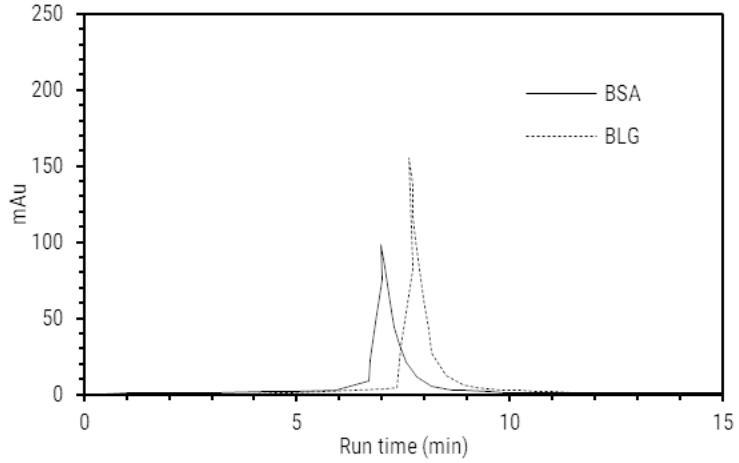

Figure 4.2: Overlay of BSA and BLG chromatograms from SEC-HPLC showing the overlapping area

Calibration method from work of El-Sayed and Chase was used further to get the calibration curves [188]. Several protein mixtures with different proportions

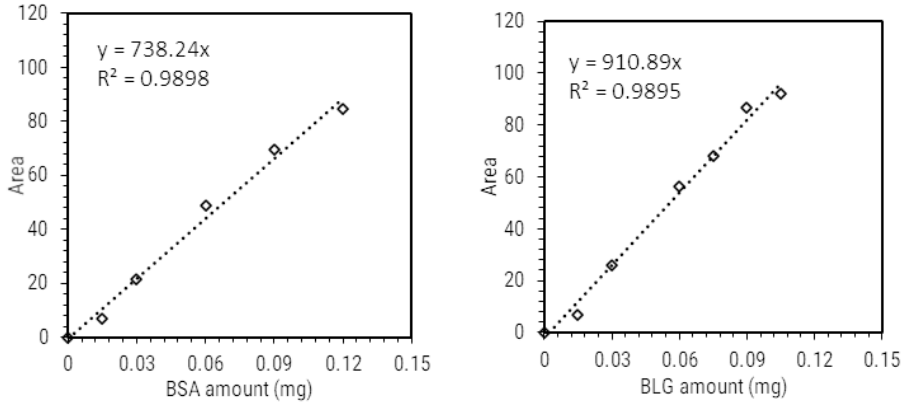

(a) (b)

Figure 4.3: SEC-HPLC standard curves for BSA (a) and BLG (b)

of BSA and BLG were run on the column. For all the samples run, total protein loaded and concentration of individual proteins were known. The area of mixture was plotted against the individual concentrations in the mixture as shown in Fig. 4.3. The curves show linearly increasing profile with regression values of 0.99 for both BSA and BLG. Equation 4.1 and 4.2 were used to find individual concentrations in the unknown mixtures.

$$c_{BSA} = \frac{A_{tot} - S_{BLG}C_{tot}}{S_{BSA} - S_{BLG}} \tag{4.1}$$

$$c_{BLG} = \frac{A_{tot} - S_{BSA}C_{tot}}{S_{BSA} - S_{BLG}} \tag{4.2}$$

4.3.1.3 HPLC

Optimised method is shown in Table 4.2. Standard curves of the proteins were estimated by injecting varying concentrations of standard proteins. Clear resolution was obtained for all the protein except BSA and ALA. hence flow rate was lowered at 39% buffer B to further resolve ALA and BSA. Figure 4.5 shows the standard curves obtained for BSA, BLG, and ALA. The curves show linearly increasing profiles with regression coefficient more than 0.99, supporting a linear fit. Though the hplc method was developed for all five whey protein resolutions, mixture of major proteins is shown here in Figure 4.4. It can be observed that the peak for

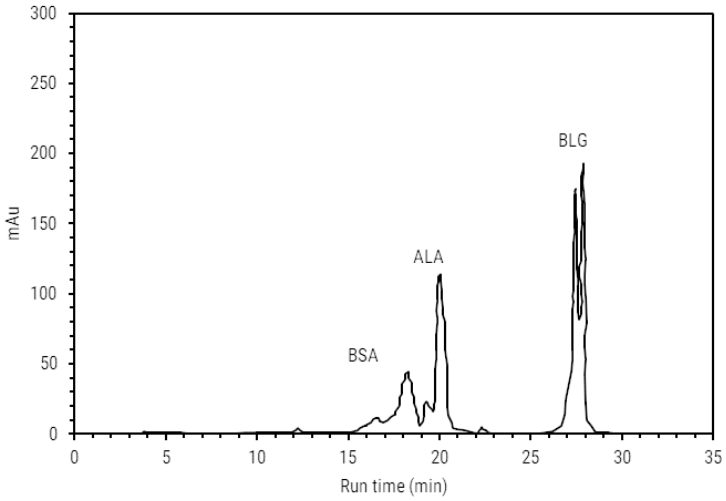

Figure 4.4: HPLC chromatogram for ALA, BSA, and BLG analysis

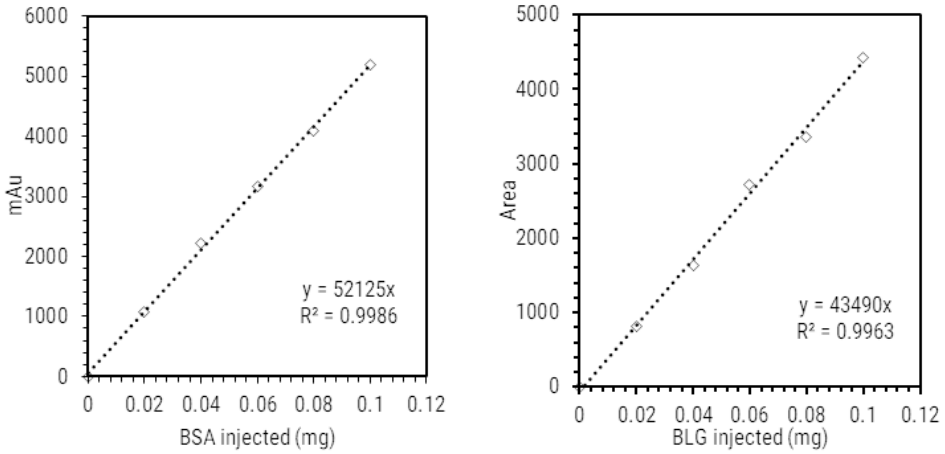

(a) (b)

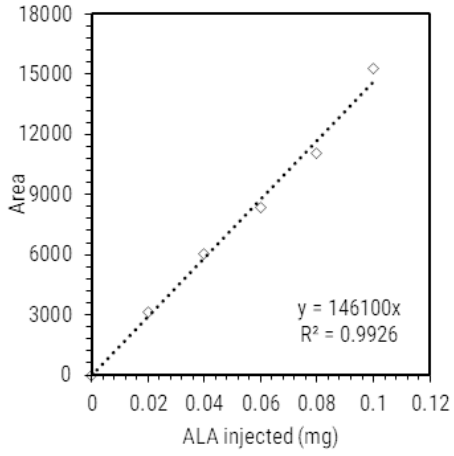

(c)

Figure 4.5: Standard curves for major whey proteins by HPLC *method 2*, BSA (a), BLG (b), and ALA (c)

Table 4.2: HPLC method optimised for resolution of five whey proteins, BSA, BLG, ALA, LF, and LP

Time (min)	%B	Flow rate (ml/min)
0	0	1
2	0	1
4	39	1
11.5	39	1
12	39	0.5
20	41	0.5
20.5	41	1
24	46	1
32	70	1
34	100	1
38	100	1
39	0	1
44	0	

BLG shows a dual peak in Figure 4.4. This was attributed to presence of two isoforms of BLG which differ in their Ala/Val contents[237]. The first isoform has 13 Ala and 12 Val, whereas second isoform has 12 Ala and 13 Val [238]. Separation of these isoforms was not attempted further as that was not the primary goal of this thesis. Standard curves were used further to calculate individual proteins from the multicomponent breakthrough mixture and is discussed later in the chapter. SDS-PAGE was not performed as the standards were pure enough to proceed for adsorption studies.

Further discussions on the results obtained is categorised by chromatography type and discussed with respect to the isotherm parameter determination those results were used for. Initially cation exchange chromatography is discussed followed by anion exchange. At the end of the chapter they are compared for their suitability in separation of major proteins.

4.3.2 Cation exchange chromatography

4.3.2.1 Determination of Langmuir parameters

Adsorption isotherm

Table 4.3 summarises the adsorption characteristics of BSA and BLG. In order to check which basic isotherm describes the data well, Langmuir, SMA, MPM and Freundlich were fitted to the experimental data as shown in the Fig. 4.6. The values of regression coefficients for Langmuir isotherm suggested a better fit to both the experimental data as compared to others. Furthermore, the value of Langmuirian equilibrium constant or separation factor, R_L lay between 0 and 1 for entire range of concentrations indicating reversible binding [239] which is favourable for chromatographic interactions [240].

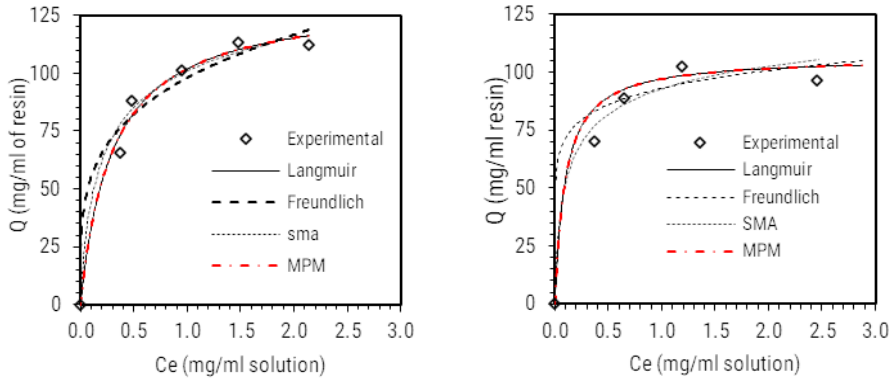

(a) (b)

Figure 4.6: Adsorption isotherms for BSA (a) and BLG (b) on SPFF^{TM} for fitting three isotherms ; Langmuir (—), Freundlich (- - -), SMA (··), and MPM (-··-)

For any globular protein, a thumb rule of surface distribution is 45% hydrophobic patches to remaining 55% ionic or hydrophilic patches. Distribution of these surfaces is interpreted in terms of protein folding suggesting that none of the chromatography techniques are purely based on a single principle such as; ion exchange, affinity, or hydrophobic interactions. There is always a combination of multiple interactions which causes the adsorption; however, one of the interaction principles dominates the binding making it a preliminary cause. From the calculation of Gibb's free energy of interaction, each such secondary interaction

Table 4.3: Summary of adsorption parameters for BSA and BLG

Parameter	**BSA**	**BLG**
Langmuir model		
Adsorption capacity Q_m (mg/ml of resin)	132.51	106.72
Dissociation constant k_d, ($\times 10^{-6}$M)	4.56	6.065
$k_{des,L}$*, ($\times 10^{-3}$ min^{-}1)	0.517	1.88
R_L at 3 mg/ml	0.5078	0.293
R_L at 8 mg/ml	0.3066	0.158
R^2	0.981	0.9875
Freundlich model		
Adsorption capacity Q_f (mg/ml of resin)	97.35	92.98
Adsorption intensity, n	3.610	8.764
Inverse of adsorption intensity, 1/n	0.277	0.1176
R^2	0.829	0.9401
MPM Langmuir model		
Q_{max} (mg/ml of resin)	132.4	106.4
k_{ads0} (ml/mg.min)	0.9455	0.2163
k_{des0} (ml/mg.ml)	0.4515	0.037
β	0.1011	0.1233
$\gamma(\times 10^{-1})$	0.951	2.163
R^2	0.9901	0.989

R_L: Langmuirian equilibrium constant,

is said to contribute around 1 kcal/mol of energy of interaction and a k_d value of 10^{-5} M gives binding energy of 7 kcal/mol in standard conditions which can prove to be sufficient for a sustainable binding [241]. The values of k_d for affinity chromatography processes lie between 10^{-8} M and 10^{-4} M [242]. Similarly for a sustained adsorption and desorption in ion exchange chromatography, the values of k_d can be assumed to lie in the same range. If the value is outside this range, it either indicates very strong or weak binding which is not suitable for chromatographic interactions. Ideally, the binding should be strong enough to retain the target protein on the resin but also be reversible enough to release the protein

during elution without application of very harsh elution conditions which may affect protein of interest. The values of k_d obtained for BSA and BLG lie within the permissible range suggesting the suitability of chromatographic process. It can be observed that the value of k_d for BLG is higher than that for BSA showing faster desorption for BLG as compared to BSA.

For Q_{max}, it is reasonable to expect value for BSA to be lower than for BLG as the net charge on BSA is smaller than the net charge on BLG due to its high electrophoretic mobility. Surprisingly, Q_{max} value was found to be higher for BSA. This might be due to non-uniform charge distribution on the surface of BSA and comparatively higher exposure of highly hydrophobic patches in case of BSA. Jeyachandran et al [243] have studied conformational changes in the protein molecule during adsorption and have shown that the hydrophobic patches influence the binding of BSA. 50% of hydrophobic patches showed influence on the binding of BSA due to conformational changes in the protein molecule upon adsorption. Effect of resin matrix on the binding of the protein is worth understanding further. Base matrix of SPFF™ is hydrophilic agarose (6% by volume). Molecules like BSA which have a tendency to change conformation when adsorbed on a solid hydrophilic surface leading to conversion of α helices into β sheets exposing more hydrophobic patches on the surface [244]. Increase in hydrophobicity at the surface promotes protein-protein binding reflecting in apparent binding capacity of BSA. Furthermore, not only the conformation but also the orientation of binding seem to play a role in binding capacity. BSA can also have different orientation while binding depending on the pH and salt concentration of the medium, affecting and changing the binding capacity [245]. It was also found in another article that the binding orientation can also be a function of concentration of BSA [244]. The Q_{max} value of BSA here further suggests that the binding can be a multilayer binding which may not be exactly predicted by Langmuir isotherm. On the other hand the BLG which has higher charge as compared to BSA, can be assumed to be under the strong electrostatic interaction between hydrophilic resin surface and ionic groups on the protein [246]. This is in support to the fact that under ionic or charged state, proteins tend to retain their structure which prevents unfolding [247]. BSA adsorption is generally limited to monolayer below 10 mg/ml concen-

tration for an exposure time of 2 hours [248]. BSA molecules have a tendency of crowding, upon longer exposure leading to undergo conformational changes. Due to considerably high molecular size and mostly surface diffusion due to competitive adsorption with BLG, multimeric structures of BSA can get formed showing an apparent maximum binding capacity. Moreover, the secondary structure of protein tends to hide the polar surfaces while exposing the hydrophobic patches on outer surface which is further involved in direct resin-protein along with protein-protein interaction [249]. If the values of Q_{max} are estimated in molar terms, it can be observed that the value for BLG is much higher than that of BSA (BSA: 2.02×10^{-3} and BLG: 6.66×10^{-3}). This suggests that the overall occupancy on the resin of BLG molecules is much higher than BSA. This is self explanatory as the molecular size of BSA is much higher than that of BLG. Value of k_d for BLG was found to be higher than BSA showing lower ionic binding strength as compared to BSA. This is also reflected in Q_{max}.

Uptake kinetics

The uptake kinetics signifies the rate of adsorption of a protein. Equations 3.39 and 3.40 represent the pseudo first order kinetic model and pseudo second order kinetic model respectively. To ensure usage of these models over film, pore and

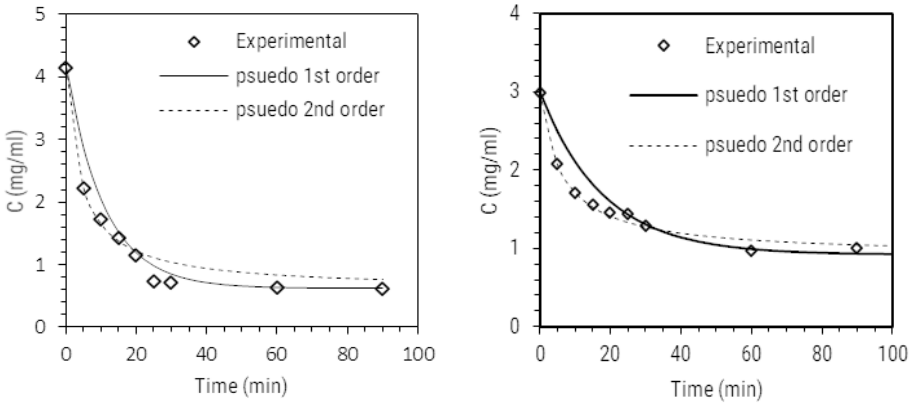

(a) (b)

Figure 4.7: Uptake kinetics comparison for BSA and BLG. a) Comparison of pseudo 1^{st} order and pseudo 2^{nd} order for BSA b) Comparison of pseudo 1^{st} order and pseudo 2^{nd} order for BLG

surface diffusion models, molecular size of protein was compared with the pore

size of the resin. The resin exclusion limit is 4000 kDa which translates into pore size of 500-1000$\mathring{A}$. The radius of protein of size of BSA and BLG were estimated to be 25.57 $\mathring{A}$ and 16.57 $\mathring{A}$ by using Equation 4.3 [250].

$$r_{min} = 0.066M^{1/3} \tag{4.3}$$

As it can be clearly noticed that sizes of proteins in discussion (BSA 66 kDa and BLG 16 kDa) are very small as compared to the pore size of the macro porous resin under consideration. This shows that pore diffusion may contribute in mass transfer. However, it was decided to ignore it for this work to see if more simplistic and basic models can predict the experimental data.

Table 4.4: Analysis of uptake kinetics

Parameter	**BSA**	**BLG**
Pseudo first order		
k_1 ($\times 10^{-2}$) (min-1)	9.19	5.68
R^2	0.969	0.759
Correlation Coefficient	0.9847	0.872
Pseudo second order		
k_2 ($\times 10^{-3}$) (ml/mg.min)	1.36	1.51
R^2	0.9837	0.9872
Correlation Coefficient	0.9918	0.9936

Fig. 4.7 shows the model fitting for uptake kinetics along with the experimental data. The representative parameters for the same are shown in Table 4.4. It has been proved experimentally that pseudo first order kinetics supports physical adsorption and second order kinetics indicates chemical adsorption. As in case of chemical adsorption, the strength of the bonds is highest between the surface and the protein molecules, once the monolayer is occupied, the adsorption at the second layer is not promoted. This monolayer adsorption is well described by Langmuir isotherm. For first order kinetics, where physical forces are involved in adsorption, multimeric adsorption mechanism can be seen. This is also reflected from the equation for pseudo first order kinetics which has exponential term. It

can be seen that the pseudo second order kinetics fits the kinetic data better (better regression coefficient and correlations coefficient).

As shown in Table 4.4, it can be observed that for pseudo second order kinetics, uptake kinetic constants for BSA and BLG show almost same values. Value of uptake kinetic constant depends on diffusivity of the protein in the medium, accessibility for number of molecules to the surface, and charge interactions [251]. Molecular diffusivity is a characteristic of molecular size as mentioned earlier. When two molecules have same kinetic constant, number of factors can be considered. First being, they have same molecular diffusivity (same molecular radius) and secondly they have equivalent access to the surface available in order to react or bind to the surface [252]. As it is known that BSA (66 kDa) is a bigger molecule as compared to BLG dimer (36 kDa), the diffusivity for BLG is higher than BSA at both the surfaces and internal pores. The value of k_2 represents a lumped kinetic constant for both surface and internal pores, hence it is not a surprise that the values are closer. This means that accessibility for both the molecules is close. It also suggest that more number of BLG molecules are interacting with the surface in order to occupy equivalent surface as BSA. Higher accessibility of the surface due to higher diffusivity can also mean uptake of one protein by displacement of the other, however further inference about displacement can be drawn when two molecules compete for adsorption later in this chapter. Even though pseudo 1^{st} order shows a good fit, it is an exponential function and its use directs to multimeric form of a BSA getting adsorbed or a multilayer adsorption which can be confirmed by breakthrough studies further. It is well known that multilayer or multimeric adsorption is not predicted well by Langmuir isotherm [253].

4.3.2.2 Determination of MPM parameters

As MPM model is derived from Langmuir model, the parameters were found to be analogous to Langmuir. Binding capacity values were closer to Langmuir isotherm. Parameters k_{ads0} and k_{des0} describe the rate of adsorption and desorption of the protein respectively. Adsorption rate constant was found to be higher for BSA and compared to BLG as additional hydrophobic interactions might be helping in adsorption. Whilst comparing the values of k_{des}^{m}, it was realised that the desorp-

tion is higher for BSA. This can be attributed to hydrophobicity of BSA interfering in the strength of ionic interactions. Molar k_{dmpm} values were calculated to be 5.73×10^{-6} M and 5.05×10^{-6} M respectively for BSA and BLG which were found comparable to k_d values estimated from Langmuir isotherm. Value of β represents an extent of ionic interactions happening during the protein binding. This can be interpreted as, higher the value of β, stronger is the interaction of the protein with the matrix. BLG shows higher β value than BSA which can be an effect of the electrophoretic mobility.

4.3.2.3 Determination of SMA parameters

Column physical parameters

Based on moment analysis of the pulse injections, external porosity of the column was determined to 0.363 ± 0.024 whereas the particle porosity was estimated to be 0.880 ± 0.018. Total porosity for column was determined to be 0.923 ± 0.012. Column packing showed asymmetry factor of 1.12 (acceptable criteria is 0.8-1.2). Height equivalent to theoretical plates was found to be 0.00131 cm and net transfer units were observed to be 1315.69. Asymmetry of the column was 1.16 which was acceptable. Ionic capacity was determined to be 2345.7 ± 20.32 mM/ml resin which compares to the reported value for SP sepharose from GE is 1800-2400 mM/ml resin [254].

Gradient elution

The values of retention volume and gradient volumes were used in Equation 3.23 and parameters for different gradient lengths were obtained. Table B.1 shows the summary of gradient runs and Figure 4.8 shows the gradient runs. It can be seen that the retention volume increases with decrease in the slope of gradient during elution. Retention time was observed to move forward as well due to slower change in the salt concentration.

When the gradients of 0-100$\%$ were run, it was observed that BSA and BLG eluted at 21$\%$ and 68$\%$ of the salt concentration respectively. This supports slow desorption of BSA. Table 4.5 shows the comparison of SMA parameters obtained from experiments. In the fitted parameters, both proteins show significant dif-

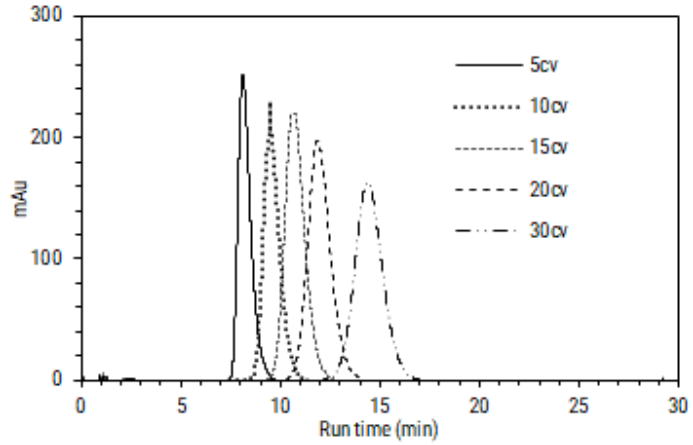

(a)

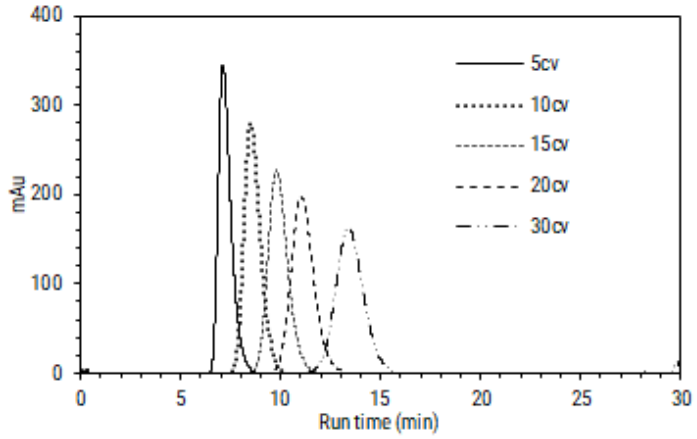

(b)

Figure 4.8: Comparison of elution profiles for (a) BSA and (b) BLG at different gradient lengths

ference in charge and equilibrium constant values. As the charge value defines the number of salt ions being displaced by a protein molecule in order to adsorb onto the resin, double the charge value along with $\frac{1}{9}$th equilibrium constant suggests stronger adsorption for BLG as compared to BSA. Conversely, BSA was eluted later than BLG showing slower desorption. Steric hindrance factor is a property influenced by molecular weight of protein which can cause screening of charges available for exchange. BSA having higher σ value emphasizes on this concept. Similar trend is seen in parameters determined from empirical equations.

The values differed considerably from those which were derived by inverse curve fitting method. The reason can be, difference of interactions between static to dynamic studies. Parameters found from experiments were less than those ob-

Table 4.5: Comparison of SMA isotherm parameters for BSA and BLG from gradient experiments and isotherm fitting

Protein	Method	v	k_{eq}	σ
BSA	Exp	1.349$\pm$0.093	0.5166$\pm$0.075	2.475$\pm$0.292
	Fit	2.176	0.914	12.415
BLG	Exp	1.45$\pm$0.106	0.0776$\pm$0.0121	1.399$\pm$0.127
	Fit	3.219	0.101	6.948

Exp=Experimental, Fit= adsorption curve fit

tained by fitting. Comparing these parameters may not be wise as the adsorption experiment assesses continuous adsorption-desorption phenomena for 3 hours which is much higher than the cycle time of the longest gradient run. Another factor to consider is the difference between the buffer environments of the two experiments where first has just the equilibration buffer whereas second has elution buffer gradient. The effect of continuous flow can reduce the residence time of the protein around the resin particle reducing the steric effects and charges displaced. The decrease in residence time also reflected in decrease in equilibrium constant for dynamic conditions for both the molecules. Another reason for this can be limited loading done in column operations which might lead to high adsorption rates decreasing the overall equilibrium constant. Estimation of steric hindrance factors for BSA and BLG was done from the respective breakthrough curves using the breakthrough volume in Equation 3.24.

4.3.2.4 Single component breakthrough: Experimental

Figure 4.9 and 4.10 show the breakthrough for BSA and BLG at different loading velocities respectively and the prediction using *ExProSim:IC*.

It is wise to discuss experimental breakthrough curves first before comparing them with the predicted data. There are two main characteristic features of breakthrough curve which should be looked at. First is the breakthrough point which shows the maximum binding capacity of the resin for the protein molecule and second being the steepness of the breakthrough curve which determines the extent to which the capacity of an adsorbent bed can be utilised. This helps in determining dynamic binding capacity (DBC) which shows maximum amount of

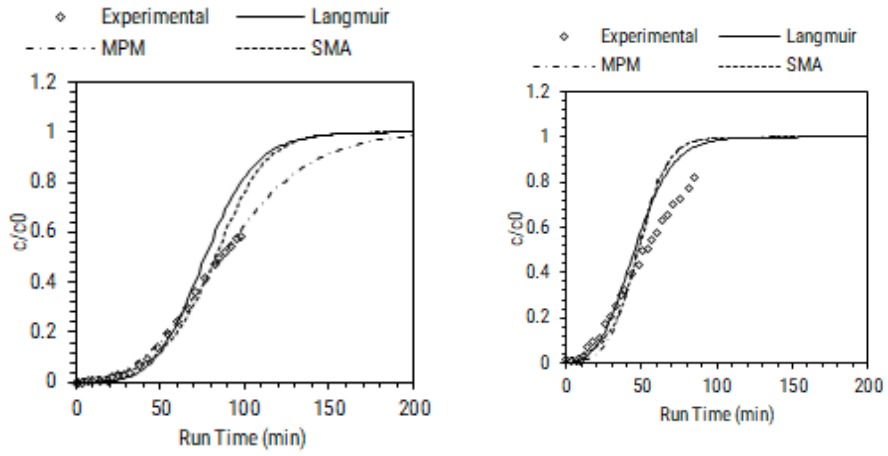

Figure 4.9: Comparison of predicted vs experimental data for breakthrough of BSA at various linear velocities, a) 0.5 ml/min (77.95 cm/hr) b) 1 ml/min (155.9 cm/hr); Langmuir(-), MPM (-·-), SMA (–), experimental (◇)

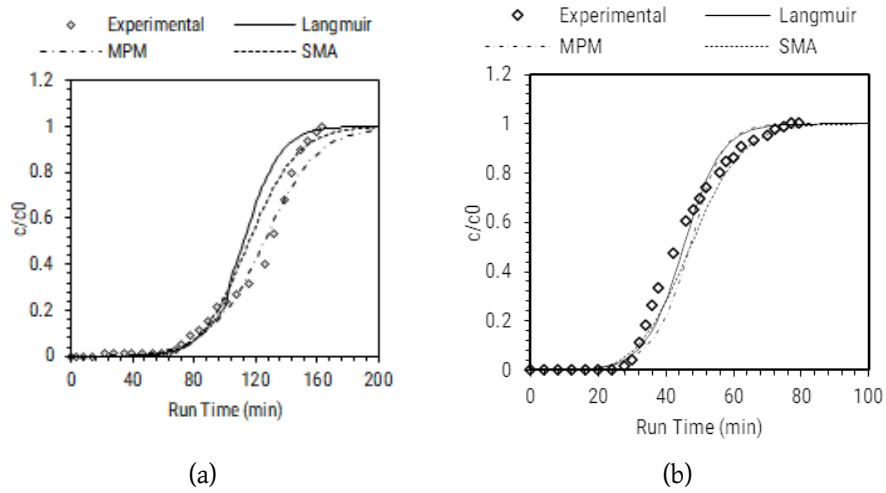

Figure 4.10: Comparison of predicted vs experimental data for breakthrough of BLG at various linear velocities, a) 0.5 ml/min (77.95 cm/hr) b) 1 ml/min (155.9 cm/hr); Langmuir(-), MPM (-·-), SMA (–), experimental (◇)

protein which can be loaded onto the column without any unnecessary loss.

Breakthrough curves for both BSA and BLG follow a logical pattern showing decrease in the breakthrough time as the velocity increases. Even the slope of breakthrough curve was found to increase with increase in velocity showing early saturation of the column. The error for 10% of the breakthrough point was less than 5% for both BSA and BLG. This can be interpreted as very minute error for the range of variation in the velocity under consideration.

Further dynamic binding capacities for both proteins were determined from

10% breakthrough volume and is shown in Table 4.6 [255].

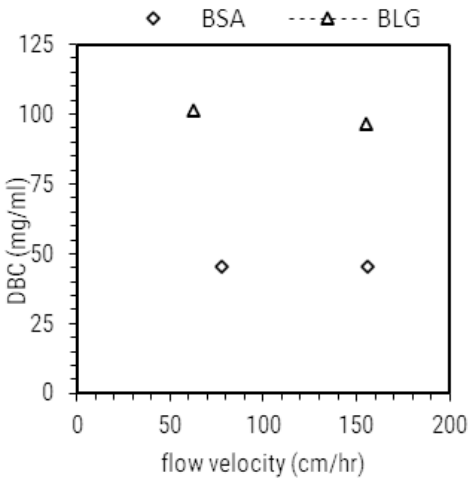

Figure 4.11: DBC versus flow velocity for two proteins a)BSA (-◇-) and b)BLG (-△-) at 77.94 and 155.88 cm/hr

Fig. 4.11 shows the effect of flow velocity on DBC of proteins. As expected the DBC was found to decrease slightly with increase in the velocity. This can be accounted for decrease in the residence time for the interaction of proteins with the resin. It is evident that DBC is less than SBC because of the amount of time and loading which is available during the experiments.

Table 4.6: Comparison of DBC for BSA and BLG on cation exchanger SPFF

Protein	**10% BT volume (ml)**	**DBC (mg/ml)**
BSA	22.75±0.2	45.37±0.5
BLG	31.8±0.8	98.61±2.49

10% BT=Breakthrough volume for 10% of breakthrough achieved. The values are averaged for all the flow rates and standard deviation is mentioned.

On comparison with the Q_{max} from static studies, the values for DBC of BLG were found to be 5% less than SBC which is a reasonable estimate suggesting that the binding for BLG is quick and firm. On the other hand, DBC for BSA was found to be significantly lower than SBC ($\approx$ 66% lower) which suggests multimeric ad sorption. In case of static binding the adsorption could sustain as the sample collection after ensuring that the equilibrium was established. However, DBC was found during operating conditions on column for just enough residence time for

protein-resin binding leading to continuous equilibrium-non equilibrium conditions. Breakthrough curve shows continuous release of BSA from the column owing to its inability to sustain the hydrophobic binding under dynamic conditions leading to non-saturation. The observed behaviour can be supported further considering conformational composition of BSA of 54% α-helix and 40% β-sheets [256] and its ability to convert from α helical structure to β sheets [257] on adsorption. Experimental breakthrough curve also provides proof for expected behaviour of BSA on ion exchange column in close proximity to its isoelectric point. Such an observation has also been made by Skidmore et al [3].

4.3.2.5 Breakthrough simulations with *ExProSim:IC*

Experimental profiles were compared further with the simulation outputs for both BSA and BLG breakthrough for different loading velocities as shown in Fig. 4.9 and 4.10. Simulations were performed with two thermodynamic models Langmuir and SMA along with EDM. The results are discussed further.

EDM-Langmuir model

When predicted with experimental parameters as inputs, the breakthrough curves overestimated the maximum binding capacity for both BSA and BLG. This might be because of different adsorption times and mechanism in static studies as compared to dynamic studies. As experimental profiles were not matched by both curves, it was decided to adjust the input parameters in order to fit to the experimental curves. It was logical to use the values of Q_{max} same as DBC predicted from breakthrough profiles. Values of k_d were increased for both the proteins ensuring the resultant k_d of BSA stays higher than BLG as BSA shows continuous desorption and slower binding. Equilibrium dissociation constant were kept constant as equilibrium constants are generally independent of the residence time. The values of k_1 were also increased further to ensure faster adsorption. Resultant k_1 value for BLG was three times of BSA as faster adsorption is expected for ionic interactions for BLG than BSA. The modifications done in the parameters for both BSA and BLG are shown in Table 4.7.

It is observed from Figure 4.9 and 4.10 that the onset of breakthrough was pre-

Table 4.7: Modified model parameters for major whey proteins simulation using EDM:Langmuir models for SPFF cation exchanger

Protein	Constant	Value	Multiplication factor	Modified value
BSA	Q_{max} (mg/ml of resin)	132.5	3	397.5
	k_d ($\times 10^{-6}$M)	4.566	20	91.3
	k_1 ($\times 10^{-3}$ml/mg.min)	1.36	15	20.4
BLG	Q_{max} (mg/ml of resin)	106.72	1.8	191.52
	k_d ($\times 10^{-6}$M)	6.065	12	72.81
	k_1 ($\times 10^{-3}$ ml/mg.min)	1.51	40	60.4

dicted successfully by the simulation tool with 10% breakthrough at more than 95% accuracy for both BSA and BLG for both flowrates. For all BSA breakthrough curves, no saturation was observed which has been explained earlier in the chapter. As the curves for BSA progressed at a very slow rate, it could not be captured completely by the model simulations. This can be attributed to absence of hydrophobicity considerations in the model used. Apparent value of Q_{max} for BSA was increased by three times in order to match to the experimental curve. This proves that there is a continuous release of BSA from the resin which does not let the resin to saturate allowing more protein to adsorb continuously. Best fit was obtained when the binding capacity was set to the DBC value determined from experimental data. It also appeared that the binding capacity of BSA might be higher than the estimated values from the static experiments but the overall capacity could not be calculated because of the unsaturation. Breakthrough was predicted successfully up to 50% saturation but further slow desorption could not be predicted and the error was higher before the saturation was predicted correctly towards saturation. Further attempts were made to achieve a better fit to the experimental profile by changing the kinetic constants further but it caused mismatch in the earlier part of the breakthrough curves. As estimation of DBC was a focus here, predictions were concluded to satisfy the accuracy of the early part of

breakthrough curves. For BLG breakthrough, it is important to notice that the experimental curve showed an unexpected dip in the slope around 40% saturation which was not predicted by Langmuir isotherm.

EDM-MPM model

Table 4.8: Modified model parameters for major whey protein simulation using EDM:MPM models for cation exchange

Protein	Parameter	Value	Multiplier	Modified value
BSA	Q_{max} $(mg/mlofresin)$	132.4	2	264.69
	k_{des0} $(ml/mg.min)$	0.4515	0.35	0.158
	k_{ads0} $(ml/mg.min)$	0.9455	0.05	0.0473
	β	0.1011	1	0.1011
	γ	0.951	1	0.951
BLG	Q_{max} $(mg/mlofresin)$	106.4	1.8	191.52
	k_{des0} $(ml/mg.min)$	0.037	1.8	0.066
	k_{ads0} $(ml/mg.min)$	0.2163	0.25	0.0541
	β	0.1233	1	0.1233
	γ	0.2163	1	0.2163

Comparison between experimental breakthrough and MPM simulations is shown in Figures 4.9 and 4.10. Modified MPM parameters are shown in Table 4.8. Model performed better than Langmuir and SMA for prediction of both BSA and BLG at lower flow rate of 0.5 ml/min. Error throughout the curve was found to be less than 5% which is an excellent match. Similar fit was obtained at 1 ml/min flow rate showing accuracy of the tool at changing flowrates. The adjustment in parameters reflected similar trend as in case of Langmuir predictions. Adjusted parameters for BSA showed lower adsorption and higher desorption rates supporting the continuous release of BSA from the resin. This proves weaker binding which was also reflected from the k_d values of Langmuir isotherm. Values for k_{dmpm} determined from resultant constants (2.08 and 0.691 for BSA and BLG respectively) and compared with k_{dmpm} values before modifications (0.297 and

0.097, for BSA and BLG respectively). It was seen that BLG had lower equilibrium dissociation value indicating stronger binding. Relative change in the k_{dmpm} values before and after modifications was a reflective of shift in the desorption curves for both the proteins.

EDM-SMA model

As primary SMA parameters were determined by two different methods which further can serve as initial guesses for breakthrough predictions, it was important to decide which ones should be used for simulations. As inverse fit method provides an easier way and lesser experiments, it was chosen over gradient experimental method. Parameters were further adjusted in order to fit to the experimental data.

Table 4.9: Modified model parameters for major whey proteins simulation using EDM:SMA models for cation exchange

Protein	Fitted Parameters	Value	Multiplier	Modified value
BSA	v	2.176	0.6	1.31
	k_{eq} $(\times 10^{-2})$	91.4	0.05	4.57
	σ	12.415	0.2	2.475
BLG	v	3.219	0.15	0.487
	k_{eq} $(\times 10^{-2})$	10.1	0.38	3.83
	σ	6.948	0.372	2.589

Modified parameters are shown in Table 4.9. SMA isotherm predictions were seen to predict breakthrough curves better than Langmuir isotherm. For BLG, SMA performed better than Langmuir throughout the curve at both velocities. In order to match the curve for BSA, steric hindrance factor was reduced. Other parameter modifications show that the charge value is lower supporting more ionic interactions and higher k_{eq} value looser binding as compared to BLG. Adjusted σ values are same for both proteins suggesting no significant effect of steric factors on difference in binding of proteins to resin. Compilation of curve to curve errors for breakthrough predictions are showed in Table B.20. RMSE values for BSA are higher than that for BLG for all the isotherms. Moreover, predictions for MPM were found to be better than other two isotherms. This can be attributed to more

number of parameters for predicting the breakthrough. However, comparison based on point by point comparison is more relatable for correlating experimental data.

4.3.2.6 Multicomponent breakthrough: Experimental

Experimental breakthrough

The combined breakthrough profile and individual profiles obtained from the HPLC-SEC analysis of the samples collected are shown in Figure 4.12.

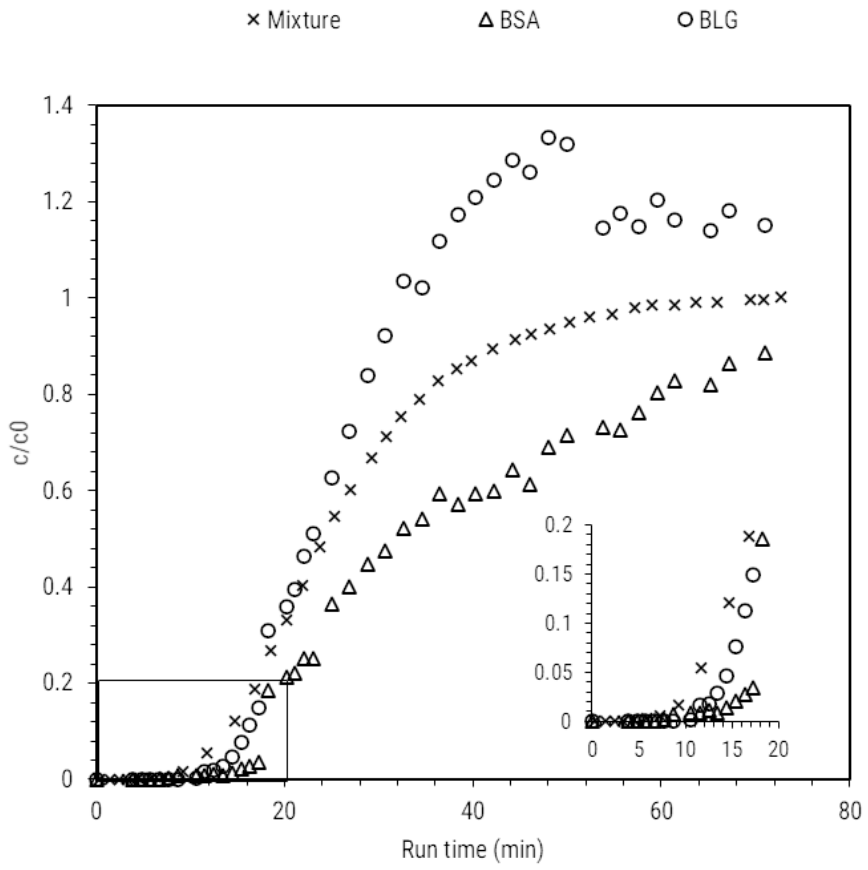

Figure 4.12: Experimental breakthrough curves for multicomponent system and individual breakthrough curves from HPLC-SEC for BSA and BLG for 1 ml/min flow rate, (BSA △, BLG ○ and combined ×)

The experiment for multicomponent breakthrough was stopped when the mixture reached saturation concentration. Interestingly when individual concentrations were determined, it was observed that BSA was almost reaching saturation and BLG was over saturated. As explained in the earlier section, BSA has a ten-

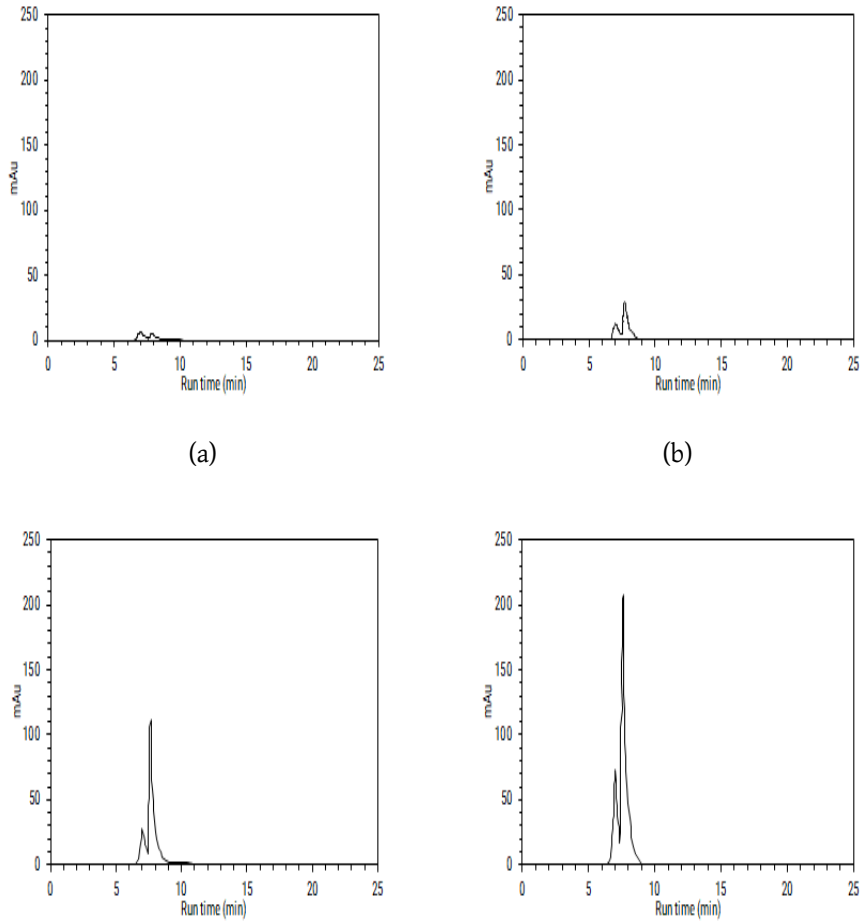

Figure 4.13: Comparison of SEC-HPLC profiles of samples at different breakthrough points on multicomponent breakthrough curve of BSA and BLG for cation exchange

dency to show linear profile due to continuous adsorption and desorption. It can also be seen in Figure 4.13 that slow release of both the proteins happen with time. Figure 4.13(a) to 4.13(d) show the individual SEC-HPLC profiles at 0%, 10%, 50%, and 100% breakthrough points. As suggested by the SEC-HPLC profiles, BLG profile shows rapid increase in concentration whereas BSA was seen to increase slowly as compared to BLG. It can be seen that the breakthrough for BLG in multicomponent system shifted from 28 min to 12 minutes as compared to single component BLG breakthrough, whereas breakthrough for BSA increased from 7 to 15 min. This is also supported by the SEC-HPLC profiles where BLG was found to saturate faster than BSA. This can be attributed to different mechanisms of mass transfer in the column for the two proteins in consideration. As BLG reaches satu-

ration faster, it can be considered to be electrokinetically transported whereas the transfer for BSA can be considered to be diffusion driven. This potentially raised the possibility of BSA displacing BLG due to relatively slower transport through the column. Increased desorption rates and early saturation of BLG, indicated clear displacement. Concentration of BLG was observed to reach over the inlet concentration and which can be attributed to increase in concentration locally due to displacement of the protein. On the other hand curve for BSA was not saturated till the end of breakthrough. This might be due to slow intermolecular hydrophobic interactions for BSA as explained in Section 4.3.2.1.

4.3.2.7 Breakthrough simulations with *ExProSim:IC*

EDM-Langmuir model *ExProSim:IC* was used further to predict the competitive breakthrough profiles. The simulations profiles are shown in Figure 4.14. The predictions obtained from experiments under-predicted the breakthrough curves. Obvious decrease in the binding capacity was attributed to competition between the molecules for the binding sites in the resins. The competition between the proteins affected the kinetics by increasing the desorption rates. Desorption constants for BLG and BSA were increased by 100 times and 20 times respectively. Higher increase in BLG desorption can be attributed to the displacement phenomena. Modified model parameters are summarised in Table 4.10.

Table 4.10: Modified model parameters for EDM-Langmuir model system for multicomponent breakthrough predictions of BSA and BLG using *ExProSim:IC*

Protein	Constant	Value	Multiplier	Modified value
BSA	Q_{max} (mg/ml of resin)	132.5	0.25	33.125
	k_d ($\times 10^{-6}$M)	4.566	15	68.49
	k_1 ($\times 10^{-3}$ml/mg.min)	1.36	20	27.2
BLG	Q_{max} (mg/ml of resin)	106.72	0.25	26.68
	k_d ($\times 10^{-6}$M)	6.065	100	606.5
	k_1 ($\times 10^{-3}$ml/mg.min)	1.5132	100	151.32

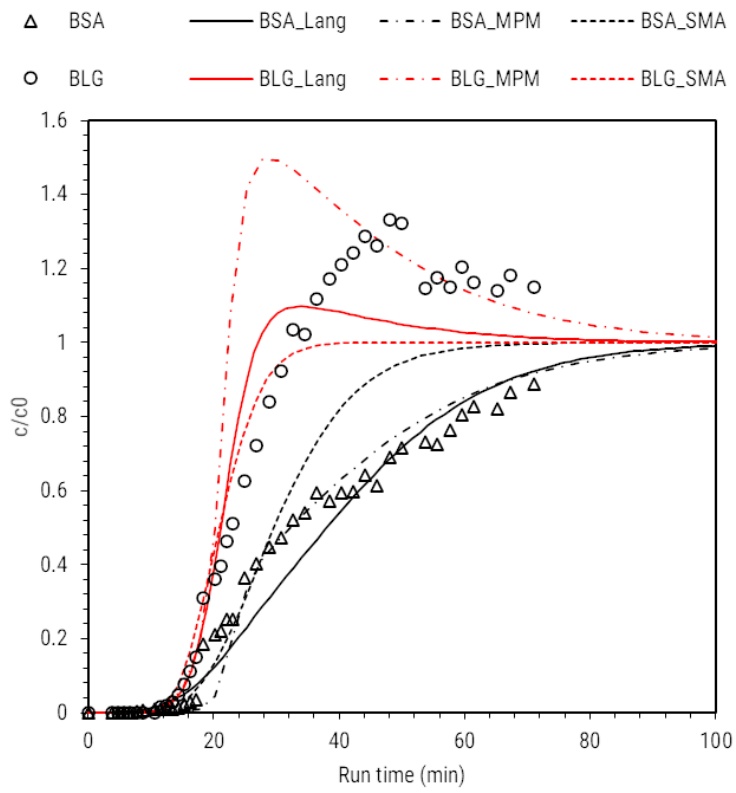

Figure 4.14: Comparison of *ExProSim:IC* simulations with EDM vs experimental breakthrough curves for multicomponent system of BSA and BLG for 1 ml/min flow rates. Predicted curves for BSA; Langmuir —, SMA · ·, MPM - ·-, and BLG; Langmuir —, SMA · ·, MPM -·-, Experimental (BSA ◇, BLG o)

For the best match, values of adsorption rate constant for BLG was also changed by 100 times assuming fast adsorption and desorption for it due to high charge and rapid displacement. It is important to notice that Q_{max} values were reduced to 25%of SBC for getting the best fit and it can be said that multicomponent systems led to huge decline in the binding capacity of both proteins. 75% decline in BSA capacity was from apparent value of binding capacity whereas actual decrease from DBC was 24%. On the other hand, decrease in BLG from DBC was 72%. This further supports displacement effect in the column. Breakthrough curves were predicted using *ExProSim:IC* with decent accuracy for multicomponent system. Breakthrough point of 10% breakthrough value was predicted to 95% accuracy.

EDM-MPM model MPM parameters from adsorption inverse fit were used initially to predict the multicomponent breakthrough but the results obtained were

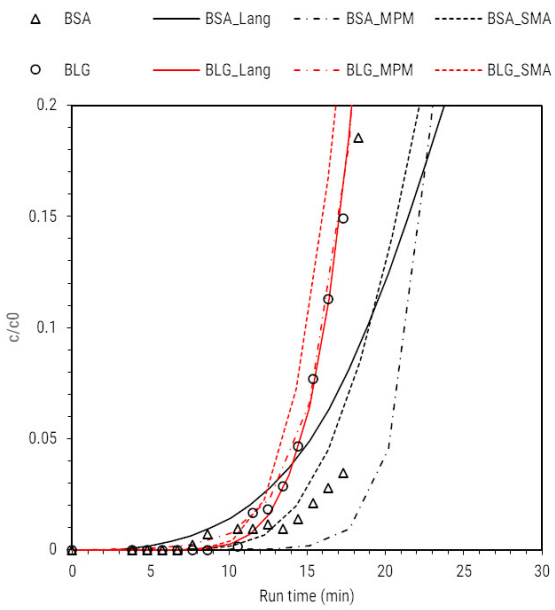

Figure 4.15: Zoomed version for a better comparison of breakthrough points in multicomponent breakthrough predictions using *ExProSim:IC* for all the models for BSA and BLG at 1 ml/min. Predicted curves for BSA; Langmuir —, SMA · ·, MPM - ·-, and BLG; Langmuir —, SMA · ·, MPM -·-, Experimental (BSA ◇, BLG o)

not satisfactory. Hence, parameters were modified as shown in Table 4.11. Both the curves were well predicted up to 50% of breakthrough. Better predictions were obtained for BSA by MPM models as compared to predictions obtained using earlier models. Expected decline in the binding capacity was observed which can be attributed to competition of the proteins for binding sites. Values of desorption constants were increased for both the proteins with higher change in desorption rate of BLG suggesting its displacement. The overshoot of BLG due to displacement was predicted by MPM model unlike earlier models, however it was predicted earlier than the experimental data. Modified equilibrium constant for Langmuir was lesser by 10 fold than that of MPM. It can be said that the overshoot was a reflection of high increase in equilibrium constant for MPM isotherm due to increase in desorption constant.

EDM-SMA model Furthermore, multicomponent breakthrough was predicted by performing simulations using EDM and SMA isotherm. This is as shown in Fig. 4.14. Modified parameters for SMA are shown in Table 4.12.

Charge values were reduced reflecting change in binding capacity for both proteins. BLG binding was considerably reduced as compared to BSA support-

Table 4.11: Modified model parameters for EDM-MPM model system for multicomponent breakthrough predictions of BSA and BLG using *ExProSim:IC*

Protein	Parameter	Value	Multiplier	Modified value
BSA	Q_{max} $(mg/mlofresin)$	132.4	0.22	29.1
	k_{des0} $(ml/mg.min)$	0.4515	5	2.26
	k_{ads0} $(ml/mg.min)$	0.9455	1	0.9455
	β	0.1011	15	1.52
	γ	0.951	1	0.951
BLG	Q_{max} $(mg/mlofresin)$	106.4	0.3	31.9
	k_{des0} $(ml/mg.min)$	0.037	10	0.37
	k_{ads0} $(ml/mg.min)$	0.2163	1	0.2163
	β	0.1233	1	0.1233
	γ	0.2163	1	0.2163

Table 4.12: Modified model parameters for EDM-SMA model system for multicomponent breakthrough predictions of BSA and BLG using *ExProSim:IC*

Protein	Parameter	Value	Multiplier	Modified value
BSA	v	2.176	0.124	0.27
	k_{eq}	0.914	0.8	0.7312
	k_a $(\times 10^{-3} ml/mg.min)$	1.36	2000	2720
	σ	12.415	0.2	2.483
BLG	v	3.219	0.033	0.0106
	k_{eq}	0.101	5.3	0.535
	k_a $(\times 10^{-3} ml/mg.min)$	1.51	50000	75500
	σ	6.948	0.36	2.49

ing the displacement effect. Modified adsorption constant values suggested high rates of adsorption for BLG whereas equilibrium constant showed continuous desorption for BSA. It can be observed that 10% breakthrough was predicted accurately for both BSA and BLG with -3.4% and 1.79% error. The simulation curve for BLG followed the experimental profile further very closely within 5% error till saturation but overshoot of the experimental profile was not predicted. Simula-

tion curve for BSA followed up experimental profile till 50% inlet concentration and further reached saturation quickly. When compared with predictions from Langmuir, SMA gave better match to the experimental data for both proteins. A better comparison of 'curve to curve errors can be seen in Table B.21

This exercise gives an example that adjustment of constants becomes more logical if the experimental phenomena can be understood. Fitting the curves to minimise the errors would be another way to adjust constants; however, it was more useful to rely on molecular and experimental knowledge. This can also help in troubleshooting the problems in the process.

Details point by point errors are shown in Table B.4. Table B.21 shows the errors based on curve to curve comparison. It can be said that SMA and MPM showed a better performance as compared to Langmuir isotherm.

This concludes the cation exchange chromatography for major whey proteins. As the process was operated above the isoelectric point of ALA, the discussed methodology did not serve the objective of assessment of all major proteins. This was due to stronger binding at lower pH values making the process less feasible for operation.

4.3.3 Anion exchange chromatography

As it was important to know which among cation and anion is better for major whey proteins, further section describes experimental studies on anion exchange. Simulation studies were also carried out which serve as additional experimental validation platform for *ExProSim:IC*. The structure of the section is similar to cation exchange studies carried out earlier.

4.3.3.1 Determination of Langmuir parameters

Adsorption isotherm

To find out the adsorption behaviour of protein molecules, different isotherms were fitted to the experimental data. The parameters obtained from the best isotherm fit of all the proteins are presented in Table 4.13. Obtained fits are shown in Figure 4.16. Regression coefficients were slightly better for Langmuir and MPM isotherm as compared to Freundlich suggesting monolayer adsorption for all the proteins. Langmuir isotherm showed the best match to experimental data for BSA, BLG, and ALA. The values of Langmuirian equilibrium constant, R_L were found to be between 0 and 1 for entire range of inlet concentrations for all the proteins indicating favourable single layer reversible adsorption [240].

As discussed in earlier Sections, any globular protein has a combination of hydrophilic and hydrophobic regions on its surface which contribute when a protein binds to an adsorbent. The binding strength due to these multiple interactions is denoted by an equilibrium constant k_d, whereas extent of binding is referred as Q_{max}. Values of k_d for all the proteins lie within 10^{-8} M and 10^{-4} M showing suitability of adsorption for chromatography [242]. It can be observed that the value of k_d for BLG is lower than ALA and BSA. Higher k_d value can mean either higher desorption rate or lesser adsorption rate. The adsorption rate kinetic constant is determined by uptake kinetics section hence further discussion on k_d is given there. It is reasonable to assume that interactions happening are mostly ionic interactions as the operating pH used here is 6.9 which is considerably higher than the isoelectric points of all the proteins. Farther the isoelectric point of the protein, greater are the charges on the protein leading to more potential for ionic

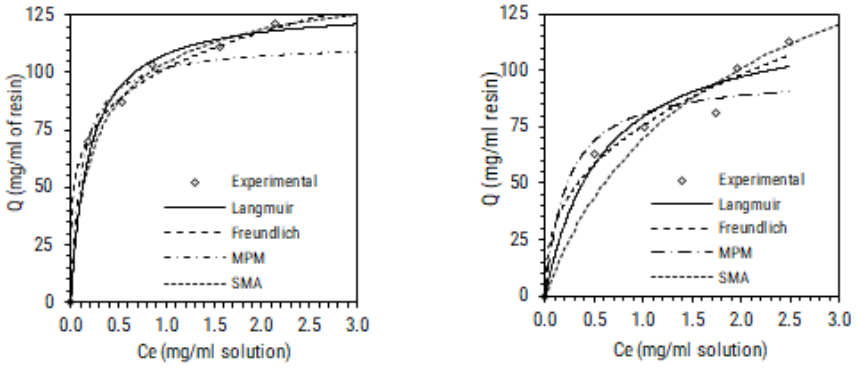

(a)

(b)

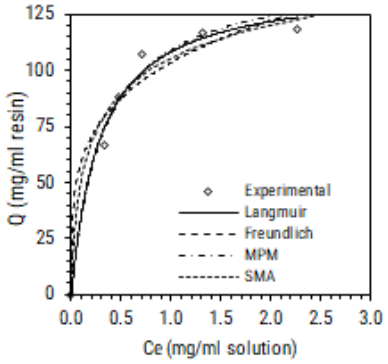

(c)

Figure 4.16: Adsorption isotherms for major whey proteins on Capto Q anion exchanger; a) BSA, b) BLG, and c) ALA

interactions. The order of extent of binding based on electrokinetic potential can be seen as expected (BLG<BSA<ALA). Q_{max} for ALA was highest amongst the proteins. However, value of Q_{max} for BLG was found to be higher than expected. This was attributed to formation of dimer of BLG which can cause stronger binding leading to slower but higher retention [258, 259]. It has been reported that BLG dimeric form is prevalent at neutral pH [236]. Furthermore, it has been proved by Mercadante et al. that BLG dimer exerts strong ionic properties in its native structural form [260]. Adsorption capacity is underestimated by Freundlich model with less regression coefficients and hence it was not considered further.

Table 4.13: Summary of adsorption parameters for major whey proteins on CaptoQ anion exchanger

Parameter	**BSA**	**BLG**	**ALA**
Langmuir model			
Q_{max} (mg/ml of resin)	128.8	125.09	139.4
k_d, ($\times 10^{-6}$M)	2.92	0.3187	2.052
*k^l_{des}, ($\times 10^{-2}$ min$^{-}1$)	1.46	0.106	0.229
R_L at 3 mg/ml	0.0578	0.132	0.0.098
R_L at 8 mg/ml	0.0213	0.061	0.0232
R^2	0.991	0.981	0.987
Freundlich model			
Q_f (mg/ml of resin)	101.7	75.69	103.4
n	4.78	2.662	4.175
1/n	0.209	0.376	0.239
R^2	0.956	0.949	0.962
MPM Langmuir model			
Q_{max} (mg/ml of resin)	127.2	96.88	101.5
k_{ads0} (ml/mg.min)	1.606	1.206	1.299
k_{des0} (ml/mg.ml)	2.271	1.818	0.4933
β	0.029	0.064	0.605
γ	1.457	1.386	1.802
$D_{ax}(\times 10^{-2})$	4.791	4.84	3.21
R^2	0.9834	0.9856	0.9821

R_L: Langmuirian equilibrium constant,
*estimated from pseudo 2^{nd}
order uptake kinetic values

Uptake kinetics

The uptake kinetics signifies the rate of adsorption of a protein. Although adsorption process happens at a particle and pore surfaces or in the films at the surfaces, here lumped kinetic models are implemented. The Equations 3.39 and 3.40 were used to find if the adsorption in physical or chemical respectively.

Fig. 4.17 represents the model fitting for uptake kinetics along with the experimental data. The representative parameters for the same have been shown

in Table 4.14. It can be seen that the pseudo second order kinetics fits the kinetic data better for all the proteins (better regression coefficient and correlations coefficient). This means that the adsorption is a chemical adsorption.

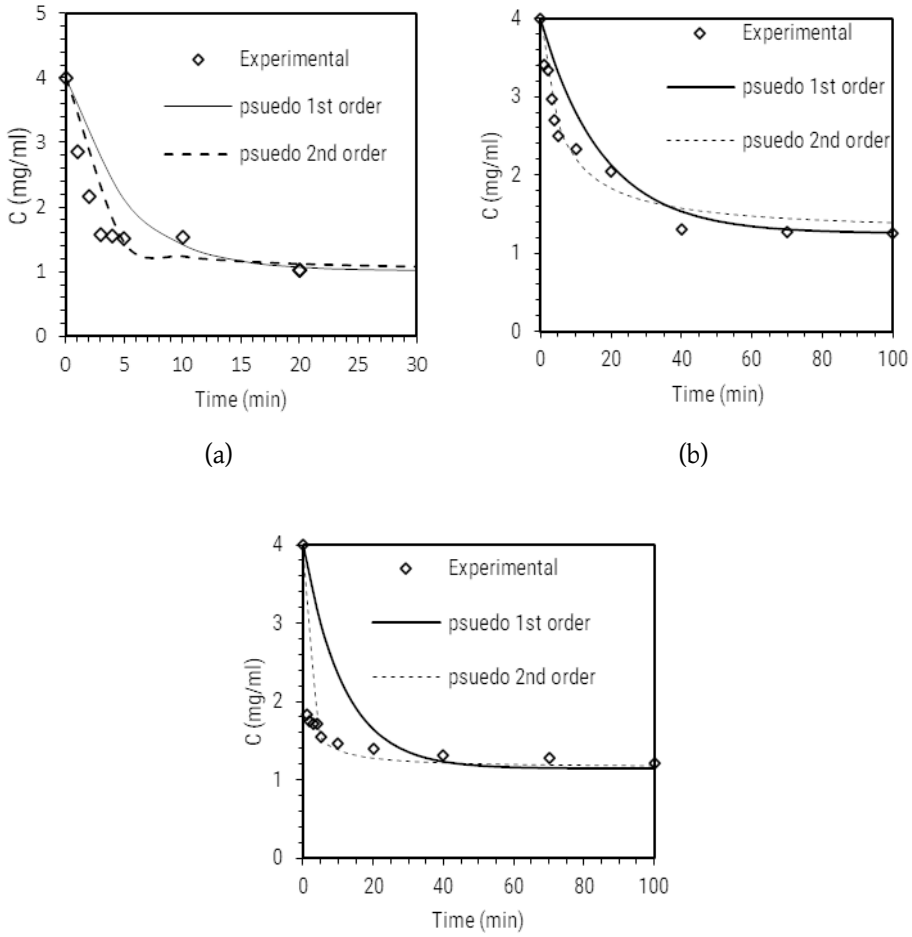

Figure 4.17: Uptake kinetics for major whey proteins on CaptoQ anion exchanger, a) Comparison of pseudo 1^{st} order and pseudo 2^{nd} order for BSA b) Comparison of pseudo 1^{st} order and pseudo 2^{nd} order for BLG c) Comparison of pseudo 1^{st} order and pseudo 2^{nd} order for ALA

It can be observed that for pseudo second order kinetics, uptake kinetic constants, k_2 for BSA and ALA were almost same. Even though there are differences in the molecular size of the proteins, the uptake rate was observed to be the same. It is fair to assume that BSA can get adsorbed at the surface easily because of its larger size than ALA. ALA on the other hand, has higher net charge making its adsorption rate higher due to ionic attractions. Adsorption constant for BLG is very low as compared to both BSA and ALA in spite of the dimeric configuration. This

Table 4.14: Parameters for uptake kinetics of major whey proteins for CaptoQ anion exchanger

Parameter	BSA	BLG	ALA
Pseudo first order			
k_1 ($\times 10^{-2}$) (min-1)	9.19	2.35	2.35
R^2	0.749	0.759	0.8072
Correlation Coefficient	0.9847	0.872	0.9023
Pseudo second order			
k_2($\times 10^{-3}$) (ml/mg.min)	7.56	1.81	7.86
R^2	0.9907	0.9832	0.991
Correlation Coefficient	0.9918	0.9936	0.9897

can be attributed to stronger binding due to protein-protein interaction making it difficult for other BLG molecules to move through the medium. Desorption constants were determined for all the proteins using k_d and k_2 values. The desorption rate was found to be very low for BLG (0.0032 min^{-1}) as compared to 0.039 for BSA and 0.0273 for ALA. This shows that desorption rate constants follow the order as BLG<ALA<BSA as supported by the breakthrough curve later in this chapter. Least desorption rate confirms strongest binding for BLG dimer due to additional charge interactions. It is important to note that the constants are fitted to the experimental curve from empirical models and may not give exact idea of what is happening during the binding kinetics. Further, it is important to consider effect of salt during the adsorption and hence further models are explored.

4.3.3.2 Determination of MPM parameters

MPM isotherm accounts for the salt as inert entity and includes the modified equilibrium coefficient based on salt concentration. Farther the isoelectric point of the protein, greater are the charges on the protein leading to more potential for ionic interactions. Parameters k_{ads0} and k_{des0} describe the resultant rate of uptake and release of the protein. The values obtained suggest higher rate of adsorption for BSA with comparable rates for ALA and BLG. However, the rate of desorption is very less for ALA as compared to BSA and BLG, confirming stronger binding to

the resin in batch conditions. Value of β represents an extent of ionic interactions happening during the protein binding. This can be interpreted as, higher the value of β, higher is the interaction of the protein with the matrix. It can be seen that ALA shows highest interaction with the adsorbent in the batch studies followed by BLG and BSA respectively. BLG shows higher β value than BSA which is in contrast to its electrophoretic mobility. This can be attributed to the dimer formation at the operating pH of 6.9.

4.3.3.3 Determination of SMA parameters

The fit for SMA isotherm was not as good as Langmuir or MPM as the regression coefficient was less than 0.97 for all the proteins. However, SMA isotherm considers salt interactions while adsorption is happening hence it was considered for the further parameter estimation. For determination of SMA parameters, column parameters were estimated.

Column physical parameters

Based on moment analysis of the pulse injections, external porosity of the column was determined to 0.41$\pm$0.014 whereas the particle porosity was estimated to be 0.860$\pm$0.0183. Total porosity for column was determined to be 0.913$\pm$0.010. Height equivalent to theoretical plates was found to be 3.01×10^{-4} cm and net transfer units were observed to be 8211.66. Asymmetry of the column was 1.08 which was acceptable. Ionic capacity was determined to be 1868.96$\pm$25.62 mM/ml resin which compares to the reported value for CaptoQ from GE is 1600-2200 mM/ml resin [254].

Gradient elution

BSA, BLG, and ALA eluted at 35$\%$, 47$\%$ and 55$\%$ respectively on the salt gradient. The gradient experiments were further performed for all the proteins between 0$\%$ to 100$\%$ for different gradient slopes to find out SMA parameters from the retention volumes. The gradient curves for the proteins are as shown in Figure 4.18. Table B.2 shows the summary of gradient runs.

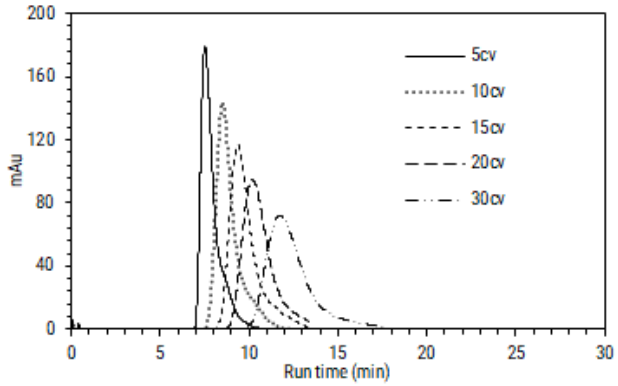

(a)

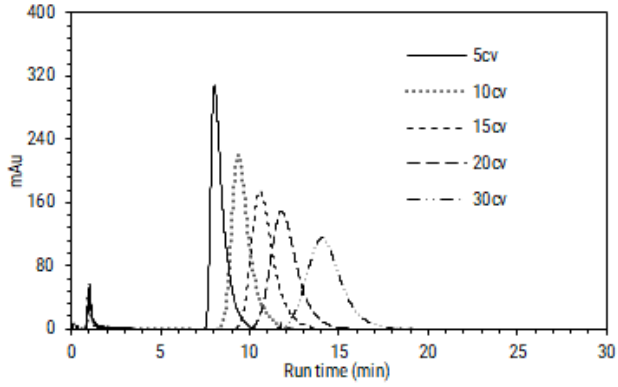

(b)

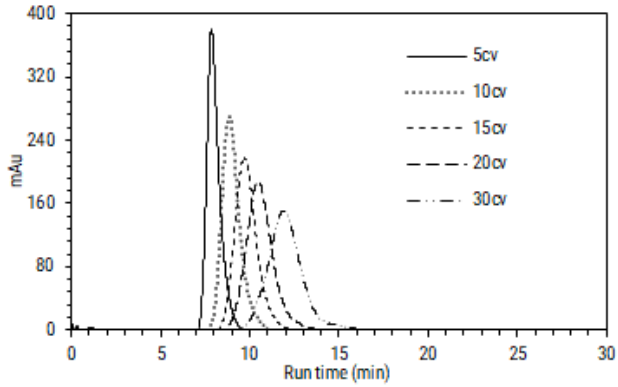

(c)

Figure 4.18: Comparison of elution profiles for (a) BSA, (b) BLG, and (c) ALA at different gradient lengths

It can be seen that the retention volume increases with decrease in the slope of gradient during elution. Retention time was observed to move forward due to slower change in the salt concentration. Table 4.15 shows the comparison of SMA

parameters obtained from experiments and inverse fit method. As the charge value in SMA defines the number of salt ions being displaced by a protein molecule in order to adsorb onto the resin. Higher values of v and least k_{eq} for ALA supports strongest binding amongst proteins. Steric hindrance factor is a property influenced by molecular weight of protein which can cause screening of charges available for exchange. BSA having higher σ value shows highest steric factor. Similar trend is seen in experimental parameters as well except the values vary with different multiplier. This trend is seen for both experimental and inverse fit values. Values for experimental and inverse fit were distant from each other. The reason can be difference of interactions between static to dynamic studies. Comparing these parameters may not be wise considering different set-ups and environments used for them. As these parameters are to be used for simulation initial guesses, any of the sets can work well. Inverse fit parameters were chosen for initial guesses as they are obtained with lesser experimental efforts.

Table 4.15: Comparison of SMA isotherm parameters for BSA, ALA, and BLG from gradient experiments and isotherm fitting

Protein	Method	v	k_{eq}	σ
BSA	Exp	0.223±0.018	0.550±0.023	6.711±0.273
	Fit	1.931	0.193	9.715
BLG	Exp	0.505±0.026	0.071±0.001	4.848±0.35
	Fit	1.737	0.069	5.612
ALA	Exp	0.972±0.009	0.002±0.001	4.702±0.076
	Fit	3.27	0.0015	4.015

Exp=Experimental, Fit= adsorption curve inverse fit

4.3.3.4 Single component breakthrough: Experimental

First experimental curves are discussed to understand how the proteins interact with the resin in dynamic conditions of over-loading. Figures 4.19, 4.20, and 4.21 show the breakthrough for BSA, BLG, and ALA at different loading velocities respectively along with the prediction using *ExProSim:IC*. The slope of breakthrough curve was found to increase with increase in velocity showing early saturation of the column. Breakthrough for BSA was obtained the earliest followed by ALA and

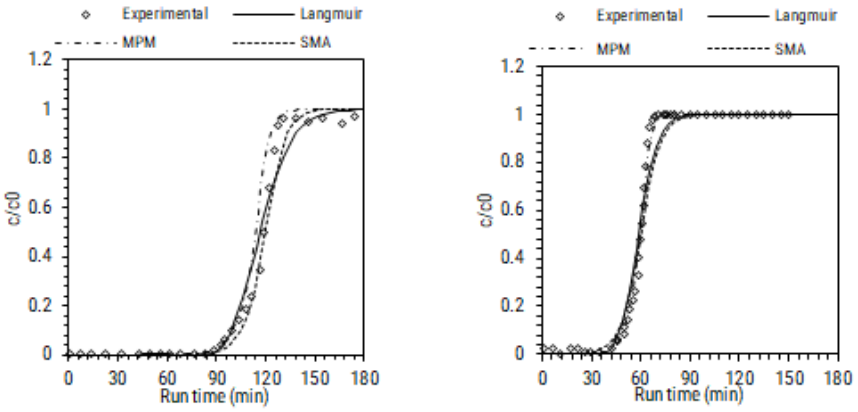

(a) (b)

Figure 4.19: Comparison of experimental breakthrough curves for BSA at two velocities a) 77.95 cm/hr b) 155.9 cm/hr with simulated breakthrough curves using three thermodynamic models Langmuir (—), MPM (- · -), SMA (- -)

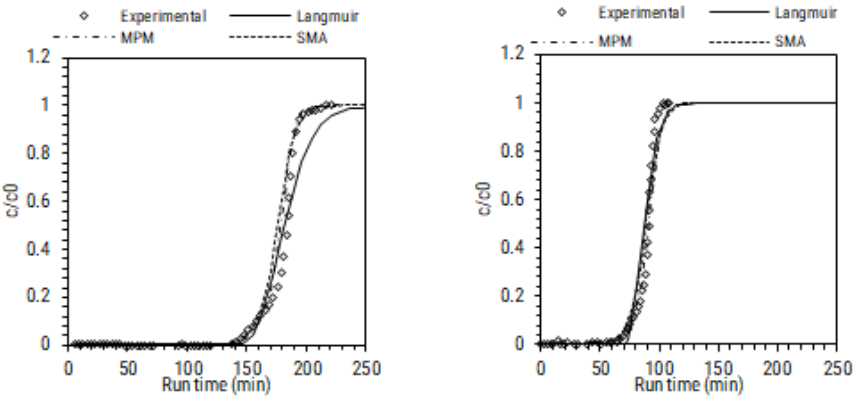

(a) (b)

Figure 4.20: Comparison of experimental breakthrough curves for BLG at two velocities a) 77.95 cm/hr b) 155.9 cm/hr with simulated breakthrough curves using three thermodynamic models Langmuir (—), MPM (- · -), SMA (- -)

BLG respectively.

Further 10% breakthrough values were used for each protein curve to find the dynamic binding capacity using Equation 3.25. The values of DBC for BLG were highest followed by ALA and BSA. Figure 4.22 shows the effect of flow velocity on DBC of proteins. As expected the DBC was found to decrease slightly with increase in the velocity. This can be accounted for decrease in the residence time for the interaction of proteins with the resin. It is evident that DBC is less than SBC because of the amount of time and loading which is available during the experiments. On

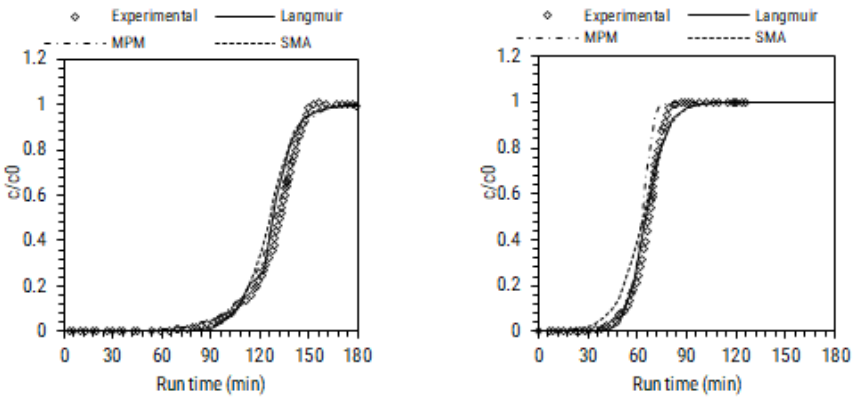

(a) (b)

Figure 4.21: Comparison of experimental breakthrough curves for ALA at two velocities a) 77.95 cm/hr b) 155.9 cm/hr with simulated breakthrough curves using three thermodynamic models Langmuir (—), MPM (- · -), SMA (–)

comparison with the Q_{max} for static studies, the values for DBC of BSA, ALA, and BLG were found to be very low than SBC which shows a looser binding in dynamic conditions. On the other hand, DBC for BLG was found to be very high as compared to its SBC. This shows stronger binding of BLG to the resin. The rise is very high as compared to ionic interactions BLG can exert which means there might be few physical forces such as hydrophobic interactions involved in the binding.

4.3.3.5 Breakthrough simulations with *ExProSim:IC*

EDM-Langmuir model

The values obtained from experimental fits of adsorption isotherm were used to predict the breakthrough curves for the first time. For all the proteins the match was far from the acceptable error criteria of 5% for experimental points and even curve to curve regression was 0.8. The parameters from experiments were adjusted further to fit the simulation curves to experimental curves. Changes in Q_{max} were made according to the DBC values obtained from breakthrough curve, whereas for k_d and k_1 were adjusted to match to the slope of the breakthrough curve based on the understanding we have gained from static experiments. The modifications done in the parameters for both BSA and BLG are shown in Table 4.16.

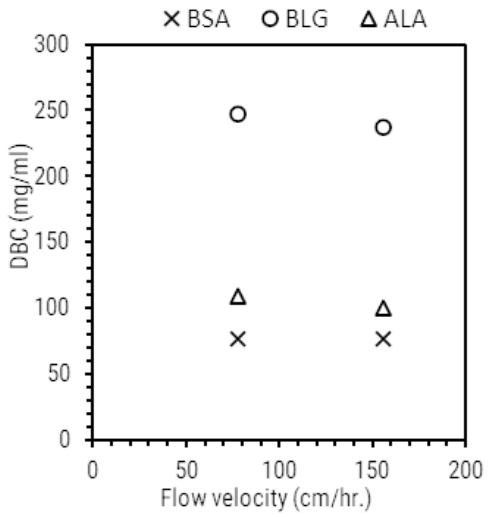

Figure 4.22: DBC versus flow velocity (77.94 and 155.88, cm/hr) for major whey proteins for CaptoQ anion exchanger; BSA (⋄), BLG (○), and ALA (△)

Table B.5 in Appendix B shows the error estimated with respect to various points on the breakthrough curve. Table B.22 shows comparison of regression and RMSE error values. It can be said that the onset and 10% breakthrough of all the breakthrough curves was predicted successfully by the simulation tool with more than 95% accuracy for all the proteins. Increase in error was observed as the curve progressed further but it remained below 10% throughout the curve even at higher velocity. All the curves showed complete saturation when compared with experimental data. From the experimental profiles it was realised that the parameters, mainly Q_{max} will need a major change for BLG in order to accommodate the dimer effect. Hence it was increased by two times. Along with that, the adsorption constant was increased and desorption constant was decreased to show higher binding. Change in rate constant k_d changed the slope of the breakthrough curve, whereas change in Q_{max} and k_1 changes the location of the breakthrough point. When k_{des} was calculated from the values of k_d and k_1; ALA showed slightly higher desorption rate than other proteins.

EDM-MPM model

As the initial simulations obtained using inverse fit MPM parameters were far from satisfactory, model parameters were modified further. The changed parameters are shown in Table 4.17. Simulations carried out using MPM-EDM models

Table 4.16: Modified model parameters for major whey proteins simulation using EDM:Langmuir models for Capto Q anion exchanger

Protein	Constant	Value	Multiplier	Modified value
BSA	Q_{max} (mg/ml of resin)	128.8	0.75	96.6
	k_d ($\times 10^{-6}$M)	2.924	0.5	1.462
	k_1 ($\times 10^{-3}$ml/mg.min)	7.56	15	113.4
BLG	Q_{max} (mg/ml of resin)	125.09	2.4	300.22
	k_d ($\times 10^{-6}$M)	3.187	0.5	1.594
	k_1 ($\times 10^{-3}$ ml/mg.min)	1.37	40	54.8
ALA	Q_{max} (mg/ml of resin)	139.4	1	139.4
	k_d ($\times 10^{-6}$M)	20.52	0.2	4.105
	k_1 ($\times 10^{-3}$ ml/mg.min)	7.81	10	78.1

were as accurate as that of Langmuir isotherm in predicting the onset and 10% breakthrough. As it can be seen in Table B.5 in Appendix B, error for MPM predictions remained below 5% throughout the curve even at higher velocity making it a better isotherm model than Langmuir for breakthrough prediction. Changed parameters revealed that desorption rate was lowest for BLG suggesting stronger binding. The value of β suggested weaker binding for BSA than other two proteins resulting in earlier breakthrough. It was observed that change in γ value did not affect the shape of the breakthrough curve. This might be due to major modifications made in k_{des0} values which makes the effect of change in gamma negligible. On the other hand, γ is multiplied by salt concentration which is quite low (0.025 M) so very small change in it wont reflect in the breakthrough curve. Modified β values for the proteins were compared further. As β for both BLG and ALA show high values as compared to BSA, comment can be made about binding strength being higher for both. Overall dissociation constant k_{dmpm}=$\left(\frac{kdes0\times S^{\beta}}{k_{ads0}\times exp(\gamma\times S)}\right)$ was determined for MPM isotherm to relate to Langmuir isotherm to Figure out why

ALA showed early breakthrough in spite of stronger binding. k_{dmpm} values for ALA was found to be very high as compared to both BLG and BSA suggesting faster adsorption-desorption. k_{dmpm} for BLG was very low indicating stronger binding.

Table 4.17: Modified model parameters for major whey proteins simulation using EDM:MPM models for Capto Q anion exchanger

Protein	Parameter	Value	Multiplier	Modified value
BSA	Q_{max} $(mg/mlofresin)$	127.2	0.7	89.53
	k_{des0} $(ml/mg.min)$	2.27	0.013	2.95×10^{-2}
	k_{ads0} $(ml/mg.min)$	1.61	0.1	0.1606
	β	0.029	1	0.029
	γ	1.457	2	2.914
	$D_{ax}(\times10^{-2})$	4.791	4	19.3
BLG	Q_{max} $(mg/mlofresin)$	96.88	1.5	145.32
	k_{des0} $(ml/mg.min)$	1.818	0.001	1.818×10^{-3}
	k_{ads0} $(ml/mg.min)$	1.21	0.1	0.121
	β	0.064	10	0.64
	γ	1.386	1	1.386
	$D_{ax}(\times10^{-2})$	4.84	3	14.5
ALA	Q_{max} $(mg/mlofresin)$	101.5	1	101.5
	k_{des0} $(ml/mg.min)$	0.493	0.018	9.076×10^{-3}
	k_{ads0} $(ml/mg.min)$	1.29	0.1	0.129
	β	0.61	1.05	0.635
	γ	1.802	1	1.802
	$D_{ax}(\times10^{-2})$	3.21	2	6.42

EDM-SMA model

As SMA parameters were determined by two different methods, it was important to decide which ones should be used for simulations. As inverse fit method provides an easier way and lesser experiments, it was chosen over gradient experimental method. Parameters were further adjusted in order to fit to the experi-

mental data.

Table 4.18: Modified model parameters for major whey proteins simulation using EDM:SMA models for Capto Q anion exchanger

Protein	Fitted Parameters	Value	Multiplier	Modified value
BSA	v	1.931	0.61	1.772
	k_{eq} $(\times 10^{-2})$	19.26	1.5	28.89
	σ	9.715	0.8	7.772
BLG	v	1.737	0.91	1.58
	k_{eq} $(\times 10^{-2})$	6.85	0.25	1.7125
	σ	5.612	1	5.612
ALA	v	3.27	0.385	1.259
	k_{eq} $(\times 10^{-2})$	0.156	10	1.56
	σ	4.015	1	4.015

Modified parameters are shown in Table 4.18. Furthermore, Table B.5 in Appendix B shows errors at different breakthrough points throughout the curves at different velocities. SMA isotherm predictions were able to match the experimental breakthrough curves at all velocities with less than 5% error for all the proteins. Major change in the modified parameters was in charge value for all the proteins. When these values were compared with experimentally obtained charge values, large differences were observed. This shows obvious error in estimation of charge value experimentally. As experiments were performed at ambient temperature of $23\pm2^{\circ}$c, even small changes in temperature can affect the charge. Major variations were observed when breakthrough was estimated at charge values obtained from experiments indicating high sensitivity to charge. Hence, fitting of this parameter was utmost necessary for getting a better fit. Charge values were compared for all the proteins. BLG showed highest value considering its strongest binding. On the other hand, k_{eq} values for BLG and ALA were comparable. It was also noticed that steric factor did not influence much for the to the shape of the curve for the low molecular weight proteins, hence it was kept constant.

Even though the comparisons were based on point to point comparison for better experimental understanding, errors for curve to curve comparison are shown in Table B.22. Predictions with MPM model give better regression coefficients as

Table 4.19: Comparison of experimental dynamic binding capacity with simulation models for BSA, BLG, and ALA for Capto Q anion exchanger

Protein	Inlet conc. (mg/ml)	DBC (mg/ml)	Langmuir		MPM		SMA	
		Experimental	value	% error	value	% error	value	% error
BSA	1.5	74.400±0.2	73.313	1.46%	72.338	2.77%	75.038	-0.86%
BLG	3	232.950±1.45	232.350	0.26%	234.675	-0.74%	230.625	1.00%
ALA	2	100.750±2.175	97.105	3.62%	100.710	0.04%	97.300	3.42%

compared to other thermodynamic models. Table 4.19 further shows the comparison of DBC values estimated by predicted curves from the various isotherm models to the DBC obtained from experimental breakthrough. The DBC values obtained by breakthrough are far less than the SBC values obtained by Langmuir model using adsorption experiment data. On the other hand, DBC for BLG was found to be very high. All the DBC values determined from predicted breakthrough curves matches well with the experimental DBC showing consistency of prediction using *ExProSim:IC*.

4.3.3.6 Multicomponent breakthrough: Experimental

It was expected that when all three proteins were injected together, the competition for the sites should further decrease the extent of binding of the proteins in the column. Figure 4.23 shows the multicomponent breakthrough obtained for the mixture of proteins injected (The zoomed Section in the Figure can be looked at to get a closer look). The breakthrough is achieved earlier than any of the single component breakthrough showing obvious reduction in the binding of all three proteins. Figure 4.24 shows HPLC analysis of the samples taken at onset, 10%, 50%, and 100% of breakthrough curve. It can be seen that the increase in BSA and ALA starts with steeper increase in ALA at 10%, whereas at 50%, BSA shows values above its saturation with ALA still increasing further. Till 50% of the breakthrough, BLG was not seen at the column outlet. Furthermore, at 100% breakthrough, BLG reaches to its saturation value, whereas BSA and ALA show decreasing profile from the saturation value. This may be attributed to displacement of BSA and ALA happening due to BLG. Dimer of BLG might be responsible for the slow retention of BLG.

It can be seen that the breakthrough onset for BSA, shifted from 88.6 for single

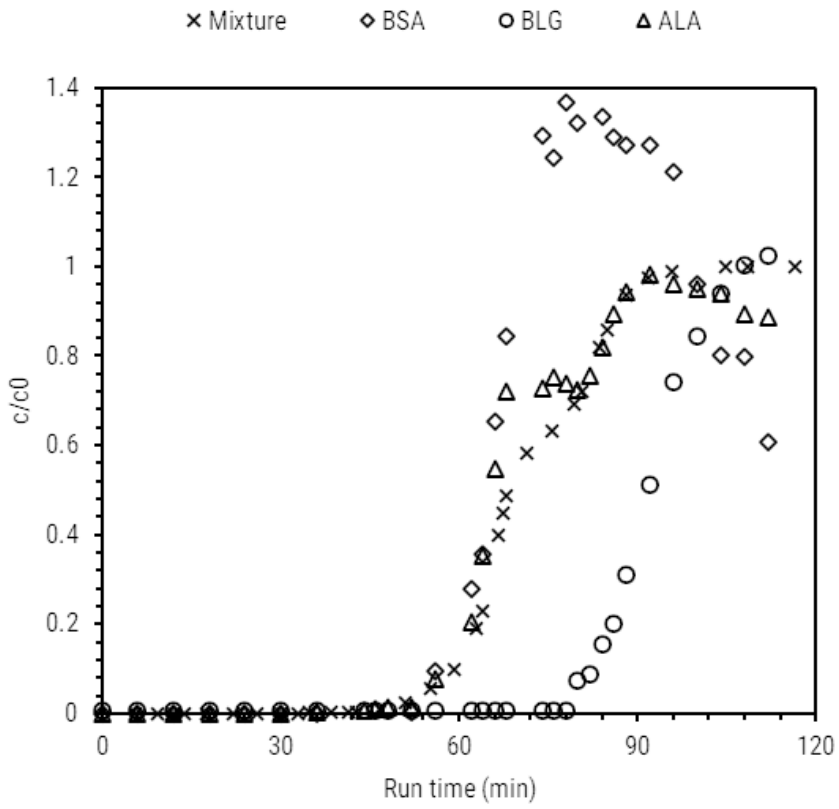

Figure 4.23: Experimental breakthrough curves for multicomponent system and individual breakthrough curves from HPLC-SEC for BSA and BLG for 1 ml/min flow rate, (BSA ◇, BLG ·, ALA △ and combined -×-)

component to 52 minutes. For ALA, it shifted from 68.87 to 48, and for BLG it shifted from 138.6 to 78 showing decrease in binding capacity for all the proteins due to competition.

4.3.3.7 Breakthrough simulations with *ExProSim:IC*

EDM-Langmuir model

Combination of EDM-Langmuir models was implemented further to predict the competitive breakthrough profiles. Predictions obtained at parameters obtained from adsorption experiments were far from satisfactory hence further modifications were done to fit to individual experimental breakthrough curves. Modified model parameters are summarised in Table 4.20.

Simulation profiles obtained for modified parameters are shown in Fig. 4.25.

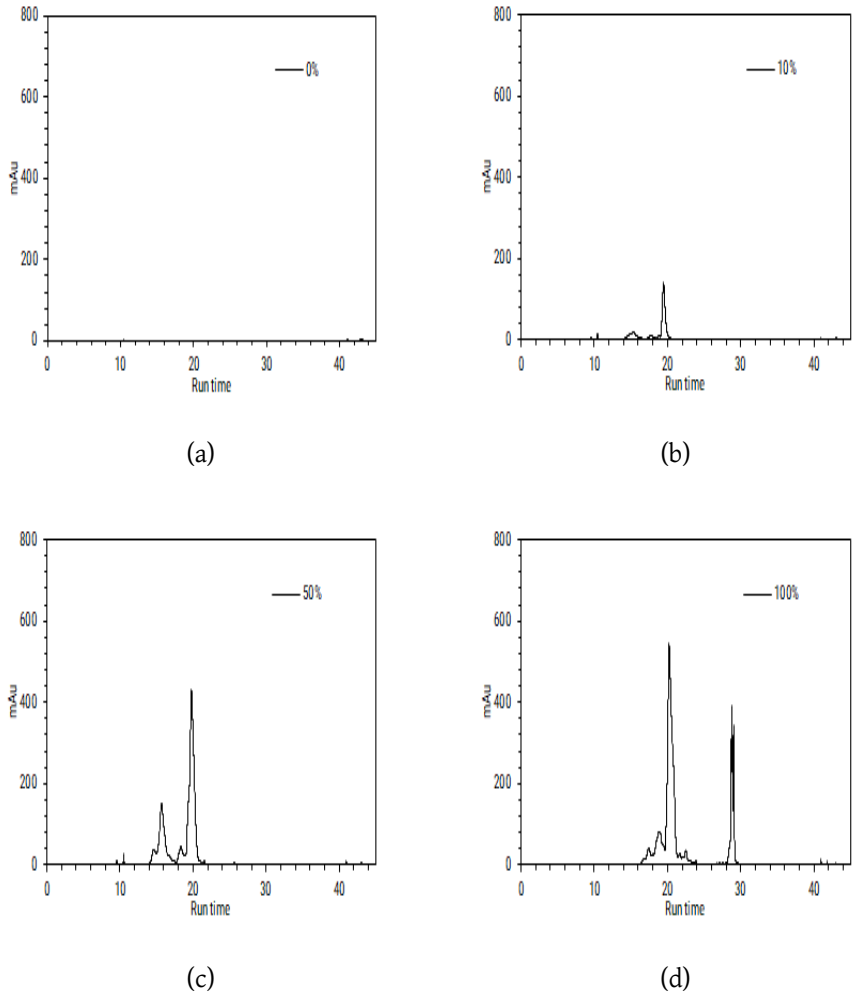

Figure 4.24: Comparison of hplc profiles of breakthrough samples taken at a) 0%bt, b) 10%bt, c) 50%bt, and d) 100%bt

Kinetics of adsorption and desorption was also affected because of the competition between the proteins showing higher desorption rates. For the best match, values of adsorption rate constant for BSA, ALA, and BLG were increased by 100,100, and 300. On the other hand, k_d value was also increased for all of them. Higher increase in k_{ads} value with marginal increase in k_d value suggests higher desorption rates for all proteins. This might be due to presence of higher number of molecules for binding leading to rapid displacement. Breakthrough curve was predicted well for BSA till 40% breakthrough but after that the error increased towards saturation. For BLG and ALA, Langmuir isotherm could predict the breakthrough data well but higher error was observed towards the end of the curve. The overshoot of BSA was best predicted by Langmuir as compared to other two

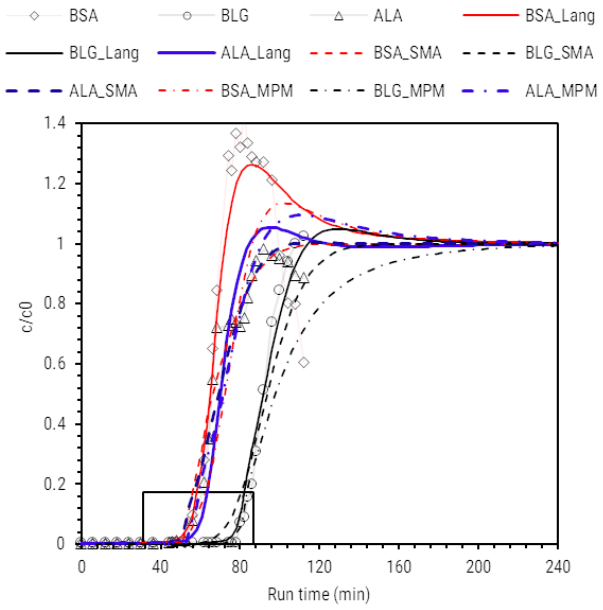

Figure 4.25: Comparison of simulated breakthrough curves with multicomponent breakthrough for major whey proteins for all the model combinations. Predicted curves for BLG; Langmuir —, SMA · ·, MPM - · -, and BSA; Langmuir —, SMA · ·, MPM - · -, ALA; Langmuir —, SMA · ·, MPM - · -, Experimental (BSA ◇, ALA △, BLG ○)

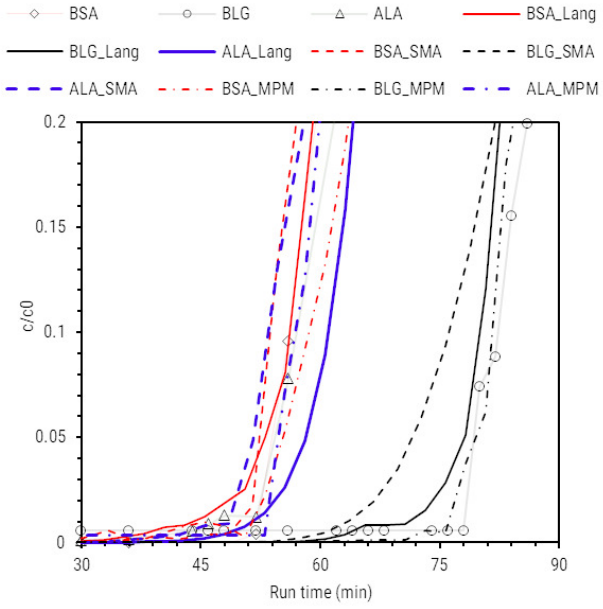

Figure 4.26: Zoomed version for a better comparison of breakthrough points in multicomponent breakthrough predictions using *ExProSim:IC* for all the models for BSA, ALA, and BLG at 1 ml/min. Predicted curves for BLG; Langmuir —, SMA · ·, MPM - · -, and BSA;Langmuir —, SMA · ·, MPM - · -, ALA ;Langmuir —, SMA · ·, MPM - · -, Experimental (BSA ◇, ALA △, BLG ○)

Table 4.20: Modified model parameters for major whey proteins multicomponent simulation using EDM:Langmuir model for Capto Q anion exchanger

Protein	Constant	Value	Multiplier	Modified value
BSA	Q_{max} (mg/ml of resin)	128.8	0.65	83.72
	k_d ($\times 10^{-6}$M)	2.924	2	5.848
	k_1 ($\times 10^{-3}$ml/mg.min)	7.56	100	756
BLG	Q_{max} (mg/ml of resin)	125.09	1.5	187.635
	k_d ($\times 10^{-6}$M)	3.187	5	15.934
	k_1 ($\times 10^{-3}$ ml/mg.min)	1.37	300	411
ALA	Q_{max} (mg/ml of resin)	139.4	0.45	62.73
	k_d ($\times 10^{-6}$M)	20.52	1	20.52
	k_1 ($\times 10^{-3}$ ml/mg.min)	7.81	100	781

isotherms.

EDM-MPM model

Furthermore, multicomponent breakthrough data was predicted using *ExProSim:IC*. Table 4.21 shows the modified parameters for fitting of the simulation curves to experimental data. Breakthrough point and 10% breakthrough was successfully predicted by *ExProSim:IC*, whereas the error was high above 80% breakthrough and beyond for all three proteins. Slight overshoot of BSA because of displacement by BLG was predicted by simulations but it couldn't match to the experimental overshoot. Error was as high as 26% for BSA because of inability to predict the overshoot. Comparison of model constants helped further in understanding the breakthrough profiles. Q_{max} value was highest for BLG, showing higher retention in the resin bed. Values of β signifies the strength of the interaction. Highest value of β for BLG supported its retention in the column, however even ALA shows higher value of β which should reflect in increased binding strength. Earlier exit

Table 4.21: Modified model parameters for major whey proteins multicomponent simulation using EDM:MPM model for Capto Q anion exchanger

Protein	Parameter	Value	Multiplier	Modified value
BSA	Q_{max} $(mg/mlofresin)$	127.2	0.7	89.53
	k_{des0} $(ml/mg.min)$	2.27	0.5	1.135
	k_{ads0} $(ml/mg.min)$	1.606	1	1.606
	β	0.029	1	0.029
	γ	1.457	1	1.457
	$D_{ax}(\times 10^{-2})$	4.791	5	23.95
BLG	Q_{max} $(mg/mlofresin)$	96.88	1.5	145.32
	k_{des0} $(ml/mg.min)$	1.818	1	1.818
	k_{ads0} $(ml/mg.min)$	1.21	0.1	0.121
	β	0.064	10	0.64
	γ	1.386	1	1.386
	$D_{ax}(\times 10^{-2})$	4.84	3	14.52
ALA	Q_{max} $(mg/mlofresin)$	101.5	1	101.5
	k_{des0} $(ml/mg.min)$	0.493	10	4.93
	k_{ads0} $(ml/mg.min)$	1.29	0.2	0.258
	β	0.61	0.5	0.305
	γ	1.802	1	1.802
	$D_{ax}(\times 10^{-2})$	3.21	3	9.63

of ALA might be attributed to very high desorption constant. Values of k_{dmpm} were found out for all the proteins. ALA showed highest value for resultant desorption constant (4.6) which explains faster release from the resin. Though the value of k_{dmpm} for BSA was least, lower β value showed weaker binding to the resin.

4.3.3.7.1 *EDM-SMA model*

Furthermore, multicomponent breakthrough was predicted by performing simulations using EDM and SMA isotherm. This is as shown in Figure 4.25. Modified

parameters for SMA are shown in Table 4.22. It can be seen that charge values were reduced to account for the possible reduction in the adsorption capacity of the proteins. Charge value for BLG was decreased marginally as compared to major decline in the charge values for ALA and BSA. This suggests displacement of ALA and BSA by BLG. Fast adsorption desorption was taken into account by increasing k_{eq} values. High increase in resultant k_{eq} supports rapid desorption for all the proteins as compared to single component breakthrough. Least value of k_{eq} was found for BLG, showing most stable binding amongst three proteins. SMA predictions showed lesser accuracy when compared with Langmuir and MPM.

Table 4.22: Modified model parameters for major whey proteins multicomponent simulation using EDM:SMA model for Capto Q anion exchanger

Protein	**Fitted Parameters**	**Value**	**Multiplier**	**Modified value**
BSA	v	1.931	0.38	0.734
	k_{eq} $(\times 10^{-2})$	19.26	15	288.9
	σ	9.715	0.1	0.9715
BLG	v	1.737	0.81	1.407
	k_{eq} $(\times 10^{-2})$	6.85	5	34.25
	σ	5.612	1	5.612
ALA	v	3.27	0.13	0.4251
	k_{eq} $(\times 10^{-2})$	0.156	500	78
	σ	4.015	1	4.015

It can be observed that onset and 10% breakthrough were predicted accurately for all the proteins. Error in SMA predictions was higher for BSA towards the end of the curve as the overshoot was not predicted by SMA isotherm. Error was found to be more than 40% from halfway through of the curve.

Table B.6 shows the overall error at different time points in the breakthrough for all the models. Dynamic binding capacity values from multicomponent breakthrough experiment were further compared with simulations as shown in Table 4.23. It can be seen that overall performance of MPM is best amongst all three models as the overall error in breakthrough and DBC was the least for MPM.

Table 4.23: Comparison of DBC from multicomponent breakthrough for anion exchange of major whey proteins

	Exp	Langmuir		MPM		SMA	
Proteins	**value**	**value**	**%error**	**value**	**%error**	**value**	**%error**
BSA	57.958	61.292	-5.75%	59.208	-2.16%	55.771	3.77%
BLG	86.292	84.625	1.93%	86.500	-0.24%	79.573	7.79%
ALA	55.875	58.375	-4.47%	58.375	-4.47%	57.958	-3.73%

4.3.4 Comparison of cation and anion exchange chromatography

We have seen that major whey proteins can be separated by implementing both cation and anion exchange chromatography techniques. However, it should be decided which performs better for separating all three proteins for future process development. In case of cation exchange, the window for selection of pH for operation is very low. At pH lower than 4.2, very harsh salt conditions are required for elution of the bound proteins which may affect the structure and properties of the proteins. Additionally, pH higher than 4.2, ALA cannot be purified as it has almost no electrokinetic potential at its isoelectric point. BSA remains slightly hydrophobic at pH 4.5, which affected its binding in a cation exchanger.

In case of anion exchange, operation window was found to be flexible enough to allow reversible binding of all the proteins to the resin. Furthermore, for cation exchange, the process has to be operated at lower pH which is not the pH of the sweet whey which is generally obtained from the industry for separating major proteins from crude stream. Sweet whey pH is generally between 6.6-7.2 which is used here for anion exchange[261]. Binding capacities obtained for anion exchanger are comparable to the binding capacities mentioned by the manufacturer for the standard proteins indicating optimum usage of the resin at the selected pH. Comparing both chromatographic methods for ease pf operation and further feasibility for scaling up, it can be inferred that anion exchange chromatography gives clear advantages over cation exchange. Hence, anion exchange was finalised for major whey protein purification studies and minor proteins were studied only for cation exchange process in Chapter 5.

4.4 Conclusion

This chapter presents a methodological approach to experimental validation of the tool *ExProSim:IC*. Experimental system for validation of the tool presented an important aspect of whey processing for high value products. Major whey protein adsorption and breakthrough were discussed in detail for both cation and anion exchange chromatography. Data generated from both experimental approaches was used for finding out parameters of the models used for simulations in *ExProSim:IC* for expeirmental validation. Cation exchange chromatography was explored for BSA and BLG, however due to restrictions imparted by operating pH, ALA was not considered. On the other hand, anion exchange chromatography was successfully implemented for all three proteins. For both methodologies, respective proteins were successfully assessed for their adsorption kinetics and model parameters were obtained by performing basic experiments such as; adsorption, column porosity, ionicity determination, and uptake kinetics. Furthermore, breakthrough experiments were performed at different velocities. Breakthrough for BSA for cation exchange was not seen to reach saturation because of prevalent hydrophobic interactions showing apparent $Q_{max}$for BSA. On the other hand, electrokinetic transfer through the column was observed for BLG showing comparable values of SBC and DBC.

For anion exchange, all the proteins reached the saturation values with consistency in SBC and DBC values. Langmuir, SMA, and MPM models were along with EDM were examined and compared for their predictability of the experimental data produced for both cation and anion exchange. All models accurately predicted the breakthrough point and 10$\%$ breakthrough which was further used in finding DBC. For most part of the curve, the predictions showed less than 5$\%$ error showing early saturation towards the end. Uneven predictions were obtained for Langmuir isotherm for both cation and anion exchange processes as compared to MPM and SMA. This can be attributed to higher number of parameters available for fitting the data. For SMA isotherm, determination of 'charge' value was not accurate experimentally. As 'Charge' has an exponential presence in the equation, its accuracy is paramount, and probably a better method for the same should be

devised. Parameters obtained from inverse fit were used successfully for predictions for both MPM and SMA eliminating the need of performing gradient experiments.

Errors shown by curve to curve comparison by determination of RMSE and coefficient of determination did not give correct representation of the fit. Even if the errors at important experimental points was high, error seemed low showing a good fit. Hence, point to point comparison was practised so that significance with respect to experiments can be derived. Point to point comparison also allowed determination and comparison of DBCs of the resin towards the proteins and their change when in competition with each other. DBC certainly gave idea about resin capacity but not performance. Also in case the resin becomes old, it will be difficult to predict even the capacity with respect to ageing of the resin. Additional considerations may be required. Comparison at 50% and 100% breakthrough gave a better idea about shape of the breakthrough and desorption of protein describing resin performance. It was observed that simulations using EDM were not efficient to predict end of the breakthrough suggesting better considerations on diffusion of the protein through the resin may be required. Higher accuracy and consistency can be obtained in predictions if POR and GRM can be implemented. For predictions of multicomponent systems by *ExProSim:IC*, Langmuir and SMA showed reasonable accuracy, whereas MPM proved to be most accurate. This can be attributed to more number of parameters to fit the data. SMA can be a better isotherm in case of prediction peaks at changing salt concentrations which is not attempted here.

Overall, it can be said that the methodology for calibration of model constants was established here and implemented in the tool. The tool developed is capable of predicting preliminary experimental outputs for proteins with wide range of properties for application of both anion and cation exchange chromatography.

Chapter 5

Minor whey protein separation

5.1 Introduction

Whey consists of major proteins such as α-lactalbumin (ALA), β-lactoglobulin(BLG), and bovine serum albumin(BSA) ($\leq$90$\%$ of total proteins) which are acidic in nature. Additionally, few minor proteins such as lactoferrin (LF) and lactoperoxidase (LP) are basic in nature and show promising therapeutic activities [262, 263, 264]. Adsorption and separation studies for major proteins have already been discussed in detail in Chapter 4 along with the respective simulation studies. This chapter focuses on studying binding characteristics of minor whey proteins on a cation exchanger for additional experimental validation of *ExProSim:IC*. Choice of cation exchange chromatography was based on two factors. Firstly, considering isoelectric points (*pI*) of LF and LP, anion exchangers will need pH higher than 9.5 for sufficient binding of minor proteins which is too harsh for the stability of LF and LP. Secondly, as the major proteins showed better performance towards anion exchangers at pH 6.9, flow-through having minor proteins can be directly processed on cation exchangers at the same pH giving a possible tandem separation.

5.2 Methodology

Along with Experiments, *ExProSim:IC* was used further to implement equilibrium dispersive model (EDM) along with various isotherm models such as Langmuir, steric mass action(SMA) and mobile phase modulator(MPM) for prediction of sin-

gle and multicomponent breakthrough curves. Methods for computation were implemented as given in Section 3.2. Data obtained from adsorption experiments was used to obtain the model constants for Langmuir, MPM, and Freundlich isotherms by inverse fitting. Once, all the model constants were determined, they were used as input for *ExProSim:IC* for simulating the breakthrough curves. For validation of simulations, predicted profiles were compared with the experimental curves and error was determined at a number of points (0%, 10%, 50%, and 100% of saturation concentration) on the curve. If the error was out of acceptable criteria ($\pm 5\%$ for 0 and 10% BT), model constants were revised logically depending on the error obtained and the simulations were repeated until the successful match was obtained. Also, curve to curve error was determined for all simulation and experimental curves.

5.2.1 Experimental

5.2.1.1 Materials and Methodology

All the protein standards and buffers required for cation sample analysis are mentioned in Section 3.3.1. LP and LF were used as model proteins and the adsorption was carried out on loose and prepacked Capto S™ resin. According to the resin manufacturer, Capto S™ offers 15-20% higher binding capacity as compared to its predecessor SPFF which was used for cation exchange studies of acidic proteins. Along with higher loading, it has high chemical stability, shows better pressure response, and processes can be operated at higher flow rates saving resultant operating times [254].

All the samples generated from batch studies were analysed at 280 ηm on UV-vis spectrophotometer. Samples generated from NGC Bio-Rad for multicomponent breakthrough curve were analysed by using HPLC *method 1*. As mentioned in Section 3.3.2.5, *method 1* was developed for sufficient resolution and clarity of the peaks for LF and LP. 1 mg/ml mixture of ALA, BLG, BSA, LF, and LP was injected at different gradients of mixture of mobile phase A (0.1% TFA in 100 % ultra-pure water) and mobile phase B (0.1% TFA in 100 % ACN) in order to get maximum resolution between LF and LP. For low pressure cation exchange equilibration and

wash buffer used was 25 mM sodium phosphate buffer at pH 6.9. 0.5 M NaCl in equilibration buffer at pH 6.9 was used for elution whereas 1 M NaOH was used for regeneration of the resin.

5.2.1.2 Sample Analysis

Total protein content of the samples from the reports received by Tatua was based on analysis from elemental analyser hence C-H-N analysis was performed for the samples. Further to check their qualitative and quantitative purity, samples were subjected to multiple assessment techniques.

Column profiles using NGC

LF and LP, 3 mg/ml and 4 mg/ml respectively were prepared in equilibration buffer. 300 μl of sample was injected onto the column to check the peak profile of the standard samples for impurity profiling. Resolution between multiple peaks (if any) was assessed. Individual breakthroughs of the samples were run at 0.5 ml/min flow rate to check if any impurities elute during flow-through to influence pure protein breakthrough profiles. For low pressure cation exchange column experiments, prepacked HiTrap Capto S column was used for frontal chromatography experiments using NGC. All the column experiments were performed at ambient temperature of 25°C.

HPLC analysis

To check purity of the samples and find out probable nature of impurities, HPLC analysis was done by injecting standard samples of the protein. HPLC purity was determined by *method 1*.

SDS-PAGE

For qualitative profiling of protein samples at various stages of column experiments as well as for the standards, SDS-PAGE was performed.

5.2.1.3 Chromatography experiments

Adsorption isotherm experiment For cation exchange adsorption, experiments were carried out for binding on Capto S resin as given in Section 3.3.3.1 and further fitted using *ExProSim:IC* to find model constants using inverse fit method.

Uptake kinetics 4 mg/ml solutions for each protein were used for the uptake kinetics experiment as given in Section 3.3.3.2. Pseudo first order and pseudo second order models were checked as given in Section 3.4.1. Uptake kinetics constant k_{ads} was found out from the best fit.

Column physical parameters Column physical parameters such as porosity and ionic capacity for SMA isotherm were determined by method mentioned in Section 3.3.5.

Gradient elution experiments Gradient experiments were performed to estimate the charge constant v_i and equilibrium constant $k_{eq,i}$. LF and LP, each 3 mg/ml were prepared and 300 μl was injected on an equilibrated column for different gradient slopes of 0.5 M sodium chloride. The values of v and k_{eq} were determined by fitting experimental data to Equation 3.23 [228].

Breakthrough experiments For LF the breakthrough was obtained at 3 mg/ml and 6 mg/ml at flow rates of 0.5, 0.75, and 1 ml/min. For LP, Breakthrough were performed at 4 mg/ml concentration at 0.5, 0.75, and 1 ml/min flow rates. Inlet parameters such as flow rate and concentration were varied to check their effect on prediction ability of *ExProSim:IC*. Breakthrough was further analysed for accuracy of predictions. Time and volumes for breakthrough point, 10$\%$ breakthrough, halfway concentration and exhaustion were recorded for comparison with simulations. σ_i was estimated by using Equation 3.24[229].

Multicomponent breakthrough For multicomponent breakthrough, LF and LP were mixed together in 4.5 mg/ml and 3 mg/ml concentrations respectively making the overall concentration of the protein solution to 3.75 mg/ml. The breakthrough was carried out in a similar fashion at 0.5 ml/min. Samples were collected throughput the experiment till the saturation. Furthermore, standard curves were prepared for LF and LP by injecting different concentrations of the protein on to the column to assess unknown sample concentrations. The samples collected from NGC were analysed on HPLC with 20 μl injection volume.

5.3 Results and Discussion

5.3.1 Sample analysis

The total protein content by C-H-N analysis based on total nitrogen was found to be 94.026% for LF and 93.88% for LP. HPLC method was finalised by comparing number of gradient runs. Two representative gradient runs are shown here in Figure 5.1. As the mixture of all the proteins was injected, initial expectation was to resolve all the proteins for analysis but then it was decided to go ahead with maximum resolution for LF and LP for this specific analysis (5.1(b) was preferred over 5.1(a)). *HPLC Method 1* is shown in Table 5.1. Figure 5.2(a) and 5.2(b) show the standard curves determined from hplc analysis and can be used for finding out concentrations of unknown samples from multicomponent breakthrough experiment.

Table 5.1: HPLC *method 1* for LF and LP resolution (%B in the table is acenotnitrile concentration in mobile phase). Flowrate is 1 ml/min

Run time (min)	**%B**
0	0
2	0
4	35
6	37
24	43
32	70
36	100
40	100
42	0
45	0

When assessment of the obtained protein samples using cation exchange chromatography was performed, no impurities were seen in LF sample as shown in Figure 5.3(a). However, chromatography run for LP showed a major impurity peak in wash fraction as can be observed in Figure 5.3(b). The SDS-PAGE as shown in Figure 5.4(a) further confirmed the presence of impurities in the LP sample. This was further confirmed by collecting the peak and loading on hplc column (Figure 5.5(b)). As breakthrough and other column experiments required a pure sample, the retained peak from multiple column experiments on a xk-16/20 (20 ml)

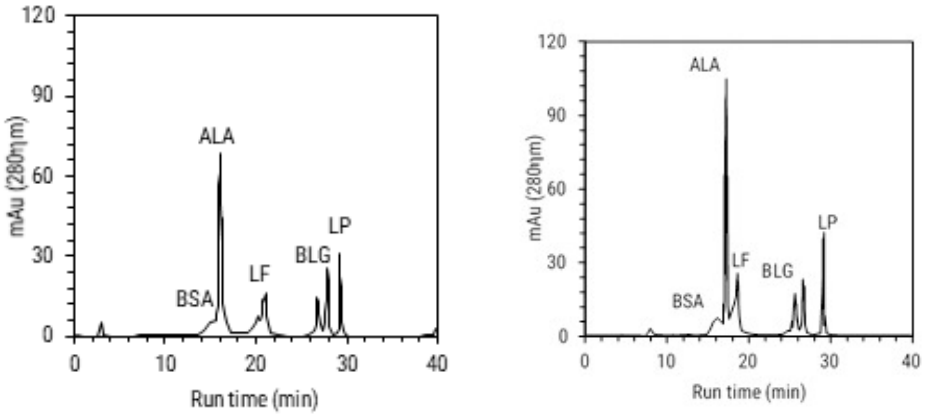

Figure 5.1: Different gradient method trials to get maximum resolution between LF and LP. Method (b) was chosen over (a)

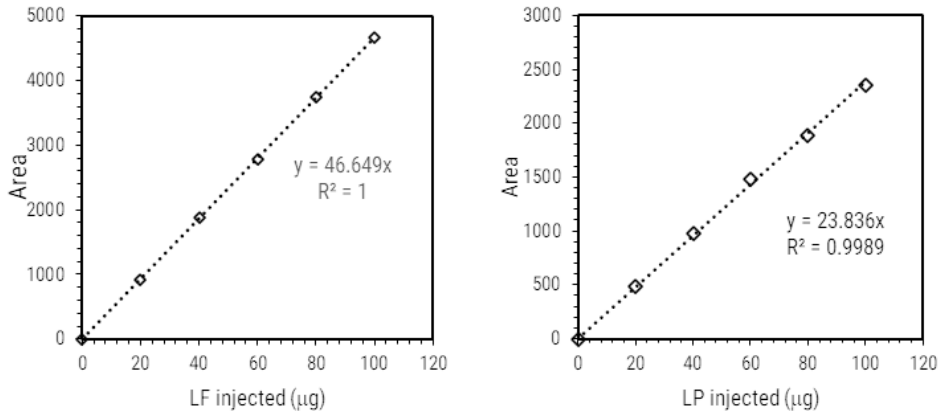

Figure 5.2: Standard curves for (a) LF and (b) LP determined from HPLC

column was collected in order to separate pure fraction of LP. The elution fractions were further concentrated and desalted using a 10 kDa minimate membrane filtration cassette. Qualitative and quantitative purity of the generated sample was checked using SDS-PAGE, NGC, and HPLC. For SDS-PAGE, the gels were overstained to ensure visibility of minor impurities. Figure 5.4(b), SDS-PAGE well 7 confirms the removal of impurity. Removal of the impurity was further confirmed by NGC (Figure 5.5(a)) and HPLC profile (Figure 5.5(b)) for LP sample. The purity of LP was improved from 88% to 97%.

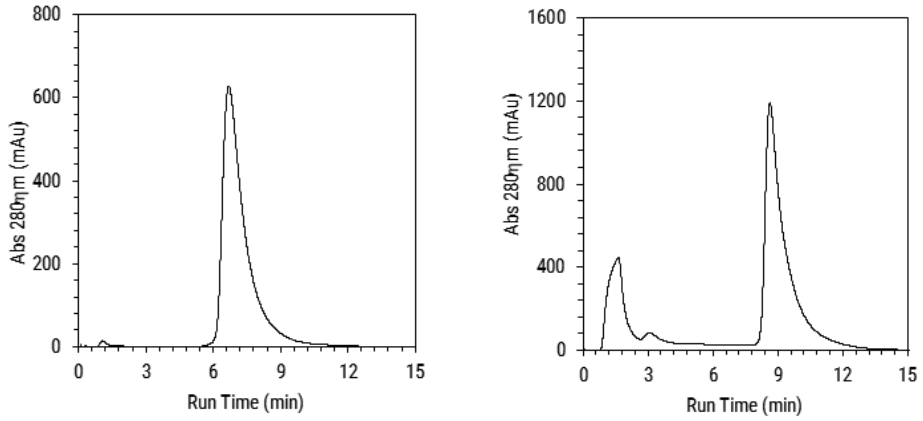

(a) (b)

Figure 5.3: LF (a) and LP (b) standard profiles on Capto S HiTrap 1 ml column

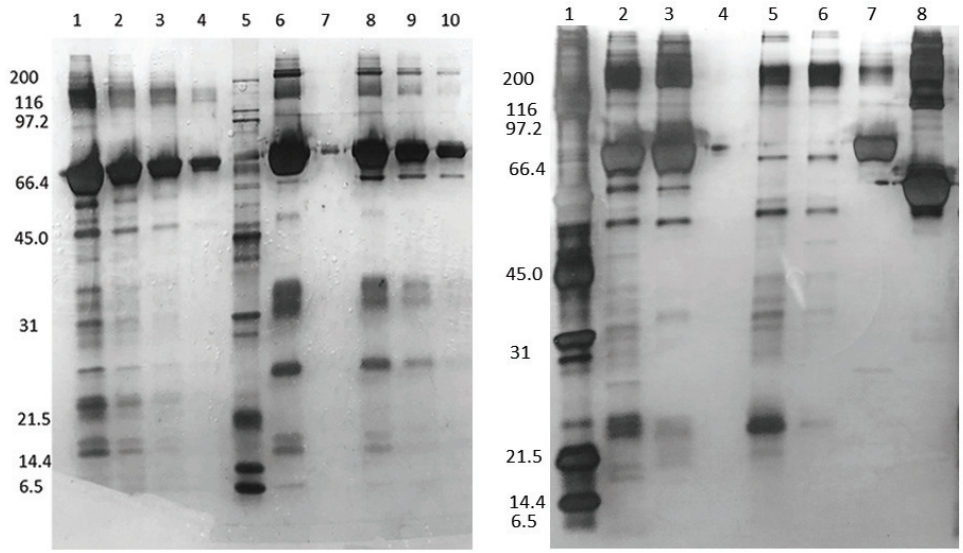

(a) (b)

Figure 5.4: a) SDS-PAGE for LF and LP at different concentrations: 1. LP 0.5 mg/ml 2. LP 0.25 mg/ml 3.LP 0.125 mg/ml 4. LP 0.0625 mg/ml 5. Broad range marker 6. LF 0.5 mg/ml 7. Blank 8. LF 0.25 mg/ml 9. LF 0.125 mg/ml 10. LF 0.0625 mg/ml b) Comparison of SDS-PAGE for LP before and after purification: 1.Broad range marker 2. LP tatua standard 3. LP sigma standard 4. Blank 5. LP fraction 1 6. LP fraction 2 7. LP elute 8. bovine serum albumin

5.3.2 Cation exchange chromatography

5.3.2.1 Determination of Langmuir parameters

Adsorption isotherms

For both the proteins, Langmuir isotherm exhibited good fit with experimental data as shown in Figure 5.6. Langmuir equilibrium constant R_L was estimated

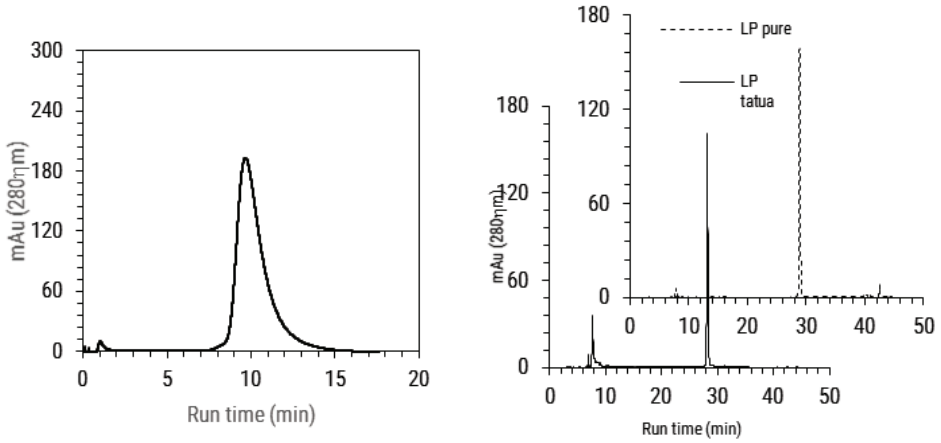

(a) (b)

Figure 5.5: a) LP profile on NGC after purification b) Comparison of HPLC profiles for LP before and after purification

in between 0 to 1 for all the inlet concentrations indicating a reversible hence favourable adsorption. Langmuir isotherm was favoured over Freundlich isotherm suggesting mono-layered adsorption. The exponent of Freundlich was estimated to be more than unity which was an underestimation of binding capacity as shown in Table 5.2.

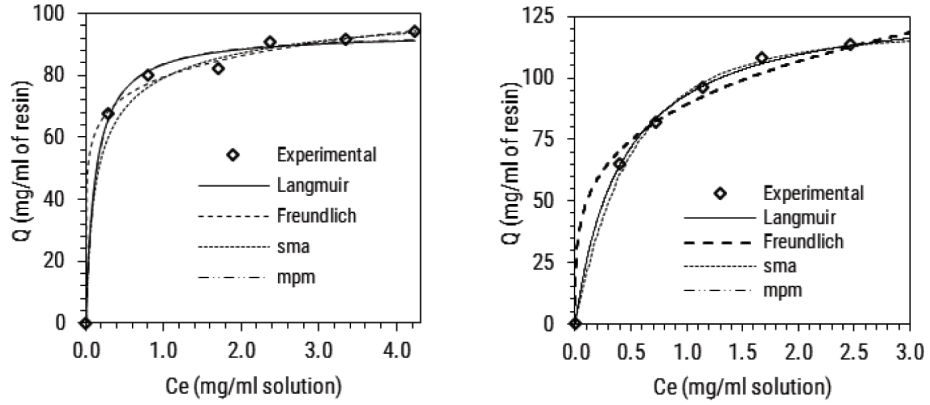

(a) (b)

Figure 5.6: Langmuir, Freundlich and SMA adsorption isotherm fit with experimental data for LF (a) and LP (b)

It is important to understand the properties of protein and how they can affect the binding kinetics before further discussion. It is known that the charges on the protein surfaces primarily take part in the ion exchange with the resin. As ex-

Table 5.2: Summary of Langmuir, Freundlich, and MPM adsorption parameters for LF and LP

Parameter	**LF**	**LP**
Langmuir model		
Q_{max} (mg/ml of resin)	93.88	132.5
k_d, ($\times 10^{-6}$M)	1.58	6.41
R_L at 3 mg/ml	0.352	0.123
R_L at 8 mg/ml	0.134	0.0581
R^2	0.9932	0.9982
Freundlich model		
Q_f (mg/ml of resin)	79.66	89.32
n	8.315	3.893
$1/n$	0.1192	0.2568
R^2	0.990	0.982
MPM Langmuir model		
Q_{max} (mg/ml of resin)	93.95	132.05
k_{ads0} (ml/mg.min)	0.8098	0.1244
k_{des0} (ml/mg.ml)	0.0818	0.0209
β	0.0119	0.2812
$\gamma(\times 10^{-3})$	6.44	0.59
R^2	0.9929	0.9901

R_L: Langmuirian equilibrium constant,

plained in Section 4.3.2.1, binding is a result of combination of forces with charged attraction as dominating force for ion exchange [241]. The k_d values obtained for LF and LP lie within this range 10^{-8} M and 10^{-4} M, indicating the suitability of the ion exchange process [242].

Ghosal and Gupta have given analytical proof that Langmuir constant can be related directly to thermodynamic equilibrium constant, K_{teq} using Vant Hoff equation [25] (Equation 5.1). Where, R is a universal gas constant (8.314 J.mol-1.K-1), ΔH^0 and ΔS^0 are standard changes in enthalpy and entropy respectively. Relation between k_d and K_{teq} is derived in the work by Ghosal and Gupta, hence

it was not discussed in detail here. The work states that value of k_d is dependent on K_{teq}. K_{teq} is a generalised thermodynamic equilibrium constant, whereas k_d is specified as adsorption equilibrium constant expressed in terms of kinetics of the process. Positive and negative ΔH^0 values represent endothermic and exothermic reaction. Positive value of ΔS^0 indicates the affinity of the sorbent towards the sorbate as the randomness near the solid liquid interface is high giving more chances for adsorption to take place. This means that change in K_{teq} value changes the extent of adsorption. This change can be accounted by measuring k_d value which also represents kinetics of adsorption. This supports that the change in k_d value shifts the equilibrium of the adsorption process which directly affects the extent of adsorption happening. k_d is mathematically represented as k_{des}/k_{ads}.

$$lnK_{teq} = -\frac{\Delta H^0}{RT} + \frac{\Delta S^0}{R} \tag{5.1}$$

Lower value of k_d suggests higher adsorption or lower desorption rate indicating stronger binding, whereas increase in the value of k_d suggests weaker binding. The dissociation constants obtained for LP was almost 4 times of that of LF suggesting loose binding for LP. On the other hand, the electrophoretic mobility depends on how far the *pI* lies from the pH of operation. *pI* further denotes the pH at which protein has minimum effective volume. At operating pH of 6.9, LF with *pI* of 7.8-8.2 should have a lesser adsorption capacity than LP having *pI* of 9.2-9.5 which was further supported by Q_{max} values as shown in Table 5.2. This means even if LF has lesser binding, it has firm adsorption on the column.

Uptake kinetics

As the uptake of protein depends on the sites at which it interacts with the resin, lumped kinetic models such as; Pseudo first order (Equation 3.39) and pseudo second order (Equation 3.40) were chosen to fit the data. As the molecular size is significantly smaller than the exclusion limit of the resin, we did not consider film theory for diffusional uptake. Concentrations used in experiments were considerably higher, therefore slow diffusion was ignored. The molecular size of the protein was determined in terms of their molecular radius using Equation 4.3 [250]. The radius of LF and LP were estimated to 32.01 and 30.21 suggesting that it was

safe to ignore additional diffusion during uptake kinetics.

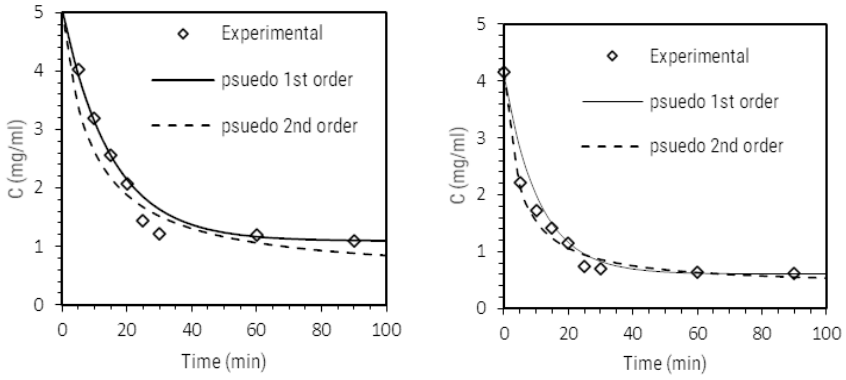

(a) (b)

Figure 5.7: Psuedo 1^{st} and 2^{nd} order uptake kinetics for LF (a) and LP (b)

Table 5.3: Uptake kinetics parameters for LF and LP

parameter	**LF**	**LP**
Psuedo first order		
k_1 ($\times 10^{-2}$) (min-1)	6.63	9.91
R^2	0.9842	0.9647
Correlation Coefficient	0.8133	0.9407
Psuedo second order		
k_2($\times 10^{-3}$) (ml/mg.min)	0.49	1.2
R^2	0.9581	0.9857
Correlation coefficient	0.9521	0.9837

It can be seen in Figure 5.7 that the uptake of LF and LP were better described by pseudo 2^{nd} order kinetics. Parameters for the fitting are shown in Table 5.3. Uptake kinetic constant k_2 for LP was found to be 2.5 times higher than that for LF. Considering higher charges on LP due to its *pI*, the faster uptake was justified. When desorption constant, k^l_{des} was determined based on k_d and k_2, it was seen that LP had very high desorption constant. This explains higher slope in the breakthrough curves.

5.3.2.2 Determination of MPM parameters

Adsorption isotherm fitted by MPM was found to coincide with that of Langmuir isotherm (Figure 5.6). Parameters obtained for MPM isotherm are shown in Table 5.2. It is evident that the values of Q_{max} are same for both isotherms. To compare the difference in dissociation between Langmuir and MPM, cumulative kinetic constants (k^m_{ads} and k^m_{des}) for MPM were calculated to determine equilibrium dissociation constant, k_{dmpm}. For LF, the value ($1.27E-6$ M) was considerably higher than LP ($7.67E-7$ M), showing difference in desorption kinetics. This means that LP has stronger attraction towards the resin as compared to LF. The values of β further concurs this observation as β value for LP was almost 10 times that for LF. Values of k_d and k_{dmpm} were almost same which explains the closeness of the fit.

5.3.2.3 Determination of SMA parameters

The value of external porosity from moment analysis of blue dextran peaks was 0.412±0.0182 and particle porosity obtained from moment analysis was 0.834±0.022. Total porosity was further calculated from these two values by using Equation 3.31, and was estimated to be 0.896±0.015. The lumped coefficient for axial dispersion was found to be 4.21×10^{-2} cm^2/min. Further the ionic capacity calculated from the titration experiment was 1345.7 mM/ml resin. The reported value for Capto S from GE is 1100-1400 mM/ml resin[254].

SMA model shows a precise fit to the adsorption experimental data for both the proteins as shown in Figure 5.6. SMA parameters were estimated experimentally as well as by data fitting. When the gradients of 0-100$\%$ were run, it was observed that LF and LP eluted at 21$\%$ and 34$\%$ of the salt concentration respectively which is in support with the electrophoretic mobility. Summary of gradient runs is shown in Table B.3. It can be seen that the results of gradient elution experiments were consistent over the range as the area under the curve was reproducible. RT for LF were found to be lesser than that of LP at all gradient lengths supporting their electrokinetic potential at operating pH. With increase in number of CVs, retention time (RT) of the protein was found to be increased. This was because of slower gradient with increase in number of gradient column volumes.

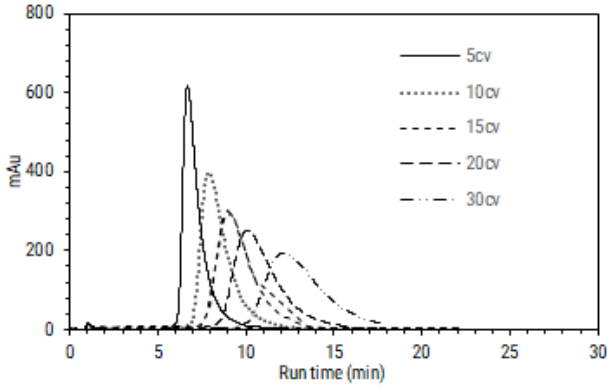

(a)

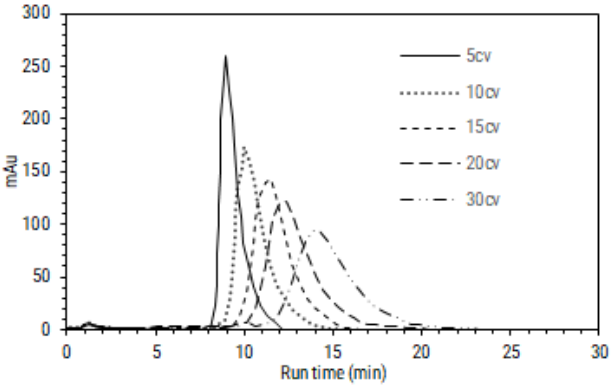

(b)

Figure 5.8: Comparison of gradient profiles for (a) LF and (b) LP at different gradient lengths

The values of v and k_{eq} were estimated from the retention volume (RV) values of the gradient experiments performed at various gradient lengths (Equation 3.23). These values were compared with the inverse fit method parameters obtained from the *patternsearch* analysis. The parameters obtained by both methods are shown in Table 5.4.

Ideally more the charge value for a protein, better is the binding strength. For the parameters obtained from elution studies, the value for characteristic charge for LF was found to be less than that of LP which supports the elution order of the proteins. However, the value of experimentally determined equilibrium constant was same for both molecules which could not be justified. In case of inverse fit method, the charge value was calculated to be higher by 23% for LF whereas it

Table 5.4: Comparison of SMA isotherm parameters from gradient experiments and isotherm fitting for LF and LP

	Protein	v	k_{eq}	σ
LF	Exp	1.7± 0.105	0.026±0.001	2.492±0.05
	Fit	2.093	0.27	9.701
LP	Exp	2.155±0.141	0.027±0.001	2.095±0.03
	Fit	0.696	17.102	10.035

Exp=Experimental, Fit= inverse fit method

decreased significantly (by 67.7%) for LP. On the other hand, equilibrium constant was found to be 10-fold higher for LF and increased to 17.102 for LP from 0.0269.

The steric hindrance factor from experiments showed a 4-fold lesser value than that of inverse fit method. Steric hindrance factor as obtained from breakthrough curves showed higher value for LF than LP which can be attributed to slight difference in the molecular weights. Values obtained by inverse fit were also very close to each other. The steric factor is a molecular weight and size based parameter which shows how much repulsive effect the size of the protein can have on adjacent binding molecules. As molecular weight of LF and LP are very close (80 and 76-78 kDa respectively), the steric factors ideally should not differ much unless there are major differences in the structure. When the structures of LF and LP were compared, it was observed that LP has a more compact structure with 2 beta sheets among α helices[170] as compared to LF which has 2 globular lobes which are linked with 3 alpha helices between them [169]. The molecular radii of the two molecules do not show much difference (compared in Section 5.3.2.1). The obvious reason of the difference in parameters of two approaches is that the base data used for 1^{st} approach was a dynamic column data; whereas, for the 2^{nd}, approach was a static adsorption data. Comparing these parameters may not be wise considering the differences in the experimental conditions. As there are two sets of parameters obtained for SMA isotherm, it was important to check the predictability depending on both sets. As inverse fit method was dependent on basic experiments, it was decided to take it as a reference for adjustment of parameters for simulations. Upon adjustment for best fit, parameters were very close to experimentally determined parameters suggesting validity of inverse fit method

for simulations.

5.3.2.4 Single component breakthrough: Experimental

The simulated and experimental breakthrough curves at different inlet concentrations and velocities for LF and different loading velocities for LP are shown in Figure 5.9 and Figure 5.10 respectively. Simulated breakthrough curves for Langmuir, SMA, and MPM isotherms as predicted by *ExProSim:IC* are shown in respective figures. Experimental breakthroughs are discussed first and then further compared with the predicted data. For LF, a prominent shift of breakthrough point can be observed with increase in velocity which can be attributed to decreasing residence time. With increase in concentration at the inlet, breakthrough was obtained earlier, suggesting crowding of molecules in the column. For LP, similar behaviour was seen where breakthrough point lowered with increase in velocity. The slope of all the curves became steeper with increase in both concentration and velocity suggesting faster saturation. All the profiles reached saturation for both the proteins suggesting steady adsorption-desorption phenomena in the column. It is noticeable that breakthrough for LP took a longer time in every case as compared to breakthrough for LF showing higher retention for LP. Further, 10$\%$ breakthrough volume was used to determine the DBC of the proteins. Figure 5.11 shows the variation in DBC with flow rate and inlet concentration. The variation in DBC values with changing concentration and a comparison of DBC for breakthrough experiments with Q_{max} obtained from Langmuir adsorption isotherm experiment is given in Table 5.5. Experimental results were found to be very consistent as the variation in 10$\%$ breakthrough volumes for different velocities was found to be less than 5$\%$ for both proteins suggesting minimal effect of changing velocity on estimated values of DBC. Whereas, DBC was under-predicted at higher concentrations of LF suggesting crowding of the protein molecules resulting in reduced residence time in the column leading to early breakthrough [255].

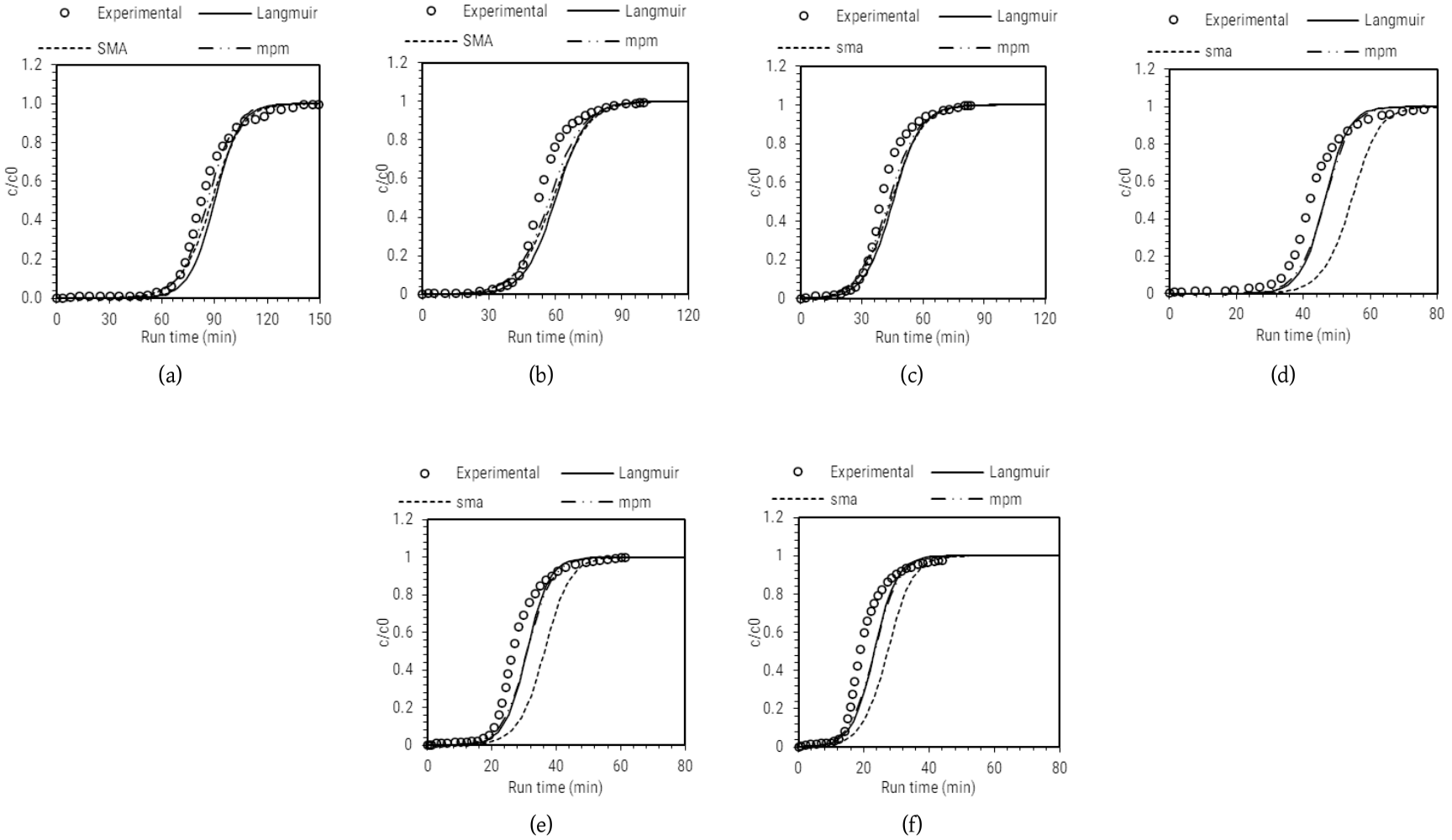

Figure 5.9: Comparison of predicted vs experimental data for breakthrough of LF at various linear velocities for inlet concentration of 3 mg/ml a) 0.5 ml/min (78.95 cm/hr) b) 0.75 ml/min (117.36 cm/hr) c) 1.0 ml/min (155.9 cm/hr) and 6 mg/ml d) 0.5 ml/min (78.95 cm/hr) e) 0.75 ml/min (117.36 cm/hr) f) 1.0 ml/min (155.9 cm/hr) , Langmuir (-), SMA (–), MPM (-···-), (experimental (◇).

Table 5.5: Comparison of DBC with Langmuir adsorption capacity at different velocities and inlet concentrations for LF and LP

Protein	Inlet Conc. (mg/ml)	10% BT volume (ml)	DBC (mg/ml)	% error from Langmuir
LF	3	32.07±2.22	92.09±6.41	1.95
	6	16.58±1.45	47.38±1.45	49.53
LP	4	44.79±0.58	128.80±1.67	2.79

10% BT=Breakthrough volume for 10% of breakthrough achieved.
The values are averaged for all the flow rates and
standard deviation is mentioned.

5.3.2.5 Breakthrough simulations with *ExProSim:IC*

Experimental breakthrough data was then compared with simulated curves from *ExProSim:IC* for Langmuir, SMA and MPM models. Input parameters for all the isotherms were adjusted in order to fit to the experimental data as the error at original model constants was very high. For a better comparison point by point comparison was used and is shown in Appendix B Table B.7 for LF and Table B.8 for LP. However, curve to curve comparison is also performed and demonstrated in Table B.24.

EDM-Langmuir model

Simulations using Langmuir-EDM were consistently close to experimental data after the parameters were adjusted to values as shown in Table 5.6. Modified model constants were assessed further to see the effect of changes in constants on the profiles. k_d value for LF was decreased by 50%, whereas LP k_d value was retained to original value. This states that the apparent dissociation constant in dynamic conditions was lesser for LF showing lesser binding strength towards resin. Resultant k_d values for both proteins showed almost 10 fold difference stating the huge difference in strength of binding. This does not support the electrophoretic mobility of the proteins suggesting presence of additional unknown interactions for decreasing desorption for LF. Q_{max} values on the other hand were increased for both proteins in order to predict the breakthrough in dynamic conditions. This suggests that additional adsorption processes are happening in the packed bed

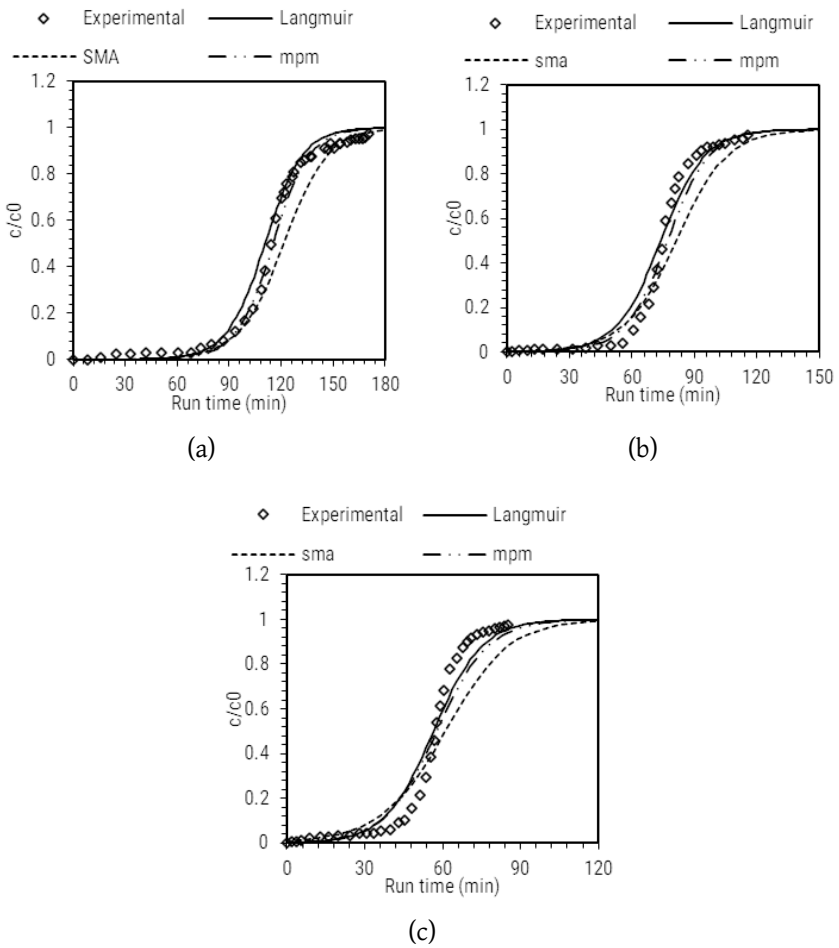

Figure 5.10: Comparison of predicted vs experimental data for breakthrough of LP 4 mg/ml at various linear velocities, a) 0.5 ml/min (78.95 cm/hr) b) 0.75 ml/min (117.36 cm/hr) c) 1 ml/min (155.9 cm/hr), Langmuir (-), SMA (–), MPM (-···-), (experimental (◇)

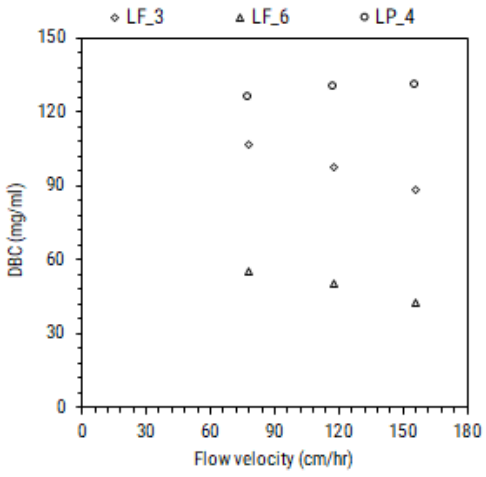

Figure 5.11: DBC versus flow velocity for two proteins LF 3 mg/ml (◇), LF 6 mg/ml (△), and LP (○) at different flow velocities 77.95, 117.36 and 155.9 cm/hr

and adsorption capacity was underestimated for both proteins during batch studies. Furthermore, modified kinetic rate constants suggested higher strength of binding for LP. It can be said that, experimentally determined Langmuir isotherm constants were not successful in relating to the nature of the protein and its binding to the resin.

For LF, 3 mg/ml inlet concentration data was predicted well at 0%, 10% and 100% for all velocities. 50% data showed higher error as the simulations over-predicted the experimental data. For inlet concentration of 6 mg/ml, faster adsorption-desorption phenomena was well-predicted by simulations but the accuracy was compromised for middle part of the curve as represented by higher error at 50% breakthrough. This can be accounted for inaccuracy of capturing the competitiveness of the protein molecules at high concentration. Similar trend was seen at all the velocities. For LP, error obtained using Langmuir-EDM was high for velocity of 1 ml/min. Errors for lower velocities were acceptable for 0%, 10%, and 100% breakthrough but 50% breakthrough was not predicted accurately. General trends of simulated breakthrough curves were observed to move farther from experimental data as the concentration and velocity were increased.

Table 5.6: Modified model parameters for single component breakthrough predictions using Langmuir isotherm

Protein	**Constant**	**Value**	**Multiplier**	**Modified value**
LF	Q_{max} (mg/ml of resin)	93.88	1.5	140.82
	k_d ($\times 10^{-6}$M)	1.366	0.5	0.683
	k_2 ($\times 10^{-3}$ml/mg.min)	0.49	100	49
LP	Q_{max} (mg/ml of resin)	132.51	1.9	251.75
	k_d ($\times 10^{-6}$M)	5.567	1	5.567
	k_2 ($\times 10^{-3}$ ml/mg.min)	1.2	20	24

EDM-SMA model

Initial predictions based on experimental parameters were not a good match to the experimental curves for both LF and LP (data not shown here). Parameters were further modified to fit the simulated data to breakthrough experimental data are shown in Table 5.7. The charge value signifies the ionic interactions happening during adsorption. Change in model constants suggested better binding strength for LP over LF, as the charge value was higher for LP. Along with charge, steric factor was modified further. Very high value of steric factor underestimated the adsorption in the column suggesting additional adsorption happening in the column.

Tuned parameters for the best fit when compared with both inverse fit parameters and parameters obtained from gradient experiments showed closer match to later suggesting better ability of gradient experiments to obtain SMA parameters. However, tuned parameters required for accurate predictions were obtained precisely by adjusting inverse fit parameters. Using inverse fit method over gradient experiments for determination of parameters can save time and resources spent in experiments. Simulations carried out by SMA-EDM model over-predicted the experimental data at 0%, 10%, and 50% for 6 mg/ml inlet concentration of LF. Error at 100% breakthrough was found minimal. For 3 mg/ml concentration, 0%, 10%, and 100% were well predicted whereas 50% showed higher error. Similar trends were obtained for LP at 4 mg/ml concentration. Accuracy of prediction using SMA-EDM was clearly lesser than Langmuir-EDM.

EDM-MPM model

Changes made to the model parameters for MPM are shown in Table 5.8. It was known from earlier results that the binding strength for LP is higher than LF. Parameters were adjusted starting from the dissociation constant. k_{des0} was adjusted for only LF to ensure there is considerable difference between equilibrium dissociation constants (k_{dmpm} values LF: 0.9714 and LP: 0.0843). Values of β shows the contribution of salt in desorption constant. Higher the value of β, lower is the desorption rate constant which increases the binding strength of the protein towards the adsorbent. Hence changes were done in β value for LF to increase

Table 5.7: Modified model parameters for single component breakthrough predictions using SMA isotherm

Protein	Fitted Parameters	Value	Multiplier	Modified value	SMA Experimental Parameters
LF	v	2.093	0.55	1.674	1.7
	k_{eq} $(\times 10^{-2})$	27	0.15	4.05	2.66
	k_a $(\times 10^{-3})$	0.49	9	4.41	-
	σ	9.701	0.5	4.851	2.492
LP	v	0.696	3	2.08	2.155
	k_{eq} $(\times 10^{-2})$	1710.2	8×10^{-4}	1.36	2.69
	k_a $(\times 10^{-3})$	1.2	2.1	2.52	-
	σ	10.035	0.25	2.51	2.095

it further. Though value of β was slightly higher for LP, not much effect on the binding was observed. On the other hand value of γS contributes into adsorption kinetics. Higher the value of gamma, higher is the adsorption kinetic rate constant (k_{ads0}) but at lower salt concentration as in this case, not much effect is seen in the profiles.

Once the logical adjustments in the parameters were made to predict the breakthrough profiles, the curves were compared with other isotherm models for their accuracy. Simulations carried out using MPM-EDM models were the most accurate predictions among the three cases compared. Breakthrough curves for LF, 3 mg/ml concentration showed accurate prediction of 0%, 10%, and 100%, whereas, middle part of the curve was not predicted well. For 6 mg/ml, predictions followed similar trend as Langmuir-EDM model with marginally better accuracy. For LP, data predicted using MPM-EDM was most accurate among all the isotherms and breakthrough curve was completely predicted up to 50% saturation and then at 100%.

Experimental results for high protein concentration shows crowding and self competition of the protein molecules not letting them bind to the matrix. Depictions made with *ExProSim:IC* were not able to predict the crowding of molecules.

Table 5.8: Modified model parameters for single component breakthrough predictions using Langmuir MPM isotherm

Protein	Parameter	Value	Multiplier	Modified value
LF	Q_{max} (mg/ml of resin)	93.95	1.1	103.345
	k_{des0} (ml/mg.min)	0.0817	15	1.225
	k_{ads0} (ml/mg.min)	0.8098	1	0.8098
	β	0.012	10	0.12
	$\gamma(\times 10^{-3})$	6.44	2	12.88
LP	Q_{max} (mg/ml of resin)	132.5	0.9	119.25
	k_{des0} (ml/mg.min)	0.0296	1	0.0296
	k_{ads0} (ml/mg.min)	0.1244	1	0.1244
	β	0.2812	1	0.2812
	$\gamma(\times 10^{-3})$	0.59	1	0.59

Experiments at higher velocities provided lesser time for the molecules to bind to the matrix resulting in earlier and faster breakthrough from the column. The change in the profiles with velocity was closely predicted by *ExProSim:IC*. The comparison between three isotherms is further shown in the form of error estimation at different concentration of the breakthrough curve. As the comparison is already discussed in earlier sections and data presented is self explanatory, it is not discussed in detail with respect to $\%$ errors.

5.3.2.6 Multicomponent breakthrough: Experimental

Figure 5.12 shows experimental and simulated breakthrough curves. During multicomponent adsorption, both the proteins compete for the sites to adsorb on the resin, the concentration shown at any point during breakthrough curve is a cumulative concentration of the proteins together. HPLC analysis was performede to segregate the proteins further into individual profiles. (The standard curves for LF and LP, and final chromatogram for maximum possible resolution of whey proteins are given in Section 5.3.1). When the DBC values of multicomponent breakthrough were compared to single component DBCs, 40$\%$ increase was observed

in DBC of LF; whereas, exact decline in DBC of LP was noted suggesting increase and decrease in residence times for LF and LP respectively (Table 5.9). Q_{max} for LF was higher as compared to LP in spite of higher electrophoretic mobility of LP suggesting displacement phenomenon for LP by LF. Lower rate of adsorption for LF and higher concentration of LF molecules can be the underlined causes for displacement of LP. It can be seen that the displacement was not prominent enough to lead to overshoot in local concentration of LP. This might be due to close k_d values for the protein when they interact with the resin in presence of each other.

Table 5.9: Comparison of DBC for single and multicomponent breakthrough experiment

Protein	**0% BT (min)**	**10% BT Time (min)**	**10% BV Time (min)**	**DBC$_{multiple}$ (mg/ml resin)**	**DBC$_{single}$ (mg/ml resin)**
LF	35	60.3	30.25	130.17	93.58
LP	25	49	24.5	93.25	131.73

BT: Breakthrough time, BV: Breakthrough volume, DBC: Dynamic binding capacity

5.3.2.7 Multicomponent breakthrough: simulations

Furthermore, *ExProSim:IC* was used to predict the breakthrough data using various models. In order to capture the effect of competition between the two proteins, the model parameters were further adjusted. For predictions using Langmuir isotherm, adjustment of model parameter Q_{max} was based on the DBC obtained from the experimental profile. Values of k_1 and k_d were further adjusted to fit the curves as shown in Table 5.10. The adjusted value of k_d showed that desorption was higher for LP than LF. The values were also close to each other showing their competitive behaviour. Minor difference between the k_d values also explains why the displacement did not lead to overshoot as in Chapter 4. The modified values for k_1 for LF was 2-fold higher than LP. Higher value of k_1 for LF suggested lower desorption in the column as compared to LP supporting the displacement. The predictability using Langmuir isotherm precisely predicted 10% onwards, however the start of the breakthrough could not be correctly predicted for both proteins.

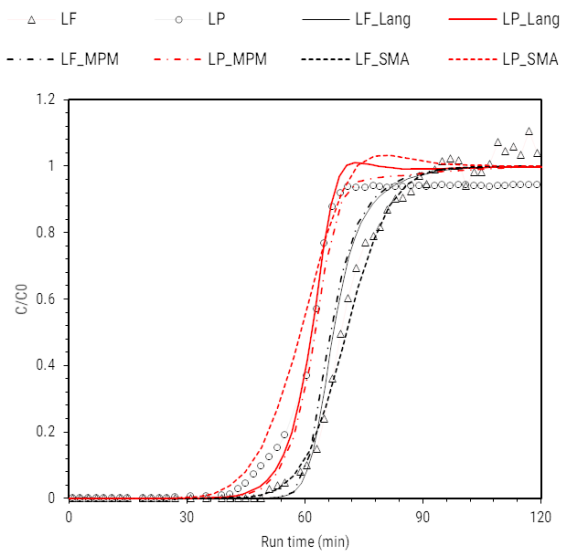

(a)

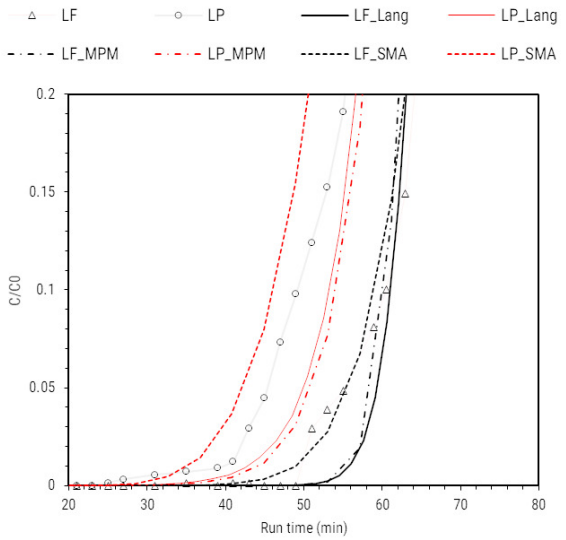

(b)

Figure 5.12: a) Multicomponent breakthrough for LF and LP at 4.5 mg/ml LP and 3 mg/ml LF ; Experimental LF-△-, LP -○-. simulated; Langmuir LP —, LF —. MPM LP -·-, LF -·-. SMA LP -···-, LF -··· , b) Zoomed version of part a)

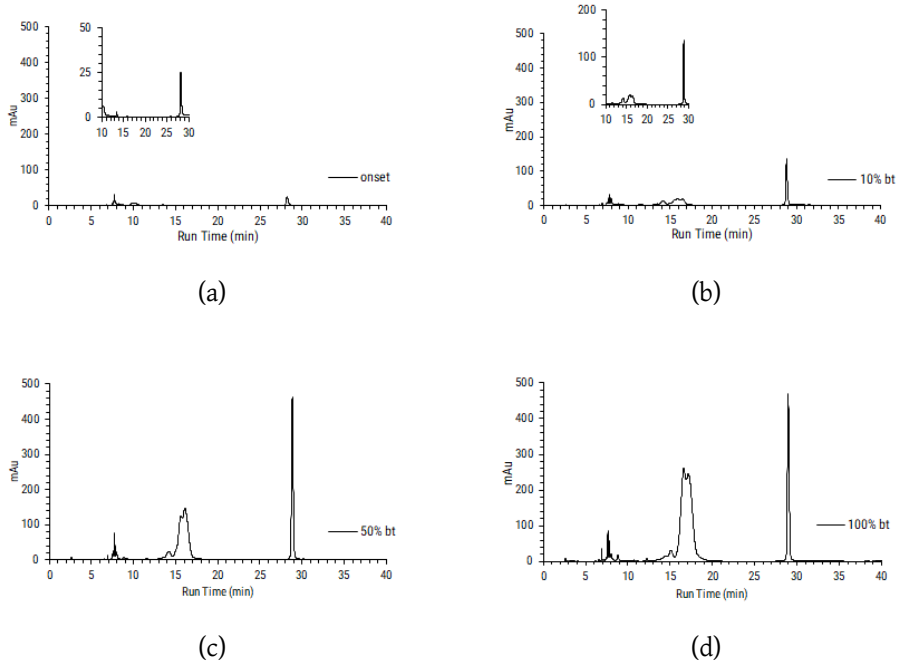

Figure 5.13: Multicomponent breakthrough curve HPLC analysis for LF and LP showing individual fractions at different breakthrough points. a) 0% bt b) 10% bt c) 50% bt d) 100% bt

Table 5.10: Modified parameters for Langmuir-EDM for multicomponent breakthrough prediction

Protein	Parameter	Value	Multiplier	Modified Value
LF	Q_{max} (mg/ml of resin)	93.88	1.3	122
	k_d ($\times 10^{-6}$ M)	1.366	50	68.3
	k_1 ($\times 10^{-3}$ ml/mg.min)	0.49	300	147
LP	Q_{max} (mg/ml of resin)	132.5	0.7	92.75
	k_d ($\times 10^{-6}$ M)	5.567	14	77.94
	k_1 ($\times 10^{-3}$ ml/mg.min)	1.2	60	72

SMA-EDM predictions for LP showed early breakthrough and highest error amongst all the isotherms. However, brealthrough for LF was predicted accurately. The parameters modified are given in Table 5.11 and the fit is shown in Figure 5.12. Charge value was modified for both proteins to account for loss of

Table 5.11: Modified parameters for SMA-EDM for multicomponent breakthrough prediction

Protein	Parameter	Value	Multiplier	Modified value
LF	v	1.7	0.85	1.445
	k_{eq}	0.0266	1	0.0266
	k_a ($\times 10^{-3}$ ml/mg.min)	0.49	600	294
	σ	2.492	1	2.492
LP	v	2.154	0.75	1.615
	k_{eq}	0.0269	1	0.0269
	k_a ($\times 10^{-3}$ ml/mg.min)	1.2	150	180
	σ	2.095	1	2.095

Table 5.12: Modified parameters for the MPM-EDM for multicomponent breakthrough prediction

Protein	Parameter	Value	Multiplier	Modified value
LF	Q_{max} (mg/ml of resin)	93.95	1.5	140.925
	k_{des0} (ml/mg.min)	.0817	90	7.353
	k_{ads0} (ml/mg.min)	.8098	1	0.8098
	β	0.012	10	0.12
	$\gamma(\times 10^{-3})$	6.44	1	6.44
LP	Q_{max} (mg/ml of resin)	132.5	0.7	92.75
	k_{des0} (ml/mg.min)	0.0296	500	14.8
	k_{ads0} (ml/mg.min)	0.1244	1	0.1244
	β	0.2812	0.6	0.168
	$\gamma(\times 10^{-3})$	0.59	1	0.59

binding capacity. It can be seen that charge value for LP was decreased by 25% as compared to 15% for LF. The modified values of forward rate constants suggest that the adsorption rate for LF was much higher (≈8-fold) than that of LP which could displace LP easily even if it was electrophoretically favoured for stronger interaction with resin. Higher uptake rate could be an effect of high inlet concentration of LF as compared to LP as elucidated by Langmuir-EDM predictions.

Table 5.13: Comparison of DBC from multiple component breakthrough curve predictions for different isotherm

Protein	Isotherm	0% BT (min)	10% BT (min)	10% BT volume (ml)	DBC (mg/ml)	% variation
	Langmuir	35	63.45	31.725	136.56	3.66%
LF	SMA	29	61.64	30.82	132.64	0.69%
	MPM	50.5	61.8	30.9	132.99	0.95%
LP	Langmuir	25	53.7	26.85	102.63	9.66%
	SMA	40.8	46.7	23.35	89.16	-4.73%
	MPM	39	54.2	27.1	103.59	10.69%

Predictions using MPM isotherm were similar to Langmuir isotherm. Modified parameters showed lesser desorption and higher adsorption rate for LF over LP supporting the displacement phenomena. β values were also changes showing increase in strength for LF and decrease in strength for LP. This also supports displacement of LP by LF. Early saturation was observed for LF; however, L breakthrough was predicted with accuracy. The details for errors are given in Table B.9 in Appendix B. As Langmuir and MPM are necessarily based on similar concepts, the salt factor included for MPM gave slight variation in the predictions. On the other hand, SMA based on mass action principle and steric hindrance of molecules, gave higher error in predictions. This might be due to sensitivity of charge factor because of exponential function. A better way of adjusting parameters for SMA may be required to get better fit. Perhaps a simple least square error method can give better estimate of SMA constants.

To compare all three isotherms, DBC was determined and compared with experimental data. The DBCs as shown in Table 5.13 matched well with the values obtained from multicomponent experimental data from Table 5.9. DBC values predicted by Langmuir were the farthest for LF. SMA and MPM gave accurate predictions, however, MPM showed higher error throughout the further curve. For LP, errors for DBC were high for all the isotherms. Even though, SMA showed early breakthrough as compared to others, it gave best predictions of DBC. Other two isotherms on the other hand, predicted rest of the curve very accurately. This can also be seen from RMSE and CoD values for the curves as given in Table B.25.

5.4 Conclusion

This chapter provides a detailed analysis of adsorption and breakthrough studies for separation of two minor whey proteins, LF and LP with experiments and process simulations. Basic adsorption data was used to determine model constants by inverse fitting which could efficiently predict the experimental breakthrough for single component systems for both LF and LP. Inverse fit method was found to be useful for estimating parameters required for simulations which is an indicative of reduction in the number of experiments required to obtain model parameters. Single component experimental breakthrough curves showed expected trend of earlier breakthrough with increase in experimental factors like concentration at inlet and process flow rate. All isotherms were able to predict the experimental data for most of the curves at lower velocities for both proteins. However, desorption kinetics was not predicted accurately for higher velocities and concentration of LF. It is ideally expected that at higher velocities, the predictions should be better for EDM, however this anomaly suggested necessity of additional diffusion considerations for more accuracy. MPM-EDM predictions were marginally more accurate when compared with Langmuir-EDM, SMA-EDM, considering there were more parameters to fit the data. For single component systems, breakthrough predictions were accurate for Langmuir-EDM and MPM-EDM with latter being marginally more precise. SMA-EDM isotherm predictions over-predicted the experimental data with higher error percentage midway of the curve. It was realised that adjustments in the charge values was crucial to get accurate prediction due to its sensitivity. Perhaps, the experiments from which the charge values are determined can be improved. The sensitivity of equilibrium constant was found very low while adjustment. If the constants were adjusted by least squares method, this would have been easily overlooked.

Furthermore, multicomponent experiments showed clear displacement of LP by LF, reducing DBC of LP by $\approx 30\%$ with equivalent increment for LF. This was unexpected as the electrophoretic mobility for LP was higher at operating pH. In case of multicomponent simulations, LF breakthrough was completely predicted by SMA, however, for LP SMA could only predict the onset and DBC well. Lang-

muir and MPM isotherms predicted the LP isotherm better than SMA. Objective here was to find an isotherm which can predict the results for the whole system, however, none of the isotherms:EDM combination predicted all the protein profiles accurately at different processing conditions. This serves as a limitation for choosing a single isotherm for single system. A combination of isotherms can serve the purpose, however, that will need exhaustive experimental validation. With the current results, preliminary predictions made with *ExProSim:IC* can help in assessing the protein binding inside the column, its competitive ability, and nature of desorption. The chapter also serves as a template for making strategies for calibration of parameters.

Chapter 6

Crude whey processing

6.1 Introduction

It has been established that *ExProSim:IC* is an efficient tool for for predicting outcomes of single and multicomponent protein standards. Further to check the usability of the tool, it is important to validate it on crude streams. Such an exercise will help to seek the areas of improvements if any. Furthermore, for a complex mixture such as whey with multiple proteins of industrial importance, understanding how proteins behave in presence of known and unknown proteins is essential for further separation. Earlier chapters have discussed in detail adsorption characteristics of major and minor proteins on anion and cation exchange chromatography respectively and it was observed that when the streams are multicomponent, the adsorption of proteins is affected by the competition with each other which can potentially affect the desired separation.

This chapter discusses experimental breakthrough studies and respective simulations of crude industrial sample of WPC. Learnings from earlier chapters were carried forward here to showcase the importance of step-wise model validation.

6.2 Methodology

6.2.1 Experimental

6.2.1.1 Materials

Respective buffer solutions were prepared as given in Chapter 4, where system was established for major proteins. Crude WPC samples were obtained from two different industries. Tatua cooperative dairy company, Morrinville, New Zealand and Warrnambool cheese and butter factory, central Victoria. HiTrap(2.5×0.7 cm) was used for ion exchange studies. Materials for UV spectrophotomentry, HPLC, SDS-PAGE, and elemental analysis are described in detail in Chapter 3.

6.2.1.2 Methods

6.2.1.3 Sample analysis

Crude sample assessment

Both samples were assessed qualitatively as well as quantitatively for the total protein content and individual protein fractions. Total protein content was determined using elemental analyser. One of the two samples which performed better in the analysis was carried forward for further studies. All other intermediate protein samples were assessed on UV-Vis spectrophotometer for finding their concentration based on standard curves provided in Figure 4.1.

HPLC

Firstly, standard curves for all the proteins were found out at optimised method by injecting different concentrations of standard protein samples (0-1 mg/ml). *Method 2* was further used to find the unknown concentrations of the samples obtained from WPC breakthrough curve. Purity and concentration of sample peaks obtained from chromatography experiments was found out by running the samples on HPLC. Details for HPLC *method 2* are given in Chapter 4

SDS-PAGE

SDS-PAGE analysis was performed for feed analysis. Standard proteins were injected in the PAGE along with WPC samples from both industries. Electrophoresis runs were carried out for 120 minutes at 100 mv and further stained by silver staining method for visualisation of the protein bands. All the sample concentrations for SDS-PAGE were measured on UV-Vis spectrophotometer first and then were diluted to keep the concentration per well to 3-5 μg for consistent staining profile.

6.2.1.4 Chromatography

Column physical parameters such as porosity, ionic capacity, v_0 were found out using method given in Section 3.3.5. Column evaluation was performed by injecting 2 $\%$ acetone at 20 cm/hr velocity and the peak was analysed for asymmetry.

Sample preparation

WPC sample for breakthrough was prepared by dissolving known amount of WPC powder in phosphate buffer at pH 6.9. As the samples were turbid visibly, they were centrifuged at 10000 rpm and then filtered through a 0.45 μm filter in order to remove the suspended solids if any. UV spectrophotometric analysis was carried out before and after clarification to find out the losses.

Breakthrough experiment

Breakthrough curve for crude whey protein mixture was determined by injecting 4 mg/ml of WPC continuously onto HiTrap CaptoQ column. The breakthrough curve was performed for anion exchange as the quantity of major proteins was found to be way higher than minor proteins. As achieving breakthrough for minor proteins was time consuming considering their low concentration in the WPC, sample analysis was focused only on major proteins. Breakthough was ended when WPC sample showed a saturation at the column outlet. Samples were taken throughout the breakthrough and were analysed on HPLC for finding out individual protein concentrations.

6.3 Results and discussion

6.3.1 Basic analysis

Crude sample assessment

WPC samples obtained from Tatua and Warrnambool are compared here. Elemental analysis of crude samples showed 73.95% and 74.21% total protein based on total nitrogen content for Tatua and Warrnambool respectively. SDS-PAGE of both crudes compared against the standard proteins is shown in Figure 6.1.

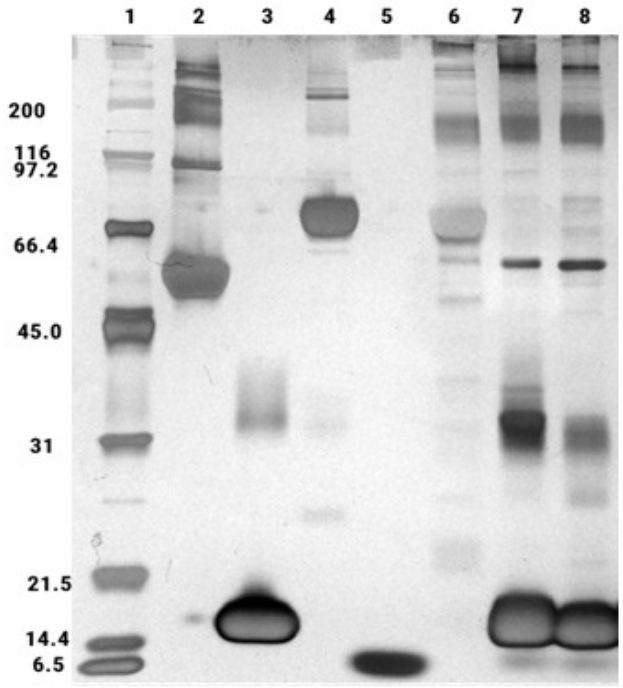

Figure 6.1: Comparison of two WPC crude samples with standard proteins; 1: BRM, 2: BSA std, 3: BLG std, 4: LF std, 5: ALA std, 6: LP std, 7: Tatua WPC, 8: Warrnambool WPC

It can be seen that the two WPC crude samples compare well with each other with prominent concentration of BLG in both of them. Low intensity bands of ALA and BSA were observed in both the samples and they show same impurity profile as well. This means that the choice of crude sample will not make much difference. As the protein standards for minor proteins were obtained from Tatua Dairy Cooperative Company, it was decided to use Tatua WPC sample for further studies.

Column evaluation

Column characteristics such as; porosity and ionic capacity for all the columns were determined in the earlier chapters. As it is important to check columns for their consistency of packing every time they are run after storage, they were evaluated to ensure desired performance [265]. Column evaluation for HiTrap column was performed and the results showed asymmetry factor of 0.93 which was acceptable to go ahead for breakthrough experiments.

HPLC analysis

Sample analysis of five whey proteins from WPC needed a robust method which can handle varying concentration of proteins and have a sensitivity to detect minute concentrations as well. Table 4.2 in Chapter 4 shows the optimised method for resolution of all the five whey proteins. Figure 6.2 demonstrates that the proteins are well separated from each other and can be analysed for their purity without interference from other proteins. Standard curves for individual proteins are shown in Figure 4.5. Equations from the standard curves were linear in nature and regression coefficient of >0.99 shows a promising fit. These equations were further used for finding the unknown concentrations of samples obtained from breakthrough experiment.

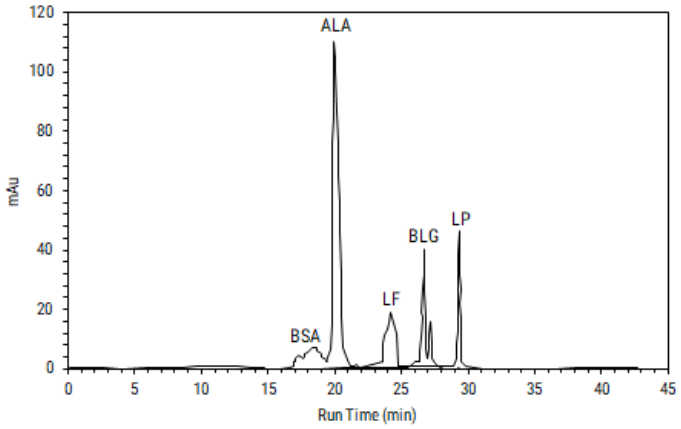

Figure 6.2: Optimised HPLC method for analysis of five whey proteins

6.3.2 WPC crude breakthrough: Experimental

Separated experimental breakthrough curves are shown in Figure 6.4 along with the zoomed Figure 6.4(b) for better view. Early breakthrough were obtained for BSA and ALA, followed by delayed breakthrough for BLG. It can be said that dimer of BLG might be responsible for its higher binding leading to late breakthrough. LP and LF were found to elute from the 1^{st} CV showing no binding to the resin at operating pH 6.9. This is obvious as the charge on minor proteins is same as the charge on the resin. Concentration of unbound LF and LP was very low hence they are not considered here for breakthrough purpose.

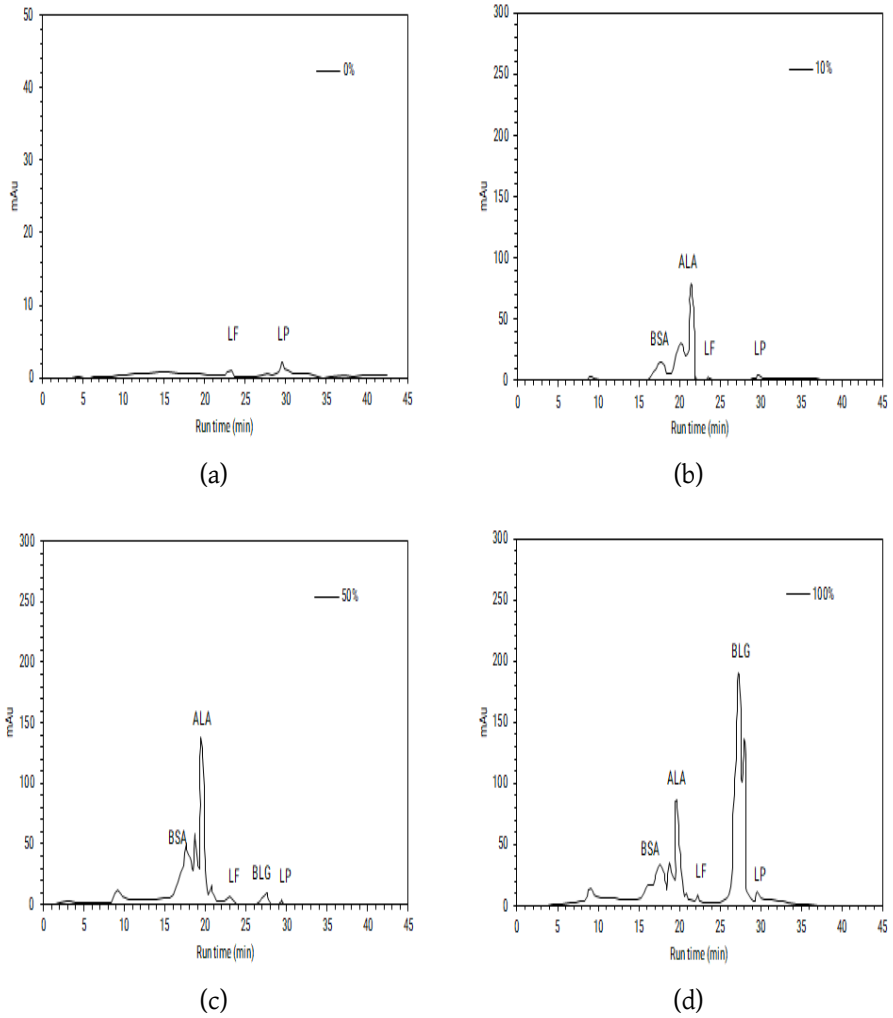

Figure 6.3: Comparison of breakthrough curve samples at different time points of the breakthrough curve for WPC

Figure 6.3 shows HPLC analysis of the samples taken at onset, 10%, 50%, and 100% of breakthrough curve. At onset, none of the major protein components

could be seen, whereas LF and LP were observed in minute quantities. At 10%, increase in both BSA and ALA were observed, whereas BLG was still in adsorption phase. At 50%, BLG slightly showed it presence at the outlet, whereas ALA and BSA were almost saturated by then. At end point of breakthrough, all the proteins were found at constant concentration, indicating complete saturation of the bed. Impurity was found consistently at retention time of 9.2 min. As it was insignificant for objectives of this thesis and minute concentration leading to unlikely interference with proteins, the impurity was left unidentified.

Experimental analysis of breakthrough curve for WPC showed similar behaviour to that of breakthrough data obtained for mixture of major proteins as given in Section 4.3.3. Figure 6.4 compares the two experimental data-sets. The only difference in the experimental conditions were concentrations of ALA and BSA being very low in WPC as compared to 2 mg/ml each in case of standard protein breakthrough. BLG concentration was comparable in both cases with WPC having slightly higher BLG concentration. When a protein is low in concentration, ideally it should take longer time to reach breakthrough, but in this case it was seen that breakthrough for ALA and BLG is achieved earlier as compared to studies with standards. This behaviour can be attributed to very high concentration of BLG in the medium which may interfere with ALA and BSA binding, leading to their early displacement out of the column. It is also observed tat BLG breakthrough from WPC was extended farther in spite of higher concentration as compared BLG breakthrough from standard proteins. Ideally, with higher concentration, early breakthrough should be achieved. In case of standard proteins, there was a healthy competition of BLG from ALA and BSA as they were in high concentration, whereas in case of WPC, very less competition was offered for BLG towards binding sites. This might have lead to higher breakthrough time. Breakthrough profile for the mixture of standards and WPC were compared further. WPC breakthrough showed early onset of the breakthrough. This can be attributed to other minor impurities in WPC which may be responsible for changing the dynamics of binding in the column as well as obscuring the UV absorbance of the experimental breakthrough curve [266]. In addition to this, early exit of ALA and BLG would have contributed in the faster concentration front at the column outlet.

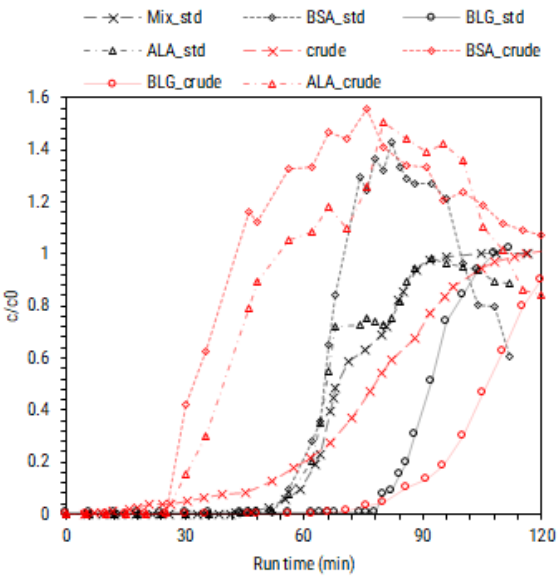

(a)

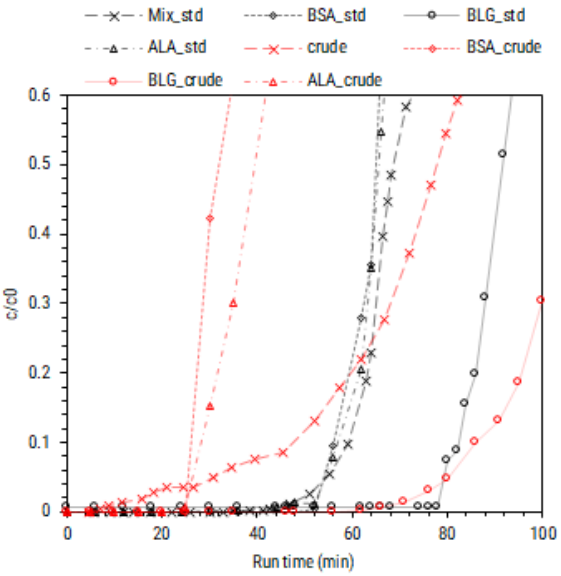

(b)

Figure 6.4: Comparison of experimental multi component breakthrough curves for WPC to that of standard proteins. WPC breakthrough; BSA -◇-, BLG -·-, ALA -△- and combined -×-. Mixture of major protein standards; BSA -◇-, BLG -·-, ALA -△- and combined -×-. b) Zoomed version of the same data for better view

6.3.3 Breakthrough simulations with *ExProSim:IC*

Furthermore, *ExProSim:IC* was implemented for prediction of the curves. Adjusted model parameters from the multicomponent breakthrough of major proteins on Capto Q were used to simulate the results. As the model constants have already

predicted breakthrough for standard proteins, it was expected that no further changes will be required in them in order to predict the experimental outcomes. When the simulations were performed, the breakthrough showed a delayed profile for ALA and BSA, due to such a low concentration of two proteins (Data not shown here). This is unlike the experimental data. Hence, minor modifications were done in the model constants to fit the data. The fitted simulations for all the model combinations are shown in Figure 6.5. Errors between experimental and simulated breakthrough for all isotherms is shown in Table B.10. The curve to curve error is presented in Table B.26.

EDM-Langmuir model

It can be seen in Table 6.1 that only parameters which were changed from model constants from Table 4.20 for simulating the experimental data using Langmuir model were the binding capacities. As accurate breakthrough was not obtained for all 3 proteins, focus was given for maintaining accuracy for the slowest desorbing protein, BLG. As observed from Figure 6.5, the onset of the breakthrough for ALA and BLG was predicted very accurately, whereas for BSA it was over-predicted. It can be seen that fit for BLG was accurate upto saturation. Ideally the parameters derived from multicomponent breakthrough of standard acidic proteins should have been able to predict the breakthrough, however adjustments in the binding capacities were required to achieve the best fits. Binding capacity for BSA and ALA were decreased by 55% and 80% respectively in order to fit to the curve. It is realised that high competition due to excess amount of the BLG, might have lead to decreased binding capacities which was also supported by simulations. This is because of difference in the concentrations profiles between two experiments. Overall desorption profiles for all the proteins were predicted correctly as no change in the adsorption or desorption profile was seen as compared to major protein standards breakthrough. Overshoot of BSA and ALA due to displacement were also predicted but high error was observed in the overshoot part.

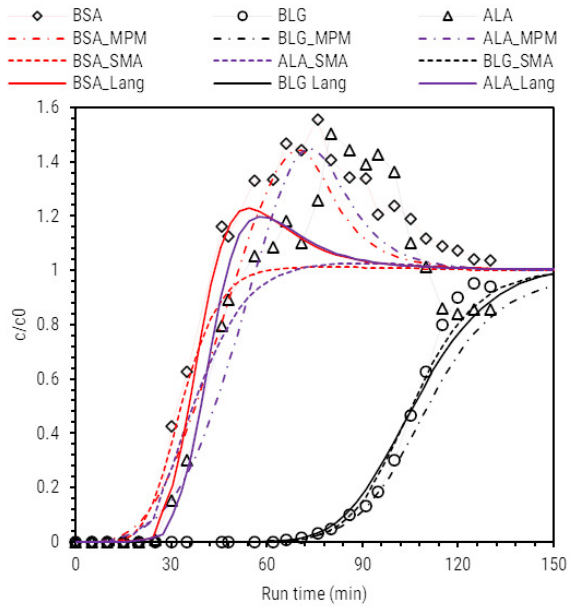

(a)

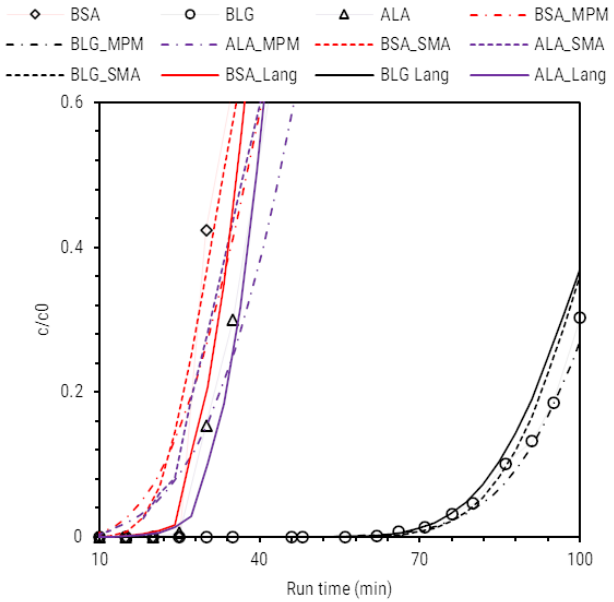

(b)

Figure 6.5: Comparison of experimental vs simulated breakthrough for WPC crude, a) experimental data; BLG -○-, ALA -△-, BSA -◇-. Simulated Langmuir; BLG —, BSA —, ALA —. Simulated MPM; BLG -·-, BSA -·-, ALA -·-. simulated SMA; BLG –, BSA –, ALA –. b) Zoomed version of the same data for better view

EDM-MPM model

The modified parameters from multicomponent breakthrough simulations for major proteins were used for carrying out simulations (Table 4.21), however predic-

Table 6.1: Modified model parameters for WPC breakthrough simulation using EDM:Langmuir model for Capto Q anion exchanger

Protein	Constant	Value	Multiplier	Modified value
BSA	Q_{max} (mg/ml of resin)	83.72	0.35	29.302
	k_d ($\times 10^{-6}$M)	5.848	1	5.848
	k_1 ($\times 10^{-3}$ml/mg.min)	756	1	756
BLG	Q_{max} (mg/ml of resin)	187.64	1	187.64
	k_d ($\times 10^{-6}$M)	15.934	1	15.934
	k_1 ($\times 10^{-3}$ ml/mg.min)	411	1	411
ALA	Q_{max} (mg/ml of resin)	62.73	0.35	21.96
	k_d ($\times 10^{-6}$M)	20.52	1	20.52
	k_1 ($\times 10^{-3}$ ml/mg.min)	781	1	781

tions were not accurate. Slight fine tuning of parameters was required with the binding capacity parameters such as Q_{max} and β as shown in Table 6.2. For BSA and ALA, MPM model showed better performance in predicting the experimental data as compared to Langmuir isotherm. The overshoots were predicted better showing displacement. Breakthrough points were accurately predicted for all three proteins. On the other hand, breakthrough of BLG was very well predicted up to 20$\%$ concentration and then saturated later than experimental data. Figure 6.5 shows the simulated data. Changes in Q_{max} values were expected due to competition of the proteins with each other. Large decrease in binding capacities for ALA were observed. Rate of adsorption of BLG was adjusted further to meet the experimental curve. This shows higher affinity of BLG towards the resin and a tendency to occupy sites available as fast as possible which might have lead to early exit of BSA and ALA. Slight decrease of binding capacity of BLG was also observed. This might be attributed to presence of impurities in the medium. Even though electrokinetically ALA has most charges amongst three, early breakthrough was

Table 6.2: Modified model parameters for multicomponent breakthrough predictions using Langmuir MPM isotherm

Protein	Parameter	Value	Multiplier	Modified value
BSA	Q_{max} $(mg/mlofresin)$	89.53	0.30	26.9
	k_{des0} $(ml/mg.min)$	1.135	1	1.135
	k_{ads0} $(ml/mg.min)$	1.606	1	1.606
	β	0.029	0.61	0.0177
	γ	1.457	1	1.457
	$D_{ax}(\times 10^{-2})$	23.95	1	23.95
BLG	Q_{max} $(mg/mlofresin)$	145.32	0.85	123.52
	k_{des0} $(ml/mg.min)$	1.818	1	1.818
	k_{ads0} $(ml/mg.min)$	0.121	8	0.968
	β	0.64	1	0.64
	γ	1.386	1	1.386
	$D_{ax}(\times 10^{-2})$	14.52	1	14.52
ALA	Q_{max} $(mg/mlofresin)$	101.5	0.25	25.375
	k_{des0} $(ml/mg.min)$	4.93	1	4.93
	k_{ads0} $(ml/mg.min)$	0.258	0.24	0.0516
	β	0.305	0.42	0.128
	γ	1.802	1	1.802
	$D_{ax}(\times 10^{-2})$	9.63	1	9.63

a result of high concentration of BLG in the medium. As the value of β signifies strength of binding to the resin, values for the best fit were found to be lower for both ALA and BSA, whereas β for BLG was kept the same suggesting stronger interactions.

EDM-SMA model Furthermore, multicomponent breakthrough was predicted by performing simulations using EDM and SMA isotherm by taking parameters from Table 4.22. Modified parameters for SMA are shown in Table 6.3. Binding capacity is generally signified by charge value in SMA isotherm. Reduction in the

Table 6.3: Modified model parameters for single component multicomponent breakthrough predictions using SMA isotherm

Protein	Fitted Parameters	Value	Multiplier	Modified value
BSA	v	0.734	0.95	0.697
	k_{eq} $(\times 10^{-2})$	288.9	1.5	385
	σ	0.9715	1	0.9715
BLG	v	1.407	1	1.407
	k_{eq} $(\times 10^{-2})$	34.25	1.2	41.1
	σ	5.612	1	5.612
ALA	v	0.4251	0.90	0.382
	k_{eq} $(\times 10^{-2})$	78	1.2	93.6
	σ	4.015	1	4.015

charge values of ALA and BSA were required for fitting the experimental data. Charge values of proteins suggest displacement of ALA and BSA by BLG. Value of k_{eq} shows the strength of the binding. Higher the value of k_{eq}, weaker is the binding. BSA showed highest value for k_{eq} indicating looser binding as compared to other two proteins. Furthermore, ALA showed the comparable value of k_{eq} to that of BLG, showing apparently strong binding, which is true electrokinetically but lower concentration in the overall mixture along with predominant existence of BLG dimer having high charges on it, might be the cause of resultant displacement.

6.4 Conclusion

Crude industrial stream in the form of whey protein concentrate (WPC) was studied for breakthrough analysis. WPC sample contained 76% protein constituting BLG (79%), followed by ALA (11%) and BSA (7%), and traces of minor proteins. The sample chosen was different in concentration profiles as compared to standard experiments which were performed in earlier chapters. Breakthrough studies provided for further exploration for usability of *ExProSim:IC*. Experimental data for breakthrough of major proteins in WPC, showed a similar behaviour to that of major protein breakthrough in Chapter 4. It was observed that ALA and BSA were displaced by BLG due to its very high concentration with respect to the competitors for binding. In case of experiments with standards, the concentrations of

proteins were equivalent. In WPC, high concentration of BLG overpowered the binding sites in the resins leading to very early breakthrough for both ALA and BSA.

Knowledge gained from earlier experimental validation was implemented here. Parameters obtained from major protein breakthrough were used for predicting experimental data. It was expected that no further adjustments will be required for successful predictions; however, slight change in the parameters was required for getting the best fit. All three protein breakthroughs were not well predicted by any of the isotherms, hence it was decided to focus on accuracy of the slowest and major component, BLG. Decent fits for other two proteins were obtained by this method. EDM-Langmuir well predicted the breakthrough onset and DBCs; however, the error throughout the curve kept was high for both ALA and BSA. The overshoot was not predicted well by Langmuir isotherm. EDM-MPM model was successful in predicting the overshoot for ALA and BSA but the desorption profiles were slightly delayed. EDM-SMA performed best in predicting slowest of the breakthrough, however, ALA and BSA overshoots were not predicted. All the thermodynamic models gave a clear idea about the adsorption and desorption patterns in the column and predicted DBCs of the proteins in WPC suggesting usability of *ExProSim:IC* in process simulations. The results were good for the models applied here but use of EDM can be a limitation when handling complex systems, as additional diffusional considerations are required.

Chapter 7

Conclusions and future work

7.1 Conclusions

The objective of this study was to formulate a preliminary simulation tool which can facilitate assessment of adsorption and desorption phenomena for further implementation into process development. Keeping in mind the scarcity of thermodynamic data for proteins, important aim was to seek for methods to determine thermodynamic model constants for protein molecules and understand their importance in implementation of the models for process development simulations. To achieve this objective, *ExProSim:IC* was developed in MATLAB 2014b incorporating EDM and three thermodynamic models; Langmuir, SMA, and MPM. In order to assess usability of the tool for design applications, it was necessary to verify its functionality and validate it. The tool was verified for its functionality by checking performance of range of model constants through a tool verification exercise. It was then verified against a well established tool, CADET for workability. Additionally, mesh independency studies were carried out to ensure its accuracy. Further, literature data was chosen for validation to assess effectiveness of the tool with variation in multiple process parameters. A potential experimental system, whey proteins was chosen further for experimental validation. Objective was to understand experimental framework required for model constant determination and their calibration. To understand and determine model parameters, basic adsorption and kinetics experiments were performed on major and minor whey proteins. Data generated from these experiments was used to find model constants by in-

verse curve fitting. A simple data fitting module was also developed in the tool. To further understand the physical significance of the model parameters, they were used in *ExProSim:IC* for simulation of breakthrough curves for three systems namely; standards of major whey protein on cation exchange, standards of major whey proteins on anion exchange, and standards of minor whey proteins on cation exchange. To apply the learnings from earlier systems, a complex industrial system of whey protein concentrate (WPC) was chosen to assess the applicability of the tool on crude systems. For each of the simulation and respective change of model constants, careful observations were made specifically related to protein behaviour in the column. Specific findings from the entire study are as follows:

Tool verification

Exercise of tool verification helped in understanding the model constants better. Basic functionality of the tool was verified for its further use, however, it required an exhaustive validation to gain confidence on the successful predictability which was further attempted in the subsequent chapters. Summary of insights from tool verification is as follows;

- Profiles obtained for all the model constants were according to the physical significance of the constants. All the simulations were highly dependent on the concentration ranges chosen based on the systems considered for every isotherm. No quantitative conclusion could be derived from this exercise and the exercise was restricted to understanding qualitative changes in the breakthrough curves with respect to changes in the model constants.

- Assessment of model constants for Langmuir isotherm showed expected increase of binding capacity with increase in Q_{max}, k_1. Binding capacity was found to decrease with increase in k_d. The slope of the breakthrough was affected by k_1 but definite effect could not be derived from such preliminary simulations.

- For SMA constants, binding of the protein was found to increase with increase in v and λ, however it was found to decrease with increase in k_{eq}

and σ. Large variations in the binding capacity were observed for minute changes in the charge value hence the adjustments for it should be done carefully. No conclusion could be derived for the shape of the curve as none of the model constants showed any effect on the shape in the chosen ranges.

- For MPM isotherm, k_{ads0} and β showed a positive correlation with binding capacity. Increase in k_{des0} showed decrease in binding of protein. γ showed a significant effect on the binding capacity which is often overlooked for ion exchange operations. It is a property of a protein and is highly system dependent. β was found to be analogous to v in SMA and special attention should be given for their calibration.

- Major observation from comparison with CADET was that, *ExProSim:IC* simulations showed high errors for all preliminary simulations. Obvious difference of GRM against EDM might also lead to this error. As predictions from CADET are accurate due to its exhaustive validation, model constants were modified based on knowledge gained from model constants assessment exercise to achieve the best fit. As the modifications were done by trial and error, it can take additional efforts to obtain a best fit. Even though results were comparable for both tools after modifications, it is just a representative example and no comparative statements can be derived from this.

- Mesh independency exercise helped in finding meshing parameters for a convergent solution. It was realised that keeping the time interval and axial interval below the optimised value helped in consistently getting a convergent solution.

Literature based validation

Understanding gained from tool verification was efficiently used to vary the model constants to get the best fit. Literature based validation presented further proof that *ExProSim:IC* can help generate system specific model constants which can predict the data to reasonable accuracy. Summary of insights from literature based validation is as follows;

- Best fit was decided based on physical and chemical significance of the simulated curve from the experimental curve. 'point to point' comparison of the curves was found to be more efficient in order to relate the data to the experimental model constants. 'Curve to curve' error was presented but it could not give that give physical comparison of the data.

- For Langmuir model, single and multicomponent breakthrough for ALA and BLG were well predicted. Secondly, IgG breakthrough was predicted at different inlet concentrations showing sensitivity of the tool towards change in concentration. Simulations for BSA and Lysozyme breakthrough curves were better fits than the simulations given in the paper showing superiority of prediction by *ExProSim:IC*.

- For SMA isotherm, predictions performed for different salt concentrations matched considerably well (error<5%) with the experimental data showing ability of the tool to predict at different ionic strengths.

- For MPM model, various protein molecules such as IgG, transferrin, and insulin which have different hydrophobicities were used for validation at different salt concentrations and ExProSim:IC showed accurate results to that of experimental data (error<3%).

- The variation in parameters was performed strategically for all the simulation runs to get the fit to experimental data. The tool established reasonable accuracy for all three isotherm models for different proteins at various processing conditions such as; flow velocity, column configuration, protein molecular weights (ranging from 6 kDa to 150 kDa), and buffer salt concentrations.

Experimental validation

For experimental validation of the tool, major proteins; BSA, ALA, and BLG were studied for adsorption characteristics and breakthrough on both anion and cation exchange chromatography, whereas minor proteins were studied for cation exchange chromatography. This experimental system provided experimental vali-

dation of 5 different proteins of range of physical and chemical properties. Significant findings of the experimental validation are as follows:

Summary from experiments

- For cation exchange, apparently higher binding was found for BSA in spite of its low electrokinetic potential. This was due to higher hydrophobicity at pH 4.5 leading to slower release from the column as observed in the breakthrough. On the other hand, it was not possible to include ALA in the cation exchange chromatography process because it lay on opposite side of the binding spectrum at pH 4.5. This suggested that cation exchange is unfavourable for major protein separation. No saturation was seen for BSA breakthrough due to continuous release from the resin due to loose hydrophobic interactions, whereas BLG showed better binding and breakthrough kinetics due to strong ionic interactions.

- For anion exchange chromatography binding of protein was found in the order of their electrokinetic potential suggesting interactions were mostly ionic. This was also supported by saturation obtained in individual breakthrough curves suggesting ionic adsorption-desorption behaviour of proteins. Multicomponent breakthrough showed slight displacement of BSA and ALA by BLG pertaining to the presence of dimer of BLG at pH 6.9.

- Anion exchange chromatography was found superior for separation of major proteins considering the operating pH for crude whey protein stream is $\approx$ 6-7 and overall binding characteristics explained. As anion exchange was finalised for major proteins, minor proteins were studied by cation exchange chromatography. Adsorption isotherm characteristics showed higher binding capacity for LP due to higher ionicity at pH 6.9.

- It was observed that crude whey breakthrough showed similar behaviour to that of major proteins breakthrough except the displacement of ALA and BSA was higher as reflected in the early rise and overshoot for both. This was attributed to very high concentration of BLG in the WPC which predominantly occupied all the sites possible till saturation pushing the low

concentration protein molecules to saturate earlier than expected.

Simulations

- Parameter estimation module from *ExProSim:IC* was successfully used to determine the model constants. For all the proteins in discussion, initial guesses from inverse fit method were successfully used for simulations eliminating the need of carrying out elution gradient experiments for SMA and MPM models. Simulations carried out by making adjustments in parameters helped understand their effect on experimental data.

- For cation exchange of major proteins, most accurate predictions by *ExProSim:IC* for BSA was given by MPM isotherm for both the proteins for single component isotherm, whereas rest of them could predict the breakthrough up to 50%. For a multicomponent breakthrough BLG was found to be displaced by BSA. Implementation of EDM-MPM model gave best prediction amongst three isotherms followed by SMA and Langmuir. Better performance of MPM can be attributed to consideration of both hydrophobic as well as salt interactions which play role in case of these two proteins as the operating pH is very close to the isoelectric points of the proteins. This suggested that the choice of a model may be dependent on protein-resin properties.

- For anion exchange of major proteins, all three thermodynamic models were used effectively for the predictions with SMA being slightly superior at predicting breakthrough curves due to highly ionic interactions. This can be attributed to nature of SMA where exchange of charged proteins with salt ions is primarily modelled, whereas for Langmuir and MPM the model is based on proteins binding on the vacant sites rather than actual exchange of ions. This observation was also made in case of cation exchange for minor proteins. Having mostly ionic interactions, SMA showed better predictability for both single and multicomponent experimental data. However, v was found to be highly sensitive for the model and its adjustment can be critical to get correct fit. This also suggested that there is scope in the improve-

ment for experimental determination of v. It can further be said that MPM was more useful when hydrophobic interactions were considerable in the binding, otherwise predictions were almost similar to Langmuir isotherm.

- For crude WPC, simulated breakthrough curves could correctly predict the breakthrough points for all the proteins using all combinations of the models. This can help in finding out dynamic binding capacities and retention patterns of the proteins in the column. It was observed that slower ionic interactions such as BLG adsorption-desorption, was predicted well by EDM-SMA as the isotherm is designed based on exchange of salt ions for protein molecules.

- DBC values were successfully predicted for all the simulations in this work, however shape of the curve was often not predicted to accuracy. DBC values can be helpful in designing the experiments, however as the resin gets older, it will be difficult to reply on same set of simulation model constants which were developed for fresh resin.

- It was concluded from number of simulations that the end of the breakthrough was not predicted consistently using any of the isotherms. It can be said that use of EDM might not be suitable for predicting desorption regime of the curve as more diffusion considerations may be required. This was also realised while simulating results for a crude systems such as WPC. This suggested the need of further extensibility of the tool to incorporate POR and GRM.

7.2 Future work

The thesis provides a basic framework of implementation of modelling and simulations for ion exchange chromatography. Nevertheless, there are areas of improvement for further validation and extensibility of the tool.

Tool improvement

A preliminary exercise of tool verification is presented here. In order to improve the code to handle complex systems, an exhaustive code to code validation can be attempted with respect to several well established tools such as CADET, ChromX, and Chromulator. In order to derive more understanding on model constants and their interrelations if any, a DoE exercise can be run in a tool verification process, where all the parameters are varied at together. Age of the resin can also be included as a variable. This will give optimised thermodynamic constants which can be robust for simulations at any stage of the process. Even if the quantitative measurements are presented for the errors between simulations and experiments, model constant modifications are based on educated trial and error guesses, and error minimisation. Further improvement is required to incorporate quantitative measurement of effect of model constants on protein profiles. It can be facilitated by exhaustive simulations for a system of protein and resin.

Experimental validation using *ExProSim:IC* from chapter 6 showcased that the accuracy of the tool reduced to <90% for 50% of the curve while predicting the breakthrough for crude industrial stream. It will be extremely helpful to validate the tool with other complex feed streams to gain more reliability. Models implemented in current structure of *ExProSim:IC*, may not describe the underlined physical phenomena for complex industrial streams with slower diffusion. Further extensibility of the tool towards incorporating mass transfer models such as; POR, GRM can be explored. While *ExProSim:IC* successfully predicts breakthrough data, it should be extended to loading and elution studies for peak prediction. The peak prediction should be aimed at varying lengths of linear gradients, multistep isocratic gradients, or a combination of both. Following peak prediction, systems must be chosen or established for validation of peak prediction for different scales of chromatography to ensure scalability of the tool [46]. Experiments and simulations in this thesis are from 1 ml scale. Further studies on length-wise and diametrical scale up can be taken up to check the predictability at higher flow rates and loading conditions.

Experiments and simulations in this thesis are carried out at constant pH. As pH is a critical parameter for ion exchange chromatography, incorporating pH

based model [267] and validating them will be beneficial for process optimisation at lab scale.

Tool integration

Importance of DoE and QbD in chromatography process development is mentioned in chapter 2. Following peak prediction, *ExProSim:IC* can be implemented for design space characterisation [120] and process optimisation [114], however for integration with DoE and QbD tools, will need additional sensitivity and uncertainty analysis [130]. Recently, statistical tools have been applied in hyphenation of chromatography operations with analytical techniques for online monitoring [268]. Simulation tools based on mechanistic models are gaining popularity in this field. Implementation of simulation tools such as *ExProSim:IC*, can speed up online troubleshooting process. Furthermore, integration with other modelling platforms such as CFD can give additional insights of the process and equipment design for chromatography. A lot of improvements related to enrichment of solvers, model selection based on process requirements, and data processing are required in the tool before it can be integrated with high end techniques like PAT and CFD.

Appendix A

A.1 Mass transfer equations

[1]

A.1.1 General Rate Model

$$\epsilon_e \frac{\partial c_i}{\partial t} = -u\frac{\partial c_i}{\partial x} + \epsilon_e D_L \frac{\partial^2 c_i}{\partial^2 x} - \frac{3}{r_p}(1-\epsilon_e)k_{ext,i}(c_i - c_{p,i}) \tag{A.1}$$

Where, r is the radius of resin particle. $k_{ext,i}$ corresponds to the fluid to particle mass transfer coefficient, and D_L corresponds to overall dispersion coefficient. Factor $\frac{3}{r_p}$ accounts for the surface to volume ratio of a spherical bead of the resin particle. Furthermore, the mass transfer in the stationary phase is controlled by pore diffusion which can be explained by following equation,

$$\frac{\partial c_{p,i}}{\partial t} = D_{eff,i}\Big(\frac{\partial^2 c_{p,i}}{\partial^2 r} + \frac{2}{r}\frac{\partial c_{p,i}}{\partial r}\Big) - \frac{(1-\epsilon_p)}{\epsilon_p}\frac{\partial q_i}{\partial t} \tag{A.2}$$

Where, $c_{p,i}$ is the concentration of protein in the pores, $D_{eff,i}$ represents the effective particle diffusion coefficient which accounts for both $D_{p,i}$ and $D_{s,i}$ which are particle and surface diffusion coefficients where, q_{eq} gives equilibrium stationary phase concentration.

$$D_{eff,i} = \epsilon_p D_{p,i} + (1-\epsilon_p)D_{s,i}\frac{\partial q_{eq,i}}{\partial c_{p,i}} \tag{A.3}$$

[1] Abbreviations and symbols for appendix A is covered in nomenclature section. Any additional notations are mentioned below the respective equations

The Initial conditions are as follows:

$$c_i(0,x) = c_i^0$$
$$c_{p,i}(0,x) = 0$$
$$q_i(0,x) = 0$$
$$(for 0 < x < L) \quad \text{(A.4)}$$

In addition to this, two sets of boundary conditions are required, one at the column inlet and the other at the column outlet. Boundary conditions for equation are, at the column inlet where $x = 0$

$$u.c'_{f,i} - u_0 c_i^0 = -\epsilon_e D_L \frac{\partial c_i}{\partial x} \quad \text{for} \quad t = 0 \quad \text{(A.5)}$$

Where, u_0 is velocity at zero time, $c'_{f,i}$ is feed concentration, and c_0^i is initial concentration at inlet.

$$c'_{f,i} = c_i^0 \quad \text{for} \quad 0 < t < t_p \quad \text{(A.6)}$$

$$c'_{f,i} = 0 \quad \text{for} \quad t_p < t \quad \text{(A.7)}$$

condition at the column outlet at x=L is,

$$\frac{\partial c_i}{\partial x} \quad \text{for} \quad t <= 0 \quad \text{(A.8)}$$

Boundary conditions for the second equation A.2 are;

$$D_{eff}.\frac{\partial c_{p,it,r}}{\partial r} = k_{ext,i}[c_i - c_{p,i(t,r)}]$$
$$\text{for} \quad t > 0 \quad , \quad r = r_p \quad \text{(A.9)}$$

$$\frac{\partial c_{p,i}(t,r)}{\partial r} = 0 \quad \text{for} \quad t > 0 \quad , \quad r = 0 \quad \text{(A.10)}$$

A.1.2 Pore Diffusion Model

$$\epsilon_e \frac{\partial c_i}{\partial t} + u\frac{\partial c_i}{\partial z} = \epsilon_e D_L \frac{\partial^2 c_i}{\partial^2 z} - (1-\epsilon_e)k_i a_p(c_i - \bar{c}_{p,i}) \tag{A.11}$$

$$\epsilon_p \frac{\partial \bar{c}_{p,i}}{\partial t} + (1-\epsilon_p)\frac{\partial \bar{q}_i}{\partial t} = k_i a_p(c_{p,i} - \bar{c}_{p,i}) \tag{A.12}$$

where, a_p is area of particle, $\bar{c}_{p,i}$ and $\bar{q}_i$ denote average concentrations in the stagnant fluid phase contained in the pores and in the solid phase respectively, and k_i is an overall mass transfer coefficient. The initial and boundary conditions are similar to GR model. The axial dispersion is further calculated through Gunn correlation [269],

$$\epsilon_e \frac{D_L}{d_p u} = \frac{ReSc}{4\alpha_1^2(1-\epsilon)}(1-p^2) + \left(\frac{ReSc}{4\alpha_1^2(1-\epsilon)}\right)^2 p(1-p)^3 \times \left(\frac{-4\alpha_1^2 11(1-\epsilon_e)}{p(1-p)ReSc}\right)\frac{\epsilon_e}{\gamma ReSc} \tag{A.13}$$

where, $p = 0.17 + 0.3310^{-24/Re}$ and Sc and Re are Schmidt and Reynolds numbers respectively, with $Sc = \eta/\rho D_m$ and $Re = d_p u\rho/\eta$. The value of k_i is further given by,

$$k_i = \left[\frac{1}{k_{ext,i}} + \frac{1}{k_{int,i}}\right]^{-1} \tag{A.14}$$

where, $k_{ext,i}$ and $k_{int,i}$ are the external and the internal mass transfer coefficients, respectively. The internal mass transfer coefficient can be calculated as follows,

$$k_{int,i} = \frac{10 D_{eff,i}}{d_p} \quad \text{with} \quad D_{eff,i} = \frac{\epsilon_p D_{m,i}}{\gamma_p} \tag{A.15}$$

Where, $D_{eff,i}$ is effective diffusion coefficient and $D_{m,i}$ is molecular diffusivity which can be found out by,

$$Dm, i = 9.40 \times 10^{-15}.\frac{T}{\eta MW_i^{\frac{1}{3}}} \quad \text{for} \quad MW_i > 1000 \tag{A.16}$$

$$D_{m,i} = 9.96 \times 10^{-16}\frac{T}{\eta V_m^{\frac{1}{3}}} \quad \text{for} \quad M_i < 1000 \tag{A.17}$$

T is the temperature($Kelvin$), η the viscosity of the solvent, and M_i and $V_{m,i}$ are the molecular weight and atomic volume respectively of the component in question. The tortuosity factor γ_t was calculated according to $\gamma_t = (2 - \epsilon_p)^2/\epsilon_p$, where ϵ_p is the particle porosity, which was calculated according to,

$$\epsilon_t = \epsilon_e + (1 - \epsilon_e)\epsilon_p \tag{A.18}$$

where, ϵ_t is the total column porosity and ϵ_e is the external column porosity. The value of the external mass transfer coefficient was calculated from the Sherwood number, Sh, according to Wilson-Geankoplis correlation [270],

$$Sh = \frac{k_{ext,i}d_p}{D_m} = \frac{1.09}{\epsilon_e}Sc^{1/3}Re^{1/3} \tag{A.19}$$

where Schmidt number and Reynolds number are given as,

$$\begin{aligned} Sc &= \frac{\eta}{\rho D_m} \\ Re &= \frac{\rho u d_p}{\eta} \end{aligned} \tag{A.20}$$

A.1.3 Transpot dispersive model

Mass transfer equation for TDM is same as EDM (Equation 3.1). EDM uses equilibrium form of isotherm for estimation of concentrations. however, following is equation is used in TDM. The kinetic forms change with change in isotherm. These models were used together for both equilibrium and kinetic simulations of the experimental systems in this work.

$$\frac{\partial q_i}{\partial t} = k_m q_{eq}(c_i) - q_i \tag{A.21}$$

here, q_{eq} is the concentration in the adsorption monolayer at the adsorbent surface in equilibrium with the concentration q_i in the mobile phase. D_{app} is apparent dispersion coefficient which replaces the axial dispersion coefficient in EDM.

A.1.4 Ideal model

Ideal model is the simplest form of mass transfer where, no diffusion is considered.

$$\frac{\partial c_i}{\partial t} + F\frac{\partial q_i}{\partial t} + u\frac{\partial c_i}{\partial x} = 0 \tag{A.22}$$

Appendix B

Table B.1: Summary of gradient elution studies for BSA and BLG

Protein	Gradient length	RT (min)	RV (ml)	Area
	5	8.19	8.18	118.46
	10	9.47	9.48	115.66
BSA	15	10.81	10.82	119.14
	20	12.04	12.02	119.12
	30	14.03	14.04	113.43
	5	6.82	6.81	270.01
	10	8.19	8.18	273.35
BLG	15	9.44	9.42	263.96
	20	10.62	10.61	262.96
	30	12.88	12.87	269.28

Table B.2: Summary of gradient elution studies for major whey proteins on CaptoQ anion exchanger

Proteins	Gradient length (CV)	RT (min)	RV (ml)	Area (ml*mAU)
	5	7.22	7.21	171.65
	10	8.2	8.18	182.56
BSA	15	9.03	9.02	187.42
	20	9.82	9.8	189.72
	30	11.35	11.34	181.24
	5	7.76	7.745	266.10
	10	9.045	9.03	268.89
BLG	15	10.22	10.21	264.12
	20	11.37	11.355	266.06
	30	13.525	13.515	266.51
	5	7.6	7.58	318.57
	10	8.52	8.505	322.58
ALA	15	9.34	9.32	325.04
	20	10.12	10.1	329.27
	30	11.48	11.46	326.06

Table B.3: Summary of gradient elution studies for LF and LP

Protein	Gradient length	RT (min)	RV (ml)	Area
	5	6.68	6.68	723.77
	10	7.87	7.87	733.90
LF	15	8.98	8.98	739.26
	20	10.07	10.07	729.54
	30	12.13	12.13	717.84
	5	8.56	8.56	345.84
	10	9.66	9.66	357.37
LP	15	10.71	10.71	363.21
	20	11.68	11.68	362.18
	30	13.55	13.55	360.95

Table B.4: Comparison of *Exprosim:IC* Langmuir, MPM, and SMA simulation to experimental data at different breakthrough percentage for multicomponent breakthrough for BSA and BLG

			Langmuir		**MPM**		**SMA**	
	BT %	**Experimental**	**sim**	**% error**	**sim**	**% error**	**sim**	**% error**
BSA	0	15.60	16.10	-3.21	16.00	-2.56	15.10	3.21
	10	16.50	17.20	-4.24	17.10	-3.64	16.30	1.21
	50	32.64	37.81	-15.84	31.70	2.88	29.60	9.31
	100	-	76.89	-	74.50	-	64.60	-
BLG	0	14.40	14.20	1.39	14.00	2.78	14.20	1.39
	10	16.30	15.90	2.45	16.00	1.84	16.10	1.23
	50	23.10	21.80	5.63	22.30	3.46	22.00	4.76
	100	34.56	27.73	19.76	34.56	22.72	36.70	-6.19

Table B.5: Estimation of error between experiment and *Exprosim:IC* simulation profiles for different isotherms for anion exchange single component breakthrough

Flowrate (ml/min)	**Model**		**BSA**			**BLG**			**ALA**		
			Exp	**Sim**	**error**	**Exp**	**Sim**	**error**	**Exp**	**Sim**	**error**
0.5	*Langmuir*	0%	88.6	87.6	1.13%	138.6	144.3	-4.11%	68.67	67.2	2.14%
		10%	99.2	98.5	0.71%	158.2	157.3	0.57%	105.1	107.02	-1.83%
		50%	119.29	113.6	4.77%	184.1	182.6	0.81%	132.25	130.4	1.40%
		100%	132.4	142.3	-7.48%	217.12	241.2	-11.09%	185.2	180.6	2.48%
		$V_{10\%b}$	49.6	49.25	0.003	79.1	78.65	0.003	52.55	53.51	-0.009
	MPM	0%	88.6	87.5	1.24%	138.6	138.18	0.30%	68.67	65.8	4.18%
		10%	99.2	98.9	0.30%	158.2	161.2	-1.90%	105.1	101.81	3.13%
		50%	119.29	115.2	3.43%	184.1	177.6	3.53%	132.25	129.3	2.23%
		100%	132.4	128.3	3.10%	217.12	219.4	-1.05%	185.2	184.24	0.52%
		$V_{10\%b}$	49.6	49.45	0.001	79.1	80.6	-0.009	52.55	50.905	0.015
	SMA	0%	88.6	89.9	-1.47%	138.6	135.6	2.16%	68.67	69.8	-1.65%
		10%	99.2	104.1	-4.94%	158.2	154.5	2.34%	105.1	104.2	0.86%
		50%	119.29	121.4	-1.77%	184.1	175.7	4.56%	132.25	126.4	4.42%
		100%	132.4	135.6	-2.42%	217.12	213.4	1.71%	185.2	176.8	4.54%
		$V_{10\%b}$	49.6	52.05	-0.024	79.1	77.25	0.011	52.55	52.1	0.004
1	*Langmuir*	0%	34.3	35.8	-4.37%	65.6	63.2	3.66%	36.2	37.1	-2.49%
		10%	49.6	47.2	4.84%	76.2	77.8	-2.10%	48.2	47.2	2.07%
		50%	59.2	56.9	3.89%	90.97	92.3	-1.46%	66.8	65.4	2.10%
		100%	80.61	86.2	-6.93%	105.1	108.3	-3.04%	87.2	90.6	-3.90%
		$V_{10\%b}$	49.6	47.2	0.048	76.2	77.8	-0.021	48.2	47.2	0.020
	MPM	0%	34.3	35.4	-3.21%	65.6	62.3	5.03%	36.2	35.1	3.04%
		10%	49.6	48.3	2.62%	76.2	74.3	2.49%	48.2	46.2	4.15%
		50%	59.2	58.1	1.86%	90.97	88.2	3.04%	66.8	63.5	4.94%
		100%	80.61	79.1	1.87%	105.1	108.4	-3.14%	87.2	83.5	4.24%
		$V_{10\%b}$	49.6	48.3	0.026	76.2	74.3	0.024	48.2	46.2	0.041
	SMA	0%	34.3	33.9	1.17%	65.6	66	-0.61%	36.2	35.2	2.76%
		10%	49.6	48	3.23%	76.2	76.5	-0.39%	48.2	45.2	6.22%
		50%	59.2	59	0.34%	90.97	92.6	-1.79%	66.8	64.3	3.74%
		100%	80.61	85.6	-6.19%	105.1	109.1	-3.81%	87.2	91.3	-4.70%
		$V_{10\%b}$	49.6	48	0.032	76.2	76.5	-0.004	48.2	45.2	0.062

Table B.6: Estimation of error between experiment and *Exprosim:IC* simulation profiles for different isotherms for multicomponent breakthrough

Model		**BSA**			**BLG**			**ALA**		
		Exp	**Sim**	**%error**	**Exp**	**Sim**	**%error**	**Exp**	**Sim**	**%error**
	0%	52	53.03	-1.98%	78	79.6	-2.05%	48	49.8	-3.75%
	10%	56	59.2	-5.71	83.2	81.6	1.92	54	56.4	-4.44
Langmuir	50%	64	73.3	-14.53	90	96.4	-7.11	66	73.4	-11.21
	100%	70	88.38	-26.26	108	132.5	-22.69	92	93.1	-1.20
	V10%b	28	29.6	-5.71	41.6	40.8	1.92	27	28.2	-4.44
	0%	52	51.2	1.54%	78	74.9	3.97%	48	49.8	-3.75%
	10%	56	57.2	-2.14	83.2	83.4	-0.24	54	56.4	-4.44
MPM	50%	64	70.1	-9.53	92	98.48	-7.04	66	71.2	-7.88
	100%	70	86.2	-23.14	112	195.6	-74.64	92	92.2	-0.22
	V10%b	28	28.6	-2.14	41.6	41.7	-0.24	27	28.2	-4.44
	0%	52	50.2	3.46	78	70.5	9.62	48	46.2	3.75
	10%	56	53.9	3.75	83.2	76.75	7.75	54	56	-3.70
SMA	50%	64	68.1	-6.41	90	92.2	-2.44	66	69.8	-5.76
	100%	70	89.2	-27.43	108	136.2	-26.11	92	104	-13.04
	V10%b	28	26.95	3.75	41.6	38.375	7.75	27	28	-3.70

Table B.7: Comparison of breakthrough points for LF for different breakthrough percentage

Inlet Conc (mg/ml)	Flow rate (ml/min)	BT%	Experimental (min)	Langmuir	% Error	SMA	% Error	MPM	% Error
3	0.5	0	52.13	54.23	-4.04	53.26	-2.19	54.01	-3.62
		10	68.80	72.27	-5.04	68.93	-0.19	68.69	0.16
		50	80.48	90.6	-12.57	88.44	-9.89	85.3	-5.99
		100	149.80	132.73	11.40	131.66	12.11	133.33	10.69
	0.75	0	25.50	28.35	-11.18	26.13	-2.47	26.2	-2.74
		10	43.61	44.1	-1.12	41.21	5.52	41.68	4.43
		50	52.50	59.5	-13.33	59.29	-12.94	57.2	-8.95
		100	99.8	105.8	-6.01	99.49	0.30	98.98	0.82
	1	0	16.53	17.2	-4.05	16.08	2.73	16.16	2.24
		10	28.76	28.68	0.30	27.95	2.82	27.91	2.99
		50	39.6	44.9	-13.38	44.32	-11.92	43.2	-9.09
		100	83.60	80.67	3.50	83.42	0.22	82.88	0.86
6	0.5	0	29.6	31.93	-7.88	34.7	-17.23	30.3	-2.36
		10	34.2	38.05	-11.26	44.2	-29.5	37.93	-10.91
		50	42.20	46.2	-9.48	54.21	-28.46	46.46	-10.09
		100	80.70	77.2	3.58	76.38	4.61	76.76	4.13
	0.75	0	13.25	14.2	-7.19	18.9	-42.67	14.1	-6.44
		10	21.84	23.52	-7.69	27.13	-24.22	22.22	-1.74
		50	26.6	30.4	-14.29	34.5	-29.70	31.2	-17.29
		100	61.40	58.84	4.17	57.38	6.55	56.57	7.87
	1	0	7.12	8.4	-17.98	10.5	-47.47	8.2	-15.17
		10	14.92	15.13	-1.38	18.92	-26.81	15.2	-1.88
		50	18.98	22.5	-18.55	27.2	-43.31	23.2	-22.23
		100	44.13	40.36	8.54	41.26	6.5	40.4	8.45

BT% denotes percentage of the maximum concentration reached

Table B.8: Comparison of breakthrough points for LP for different breakthrough percentage for single component breakthrough

Inlet Conc (mg/ml)	Flow rate (ml/min)	BT%	Experimental (min)	Langmuir	% Error	SMA	% Error	MPM	% Error
4	0.5	0	67.22	68.66	-2.14	68.99	-2.63	70.71	-5.19
		10	90.02	91.12	-1.22	91.12	-1.22	92.43	-2.68
		50	113.89	112.61	1.12	112.61	1.12	115.15	-1.11
		100	170.3	149.58	12.17	149.58	12.17	169.7	0.35
	0.75	0	31.52	32.13	-1.93	32.323	-2.54	32.32	-2.53
		10	60.46	51.8	14.32	54.32	10.15	56.31	6.86
		50	75.63	75.23	0.53	81.34	-7.55	76.77	-1.51
		100	115.78	109.24	5.65	126.04	-8.87	141.41	-22.14
	1	0	11.01	13.45	28.07	12.12	-10.18	18.18	-65.12
		10	43.25	33.61	14.51	35.67	17.53	36.36	15.93
		50	57.30	55.46	3.21	60.89	-6.27	57.67	-0.65
		100	85.33	104.2	-22.11	117.17	-37.31	105.05	-23.11

BT% denotes percentage of the maximum concentration reached

Table B.9: Comparison of breakthrough points at different breakthrough stages of multicomponent breakthrough of LF and LP

Protein	BT %	Experimental (min)	Langmuir	% error	SMA	% error	MPM	% error
Lactoferrin	0%	50	54.2	8.40	49.6	-0.80	50.2	0.40
	10%	61.22	63.45	3.64	61.64	0.69	61.8	0.95
	50%	69	66.8	-3.19	72.56	5.16	66.47	-3.67
	100%	90.91	88.89	2.22	97.96	-7.75	93.44	-2.78
Lactoperoxidase	0%	28.57	31.6	10.61	27.8	-2.7	28.5	-0.25
	10%	49	52.9	7.96	46.8	-4.49	53.7	9.59
	50%	61.6	61.8	0.32	58.8	-4.55	62.3	1.14
	100%	73	73.47	0.64	77.55	6.23	70.4	-3.56

Table B.10: Comparison of breakthrough points at different breakthrough stages of WPC breakthrough

		BSA			ALA			BLG		
	% BT	Exp	Sim	% Error	Exp	Sim		Exp	Sim	% Error
Langmuir	0	20	22.2	11	29	28.1	-3.103	71	71.2	0.281
	10	24	27.4	14.166	32	30.3	-5.312	86	84.84	-1.348
	50	32.1	36.36	13.271	42	39.93	-4.928	107	106.6	-0.374
	100	45.6	45.45	-0.328	55.4	48.7	-12.093	128	142.1	11.015
	v10%	24	27.4	14.166	32	30.3	-5.3125	86	84.84	-1.348
MPM	0	20	17.3	-13.5	29	25.7	-11.379	71	70.8	-0.282
	10	24	27.7	15.416	32	36.5	14.063	86	87.1	1.279
	50	32.1	35.6	10.903	42	43.8	4.286	107	109.6	2.429
	100	45.6	48.5	6.359	55.4	60.67	9.512	128	145.7	13.828
	v10%	24	27.7	15.416	32	36.5	14.0625	86	87.1	1.279
SMA	0	20	15.2	-24	29	24.1	-16.896	71	72.7	2.394
	10	24	24.34	1.416	32	29.1	-9.0625	86	86.1	0.116
	50	32.1	33.33	3.831	42	38.6	-8.095	107	107	0
	100	45.6	55.6	21.929	55.4	72.2	30.324	128	130.2	1.718
	v10%	24	24.34	1.416	32	29.1	-9.063	86	86.1	0.116

Table B.11: Summary of errors for axial coordinate mesh number variation

	ALA		BLG	
Nx	**RMSE**	**CoD**	**RMSE**	**CoD**
5-10	9.961E-4	0.9900	6.11E-04	0.9806
10-15	1.853E-09	0.9916	6.28E-09	0.9872
15-20	3.450E-09	0.9917	8.83E-09	0.9917
20-25	2.605E-09	0.9917	6.09E-09	0.9917
25-30	1.730E-09	0.9917	3.88E-09	0.9917
30-35	2.889E-09	0.9917	2.53E-09	0.9917
35-40	7.930E-10	0.9917	1.73E-09	0.9917
40-45	5.666E-10	0.9917	1.17E-09	0.9917
45-50	9.82939E-10	0.9917	1.30E-09	0.9919

Table B.12: Summary of errors for time coordinate mesh number variation

	ALA		BLG	
Nt	**RMSE**	**CoD**	**RMSE**	**CoD**
10-20	1.49E-05	0.946	5.07E-04	0.941
20-30	4.69E-07	0.967	1.81E-07	0.966
30-40	1.51E-07	0.975	6.98E-07	0.975
40-50	2.54E-09	0.990	2.83E-07	0.990
50-60	1.23E-09	0.991	1.20E-07	0.990
60-70	1.43E-09	0.991	1.13E-07	0.989

Table B.26: Compilation of errors for breakthrough prediction for anion exchange of whey protein concentrate

		BSA	BLG	ALA
Lang	*MSE*	0.0558	0.0060	0.0338
	SD MSE	0.0698	0.0119	0.0515
	RMSE	0.0006	0.0001	0.0084
	CoD	0.9388	0.9523	0.9223
SMA	*MSE*	0.0595	0.0011	0.0436
	SD MSE	0.0748	0.0024	0.0588
	RMSE	0.0000	0.0000	0.0003
	CoD	0.9527	0.9730	0.9162
MPM	*MSE*	0.0597	0.0057	0.0392
	SD MSE	0.1030	0.0124	0.0626
	RMSE	0.0000	0.0000	0.0000
	CoD	0.9189	0.9790	0.9207

Table B.13: Summary of errors for single component predictions from El Sayed and Chase et al. [1]

	ALA		**BLG**	
	ExProSim:IC	ElSayed sim	ExProSim:IC	ElSayed sim
MSE	0.0116	0.0051	0.0039	0.0041
SD MSE	0.0191	0.0070	0.0074	0.0066
RMSE	5.06E-04	3.92E-03	1.15E-05	7.20E-04
CoD	0.9399	0.9254	0.9538	0.9449

Table B.14: Errors for Langmuir:EDM multicomponent breakthrough prediction from El Sayed and Chase [1]

	ALA		**BLG**	
	Exprosim:IC	ElSayed sim	Exprosim:IC	ElSayed sim
MSE	0.0069	0.0062	0.0065	0.0002
SD MSE	0.0109	0.0094	0.0089	0.0003
RMSE	1.27E-3	1.08E-2	3.09E-5	7.24E-4
CoD	0.9384	0.9044	0.9498	0.9318

Table B.15: Errors for Langmuir:EDM prediction from H. Bak et al. [2]

	20%		**33%**		**50%**		**100%**	
	Exprosim	sim	Exprosim	sim	Exprosim	sim	Exprosim	sim
MSE	0.0006	0.1349	0.0011	0.0712	0.0002	0.1773	0.0177	0.1610
CoD	0.0010	0.2134	0.0028	0.1076	0.0005	0.2513	0.0486	0.2141
RMSE	0.0020	0.0028	0.0002	0.0005	0.0006	0.0015	0.0000	0.0004
CoD	0.9116	0.8564	0.9812	0.8258	0.9509	0.7216	0.9311	0.6711

Table B.16: Errors for Langmuir:EDM breakthrough prediction from Skidmore and Chase [3]

	BSA		**Lysozyme**	
	Exprosim	sim	Exprosim	sim
MSE	0.0274	0.0237	0.0042	0.0003
CoD	0.0283	0.0282	0.0107	0.0005
RMSE	0.0004	0.0006	0.0000	0.0001
CoD	0.9801	0.9419	0.9745	0.9517

Table B.17: Compilation of errors EDM:SMA simulations for Insulin and Transferrin

	Insulin		**Transferrin**	
	Exprosim	sim	Exprosim	sim
MSE	0.0016	0.0005	0.0014	0.0003
CoD	0.0045	0.0010	0.0031	0.0007
RMSE	0.0007	0.0087	0.0005	0.0013
CoD	0.9872	0.9656	0.9867	0.9468

Table B.18: Errors for Langmuir:SMA multicomponent breakthrough prediction from Jozwik et al. [5]

Salt%	**0%**		**1%**		**2%**		**3%**	
	Exprosim	sim	Exprosim	sim	Exprosim	sim	Exprosim	sim
MSE	0.0027	0.0081	0.0062	0.0013	0.0467	0.0586	0.0140	0.0716
CoD	0.0052	0.0158	0.0142	0.0017	0.0885	0.0659	0.0301	0.1134
RMSE	0.0002	0.0008	0.0004	0.0008	0.0006	0.0015	0.0004	0.0010
CoD	0.9813	0.9364	0.9760	0.9616	0.8889	0.8844	0.7682	0.8510

Table B.19: Compilation of errors for EDM:MPM simulations for Transferrin, Insulin, and IgG

	Transferrin		**Insulin**		**IgG**	
	Exprosim	sim	Exprosim	sim	Exprosim	sim
MSE	0.0002	0.0008	0.0002	0.0008	0.0001	0.0001
CoD	0.0006	0.0012	0.0006	0.0012	0.0003	0.0001
RMSE	0.0000	0.0001	0.0000	0.0001	0.0000	0.0004
CoD	0.9944	0.9788	0.9944	0.9788	0.9991	0.9823

Table B.20: Compilation of errors for single component breakthrough prediction for cation exchange of BSA and BLG

		BSA		BLG	
	Flow rate (ml/min)	0.5	1	0.5	1
Lang	*MSE*	0.0001	0.0133	0.0173	0.0100
	CoD	0.0002	0.0145	0.0345	0.0156
	RMSE	1.43E-4	9.36E-4	1.31E-6	7.01E-7
	CoD	0.9858	0.9769	0.9503	0.9639
SMA	*MSE*	0.0020	0.0164	0.0081	0.0036
	CoD	0.0043	0.0202	0.0168	0.0063
	RMSE	1.39E-3	2.27E-3	1.07E-10	5.34E-6
	CoD	0.9631	0.9641	0.9615	0.9674
MPM	*MSE*	0.0061	0.0259	0.0021	0.0057
	CoD	0.0121	0.0256	0.0031	0.0105
	RMSE	7.95E-4	1.07E-3	1.61E-5	1.12E-4
	CoD	0.9714	0.9704	0.9780	0.9605

Table B.21: Compilation of errors for multi component breakthrough prediction for anion exchange of BSA and BLG

		BSA	BLG
Lang	*MSE*	0.0046	0.0208
	CoD	0.0066	0.0223
	RMSE	0.0001	0.0000
	CoD	0.9214	0.9197
SMA	*MSE*	0.0219	0.0240
	CoD	0.0239	0.0279
	RMSE	0.0000	0.0000
	CoD	0.9572	0.9502
MPM	*MSE*	0.0026	0.0775
	CoD	0.0054	0.1629
	RMSE	0.0003	0.0004
	CoD	0.9589	0.8670

Table B.22: Compilation of errors for single component breakthrough prediction at two flow rates for anion exchange of major whey proteins

		BSA		**BLG**		**ALA**	
Flow rate (ml/min)		0.5	1	0.5	1	0.5	1
Lang	*MSE*	0.0026	0.0024	0.0036	0.0046	0.0017	0.0012
	CoD	0.0062	0.0068	0.0080	0.0106	0.0050	0.0027
	RMSE	0.0008	0.0005	0.0006	0.0027	0.0002	0.0002
	CoD	0.9818	0.9677	0.9547	0.9098	0.9518	0.9350
SMA	*MSE*	0.0024	0.0030	0.0049	0.0035	0.0034	0.0040
	CoD	0.0067	0.0103	0.0173	0.0076	0.0090	0.0079
	RMSE	0.0009	0.0004	0.0006	0.0016	0.0001	0.0006
	CoD	0.9831	0.9674	0.9651	0.9517	0.9688	0.9616
MPM	*MSE*	0.0048	0.0004	0.0024	0.0024	0.0010	0.0064
	CoD	0.0171	0.0013	0.0092	0.0069	0.0021	0.0192
	RMSE	0.0006	0.0025	0.0005	0.0000	0.0001	0.0000
	CoD	0.9818	0.9857	0.9785	0.9730	0.9840	0.9687

Table B.23: Compilation of errors for multi component breakthrough prediction for anion exchange of major whey proteins

		BSA	**BLG**	**ALA**
Lang	*MSE*	0.0182	0.0016	0.0100
	CoD	0.0447	0.0031	0.0191
	RMSE	0.0000	0.0009	0.0000
	CoD	0.9491	0.9727	0.9580
SMA	*MSE*	0.0595	0.0061	0.0039
	CoD	0.1047	0.0115	0.0087
	RMSE	0.0045	0.0009	0.0008
	CoD	0.9055	0.9604	0.9616
MPM	*MSE*	0.0734	0.0162	0.0093
	CoD	0.1268	0.0357	0.0195
	RMSE	0.0000	0.0009	0.0001
	CoD	0.9046	0.9712	0.9555

Table B.24: Compilation of errors for single component breakthrough prediction for cation exchange of minor whey proteins

		LF (3 mg/ml)			**LF (6 mg/ml)**			**LP (4 mg/ml)**		
	Flow Rate (ml/min)	0.5	0.75	1	0.5	0.75	1	0.5	0.75	1
Lang	*MSE*	0.0067	0.0118	0.0082	0.0039	0.0107	0.0144	0.0021	0.0035	0.0077
	SD MSE	0.0158	0.0245	0.0166	0.0076	0.0244	0.0284	0.0041	0.0055	0.0102
	RMSE	0.0002	0.0007	0.0009	0.0013	0.0016	0.0020	0.0000	0.0003	0.0001
	CoD	0.9715	0.9604	0.9635	0.9716	0.9510	0.9319	0.9860	0.9761	0.9594
SMA	*MSE*	0.0034	0.0086	0.0060	0.0526	0.0488	0.0532	0.0053	0.0104	0.0134
	SD MSE	0.0081	0.0174	0.0119	0.1002	0.0870	0.0825	0.0123	0.0189	0.0185
	RMSE	0.0000	0.0006	0.0006	0.0011	0.0011	0.0016	0.0009	0.0008	0.0008
	CoD	0.9854	0.9731	0.9757	0.8904	0.8957	0.8819	0.9653	0.9483	0.9360
MPM	*MSE*	0.0014	0.0051	0.0037	0.0073	0.0101	0.0141	0.0010	0.0030	0.0059
	SD MSE	0.0031	0.0108	0.0076	0.0173	0.0230	0.0271	0.0013	0.0055	0.0070
	RMSE	0.0004	0.0007	0.0008	0.0021	0.0019	0.0017	0.0000	0.0006	0.0011
	CoD	0.9831	0.9694	0.9680	0.9618	0.9470	0.9243	0.9858	0.9750	0.9631

Table B.25: Compilation of errors for multi component breakthrough prediction for cation exchange of minor whey proteins

		LF	**LP**
Lang	*MSE*	0.0022	0.0232
	SD MSE	0.0038	0.0447
	RMSE	2.36E-5	6.28E-7
	CoD	0.9623	0.9774
SMA	*MSE*	0.0041	0.0177
	SD MSE	0.0088	0.0315
	RMSE	3.41E-5	1.34E-4
	CoD	0.9714	0.9564
MPM	*MSE*	0.0029	0.0457
	SD MSE	0.0065	0.1115
	RMSE	6.87E-5	1.68E-8
	CoD	0.9699	0.9842

Bibliography

[1] Mayyada MH El-Sayed and Howard A Chase. Purification of the two major proteins from whey concentrate using a cation-exchange selective adsorption process. *Biotechnology progress*, 26(1):192–199, 2010.

[2] Hanne Bak, Owen RT Thomas, and Jens Abildskov. Lumped parameter model for prediction of initial breakthrough profiles for the chromatographic capture of antibodies from a complex feedstock. *Journal of chromatography B*, 848 (1):131–141, 2007.

[3] Graham L Skidmore, Brenda J Hortsmann, and Howard A Chase. Modelling single-component protein adsorption to the cation exchanger s sepharose® ff. *Journal of Chromatography A*, 498:113–128, 1990.

[4] David Karlsson, Niklas Jakobsson, Karl-Johan Brink, Anders Axelsson, and Bernt Nilsson. Methodologies for model calibration to assist the design of a preparative ion-exchange step for antibody purification. *Journal of chromatography a*, 1033(1):71–82, 2004.

[5] Magdalena Jozwik, Krzystof Kaczmarski, and Ruth Freitag. Investigation of the steric mass action formalism in the simulation of breakthrough curves on a monolithic and a packed bed column. *Journal of Chromatography A*, 1073 (1):111–121, 2005.

[6] David Karlsson, Niklas Jakobsson, Anders Axelsson, and Bernt Nilsson. Model-based optimization of a preparative ion-exchange step for antibody purification. *Journal of Chromatography A*, 1055(1-2):29–39, 2004.

[7] Eric Langer and Joel Ranck. Capacity bottleneck squeezed by downstream processes. *BioProcess Int*, 4(3):14–18, 2006.

[8] Eric S Langer. Downstream production challenges in 2007. *Bioprocess International*, 5(6):22–28, 2007.

[9] EN Lightfoot. Speeding the design of bioseparations: A heuristic approach to engineering design. *Industrial & engineering chemistry research*, 38(10): 3628–3634, 1999.

[10] Ana S. Simaria, Richard Turner, and Suzanne S. Farid. A multi-level meta-heuristic algorithm for the optimisation of antibody purification processes. *Biochemical Engineering Journal*, 69:144 – 154, 2012.

[11] Abhinav A Shukla, Brian Hubbard, Tim Tressel, Sam Guhan, and Duncan Low. Downstream processing of monoclonal antibodies—application of platform approaches. *Journal of Chromatography B*, 848(1):28–39, 2007.

[12] ICH Harmonised Tripartite Guideline. Guidance for industry: Q8 (r2), pharmaceutical development. In *International Conference on Harmonisation of Technical Requirements for Registration of Pharmaceuticals for Human Use (ICH), US Department of Health and Human Services, Food and Drug Administration, Rockville*, 2009.

[13] Attila Felinger. Tingyue gu: Mathematical modeling and scale-up of liquid chromatography: with application examples. *Analytical and bioanalytical chemistry*, 408(18):4827, 2016.

[14] Tobias Hahn, Thiemo Huuk, Vincent Heuveline, and Jurgen Hubbuch. Simulating and optimizing preparative protein chromatography with chromx. *Journal of Chemical Education*, 92(9):1497–1502, 2015.

[15] Eric von Lieres and Joel Andersson. A fast and accurate solver for the general rate model of column liquid chromatography. *Computers & chemical engineering*, 34(8):1180–1191, 2010.

[16] Alois Jungbauer and Rainer Hahn. Ion-exchange chromatography. In *Methods in enzymology*, volume 463, pages 349–371. Elsevier, 2009.

[17] J Norton Wilson. A theory of chromatography. *Journal of the American Chemical Society*, 62(6):1583–1591, 1940.

[18] AJP Martin and RL Mo Synge. A new form of chromatogram employing two liquid phases: A theory of chromatography. 2. application to the micro-determination of the higher monoamino-acids in proteins. *Biochemical Journal*, 35(12):1358, 1941.

[19] Leon Lapidus and Neal R Amundson. Mathematics of adsorption in beds. vi. the effect of longitudinal diffusion in ion exchange and chromatographic columns. *The Journal of Physical Chemistry*, 56(8):984–988, 1952.

[20] Irving Langmuir. The constitution and fundamental properties of solids and liquids. part i. solids. *Journal of the American Chemical Society*, 38(11):2221–2295, 1916.

[21] Jozsef Toth. *Adsorption*. CRC Press, 2002.

[22] Elias I Franses, Faisal A Siddiqui, Dong June Ahn, Chien-Hsiang Chang, and Nien-Hwa Linda Wang. Thermodynamically consistent equilibrium adsorption isotherms for mixtures of different-sized molecules. *Langmuir*, 11(8): 3177–3183, 1995.

[23] Ajoy Velayudhan and Csaba Horváth. Preparative chromatography of proteins: Analysis of the multivalent ion-exchange formalism. *Journal of Chromatography A*, 443:13–29, 1988.

[24] Arvind Rajendran and Wenda Chen. Binary retention time method for rapid determination of competitive langmuir isotherm parameters. *Separation and Purification Technology*, 67(3):344–354, 2009.

[25] Partha S Ghosal and Ashok K Gupta. Determination of thermodynamic parameters from langmuir isotherm constant-revisited. *Journal of Molecular Liquids*, 225:137–146, 2017.

[26] Kanji Miyabe. Moment equations for chromatography based on langmuir type reaction kinetics. *Journal of Chromatography A*, 1356:171–179, 2014.

[27] Wayne R Melander, Ziad El Rassi, and Csaba Horváth. Interplay of hydrophobic and electrostatic interactions in biopolymer chromatography: effect of

salts on the retention of proteins. *Journal of Chromatography A*, 469:3–27, 1989.

[28] David Karlsson, Niklas Jakobsson, Karl-Johan Brink, Anders Axelsson, and Bernt Nilsson. Methodologies for model calibration to assist the design of a preparative ion-exchange step for antibody purification. *Journal of chromatography a*, 1033(1):71–82, 2004.

[29] David Karlsson, Niklas Jakobsson, Anders Axelsson, and Bernt Nilsson. Model-based optimization of a preparative ion-exchange step for antibody purification. *Journal of Chromatography A*, 1055(1):29–39, 2004.

[30] Clayton A Brooks and Steven M Cramer. Steric mass-action ion exchange: displacement profiles and induced salt gradients. *AIChE Journal*, 38(12): 1969–1978, 1992.

[31] Amitava Kundu, Kristopher A Barnthouse, and Steven M Cramer. Selective displacement chromatography of proteins. *Biotechnology and bioengineering*, 56(2):119–129, 1997.

[32] Joseph A Gerstner and Steven M Cramer. Cation-exchange displacement chromatography of proteins with protamine displacers: Effect of induced salt gradients. *Biotechnology progress*, 8(6):540–545, 1992.

[33] Harish Iyer, Sarah Tapper, Philip Lester, Bradley Wolk, and Robert van Reis. Use of the steric mass action model in ion-exchange chromatographic process development. *Journal of Chromatography A*, 832(1):1–9, 1999.

[34] Naeimeh Faraji, Yan Zhang, and Ajay K Ray. Determination of adsorption isotherm parameters for minor whey proteins by gradient elution preparative liquid chromatography. *Journal of Chromatography A*, 1412:67–74, 2015.

[35] A Osberghaus, S Hepbildikler, S Nath, M Haindl, E von Lieres, and J Hubbuch. Determination of parameters for the steric mass action model—a comparison between two approaches. *Journal of Chromatography A*, 1233:54–65, 2012.

[36] Magdalena Jozwik, Krzystof Kaczmarski, and Ruth Freitag. Investigation of the steric mass action formalism in the simulation of breakthrough curves

on a monolithic and a packed bed column. *Journal of Chromatography A*, 1073 (1):111–121, 2005.

[37] Sugunakar Y Patro and Todd M Przybycien. Self-interaction chromatography: a tool for the study of protein–protein interactions in bioprocessing environments. *Biotechnology and bioengineering*, 52(2):193–203, 1996.

[38] Karin Westerberg. *Modeling for Quality and Safety in Biopharmaceutical Production Processes*. Department of Chemical Engineering, Lund University, 2012.

[39] Jørgen M Mollerup. Applied thermodynamics: A new frontier for biotechnology. *Fluid phase equilibria*, 241(1):205–215, 2006.

[40] Juliane Diedrich, William Heymann, Samuel Leweke, Stephen Hunt, Robert Todd, Christian Kunert, Will Johnson, and Eric von Lieres. Multi-state steric mass action model and case study on complex high loading behavior of mab on ion exchange tentacle resin. *Journal of Chromatography A*, 1525:60–70, 2017.

[41] Gautham P Jeppu and T Prabhakar Clement. A modified langmuir-freundlich isotherm model for simulating ph-dependent adsorption effects. *Journal of contaminant hydrology*, 129:46–53, 2012.

[42] Fabian Zehender, Andre Ziegler, H-J Schonfeld, and Joachim Seelig. Thermodynamics of protein self-association and unfolding. the case of apolipoprotein ai. *Biochemistry*, 51(6):1269–1280, 2012.

[43] Georges Guiochon. Preparative liquid chromatography. *Journal of Chromatography A*, 965(1):129–161, 2002.

[44] K Kaczmarski and J Ch Bellot. Effect of particle-size distribution and particle porosity changes on mass-transfer kinetics. *Acta Chromatographica*, pages 22–37, 2003.

[45] MA Quarry, MA Stadalius, TH Mourey, and LR Snyder. General model for the separation of large molecules by gradient elution: sorption versus precipitation. *Journal of Chromatography A*, 358:1–16, 1986.

[46] Spyridon Gerontas, Magnus Asplund, Rolf Hjorth, and Daniel G Bracewell. Integration of scale-down experimentation and general rate modelling to predict manufacturing scale chromatographic separations. *Journal of Chromatography A*, 1217(44):6917–6926, 2010.

[47] Tingyue Gu, Gow-Jen Tsai, and George T Tsao. Simulation of multicomponent elution with the mobile phase containing competing modifiers. *Separations Technology*, 1(4):184–194, 1991.

[48] Niklas Borg, Yan Brodsky, John Moscariello, Suresh Vunnum, Ganesh Vedantham, Karin Westerberg, and Bernt Nilsson. Modeling and robust pooling design of a preparative cation-exchange chromatography step for purification of monoclonal antibody monomer from aggregates. *Journal of Chromatography A*, 1359:170–181, 2014.

[49] Shamsul Qamar, Fouzia Abdul Sattar, Javeria Nawaz Abbasi, and Andreas Seidel-Morgenstern. Numerical simulation of nonlinear chromatography with core–shell particles applying the general rate model. *Chemical Engineering Science*, 147:54–64, 2016.

[50] Wojciech Pikatkowski, Dorota Antos, and Krzysztof Kaczmarski. Modeling of preparative chromatography processes with slow intraparticle mass transport kinetics. *Journal of Chromatography A*, 988(2):219–231, 2003.

[51] Massimo Morbidelli, Alberto Servida, Giuseppe Storti, and Sergio Carra. Simulation of multicomponent adsorption beds. model analysis and numerical solution. *Industrial & Engineering Chemistry Fundamentals*, 21(2):123–131, 1982.

[52] Deqiang Mu, Zhong-Sheng Liu, Cheng Huang, and Ned Djilali. Determination of the effective diffusion coefficient in porous media including knudsen effects. *Microfluidics and Nanofluidics*, 4(3):257–260, 2008.

[53] AM Lenhoff. Multiscale modeling of protein uptake patterns in chromatographic particles. *Langmuir*, 24(12):5991–5995, 2008.

[54] JF Langford, MR Schure, Y Yao, SF Maloney, and AM Lenhoff. Effects of pore structure and molecular size on diffusion in chromatographic adsorbents. *Journal of Chromatography A*, 1126(1):95–106, 2006.

[55] Bertrand Coquebert de Neuville, Abhijit Tarafder, and Massimo Morbidelli. Distributed pore model for bio-molecule chromatography. *Journal of Chromatography A*, 1298:26–34, 2013.

[56] Muhammad Sahimi and Valerie L Jue. Diffusion of large molecules in porous media. *Physical review letters*, 62(6):629, 1989.

[57] Shumaila Javeed, Shamsul Qamar, Andreas Seidel-Morgenstern, and Gerald Warnecke. Efficient and accurate numerical simulation of nonlinear chromatographic processes. *Computers & Chemical Engineering*, 35(11):2294–2305, 2011.

[58] Bingchang Lin, Sadroddin Golshan-Shirazi, and Georges Guiochon. Effect of mass transfer coefficient on the elution profile in nonlinear chromatography. *The Journal of Physical Chemistry*, 93(8):3363–3368, 1989.

[59] RJ Schotting, H Moser, and SM Hassanizadeh. High-concentration-gradient dispersion in porous media: experiments, analysis and approximations1. *Advances in Water Resources*, 22(7):665–680, 1999.

[60] Edward J Close, Jeffrey R Salm, Daniel G Bracewell, and Eva Sorensen. A model based approach for identifying robust operating conditions for industrial chromatography with process variability. *Chemical Engineering Science*, 116:284–295, 2014.

[61] Paweł Szabelski and Krzysztof Kaczmarski. Theoretical investigations of the chromatographic separation of interacting enantiomers. *Journal of Chromatography A*, 1113(1):74–83, 2006.

[62] F Gritti, W Piatkowski, and G Guiochon. Comparison of the adsorption equilibrium of a few low-molecular mass compounds on a monolithic and a packed column in reversed-phase liquid chromatography. *Journal of Chromatography A*, 978(1):81–107, 2002.

[63] Joanna Kostka, Fabrice Gritti, Krzysztof Kaczmarski, and Georges Guiochon. Modified equilibrium-dispersive model for the interpretation of the efficiency of columns packed with core–shell particle. *Journal of Chromatography A*, 1218(32):5449–5455, 2011.

[64] O Lisec, P Hugo, and A Seidel-Morgenstern. Frontal analysis method to determine competitive adsorption isotherms. *Journal of Chromatography A*, 908 (1):19–34, 2001.

[65] Weiqiang Hao, Bin Di, Bangyi Yue, Qiang Chen, Shun Wu, and Peipei Zhang. Equivalence between the equilibrium dispersive and the transport model in describing band broadening in analytical gradient liquid chromatography. *Journal of Chromatography A*, 1369:191–195, 2014.

[66] Douglas M Ruthven. *Principles of adsorption and adsorption processes*. John Wiley & Sons, 1984.

[67] Michael W Phillips, Guhan Subramanian, and Steven M Cramer. Theoretical optimization of operating parameters in non-ideal displacement chromatography. *Journal of Chromatography A*, 454:1–21, 1988.

[68] Georges Guiochon, Attila Felinger, and Dean GG Shirazi. *Fundamentals of preparative and nonlinear chromatography*. Academic Press, 2006.

[69] Sadroddin Golshan-Shirazi and Georges Guiochon. Experimental characterization of the elution profiles of high concentration chromatographic bands using the analytical solution of the ideal model. *Anal. Chem.;(United States)*, 61(5), 1989.

[70] Georges Guiochon and Sadroddin Golshan-Shirazi. A retrospective on the solution of the ideal model of chromatography. *Journal of Chromatography A*, 658(2):173–177, 1994.

[71] Guoming Zhong, Torgny Fornstedt, and Georges Guiochon. Profiles of large-size system peaks and vacancy bands in liquid chromatography i. analytical solution of the ideal model. *Journal of Chromatography A*, 734(1):63–74, 1996.

[72] Sadroddin Golshan-Shirazi and Georges Guiochon. Analytical solution for the ideal model of chromatography in the case of langmuir isotherm. *Anal. Chem.;(United States)*, 60(21), 1988.

[73] S Golshan-Shirazi and G Guiochon. The ideal model of chromatography. In *Theoretical Advancement in Chromatography and Related Separation Techniques*, pages 1–33. Springer, 1992.

[74] Anna A Lysova, Igor V Koptyug, Alexander V Kulikov, Valery A Kirillov, Renad Z Sagdeev, and Valentin N Parmon. Nuclear magnetic resonance imaging of an operating gas–liquid–solid catalytic fixed bed reactor. *Chemical Engineering Journal*, 130(2-3):101–109, 2007.

[75] Laurie A Cardoza, Valentino K Almeida, Amy Carr, Cynthia K Larive, and David W Graham. Separations coupled with nmr detection. *TrAC Trends in Analytical Chemistry*, 22(10):766–775, 2003.

[76] Jürgen Ulpts, Wolfgang Dreher, Miriam Klink, and Jorg Thöming. Nmr imaging of gas phase hydrogenation in a packed bed flow reactor. *Applied Catalysis A: General*, 502:340–349, 2015.

[77] Michael Harasek, Georg Paul, Christian Jordan, and Anton Friedl. Cfd-simulation of preparative chromatographic columns: Effect of the distributor and the column design on the separation performance. *Institute of Chemical Engineering, Fuel and Environmental Technology, Vienna University of Technology, ECCE*, 2001.

[78] A Jafari, P Zamankhan, SM Mousavi, and K Pietarinen. Modeling and cfd simulation of flow behavior and dispersivity through randomly packed bed reactors. *Chemical Engineering Journal*, 144(3):476–482, 2008.

[79] Naveen Pathak, Carney Norman, Sourav Kundu, Suresh Nulu, Mark Durst, and Zhiwu Fang. Modeling flow distribution in large-scale chromatographic columns with computational fluid dynamics. *BioProcess Int*, 6:72–81, 2008.

[80] Chris Johnson, Venkatesh Natarajan, and Chris Antoniou. Evaluating two

process scale chromatography column header designs using cfd. *Biotechnology progress*, 30(4):837–844, 2014.

[81] Jiří J Klemeš, Petar Sabev Varbanov, and Peng Yen Liew. *24th European Symposium on Computer Aided Process Engineering: Part A and B*, volume 33. Elsevier, 2014.

[82] D Brynn Hibbert. Experimental design in chromatography: a tutorial review. *Journal of chromatography B*, 910:2–13, 2012.

[83] Marcos Almeida Bezerra, Ricardo Erthal Santelli, Eliane Padua Oliveira, Leonardo Silveira Villar, and Luciane Amélia Escaleira. Response surface methodology (rsm) as a tool for optimization in analytical chemistry. *Talanta*, 76(5):965–977, 2008.

[84] Bieke Dejaegher and Yvan Vander Heyden. Experimental designs and their recent advances in set-up, data interpretation, and analytical applications. *Journal of pharmaceutical and biomedical analysis*, 56(2):141–158, 2011.

[85] Anthony C Atkinson and Randall D Tobias. Optimal experimental design in chromatography. *Journal of Chromatography A*, 1177(1):1–11, 2008.

[86] Luciana Vera Candioti, María M De Zan, María S Cámara, and Héctor C Goicoechea. Experimental design and multiple response optimization. using the desirability function in analytical methods development. *Talanta*, 124:123–138, 2014.

[87] Sergio Luis Costa Ferreira, Roy Edward Bruns, Erik Galvao Paranhos da Silva, Walter Nei Lopes Dos Santos, Cristina Maria Quintella, Jorge Mauricio David, Jailson Bittencourt de Andrade, Marcia Cristina Breitkreitz, Isabel Cristina Sales Fontes Jardim, and Benicio Barros Neto. Statistical designs and response surface techniques for the optimization of chromatographic systems. *Journal of Chromatography A*, 1158(1-2):2–14, 2007.

[88] Amir M Ramezani, Saeed Yousefinejad, Mohammad Nazifi, and Ghodratollah Absalan. Response surface approach for isocratic separation of some

natural anthraquinone dyes by micellar liquid chromatography. *Journal of Molecular Liquids*, 242:1058–1065, 2017.

[89] Pierre Lebrun, Bruno Boulanger, Benjamin Debrus, Philippe Lambert, and Philippe Hubert. A bayesian design space for analytical methods based on multivariate models and predictions. *Journal of biopharmaceutical statistics*, 23(6):1330–1351, 2013.

[90] Pierre Lebrun, Bruno Boulanger, Philippe Hubert, Benjamin Debrus, and Bernadette Govaerts. Statistical models and multi-criteria optimization techniques in chromatography. 2006.

[91] Manuel David Peris-Díaz, Miguel A Sentandreu, and Enrique Sentandreu. Multiobjective optimization of liquid chromatography–triple-quadrupole mass spectrometry analysis of underivatized human urinary amino acids through chemometrics. *Analytical and bioanalytical chemistry*, pages 1–10, 2018.

[92] Edward Close, Daniel G Bracewell, and Eva Sorensen. A model based approach to an adaptive design space in chromatography. In *Computer Aided Chemical Engineering*, volume 32, pages 115–120. Elsevier, 2013.

[93] Beckley K Nfor, Tangir Ahamed, Gijs WK van Dedem, Peter DEM Verhaert, Luuk AM van der Wielen, Michel HM Eppink, Emile JAX van de Sandt, and Marcel Ottens. Model-based rational methodology for protein purification process synthesis. *Chemical Engineering Science*, 89:185–195, 2013.

[94] Rushd Khalaf, Julia Heymann, Xavier LeSaout, Florence Monard, Matteo Costioli, and Massimo Morbidelli. Model-based high-throughput design of ion exchange protein chromatography. *Journal of Chromatography A*, 1459: 67–77, 2016.

[95] Malay K Das and Tapash Chakraborty. Ann in pharmaceutical product and process development. In *Artificial Neural Network for Drug Design, Delivery and Disposition*, pages 277–293. Elsevier, 2016.

[96] Gang Wang, Till Briskot, Tobias Hahn, Pascal Baumann, and Jürgen Hubbuch. Estimation of adsorption isotherm and mass transfer parameters in protein chromatography using artificial neural networks. *Journal of Chromatography A*, 1487:211–217, 2017.

[97] Josef Havel, Michael Breadmore, Miroslav Macka, and Paul R Haddad. Artificial neural networks for computer-aided modelling and optimisation in micellar electrokinetic chromatography. *Journal of Chromatography A*, 850 (1-2):345–353, 1999.

[98] Kelly Munro, Thomas H Miller, Claudia PB Martins, Anthony M Edge, David A Cowan, and Leon P Barron. Artificial neural network modelling of pharmaceutical residue retention times in wastewater extracts using gradient liquid chromatography-high resolution mass spectrometry data. *Journal of Chromatography A*, 1396:34–44, 2015.

[99] Dirk C Hinz. Process analytical technologies in the pharmaceutical industry: the fda's pat initiative. *Analytical and bioanalytical chemistry*, 384(5):1036–1042, 2006.

[100] Mayyada MH El-Sayed and Howard A Chase. Simulation of the breakthrough curves for the adsorption of α-lactalbumin and β-lactoglobulin to sp sepharose ff cation-exchanger. *Biochemical Engineering Journal*, 49(2):221–228, 2010.

[101] Prashant Kumar, Pei Wen Lau, Sandeep Kale, Stuart Johnson, Vishnu Pareek, Ranjeet Utikar, and Arvind Lali. Kafirin adsorption on ion-exchange resins: Isotherm and kinetic studies. *Journal of chromatography A*, 1356:105–116, 2014.

[102] Krzysztof Kaczmarski, Dorota Antos, Hong Sajonz, Peter Sajonz, and Georges Guiochon. Comparative modeling of breakthrough curves of bovine serum albumin in anion-exchange chromatography. *Journal of Chromatography A*, 925(1):1–17, 2001.

[103] Amit S Patil and Anil M Pethe. Quality by design (qbd): A new concept for development of quality pharmaceuticals. *Int J Qual Assur*, 4:13–9, 2013.

[104] Anurag S Rathore. Quality by design (qbd)-based process development for purification of a biotherapeutic. *Trends in biotechnology*, 34(5):358–370, 2016.

[105] Lalita Kanwar, Anurag Rathore, and Apurva Manvar. Enablers for qbd implementation: Mechanistic modeling for ion-exchange membrane chromatography. In *ABSTRACTS OF PAPERS OF THE AMERICAN CHEMICAL SOCIETY*, volume 253. AMER CHEMICAL SOC 1155 16TH ST, NW, WASHINGTON, DC 20036 USA, 2017.

[106] Cleo Kontoravdi, Nouri J Samsatli, and Nilay Shah. Development and design of bio-pharmaceutical processes. *Current Opinion in Chemical Engineering*, 2 (4):435–441, 2013.

[107] David K Lloyd and James Bergum. Application of quality by design (qbd) to the development and validation of analytical methods. In *Specification of Drug Substances and Products*, pages 29–72. Elsevier, 2013.

[108] Luca Nompari, Serena Orlandini, Benedetta Pasquini, Cristiana Campa, Michele Rovini, Massimo Del Bubba, and Sandra Furlanetto. Quality by design approach in the development of an ultra-high-performance liquid chromatography method for bexsero meningococcal group b vaccine. *Talanta*, 178:552–562, 2018.

[109] Mike McBrien. Practical implications of quality by design to chromatographic method development. *Chromatogr. Today*, 3:30–34, 2010.

[110] Anurag S Rathore. Qbd/pat for bioprocessing: moving from theory to implementation. *Current opinion in chemical engineering*, 6:1–8, 2014.

[111] Marcus Degerman, Niklas Jakobsson, and Bernt Nilsson. Constrained optimization of a preparative ion-exchange step for antibody purification. *Journal of Chromatography A*, 1113(1):92–100, 2006.

[112] A Osberghaus, S Hepbildikler, S Nath, M Haindl, E Von Lieres, and J Hubbuch. Optimizing a chromatographic three component separation: A comparison of mechanistic and empiric modeling approaches. *Journal of Chromatography A*, 1237:86–95, 2012.

[113] Karsten-Ulrich Klatt, Felix Hanisch, Guido Dünnebier, and Sebastian Engell. Model-based optimization and control of chromatographic processes. *adsorption*, 2(x2):1, 2000.

[114] Niklas Borg, Karin Westerberg, Niklas Andersson, Eric von Lieres, and Bernt Nilsson. Effects of uncertainties in experimental conditions on the estimation of adsorption model parameters in preparative chromatography. *Computers & Chemical Engineering*, 55:148–157, 2013.

[115] Patrik Persson, Per-Erik Gustavsson, Guido Zacchi, and Bernt Nilsson. Aspects of estimating parameter dependencies in a detailed chromatography model based on frontal experiments. *Process Biochemistry*, 41(8):1812–1821, 2006.

[116] HK Teoh, M Turner, N Titchener-Hooker, and E Sorensen. Experimental verification and optimisation of a detailed dynamic high performance liquid chromatography column model. *Computers & Chemical Engineering*, 25(4): 893–903, 2001.

[117] Food, Drug Administration, et al. Guidance for industry: Pat—a framework for innovative pharmaceutical development, manufacturing, and quality assurance. *DHHS, Rockville, MD*, 2004.

[118] Canping Jiang, Lisa Flansburg, Sanchayita Ghose, Paul Jorjorian, and Abhinav A Shukla. Defining process design space for a hydrophobic interaction chromatography (hic) purification step: application of quality by design (qbd) principles. *Biotechnology and bioengineering*, 107(6):985–997, 2010.

[119] David Gétaz, Alessandro Butté, and Massimo Morbidelli. Model-based design space determination of peptide chromatographic purification processes. *Journal of Chromatography A*, 1284:80–87, 2013.

[120] Marcus Degerman, Karin Westerberg, and Bernt Nilsson. A model-based approach to determine the design space of preparative chromatography. *Chemical engineering & technology*, 32(8):1195–1202, 2009.

[121] David Gétaz, Guido Stroehlein, Alessandro Butté, and Massimo Morbidelli. Model-based design of peptide chromatographic purification processes. *Journal of Chromatography A*, 1284:69–79, 2013.

[122] Karin Westerberg, Marcus Degerman, and Bernt Nilsson. Pooling control in variable preparative chromatography processes. *Bioprocess and biosystems engineering*, 33(3):375–382, 2010.

[123] Yichu Shan and Andreas Seidel-Morgenstern. Optimization of gradient elution conditions in multicomponent preparative liquid chromatography. *Journal of Chromatography A*, 1093(1-2):47–58, 2005.

[124] Marcus Degerman, Niklas Jakobsson, and Bernt Nilsson. Designing robust preparative purification processes with high performance. *Chemical engineering & technology*, 31(6):875–882, 2008.

[125] Anurag Rathore and Ajoy Velayudhan. Guidelines for optimization and scale-up in preparative chromatography. *Biopharm international*, 16(1):34–42, 2003.

[126] J Haag, A Vande Wouwer, S Lehoucq, and P Saucez. Modeling and simulation of a smb chromatographic process designed for enantioseparation. *Control Engineering Practice*, 9(8):921–928, 2001.

[127] Marc Bisschops and Mark Brower. Dynamic simulations as a predictive model for a multicolumn chromatography separation. *Preparative Chromatography for Separation of Proteins*, page 457, 2017.

[128] Jahirul Mazumder, Jingxu Zhu, Amarjeet S Bassi, and Ajay K Ray. Modeling and simulation of liquid–solid circulating fluidized bed ion exchange system for continuous protein recovery. *Biotechnology and bioengineering*, 104 (1):111–126, 2009.

[129] Caroline Costa Moraes, Marcio A Mazutti, Francisco Maugeri, and Susana Juliano Kalil. Modeling of ion exchange expanded-bed chromatography for the purification of c-phycocyanin. *Journal of Chromatography A*, 1281:73–78, 2013.

[130] Lena Melter, Alessandro Butte, and Massimo Morbidelli. Preparative weak cation-exchange chromatography of monoclonal antibody variants: I. single-component adsorption. *Journal of Chromatography A*, 1200(2):156–165, 2008.

[131] F Owen Hoffman and Jana S Hammonds. Propagation of uncertainty in risk assessments: the need to distinguish between uncertainty due to lack of knowledge and uncertainty due to variability. *Risk Analysis*, 14(5):707–712, 1994.

[132] Harvey M Wagner. Global sensitivity analysis. *Operations Research*, 43(6): 948–969, 1995.

[133] Eric Langer. Biopharma industry seeks downstream processing advances, 2015. URL `http://www.pharmpro.com/blog/2015/05/biopharma-industry-seeks-downstream-processing-advances`.

[134] Eric Langer. Key downstream problems decline while industry continues to demand new technologies. *BioProcess International*, 10:4, 2012.

[135] Samuel Leweke and Eric von Lieres. Chromatography analysis and design toolkit (cadet). *Computers & Chemical Engineering*, 113:274–294, 2018.

[136] William Heyman and Eric von Lieres. Cadet web interface, 2016. URL `https://www.cadet-web.de/`.

[137] Andreas Püttmann, Sebastian Schnittert, Uwe Naumann, and Eric von Lieres. Fast and accurate parameter sensitivities for the general rate model of column liquid chromatography. *Computers & Chemical Engineering*, 56:46–57, 2013.

[138] Vijesh Kumar, Samuel Leweke, Eric von Lieres, and Anurag S Rathore. Mechanistic modeling of ion-exchange process chromatography of charge variants of monoclonal antibody products. *Journal of Chromatography A*, 1426: 140–153, 2015.

[139] Clayton A Brooks and Steven M Cramer. Steric mass-action ion exchange: displacement profiles and induced salt gradients. *AIChE Journal*, 38(12): 1969–1978, 1992.

[140] Lars Freier and Eric von Lieres. Robust multi-objective global optimization of stochastic processes with a case study in gradient elution chromatography. *Biotechnology journal*, 13(1):1700257, 2018.

[141] T Hahn, V Heuveline, and J Hubbuch. Chromx-a powerful and user-friendly software package for modeling liquid chromatography processes. *Chemie Ingenieur Technik*, 84(8):1342–1342, 2012.

[142] Frieder Kroner, Dennis Elsasser, and Jurgen Hubbuch. A high-throughput 2d-analytical technique to obtain single protein parameters from complex cell lysates for in silico process development of ion exchange chromatography. *Journal of Chromatography A*, 1318:84–91, 2013.

[143] Thiemo C Huuk, Tobias Hahn, Anna Osberghaus, and Jurgen Hubbuch. Model-based integrated optimization and evaluation of a multi-step ion exchange chromatography. *Separation and Purification Technology*, 136:207–222, 2014.

[144] Gang Wang, Tobias Hahn, and Jurgen Hubbuch. Water on hydrophobic surfaces: Mechanistic modeling of hydrophobic interaction chromatography. *Journal of Chromatography A*, 1465:71–78, 2016.

[145] Tobias Hahn, Thiemo Huuk, Anna Osberghaus, Katharina Doninger, Susanne Nath, Stefan Hepbildikler, Vincent Heuveline, and Jorgen Hubbuch. Calibration-free inverse modeling of ion-exchange chromatography in industrial antibody purification. *Engineering in Life Sciences*, 2015.

[146] Pascal Baumann, Tobias Hahn, and Jorgen Hubbuch. High-throughput micro-scale cultivations and chromatography modeling: Powerful tools for integrated process development. *Biotechnology and bioengineering*, 112(10): 2123–2133, 2015.

[147] Weiwei Qin, Martin E Silvestre, Frank Kirschhofer, Gerald Brenner-Weiss, and Matthias Franzreb. Insights into chromatographic separation using core–shell metal–organic frameworks: Size exclusion and polarity effects. *Journal of Chromatography A*, 1411:77–83, 2015.

[148] Thiemo C Huuk, Till Briskot, Tobias Hahn, and Jurgen Hubbuch. A versatile noninvasive method for adsorber quantification in batch and column chromatography based on the ionic capacity. *Biotechnology progress*, 2016.

[149] Tingyue Gu, Mingqing Liu, Kwok-Shun C Cheng, Senthilkumar Ramaswamy, and Chen Wang. A general rate model approach for the optimization of the core radius fraction for multicomponent isocratic elution in preparative nonlinear liquid chromatography using cored beads. *Chemical engineering science*, 66(15):3531–3539, 2011.

[150] Tinguye Gu. Tingyue gu's chromatography simulation home page, 2017. URL `http://www.ohio.edu/people/gu/CHROM/`.

[151] Steven T Evans, Xinqun Huang, and Steven M Cramer. Using aspen to teach chromatographic bioprocessing: A case study in weak partitioning chromatography for biotechnology applications. *Chemical Engineering Education*, 44(3):198–207, 2010.

[152] Jin Seok Hur and Phillip C Wankat. Chromatographic and smb center-cut separations of ternary mixtures. *Separation Science and Technology*, 43(6): 1273–1295, 2008.

[153] Jin Seok Hur, Phillip C Wankat, Jin-Il Kim, Jeung Kun Kim, and Yoon-Mo Koo. Purification of l-phenylalanine from a ternary amino acid mixture using a two-zone smb/chromatography hybrid system. *Separation Science and Technology*, 42(5):911–930, 2007.

[154] Seon-Hee Lee, Eun Lee, and In-Ho Kim. Simulation of smb [simulated moving bed] chromatography for separation of l-ribose and l-arabinose by aspen chromatography. *KSBB Journal*, 23(2):135–141, 2008.

[155] Yifei Zang and Phillip C Wankat. Three-zone simulated moving bed with partial feed and selective withdrawal. *Industrial & engineering chemistry research*, 41(21):5283–5289, 2002.

[156] Sharon Chan, Nigel Titchener-Hooker, Daniel G Bracewell, and Eva Sørensen. A systematic approach for modeling chromatographic processes—application to protein purification. *AIChE journal*, 54(4):965–977, 2008.

[157] Marcus Almqvist. Modeling and calibration of preparative chromatography in gproms separations of protein monomers from dimers. 2009.

[158] Edward J Close, Jeffrey R Salm, Daniel G Bracewell, and Eva Sorensen. A model based approach for identifying robust operating conditions for industrial chromatography with process variability. *Chemical Engineering Science*, 116:284–295, 2014.

[159] Jason Bentley and Yoshiaki Kawajiri. Prediction-correction method for optimization of simulated moving bed chromatography. *AIChE Journal*, 59(3): 736–746, 2013.

[160] Tingyue Gu. *Mathematical Modeling and Scale-up of Liquid Chromatography: With Application Examples*. Springer, 2015.

[161] T Gu, G-J Tsai, and GT Tsao. Modeling of nonlinear multicomponent chromatography. In *Chromatography*, pages 45–71. Springer, 1993.

[162] Seyed Mohammad Taghi Gharibzahedi, Shahin Roohinejad, Saji George, Francisco J Barba, Ralf Greiner, Gustavo V Barbosa-Cánovas, and Kumar Mallikarjunan. Innovative food processing technologies on the transglutaminase functionality in protein-based food products: Trends, opportunities and drawbacks. *Trends in food science & technology*, 2018.

[163] Francesco Cacciola, Paola Dugo, and Luigi Mondello. Multidimensional liquid chromatography in food analysis. *TrAC Trends in Analytical Chemistry*, 96: 116–123, 2017.

[164] Peter Q Tranchida, Paola Donato, Francesco Cacciola, Marco Beccaria, Paola Dugo, and Luigi Mondello. Potential of comprehensive chromatography in food analysis. *TrAC Trends in Analytical Chemistry*, 52:186–205, 2013.

[165] Sharmilee P Mane, Stuart K Johnson, Marcello Duranti, Vishnu K Pareek, and Ranjeet P Utikar. Lupin seed γ-conglutin: Extraction and purification methods-a review. *Trends in Food Science & Technology*, 73:1–11, 2018.

[166] F Janakievski, O Glagovskaia, and K De Silva. Simulated moving bed chromatography in food processing. In *Innovative Food Processing Technologies*, pages 133–149. Elsevier, 2016.

[167] EA Foegeding and PJ Luck. Milk proteins| whey protein products. 2002.

[168] Sparsh Ganju and Parag R Gogate. A review on approaches for efficient recovery of whey proteins from dairy industry effluents. *Journal of Food Engineering*, 215:84–96, 2017.

[169] Susana A González-Chávez, Sigifredo Arévalo-Gallegos, and Quintín Rascón-Cruz. Lactoferrin: structure, function and applications. *International journal of antimicrobial agents*, 33(4):301–e1, 2009.

[170] Sujata Sharma, Amit Kumar Singh, Sanket Kaushik, Mau Sinha, Rashmi Prabha Singh, Pradeep Sharma, Harshverdhan Sirohi, Punit Kaur, and Tej P Singh. Lactoperoxidase: structural insights into the function, ligand binding and inhibition. *International journal of biochemistry and molecular biology*, 4(3):108, 2013.

[171] Shireen Doultani, K Nazan Turhan, and Mark R Etzel. Fractionation of proteins from whey using cation exchange chromatography. *Process biochemistry*, 39(11):1737–1743, 2004.

[172] Magdalena Lech, Anita Niesobska, and Anna Trusek-Holownia. Dairy wastewater utilization: separation of whey proteins in membrane and chromatographic processes. *Desalination and Water Treatment*, 57(48-49):23326–23334, 2016.

[173] H Carrere, A Bascoul, P Floquet, AM Wilhelm, and H Delmas. Whey proteins extraction by fluidized ion exchange chromatography: simplified modeling and economical optimization. *The Chemical Engineering Journal and The Biochemical Engineering Journal*, 64(3):307–317, 1996.

[174] Steven Jay Gerberding and CH Byers. Preparative ion-exchange chromatography of proteins from dairy whey. *Journal of Chromatography A*, 808(1):141–151, 1998.

[175] B Hernández-Ledesma, I Recio, and L Amigo. β-lactoglobulin as source of bioactive peptides. *Amino acids*, 35(2):257–265, 2008.

[176] Tuğba Bayram, Murat Pekmez, Nazlı Arda, and A Süha Yalçın. Antioxidant activity of whey protein fractions isolated by gel exclusion chromatography and protease treatment. *Talanta*, 75(3):705–709, 2008.

[177] Eugene A Permyakov and Lawrence J Berliner. α-lactalbumin: structure and function. *FEBS letters*, 473(3):269–274, 2000.

[178] Gerd Konrad and Thomas Kleinschmidt. A new method for isolation of native α-lactalbumin from sweet whey. *International Dairy Journal*, 18(1):47–54, 2008.

[179] Daniel C Carter and Joseph X Ho. Structure of serum albumin. In *Advances in protein chemistry*, volume 45, pages 153–203. Elsevier, 1994.

[180] Najwa El Kadi, Nicolas Taulier, JY Le Huerou, Marcel Gindre, Wladimir Urbach, Ifeoma Nwigwe, Peter C Kahn, and Marcel Waks. Unfolding and refolding of bovine serum albumin at acid ph: ultrasound and structural studies. *Biophysical journal*, 91(9):3397–3404, 2006.

[181] Fariba Jafary, Soheila Kashanian, and Seyed Ziyaedin Samsam Sharieat. Purification, immobilization, and characterization of bovine lactoperoxidase. *International journal of food properties*, 16(4):905–916, 2013.

[182] S Goodall, AS Grandison, PJ Jauregi, and J Price. Selective separation of the major whey proteins using ion exchange membranes. *Journal of dairy science*, 91(1):1–10, 2008.

[183] Maria João Santos, José A Teixeira, and Lígia R Rodrigues. Fractionation and recovery of whey proteins by hydrophobic interaction chromatography. *Journal of Chromatography B*, 879(7-8):475–479, 2011.

[184] Ranjit Aich, Subhasis Batabyal, and Siddhartha Narayan Joardar. Isolation and purification of beta-lactoglobulin from cow milk. *Veterinary world*, 8(5): 621, 2015.

[185] B Schlatterer, R Baeker, and K Schlatterer. Improved purification of β-lactoglobulin from acid whey by means of ceramic hydroxyapatite chromatography with sodium fluoride as a displacer. *Journal of Chromatography B*, 807(2):223–228, 2004.

[186] Linda Voswinkel, Mark R Etzel, and Ulrich Kulozik. Adsorption of beta-lactoglobulin in anion exchange membrane chromatography versus the contacting mode and temperature. *LWT-Food Science and Technology*, 79:78–83, 2017.

[187] Tirang R Neyestani, Mahmoud Djalali, and Mohamad Pezeshki. Isolation of α-lactalbumin, β-lactoglobulin, and bovine serum albumin from cow's milk using gel filtration and anion-exchange chromatography including evaluation of their antigenicity. *Protein Expression and Purification*, 29(2):202–208, 2003.

[188] Mayyada MH El-Sayed and Howard A Chase. Single and two-component cation-exchange adsorption of the two pure major whey proteins. *Journal of Chromatography A*, 1216(50):8705–8711, 2009.

[189] Clara Fuciños, Pablo Fuciños, Natalia Estévez, Lorenzo M Pastrana, Antonio A Vicente, and María Luisa Rúa. One-step chromatographic method to purify α-lactalbumin from whey for nanotube synthesis purposes. *Food chemistry*, 275:480–488, 2019.

[190] Christine Machold, Robert Schlegl, Wolfgang Buchinger, and Alois Jungbauer. Continuous matrix assisted refolding of α-lactalbumin by ion exchange chromatography with recycling of aggregates combined with ultradiafiltration. *Journal of Chromatography A*, 1080(1):29–42, 2005.

[191] Rafael CI Fontan, Luis A Minim, Renata CF Bonomo, Luis Henrique M da Silva, and Valéria PR Minim. Adsorption isotherms and thermodynamics of α-lactalbumin on an anionic exchanger. *Fluid Phase Equilibria*, 348:39–44, 2013.

[192] Xiuyun Ye, Shigeru Yoshida, and TB Ng. Isolation of lactoperoxidase, lactoferrin, α-lactalbumin, β-lactoglobulin b and β-lactoglobulin a from bovine rennet whey using ion exchange chromatography. *The international journal of biochemistry & cell biology*, 32(11-12):1143–1150, 2000.

[193] Johan Samuelsson. Simulation of continuous chromatographic processes.

[194] Gabriela Sandoval, Barbara A Andrews, and Juan A Asenjo. Elution relationships to model affinity chromatography using a general rate model. *Journal of Molecular Recognition*, 25(11):571–579, 2012.

[195] Samar N Alias, Ahmed J Ali, and Cecilia Khoshaba Haweel. Separation of bovine serum albumin using chromatographical column: Parameters and simulation. *Iraqi Journal of Chemical and Petroleum Engineering*, 11(1):1–9, 2010.

[196] Peter van Beijeren, Peter Kreis, and Tim Zeiner. Ion exchange membrane adsorption of bovine serum albumin—impact of operating and buffer conditions on breakthrough curves. *Journal of membrane science*, 415:568–576, 2012.

[197] Naeimeh Faraji, Yan Zhang, and Ajay K Ray. Determination of adsorption isotherm parameters for minor whey proteins by gradient elution preparative liquid chromatography. *Journal of Chromatography A*, 1412:67–74, 2015.

[198] Qiao-Yan Du, Dong-Qiang Lin, Zhan-Sen Xiong, and Shan-Jing Yao. One-step purification of lactoferrin from crude sweet whey using cation-exchange expanded bed adsorption. *Industrial & Engineering Chemistry Research*, 52(7): 2693–2699, 2013.

[199] Chalore Teepakorn, Koffi Fiaty, and Catherine Charcosset. Optimization of lactoferrin and bovine serum albumin separation using ion-exchange mem-

brane chromatography. *Separation and Purification Technology*, 151:292–302, 2015.

[200] Pankaj Maharjan, Eva M Campi, Kirthi De Silva, Brad W Woonton, W Roy Jackson, and Milton TW Hearn. Studies on the application of temperature-responsive ion exchange polymers with whey proteins. *Journal of Chromatography A*, 1438:113–122, 2016.

[201] Rong Rong Lu, Shi Ying Xu, Zhang Wang, and Rui Jin Yang. Isolation of lactoferrin from bovine colostrum by ultrafiltration coupled with strong cation exchange chromatography on a production scale. *Journal of Membrane Science*, 297(1-2):152–161, 2007.

[202] Naeimeh Faraji, Yan Zhang, and Ajay K Ray. Optimization of lactoperoxidase and lactoferrin separation on an ion-exchange chromatography step. *Separations*, 4(2):10, 2017.

[203] Jonatan Andersson and Bo Mattiasson. Simulated moving bed technology with a simplified approach for protein purification: separation of lactoperoxidase and lactoferrin from whey protein concentrate. *Journal of Chromatography A*, 1107(1-2):88–95, 2006.

[204] Conan J Fee and Amita Chand. Capture of lactoferrin and lactoperoxidase from raw whole milk by cation exchange chromatography. *Separation and purification technology*, 48(2):143–149, 2006.

[205] Isidra Recio and Servaas Visser. Two ion-exchange chromatographic methods for the isolation of antibacterial peptides from lactoferrin: In situ enzymatic hydrolysis on an ion-exchange membrane. *Journal of chromatography A*, 831(2):191–201, 1999.

[206] Shigeru Yoshida et al. Isolation of lactoperoxidase and lactoferrins from bovine milk acid whey by carboxymethyl cation exchange chromatography. *Journal of Dairy Science*, 74(5):1439–1444, 1991.

[207] Edward J Close, Jeffrey R Salm, Daniel G Bracewell, and Eva Sorensen. Mod-

elling of industrial biopharmaceutical multicomponent chromatography. *Chemical Engineering Research and Design*, 92(7):1304–1314, 2014.

[208] Shamsul Qamar, Noreen Akram, and Andreas Seidel-Morgenstern. Analysis of general rate model of linear chromatography considering finite rates of the adsorption and desorption steps. *Chemical Engineering Research and Design*, 111:13–23, 2016.

[209] Tivadar Farkas, James Q Chambers, and Georges Guiochon. Column efficiency and radial homogeneity in liquid chromatography. *Journal of Chromatography A*, 679(2):231–245, 1994.

[210] Chen-Jiann Lin, Tseng-Hsiang Tse, Liu-Cheng Che, and Liang-Ming Tsai. Computer aided design and analysis on distributors in dac columns. In *MATEC Web of Conferences*, volume 185, page 00024. EDP Sciences, 2018.

[211] Miner N Munk. Liquid chromatography pumping system with compensation means for liquid compressibility, June 28 1977. US Patent 4,032,445.

[212] Pierre Achener, Seth R Abbott, and Robert L Stevenson. An experimental evaluation of compressibility effects in syringe pumps for liquid chromatography. *Journal of Chromatography A*, 130:29–40, 1977.

[213] Tivadar Farkas, Michael J Sepaniak, and Georges Guiochon. Radial distribution of the flow velocity, efficiency and concentration in a wide hplc column. *AIChE journal*, 43(8):1964–1974, 1997.

[214] Michel Martin, Gilbert Blu, and Georges Guiochon. The effect of pressure on the retention time and the retention volume of an inert compound in liquid chromatography. *Journal of Chromatographic Science*, 11(12):641–654, 1973.

[215] Michel Martin, Gilbert Blu, Claude Eon, and Georges Guiochon. Optimization of column design and operating parameters in high speed liquid chromatography. *Journal of Chromatographic Science*, 12(8):438–448, 1974.

[216] Joanna Kostka, Fabrice Gritti, Georges Guiochon, and Krzysztof Kaczmarski. Modeling of thermal processes in very high pressure liquid chromatogra-

phy for column immersed in a water bath: Application of the selected models. *Journal of Chromatography A*, 1217(28):4704–4712, 2010.

[217] E Kováts and F Bruner. The science of chromatography. *Elsevier, Amsterdam, the Netherlands*, 1985.

[218] Małgorzata Gubernak, Xiaoda Liu, Krzysztof Kaczmarski, and Georges Guiochon. Mass transfer kinetics in the chromatography of insulin variants under nonlinear conditions. *Biotechnology progress*, 20(5):1496–1506, 2004.

[219] Jinglan Wu, Wei Zhuang, Hanjie Ying, Pengfei Jiao, Renjie Li, Qingshi Wen, Lili Wang, Jingwei Zhou, and Pengpeng Yang. Acetone–butanol–ethanol competitive sorption simulation from single, binary, and ternary systems in a fixed-bed of ka-i resin. *Biotechnology progress*, 31(1):124–134, 2015.

[220] J_J_ Van Deemter, FJ Zuiderweg, and A van Klinkenberg. Longitudinal diffusion and resistance to mass transfer as causes of nonideality in chromatography. *Chemical Engineering Science*, 5(6):271–289, 1956.

[221] H Scott Fogler. *Essentials of Chemical Reaction Engineering: Essenti Chemica Reactio Engi*. Pearson Education, 2010.

[222] Joseph A Gerstner and Steven M Cramer. Cation-exchange displacement chromatography of proteins with protamine displacers: effect of induced salt gradients. *Biotechnology progress*, 8(6):540–545, 1992.

[223] Shishir D Gadam, Guhan Jayaraman, and Steven M Cramer. Characterization of non-linear adsorption properties of dextran-based polyelectrolyte displacers in ion-exchange systems. *Journal of Chromatography A*, 630(1-2): 37–52, 1993.

[224] Frank W Sosulski and Gilbert I Imafidon. Amino acid composition and nitrogen-to-protein conversion factors for animal and plant foods. *Journal of Agricultural and Food Chemistry*, 38(6):1351–1356, 1990.

[225] B David Hames. *Gel electrophoresis of proteins: a practical approach*, volume 197. OUP Oxford, 1998.

[226] Wayne Wray, Teni Boulikas, Virginia P Wray, and Ronald Hancock. Silver staining of proteins in polyacrylamide gels. *Analytical biochemistry*, 118(1): 197–203, 1981.

[227] Agilent Technologies. Agilent zorbax 300sb-c18 datasheet, 2003. URL `https://www.agilent.com/cs/library/datasheets/public/820646-002f.pdf`.

[228] Abhinav A Shukla, Sung Su Bae, JA Moore, Kristopher A Barnthouse, and Steven M Cramer. Synthesis and characterization of high-affinity, low molecular weight displacers for cation-exchange chromatography. *Industrial & engineering chemistry research*, 37(10):4090–4098, 1998.

[229] A Osberghaus, S Hepbildikler, S Nath, M Haindl, E von Lieres, and J Hubbuch. Determination of parameters for the steric mass action model—a comparison between two approaches. *Journal of Chromatography A*, 1233:54–65, 2012.

[230] US FDA. Technical review guide: Validation of chromatographic methods. *Center for Drug Evaluation and Research (CDER), Rockville, MD*, 1993.

[231] Sabyasachi Sarkar, Peter W Carr, and Anu Subramanian. Identification of the mass transfer mechanisms involved in the transport of human immunoglobulin-g in n, n, n, n-ethylenediaminetetramethylenephosphonic acid-modified zirconia. *Journal of Chromatography B*, 821(2):124–131, 2005.

[232] ME Young, PA Carroad, and RL Bell. Estimation of diffusion coefficients of proteins. *Biotechnology and Bioengineering*, 22(5):947–955, 1980.

[233] Samir Hamdi, William E Schiesser, and Graham W Griffiths. Method of lines. *Scholarpedia*, 2(7):2859, 2007.

[234] Shuichi Yamamoto, Kazahiro Nakanishi, and Ryuichi Matsuno. *Ion-exchange chromatography of proteins*. CRC Press, 1988.

[235] Joachim Weiss. *Handbook of Ion Chromatography, 3 Volume Set*, volume 2. John Wiley & Sons, 2016.

[236] Michael Gottschalk, Hanna Nilsson, Helena Roos, and Bertil Halle. Protein self-association in solution: The bovine β-lactoglobulin dimer and octamer. *Protein Science*, 12(11):2404–2411, 2003.

[237] EB Kalan, RR Kraeling, and RJ Gerrits. Isolation and partial characterization of a polymorphic swine whey protein. *International Journal of Biochemistry*, 2 (8):232–244, 1971.

[238] M Dalgalarrondo, E Dufour, C Bertrand-Harb, JM Chobert, and T Haertlé. Purification and characterization of two porcine β-lactoglobulin variants by nacl salting-out and reversed phase-hplc. *Le Lait*, 72(1):35–42, 1992.

[239] Kenneth R Hall, Lee C Eagleton, Andreas Acrivos, and Theodore Vermeulen. Pore-and solid-diffusion kinetics in fixed-bed adsorption under constant-pattern conditions. *Industrial & Engineering Chemistry Fundamentals*, 5(2):212–223, 1966.

[240] Mulu Berhe Desta. Batch sorption experiments: Langmuir and freundlich isotherm studies for the adsorption of textile metal ions onto teff straw (eragrostis tef) agricultural waste. *Journal of Thermodynamics*, 2013, 2013.

[241] Jan-Christer Janson. *Protein purification: principles, high resolution methods, and applications*, volume 151. John Wiley & Sons, 2012.

[242] Haiou Yang. *Fc-binding hexamer peptide ligands for immunoglobulin purification*. North Carolina State University, 2008.

[243] YL Jeyachandran, E Mielczarski, B Rai, and JA Mielczarski. Quantitative and qualitative evaluation of adsorption/desorption of bovine serum albumin on hydrophilic and hydrophobic surfaces. *Langmuir*, 25(19):11614–11620, 2009.

[244] Joonyeong Kim and Gabor A Somorjai. Molecular packing of lysozyme, fibrinogen, and bovine serum albumin on hydrophilic and hydrophobic surfaces studied by infrared- visible sum frequency generation and fluorescence microscopy. *Journal of the American Chemical Society*, 125(10):3150–3158, 2003.

[245] Florian Dismer and Jürgen Hubbuch. A novel approach to characterize the binding orientation of lysozyme on ion-exchange resins. *Journal of Chromatography A*, 1149(2):312–320, 2007.

[246] Xiaoyu Wu and Ganesan Narsimhan. Characterization of secondary and tertiary conformational changes of β-lactoglobulin adsorbed on silica nanoparticle surfaces. *Langmuir*, 24(9):4989–4998, 2008.

[247] C Nick Pace, Gerald R Grimsley, and J Martin Scholtz. Protein ionizable groups: pk values and their contribution to protein stability and solubility. *Journal of Biological Chemistry*, 284(20):13285–13289, 2009.

[248] Valeria Militello, Carlo Casarino, Antonio Emanuele, Antonella Giostra, Filippo Pullara, and Maurizio Leone. Aggregation kinetics of bovine serum albumin studied by ftir spectroscopy and light scattering. *Biophysical chemistry*, 107(2):175–187, 2004.

[249] Cyrus Chothia. The nature of the accessible and buried surfaces in proteins. *Journal of molecular biology*, 105(1):1–12, 1976.

[250] Harold P Erickson. Size and shape of protein molecules at the nanometer level determined by sedimentation, gel filtration, and electron microscopy. *Biological procedures online*, 11(1):32, 2009.

[251] Duong D Do et al. *Adsorption analysis: equilibria and kinetics*, volume 2. Imperial college press London, 1998.

[252] Ch S Gulipalli, B Prasad, and KAILAS L Wasewar. Batch study, equilibrium and kinetics of adsorption of selenium using rice husk ash (rha). *J. Eng. Sci. Technol*, 6(5):586–605, 2011.

[253] Ajoy Velayudhan and Csaba Horváth. Adsorption and ion-exchange isotherms in preparative chromatography. *Journal of Chromatography A*, 663 (1):1–10, 1994.

[254] *Capto^{TM} S, Capto Q, and Capto DEAE*. GE Healthcare Bio-Sciences AB, 5 2012. Björkgatan 30, 751 84, Uppsala, Sweden.

[255] Poondi Rajesh Gavara, Noor Shad Bibi, Mirna Lorena Sanchez, Mariano Grasselli, and Marcelo Fernandez-Lahore. Chromatographic characterization and process performance of column-packed anion exchange fibrous adsorbents for high throughput and high capacity bioseparations. *Processes*, 3(1): 204–221, 2015.

[256] T Peters and Roberta G Reed. Serum albumin: conformation and active sites. *Albumin: structure, biosynthesis, function. Pergamon, Oxford*, pages 11–20, 1978.

[257] Ryo Ishiguro, Yasuhiro Yokoyama, Hirotaka Maeda, Aya Shimamura, Keiichi Kameyama, and Koichi Hiramatsu. Modes of conformational changes of proteins adsorbed on a planar hydrophobic polymer surface reflecting their adsorption behaviors. *Journal of colloid and interface science*, 290(1):91–101, 2005.

[258] Lenin Domínguez-Ramírez, Elizabeth Del Moral-Ramírez, Paulina Cortes-Hernández, Mariano García-Garibay, and Judith Jiménez-Guzmán. β-lactoglobulin's conformational requirements for ligand binding at the calyx and the dimer interphase: a flexible docking study. *PloS one*, 8(11):e79530, 2013.

[259] Marleen Verheul, Jan Skov Pedersen, Sebastianus PFM Roefs, and Kees G de Kruif. Association behavior of native β-lactoglobulin. *Biopolymers: Original Research on Biomolecules*, 49(1):11–20, 1999.

[260] Davide Mercadante, Laurence D Melton, Gillian E Norris, Trevor S Loo, Martin AK Williams, Renwick CJ Dobson, and Geoffrey B Jameson. Bovine β-lactoglobulin is dimeric under imitative physiological conditions: dissociation equilibrium and rate constants over the ph range of 2.5–7.5. *Biophysical journal*, 103(2):303–312, 2012.

[261] Geoffrey W Smithers. Whey and whey proteins—from 'gutter-to-gold'. *International Dairy Journal*, 18(7):695–704, 2008.

[262] Mohamed Mansour El-Loly and Mohamed Bahy Mahfouz. Lactoferrin in relation to biological functions and applications: a review. *Int. J. Dairy Sci*, 6 (2):79–111, 2011.

[263] JN De Wit and ACM Van Hooydonk. Structure, functions and applications of lactoperoxidase in natural antimicrobial systems. *Netherlands Milk and Dairy Journal*, 50:227–244, 1996.

[264] Klaas D Kussendrager and ACM Van Hooijdonk. Lactoperoxidase: physico-chemical properties, occurrence, mechanism of action and applications. *British Journal of Nutrition*, 84(S1):19–25, 2000.

[265] Anurag S RATHORE, Robert M KENNEDY, J O'DONNELL, Ivars BEMBERIS, Oliver KALTENBRUNNER, et al. Qualification of a chromatographic column: why and how to do it. *Biopharm international*, 16(3):30–40, 2003.

[266] Robert L Fahrner and Gregory S Blank. Real-time monitoring of recombinant antibody breakthrough during protein a affinity chromatography. *Biotechnology and applied biochemistry*, 29(2):109–112, 1999.

[267] Derek YC Choy, A Louise Creagh, and Charles Haynes. Improved isoelectric focusing chromatography on strong anion exchange media via a new model that custom designs mobile phases using simple buffers. *Biotechnology and bioengineering*, 111(3):552–564, 2014.

[268] Ying Hou, Canping Jiang, Abhinav A Shukla, and Steven M Cramer. Improved process analytical technology for protein a chromatography using predictive principal component analysis tools. *Biotechnology and bioengineering*, 108 (1):59–68, 2011.

[269] DJ Gunn. Axial and radial dispersion in fixed beds. *Chemical Engineering Science*, 42(2):363–373, 1987.

[270] EJ Wilson and CJ Geankoplis. Liquid mass transfer at very low reynolds numbers in packed beds. *Industrial & Engineering Chemistry Fundamentals*, 5(1): 9–14, 1966.

Every reasonable effort has been made to acknowledge the owners of copyright material. I would be pleased to hear from any copyright owner who has been omitted or incorrectly acknowledged.